THÈSE POUR OBTENIR LE GRADE DE DOCTEUR DE MONTPELLIER SUPAGRO

En Biologie Intégrative, Diversité et Amélioration des Plantes

École doctorale GAIA – Biodiversité, Agriculture, Alimentation, Environnement, Terre, Eau
Portée par l'Université de Montpellier

Unité de recherche de Biochimie & Physiologie Moléculaires des Plantes (B&PMP)

Root developmental responses to nutrient shortage and biotic conditions in wheat: identification of beneficial bacteria from wheat rhizosphere and new procedures for phenotyping root and root hair development

Présentée par Thanyakorn RONGSAWAT
Le 13 décembre 2019

Sous la direction de Hervé SENTENAC
Encadrement par Jean-Benoît PELTIER

Devant le jury composé de

M. Jean-Marc ALLAIN, Professeur, Ecole polytechnique, Palaiseau	Rapporteur
M. Jean-Marie FRACHISSE, Chargé de recherche, CNRS, Gif-sur-Yvette	Rapporteur
Mme. Brigitte BRUNEL, Professeur, SupAgro, Montpellier	Examinatrice
Mme. Maïté VICRÉ-GIBOUIN, Maître de conférences, Université de Rouen, Rouen	Examinatrice
M. Hervé SENTENAC, Directeur de recherche, INRA, Montpellier	Directeur de thèse
M. Jean-Benoît PELTIER, Chargé de recherche, INRA, Montpellier	Encadrant

UNIVERSITÉ DE MONTPELLIER

Montpellier SupAgro

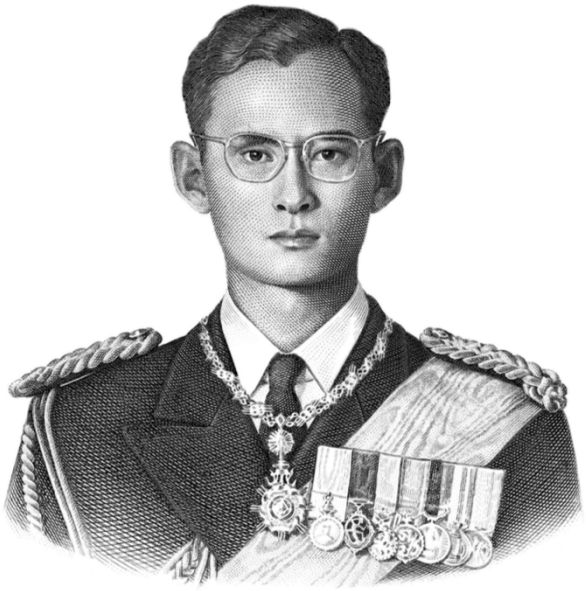

“…À partir du moment où se présentent des opportunités et des postes, il nous appartient de les saisir à bon escient sans prétexter des empêchements et sans se poser des conditions entravant l'acceptation. Une personne dynamique peut réussir dans toutes situations professionnelles. Fort du soin apporté, de l'assiduité et de l'honnêteté, les chances de réussite augmentent à coup sûr…”

“…Once there are opportunities and jobs offered,
one should be willing to do them without having any excuses or
any conditions as the obstacles. A proactive person can accomplish jobs in any types of work. Together will care, diligence and honesty, the chances of being successful are definitely increasing…”

“...เมื่อมีโอกาสและมีงานให้ทำ ควรเต็มใจทำ โดยไม่จำเป็นต้องตั้งข้อแม้หรือเงื่อนไขอันใด ไว้ให้เป็นเครื่องกีดขวาง
คนที่ทำงานได้จริงๆ นั้น ไม่ว่าจะจับงานสิ่งใดย่อมทำได้เสมอ ถ้ายิ่งมี ความเอาใจใส่
มีความขยันและซื่อสัตย์สุจริต ก็ยิ่งจะช่วยให้ประสบผลสำเร็จในงานที่ทำสูงขึ้น...”

H.M. King Bhumibol Adulyadej The Great
(1946-2016)

Photo by: BOT พระสยาม MAGAZINE

Acknowledgements

Firstly, I give sincerely acknowledge to the Erasmus Mundus ALFABET project, and the Montpellier SupAgro scholarship for their considerable financial support during my Ph.D. program.

I would like to express my appreciation to my supervisor, Dr. Hervé SENTENAC and to my co-supervisor, Dr. Jean-Benoît PELTIER for their supervision and invaluable guidance throughout the project. Besides to the mental supports, I would like to extend my gratitude for all opportunities and professtionally international cooperation, without the kindness of that this work would not be successful.

For all of my progression, I would like to thanks my committee members, Prof. Yvan MOËNNE-LOCCOZ, Prof. Philippe NORMAND, Dr. Christophe PÉRIN, and Dr. Pierre ROUMET for their comments and suggestions in completing my works.

I am taking this opportunity to greatly thanks to Dr. Ezékiel BAUDION regarding his expertise of the microbial ecology, to Volker BÄCKER for helping me in part of the MRHT and ACRT programs writing, and Dr. Jean-Baptiste THIBAUD for the electrical design.

Special thanks to Prof. Guilhem DESBROSSES and Dr. Nico NOUWEN for proving me the N_2-fixing bacteria in this study, to Pascal TILLARD for helping me in nitrogen and carbon analysis, to Carine ALCON in training of microscopy, to Florian FORT in the WinRhizo program, and to Sandrine CHAY for MP-AES training.

I would like to dedicate my thankfulness to Didier PILLOT, Madeleine AIDI, and Cécile DURAND-MORILLEAU for their supportive works, which regards to my scholarship managements.

For all members of ELSA and TICER team, I would like to give my recognition for their kindly advise and helps.

Thanks for the meaningful encouragements from Assoc. Prof. Dr. Charassri NUALSRI and Asst. Prof Dr. Korakot NAKKANONG, Faculty of Natural Resources, Prince of Songkla University, THAILAND.

Especially, thanks for the friendship to Frédéric, Nicolas, Antoine, Cyril, Minh, Alaeddine, Arthur, Jérémy B., Chu, Julien, Man Yuan, Hortense, Morgan, Jérémy V. Gabriella, Carmen, Thanh Hao, Jing, and all Thai students in Montpellier.

Finally, I would appreciated to say thousand words of “thank you” to my dearest family including my father, mother and sister for the unconditional LOVE and BELIEVE in me. You are inspired me in any ways. Thank you for being such a great role model and showing me to be the best in life and my challenges.

Table of the contents

Réponses développementales des racines aux carences nutritives et aux conditions biotiques chez le blé: identification de bactéries bénéfiques à partir de sol rhizosphérique de blé et nouvelles procédures de phénotypage du développement des racines et des poils absorbants

Chapitre 1 :

Introduction

1.1. Généralités

L'un des principaux défis de la seconde révolution verte qui s'annonce consiste à réduire les niveaux de fertilisation et d'irrigation et leurs coûts écologiques (Lynch, 2007) tout en faisant face à la forte augmentation de la population mondiale. De gros efforts de recherche visant à mieux comprendre le fonctionnement des systèmes racinaires sont nécessaires pour mettre au point de nouveaux cultivars offrant une meilleure capacité d'acquisition des ressources du sol et mieux exploiter la variation génétique de la productivité des cultures dans les sols peu fertiles (Brown *et al.*, 2013). L'architecture du système racinaire et, à l'interface du sol et des racines, la production et l'élongation des poils racinaires (PR) sont des facteurs déterminants du de la localisation et du volume du sol exploré. On sait également que i) la sécrétion racinaire de protons, d'acides organiques et d'enzymes permet la mobilisation des éléments nutritifs provenant des particules du sol et de la matière organique, et ii) le transfert/exsudation de sucres pour alimenter les symbiontes racinaires et les microbes bénéfiques est d'une importance capitale pour l'acquisition d'éléments nutritifs par les plantes et leur développement.

La présente étude est focalisée sur les poils absorbants racinaires (PR), cellules très abondantes et bien visibles surtout sur les parties racinaires jeunes. Il a été rapporté qu'un seul plant de seigle peut développer plus de 10 milliards de poils racinaires, ce qui représente une interface souterraine d'environ 400 m^2, beaucoup plus grande que celle des parties aériennes de la plante (Dittmer, 1937). La figure 1.1 montre une plantule de blé âgée de 2 semaines présentant des poils racinaires denses et longs sur presque tout le système racinaire. Le diamètre du cylindre pileux des racines dans les agrandissements affichés par les panneaux B, C et D de la figure 1.1 est environ 10 fois plus grand que celui de la racine elle-même. Le volume du cylindre pileux des racines est donc environ 100 fois supérieur à celui de la racine. En outre, pour des ions qui seraient mobiles dans la solution du sol proche de telles régions racinaires, leur probabilité d'atteindre la membrane cellulaire d'un poil racinaire serait

beaucoup plus élevée que celle d'atteindre la surface du cylindre racinaire. Nous passons ici en revue les principales fonctions des poils absorbants, en ce qui concerne la nutrition minérale des plantes, et faisons le point des tentatives d'utilisation des caractéristiques des poils absorbants dans les programmes de sélection végétale. Les processus de signalisation et les mécanismes moléculaires sous-jacents aux rôles des poils absorbants dans les interactions des plantes avec des microbes bénéfiques du sol, par exemple dans la symbiose rhizobienne (Ibanez *et al.*, 2017; Zipfel et Oldroyd, 2017), ne sont pas examinés dans la présente étude bibliographique.

1.2. Adhérence aux particules du sol, pénétration du sol et formation des manchons racinaires

L'adhérence des poils absorbants sur les particules de sol est d'une importance cruciale pour l'ancrage de l'extrémité des racines, la pénétration dans le sol et la formation de manchons racinaires (rhizosheath) (voir ci-dessous).

L'évocation rapide du rôle des poils absorbants dans « l 'ancrage des plantes », que l'on trouve souvent dans les documents sur le développement des poils absorbants, peut être perçue de manière confuse. Lorsque l'on compare la résistance aux forces de déracinement vertical entre des plantes d'Arabidopsis de génotype sauvage et des plantes mutantes altérées dans le développement des poils racinaires ou dans la production des racines latérales, la conclusion est que les poils ne contribuent pas à l'ancrage de la plante entière, dans cette définition opérationnelle (Bailey *et al.*, 2002). Par ailleurs, il est clairement établi que les poils absorbants permettent la pénétration des racines dans le sol. Par exemple, environ 80% des racines d'orge de type sauvage poussant dans couche de sol meuble au-dessus d'une couche plus compactée sont capables de pénétrer dans le sol compacté, alors que le pourcentage correspondant n'est que de 1% dans le cas de racines mutantes sans poils (Haling *et al.*, 2013). De même, dans le maïs en cours de germination sur un sol présentant une résistance au pénétromètre modérée, il a fallu environ 16 heures aux semis de type sauvage pour s'ancrer au sol, contre plus de 30 h pour les semis mutants sans poils, qui le plus souvent ne sont pas ancrés de manière sûre (Bengough *et al.*, 2016). Les forces d'ancrage étaient jusqu'à 5 fois plus faibles dans le mutant sans poil que dans les racines de type sauvage.

La force de l'adhérence fournie par les poils racinaires aux extrémités des racines en croissance dépend à la fois de la microstructure de la rhizosphère et de la taille du poil absorbant, qui déterminent la profondeur à laquelle les poils absorbants peuvent pénétrer dans la matrice du sol et les micropores. Il est tentant de supposer que, du moins chez certaines espèces, la force d'adhérence dépend également de la sécrétion de molécules adhérentes, comme le font les poils de l'haustorium de plantes parasites (Baird et Riopel, 1983; Cui *et al.*, 2016), les poils racinaires spécialisés des lianes à crampons comme le lierre (Huang *et al.,* 2016) et de l'Aracée Syngonium podophyllum (Yang et Deng, 2017).

Les mécanismes par lesquels les poils absorbants contribuent à la pénétration du sol sont également susceptibles de jouer un rôle majeur dans la formation des "manchons" racinaires. Les manchons racinaires ont été initialement décrits comme des "gaines particulières" composées de particules de sable agglutinées (Volkens, 1887). Les descriptions opérationnelles sont maintenant proposées à partir du poids du sol adhérant aux racines fraîchement excavées et soumises à un traitement d'enlèvement du sol (par exemple, agitation manuelle ou sonication dans l'eau) de vigueur standardisée (McCully, 1999; George *et al.*, 2014; Brown *et al.*, 2017; Pang *et al.*, 2017). Il est prouvé que la présence de poils absorbants dans les particules du sol est indispensable à la formation de ces manchons racinaires (Moreno-Espindola *et al.*, 2007; Shane *et al.*, 2011). Ainsi, le manchon racinaire désigne le sol qui adhère physiquement au système racinaire, tandis que la rhizosphère désigne le sol influencé par la racine, au-delà du "cylindre" du manchon (Hinsinger *et al.*, 2009: York *et al.*, 2016). Une forte corrélation a été trouvée entre la longueur du poil racinaire et le poids du manchon chez le blé (Delhaize *et al.*, 2012). La corrélation est plus faible chez l'orge (George *et al.*, 2014) et aucune corrélation significative n'a été observée chez 58 autres espèces, sauf lorsque les poils racinaires étaient extrêmement courts (Brown *et al.*, 2017). Il est possible que les manchons qui entourent les racines et qui possèdent de longs poils soient instables et aient tendance à se désintégrer pendant les mesures, ce qui donne une mauvaise corrélation. Il a également été suggéré que, lorsque la longueur des poils racinaires dépasse 300 µm environ, d'autres facteurs jouent un rôle de plus en plus important dans la formation, la taille et la stabilité des manchons, parmi lesquels (i) la densité et la morphologie des poils racinaires, par exemple des formes courbées ou crochues qui emprisonneraient plus fortement les particules de sol, et (ii) les mucilages racinaires et/ou microbiens (McCully 1999, Brown *et al.*, 2017). La présence de manchons peut jouer un rôle majeur dans de nombreuses fonctions physiologiques et l'adaptation des plantes aux conditions abiotiques et biotiques, telles que la prévention de la perte en eau, l'acquisition des nutriments et de l'eau, le recyclage des nutriments, la mise en place d'une défense mécanique contre les parasites herbivores et végétaux (Striga, Orobanches…) et la formation d'une niche favorisant la croissance pour les microbes bénéfiques (Shane 2011). Il a également été démontré que les manchons racinaires hébergent des bactéries diazotrophes (Wullstein *et al.*, 1979; Othman *et al.*, 2004) et hébergent une activité nitrogénase (Wullstein *et al.*, 1979).

Ainsi, les QTL (locus de caractères quantitatifs) pour la taille des manchons racinaires, pris comme substitut de la longueur des poils racinaires ou, dans un sens plus large, d'un trait de racine susceptible de contribuer à l'amélioration de l'alimentation du sol et de la nutrition hydrominérale, entraînant une augmentation de la production de biomasse et du rendement de plantes cultivées dans des sols à faible fertilité sont activement recherchées (Delhaize et al., 2015; Horn et al., 2016; James et al., 2016; Liu et al., 2017; Gong et McDonald, 2017; voir ci-dessous). Étroitement apparentés aux manchons racinaires, les grappes de racines dauciformes sont une structure racinaire spécialisée développée chez les carex (monocotylédones). Leur développement ne se produit que dans des genres

particuliers de Cyperaceae et Restoniacées lorsqu'ils sont cultivés avec un faible apport en P et N. Ces grappes de structures courtes en forme de carotte abritent des poils racinaires remarquablement denses et longs (Davies et al., 1973; Lamont, 1974; Shane et al., 2006). En conclusion, les manchons racinaires des racines dauciformes présentes dans les sols pauvres sont structurellement différents des racines protéoïdes, caractérisées par la production d'abondantes radicelles déterminées, mais sont fonctionnellement similaires aux racines protéoïdes (Shane et al., 2006) en termes d'abondance de poils racinaires fins et de libération d'anions organiques qui améliorent l'absorption des minéraux et de l'eau des sols appauvris en P (Albalasmeh et Ghezzehei, 2014).

1.3. Poils absorbants et acquisition de nutriments et d'eau

De très nombreuses études ont fourni des preuves indirectes ou directes que les poils absorbants contribuent de manière significative à l'acquisition d'ions nutritifs à partir du sol, et ainsi à la nutrition minérale de la plante. Les principaux éléments de preuve peuvent être triés comme suit. (i) La privation de nutriments entraîne une augmentation de la densité et de la longueur des poils absorbants (Bates et Lynch, 1996; Ma *et al.*, 2001; Schmidt et Shikora, 2001; Stettler *et al.*, 2015; Zygalakis *et al.*, 2011; Janes *et al.*, 2018). (ii) Les plantes mutantes présentant une croissance ralentie des poils absorbants sont affectées dans l'absorption des ions nutritifs et la production de biomasse; de plus, l'accumulation d'éléments nutritifs (par exemple le P) est positivement corrélée à la longueur du poil absorbant dans des conditions de faible disponibilité des éléments nutritifs ans le milieu (Brown *et al.*, 2013; Ahn *et al.*, 2004; Haling *et al*., 2014; Tanaka *et al.*, 2014; Canales e*t al.*, 2017) (iii) il a été démontré que les génotypes à poils racinaires plus longs chez l'orge et le blé étaient mieux adaptés aux sols pauvres en nutriments (Gahoonia et Nielsen, 2004; Han *et al.*, 2015; Klinsawang *et al.*, 2018). (iv) Enfin, des preuves directes que les poils racinaires contribuent à l'absorption des nutriments ont été obtenues par diverses approches électrophysiologiques (voir ci-dessous) ou en utilisant des dispositifs de croissance dédiés garantissant que seuls les poils racinaires ont accès à la source de nutriments (Gahoonia et Nielsen, 1998).

Une augmentation de la longueur et de la densité des poils résultant de la privation de nutriments a souvent été signalée pour des ions peu solubles, tels que les phosphates, le potassium, le fer et le manganèse, qui peuvent être fortement liés aux minéraux du sol et donc peu mobiles dans la solution du sol (faible capacité de diffusion par rapport à celle de NO_3^-) (Marschner, 1995). En outre, l'influence des poils absorbants sur la capacité d'absorption des éléments nutritifs est beaucoup plus importante lorsque la plante se développe dans du sol, par rapport à une culture hydroponique (Leitner *et al.*, 2010). Ces observations vont dans le sens de l'hypothèse largement acceptée selon laquelle l'augmentation de la surface de l'interface sol-racine résultant de la production de poils absorbants sous-tend fortement la contribution de ces cellules à l'acquisition d'ions nutritifs peu mobiles. En d'autres termes, les poils absorbants permettent à la racine d'augmenter le volume de sol à partir duquel des éléments nutritifs peuvent être absorbés (voir Figure 1.1). Il

convient de noter que les analyses physiques et mathématiques prédisent que l'augmentation de la longueur des poils absorbants entraîne une augmentation de l'absorption des nutriments supérieure à celle résultant d'une augmentation de la densité des poils (Zygalakis et al., 2011).

1.4. Systèmes de transport ionique au niveau de la membrane plasmique des poils absorbants: une panoplie conservée parmi les espèces végétales

Les échanges ioniques entre les cellules des poils absorbants des racines et le milieu externe ont été mis en évidence par différentes approches: l'utilisation de microélectrodes vibrantes sélectives aux ions au voisinage des poils absorbants permettant de déterminer les flux nets à partir de gradients de concentration locaux (Jones *et al*., 1995; Felle *et al.,* 1998 ; Lew, 1998; Babourina *et al.*, 2001), l'enregistrement des variations du potentiel de membrane au repos en réponse aux modifications de la composition ionique du milieu externe (Meharg et Blatt, 1995), ainsi que l'accumulation d'ions dans le cytosol des poils racinaires par imagerie fluorescente ou à l'aide de microélectrodes sélectives aux ions positionnées dans le cytosol (Bibikova *et al.*, 1997; Felle et Kepler, 1997; Felle *et al.*, 1999; Halperin et Lynch, 2003; Bai *et al.*, 2014). Ces études n'ont été menées que sur 3 espèces de plantes (*Arabidopsis*, la luzerne et la grenouillette *Limnobium stoloniferum*) et n'ont pas été généralisées à une large gamme d'ions. Elles ont par contre permis de mettre en évidence une absorption nutritionnelle des ions majeurs par les poils absorbants: K^+ (absorption couplée ou non à l'efflux de H^+), NO_3^- (couplée à l'afflux de H^+), Ca_2^+ et Na^+ (à des concentrations élevées). En outre, l'imagerie et les études utilisant des microélectrodes sélectives ont révélé des différences dans les propriétés de transport des ions en fonction du stade de développement des poils racinaires, et mis en évidence un transport polarisé des ions (Ca^{2+}, H^+) le long des poils racinaires en croissance (Bibikova *et al.*, 1997; Felle et Kepler, 1997; Felle *et al.*, 1999; Jones *et al.*, 1995; Bai *et al.*, 2014; voir ci-dessous). De telles analyses ont également mis en évidence des flux d'ions participant à des mécanismes de signalisation, par exemple dans la luzerne en réponse à des facteurs Nod, impliquant H^+, Cl^-, Ca^{2+} et K^+ (les réponses de signalisation des poils absorbants ne sont pas décrites dans le présent manuscrit).

Il est intéressant de noter que des membres de la famille des canaux Shaker et des familles de transporteurs HAK, NRT2, NRT3, AMT, PHT et Sultr sont également présents dans la mousse *Physcomitrella patens* (Garciadeblas *et al.*, 2007; Tsujimoto *et al.*, 2007 ; De Michele *et al*., 2012; Takahashi *et al*., 2012; https://phytozome.jgi.doe.gov/pz/portal.html#!info?alias=Org_Ppatens). Cette conservation des systèmes de transport assurant l'absorption des macronutriments et la conservation des conductances ioniques majeures révélée par les analyses électrophysiologiques de la membrane plasmique des poils racinaires (par patch clamp; *Cf*. ci-dessus) suggèrent que les principaux composants de l'équipement des poils impliqués dans la nutrition minérale des plantes ont été acquis très tôt au cours de l'évolution des plantes.

1.5. Poils racinaires et symbiose mycorhizienne: contribution à l'alimentation hydro-minérale des plantes

Il est bien connu que l'association symbiotique avec les champignons mycorhiziens peut également permettre à la plante d'augmenter le volume de sol exploité. Il a été proposé que les espèces végétales présentant des racines de diamètre relativement grand, une faible densité de poils et des poils de faible longueur, et donc une capacité intrinsèque limitée à absorber les éléments nutritifs du sol, tirent le plus grand bénéfice de la symbiose endomycorhizienne à arbuscules (AM) (Baylis, 1970; Brundrett, 2002; Smith et Read, 2008). Une méta-analyse récente indique cependant que la réponse à cette symbiose n'est pas corrélée au diamètre de la racine, à la longueur et à la densité des poils racinaires. En d'autres termes, observer des racines grossières chez une plante ne peut pas être considéré comme un facteur prédictif de la réponse de la croissance des plantes à la colonisation fongique par des champignons AM (Maherali, 2014).

L'investissement des photosynthétats dans l'augmentation de la production de poils absorbants et dans l'engagement dans la symbiose mycorhizienne peut être considéré comme une stratégie complémentaire pour améliorer l'acquisition des nutriments. Il convient toutefois de noter que les ectomycorhizes matures ne présentent pas de poils racinaires (Peterson et Farquhar, 1996). Cette absence est susceptible de résulter d'une incorporation des poils absorbants dans le manteau fongique. Lors de l'incorporation, les poils absorbants disparaitraient sous l'effet de la pression mécanique des hyphes (Brown et Sinclair, 1981; Thomson *et al.*, 1989). Cependant, il a également été prouvé que la sécrétion fongique de l'hypaphorine, un antagoniste de l'auxine, peut contribuer à l'absence de poils absorbants dans les ectomycorhizes en inhibant directement l'élongation des poils absorbants (Ditengou *et al.*, 2000 et 2003; Rigas *et al.*, 2013). Aucune corrrelation entre colonisation endomycorhizienne arbusculaire (AM) et développement des poils absorbants n'est clairement établie.

1.6. Interactions des poils absorbants avec les rhizobactéries promotrices de la croissance des plantes (PGPR)

La communauté microbienne vivant dans la rhizosphère à la surface des racines et nommée rhizomicrobiote (Chaparro *et al.*, 2013; Bulgarelli *et al.*, 2013) est extrêmement riche. Elle peut inclure jusqu'à 10^{10} bactéries par gramme de sol (Gans *et al.*, 2005; Roesch *et al.*, 2007), représentant une grande diversité de taxons (Kyselková *et al.*, 2009; Gomes *et al.*, 2010; Robertson-Albertyn *et al.*, 2017). Au sein de cette population, des bactéries génétiquement appelées rhizobactéries stimulant la croissance des plantes (PGPR) peuvent être recrutées par des racines pour s'engager dans des interactions bénéfiques (symbiose associative). En comparaison avec les symbiotes mutualistes (par exemple, la symbiose fixatrice d'azote dans les légumineuses), les PGPR interagissent avec un large éventail d'espèces de plantes hôtes et cette appellation générique englobe une diversité taxonomique importante,

en particulier dans les Firmicutes et dans les phyllums de Proteobactéries (Lugtenberg et Kamilova, 2009; Drogue *et al.*, 2012; Yeoh *et al.*, 2017; Garrido-Oter *et al.*, 2018). Les PGPR favorisent la croissance des plantes via des mécanismes très divers, tels que l'amélioration de la nutrition minérale des plantes résultant par exemple de la solubilisation de sources peu solubles de phosphate ou d'autres nutriments, la sécrétion de phytosidérophore, la production de phytohormones affectant le développement des racines, la mise en place facilitée de symbioses rhizobiennes ou mycorhiziennes, la protection contre les phytoparasites basés sur des mécanismes d'antagonisme ou de concurrence et / ou sur la défense des plantes, tels que la résistance systémique induite (Bashan et de-Bashan, 2010; Vacheron *et al*., 2013). Un déplacement du pH de la surface radiculaire vers des valeurs plus acides a également été signalé (Poitout *et al.*, 2017), suggérant une augmentation du taux d'excrétion de H^+ par les pompes à protons du plasmalemme et, de ce fait, une augmentation du potentiel électrochimique de H^+ qui énergize la membrane cellulaire et l'absorption des nutriments (Sentenac et Grignon, 1987; Thibaud *et al.*, 1988).

1.7. Plasticité du développement des poils absorbants et adaptation à la faible disponibilité en éléments nutritifs et aux conditions environnementales

La distribution des poils absorbants dans l'épiderme dépend de chaque espèce et il est possible de distinguer 3 types de patrons de distribution. Dans les espèces présentant un patron de type I, comme le riz ou la tomate par exemple, les poils absorbants se développent de manière aléatoire. Dans le motif de type II, présenté par des herbes telles que *Brachypodium*, les poils se développent à partir de cellules plus petites dérivées d'une division cellulaire asymétrique, les cellules plus grosses ne formant pas de poils. Dans le troisième patron, présenté par les Brassicaceae, comme Arabidopsis, et certaines de leurs familles sœurs, les lignées de cellules sont disposées longitudinalement de manière à ce que des lignées constituées de cellules différenciées en poils absorbants alternent avec des lignées de cellules sans poil.

La plupart des connaissances actuelles sur les mécanismes de développement fixés génétiquement qui régissent le destin des cellules épidermiques ont été acquis chez Arabidopsis. Dans ce modèle, le destin par défaut d'une cellule épidermique est une différenciation en poil absorbant. K'entrée d'une cellule épidermique dans le programme de développement des cellules autres que celui conduisant à la formation des cellules poils racinaires implique l'expression d'un facteur de transcription (FT) nommé GL2 (GABRA2), qui bloque la voie de différenciation en poil racinaire. Dans une cellule épidermique donnée, le niveau d'expression de GL2, et donc le destin de la cellule, est déterminé par la position relative de cette cellule par rapport aux cellules corticales sous-jacentes. Une cellule épidermique en contact avec deux cellules corticales, une position nommée "H" (pour "Hair"), se développe en une cellule de poil racinaire, tandis qu'une cellule en contact avec une seule cellule corticale, une position nommée "N" (Non-hair), entre dans le programme de développement des cellules ne différenciant pas de poil (Figure 1.7). Il est prouvé que la couche de cellules corticales émet des signaux conduisant à ce schéma de

différenciation, mais les connaissances actuelles sur la nature et les voies de transmission de ces signaux sont encore limitées.

1.8. QTL du développement des poils absorbants et relation avec le rendement de la plante

Différentes études menées sur les céréales, essentiellement l'orge, le blé et le maïs, visent à évaluer la possibilité d'exploiter la variation naturelle de la longueur des poils afin de développer des cultivars améliorés permettant des rendements durables dans des conditions de faibles intrants (fertilisation et irrigation). Dans l'orge, par exemple, un travail pionnier et de référence dans ce domaine a exploré la diversité biologique chez 38 cultivars, révélant une variations d'un facteur 4 environ de la longueur des poils racinaires, soit d'environ 0,4 mm à plus de 1,3 mm, chez des plantes cultivées en culture hydroponique, ce qui correspond aux variations observées par la suite lors d'expériences de contrôle effectuées sur le terrain (Gahoonia et Nielsen, 2004). Ensuite, un ensemble de 10 cultivars représentatifs a été testé dans des expériences sur le terrain, avec différents niveaux de disponibilité / fertilisation du sol. L'ensemble des résultats indiquait que les génotypes d'orge avec de longs poils racinaires présentaient une tolérance plus forte aux conditions de faible teneur en phosphore et exprimaient des potentiels de rendement plus élevés dans les sols à fortes concentrations de phosphore. De même, la caractérisation de lignées mutantes d'orge présentant divers phénotypes de poils racinaires, analysée à partir d'une population mutagénisée au sulfate d'éthylméthane (EMS), a montré que la longueur des poils racinaires était importante pour l'accumulation de P dans les tiges et la production de biomasse, en particulier lorsque les plantes étaient cultivées sous un stress combiné en eau et en phosphore. (Brown *et al*., 2012). Pour le rendement en grain, seule la présence de poils absorbants, et non la longueur de ceux-ci, était essentielle. Il convient toutefois de noter que la différence de longueur des poils racinaires entre les génotypes classés «poils racinaires courts» et «poils racinaires longs» (0,543 mm contre 0,690 mm) dans ces expériences était plutôt faible par rapport aux différences observées au sein du même ensemble de cultivars d'orge précédemment utilisés par Gahoonia et Nielsen (2004). Le fait que la production de biomasse végétale peut être corrélée positivement avec la longueur des poils chez l'orge a aussi été retrouvé lors du phénotypage de 175 lignées provenant d'une population d'haploïdes doublés (DH), utilisant la taille du manchon racinaire comme substitut fiable de la longueur des poils racinaires et l'index NDVI (index normalisé de différence de végétation), comme substitut de la biomasse des cultures. Cette approche a révélé que les principaux QTL (Locus de Traits Quantitatifs) pour la taille des manchons racinaires étaient associés à la masse estimée par le NDVI (Gong et McDonald, 2017). Aucun des QTL pour la taille des manchons racinaires et le rendement en grain n'ont pu être associés. Le lien complexe entre la croissance végétative et le rendement en grains dans les systèmes non irrigués (Ahmed *et al.*, 2018) pourrait expliquer le fait que la production de biomasse ne se soit pas traduite par une augmentation du rendement en grains dans ces expériences.

Chapitre 2 :

Matériels et méthodes

2.1. Stérilisation des caryopses de blé

Les caryopses de blé *Triticum turgidum* ssp. durum (cv Oued Zenati) sont, dans un premier temps, sélectionnés individuellement au niveau de leur poids et de l'aspect du germe afin de diminuer la variabilité. Les caryopses sont ensuite immergés dans 15 mL d'une solution d'hypochlorite de calcium (40 $g.L^{-1}$) et placés sous cloche à vide (2×8 min avec agitation forte entre les deux) permettant à la solution d'éliminer les bulles d'air en particulier celles prisonnières du sillon central. Sous flux laminaire et à température ambiante, les graines sont rincées 5 fois à l'eau stérile. Après le $5^{ème}$ lavage, les graines sont transférées dans un récipient contenant de l'eau stérile à 40°C, stimulant la germination, puis le récipient est incubé à 26°C pendant une nuit.

2.2. Conditions de germination et prétraitement des semences

Sous hotte à flux laminaire, les caryopses stériles sont transférés sur papier filtre stériles dans une boite de Petri et mis à germer pendant 2-3 jours à 26°C à l'obscurité. Les semences présentant des racines de 3-4 cm avec un hypocotyle bien visible (Figure 2.1, paneau B) sont transférées de nouveau dans une boite de Petri contenant 20 mL de PBS additionnés ou non de bactéries, en immergeant seulement les racines. La suspension bactérienne utilisée a été préparée en additionnant 19 mL de PBS et 1 mL de bactéries (DO_{600} initiale= 0,5 diluée à 0,1 dans du PBS). Les caryopses seuls sont ensuite traités au soufre afin de diminuer la contamination fongique dans les rhizotrons. Les graines sont "peintes" ("enrobées") 3 fois (soufre micronisé Neudorff à 640 $mg.mL^{-1}$ dilué dans de l'eau) avec séchage entre les applications successives.

2.3. Solutions nutritives

Différentes solutions nutritives ont été utilisées, toutes dérivant de la solution de Hoagland. Leur composition est donnée dans la légende ou le texte accompagnant les figures.

La solution pauvre en N (LN) contient 0,1 mM NH_4NO_3, 0,5 mM KNO_3, 5,0 mM KCl, 2,0 mM $CaCl_2$, 2,0 mM $MgSO_4$, 1,0 mM KH_2PO_4, 0,5 mM Na_2SiO_3, 0,1 mM NaFe (III) EDTA, 0,0125 mM H_3BO_3, 0,002 mM $MnCl_2$, 0,003 mM $ZnSO_4$, 0,0005 mM $CuSO_4$, 0,0001 mM Na_2MoO_4 and 0,0001 mM $NiSO_4$.

La solution correspondante riche en N (HN) contient du KNO_3 à 5,0 mM au lieu de 0,5 mM et le KCl est ramené à 0,025 mM. La concentration totale en azote dans les solutions LN et HN sont respectivement de 0,7 et 5,2 mM.

2.4. Croissance sur agar pour le phénotypage des poils absorbants

Les plantules germées sont transférées sur boite de Petri (1 plante/boite, Figure 2.3) et sur milieu gélosé (12 $g.L^{-1}$ agar, ½Hoagland sinon indiqué dans le texte). Les plantules ne sont pas inoculées mais le milieu, lui, est inoculé en mélangeant 100 µl de suspension bactérienne (DO_{600} 0,5 diluée à 0,1 dans du PBS) dans 30 ml de milieu gélosé juste avant le coulage des boites (milieu tiède). Les boites de Petri sont enveloppées au ¾ dans un plastique noir 'pour éviter de laisser les racines à la lumière) et transférées dans une chambre de culture (Aralab, photopériode de 16h, 70% d'humidité et température jour/nuit 23/20°C. Les boites sont quasi verticales (85°) pour faciliter l'adhérence des racines sur l'agarose. La croissance est assurée dans ces conditions durant 72 H avec des racines séminales développant des poils racinaires à la surface du milieu. Les photos des racines sont prises à 1 cm de l'apex racinaire (sinon précisé) en utilisant une loupe binoculaire Olympus (mode champ brillant). Les images sont analysées par ImageJ.

2.5. Croissance des plantes en « cuvette » pour le phénotypage des poils racinaires sous microscope

Les plantules sont transférées dans des « cuvettes » construites par impression 3D (Figure 2.2A). Une description détaillée du système « cuvette est disponible au chapitre 4. Chaque cuvette reçoit une plante et le transfert de la plante vers la cuvette s'effectue sous flux laminaire afin de minimiser les infections précoces. La racine séminale majeure de la plantule est glissée dans un tube connecté avec la partie inférieure de la cuvette. Ce tube est ensuite obturé par de la glu dentaire (Coltène President microSystem, light body, Coltène / Whaledent AG, Altstätten, Suisse). La cuvette est ensuite placée dans une solution nutritive, le caryopse se situant à environ 1 cm du niveau de cette solution. Un système de pompage/reflux entre 2 contenants permet l'oxygénation du matériel végétal (voir chapitre 4). Les plantes croissent pendant 3 jours en chambre de culture (photopériode de 16H, température jour/nuit 22/20°C, intensité lumineuse de 150 µE, 70% d'humidité). La cuvette est alors sortie précautionneusement de la solution hydroponique pour éviter les dommages au niveau des poils absorbants, et l'excès de liquide ôté. La cuvette est placée à l'horizontale pour recouvrir la racine principale d'une lame de microscope. Quelques gouttelettes de milieu LN sont ajoutées entre la lame et la racine (voir Figure 4.6). Les images sont prises à une distance donnée de l'apex racinaire (1 cm sinon précisé) à l'aide d'un apotome Zeiss (zoom ×5) (Microscope Zeiss Apotome, Bright field, Z-stacks mode).

2.6. Croissance en rhizotron pour le phenotypage du système racinaire et des poils absorbants

Une description détaillée des rhizotrons est fournie dans le chapitre 4. Deux graines germées sont insérées par rhizotron, une sur chaque face, de sorte à ce que les racines poussent entre la plaque de verre et un tissu polyester noir (18 µm SAATI France) enveloppant une mousse florale en polyurétane (Smithers Oasis France 11400 St Martin Lalande). L'ensemble est humidifié automatiquement par une rampe de robinets (10/rhizotrons) reliée à un réservoir de solution (voir chapitre 4, Figures 4.14 and 4.15). Les racines sont protégées de la lumière par des plaques couvertes

d'aluminium ajustées à la taille des rhizotrons. Les plantes sont mises à pousser pendant 12 jours en chambre de culture (photopériode 16H, température jour nuit 22/20°C, humidité 70% comme dans le cas des « cuvettes »). Des images à haute résolution (48 bits, 1200 ppp) du système racinaire sont obtenues grâce à un scanner (Epson Perfection V850 Pro Scanner).

2.7. Effet de souches diazotrophes sur la croissance du blé sur sol artificiel

Les caryopses de blé (cultivar Oued Zanati) sont cultivés en présence de concentrations variables en NO_3^- et en présence ou non de bactéries diazotrophes. Les douze souches suivantes ont été utilisées dans cette étud: i) *Bradyrhizobium japonicum* ORS285 et *B. japonicum* ORS285Δ*nif* (abréviation: Brad et BradΔ*nif*) fournies par Dr. Nico Nouwen (IRD Montpellier), (ii) *Frankia* sp. R43 (abréviation: Frankia, fournie par Prof. Philippe Normand, Université de Lyon, (iii) *Azospirillium lipoferum* 4B (abréviation: Azo4B) et *A. brasilense* Sp245 (abréviation: AzoSp245), obtenues auprès du Prof. Guilhem Desbrosses, Université de Montpellier et (iv) les souches A10, B1, B3-1, B-3-2, H2, I1-2 et I1-3 (abréviations: A10, B1, B3-1, B3-2, H2, I1-2 et I1-3) isolées de la rhizosphère d'un plant de blé dur cultivé à Nabatiyeh (sud Liban).

Un mélange tourbe/sable/perlite (1/1/1 v/v/v) est stérilisé à l'autoclave et inoculé ou non avec une souche diazotrophe. La suspension bactérienne et les plantules sont préparées comme décrit au § 2 (§ 2.2), sans que les plantules soient traitées au soufre. Chaque pot contenant une seule graine est couvert d'un film plastique pour ralentir la contamination possible par les bactéries présentes dans la chambre de culture. Les plantes sont laissées pendant 30 j en chambre de culture (conditions de culture voir § 2.5) avant d'être phénotypées (voir Figure 2.4) et arrosées périodiquement (tous les 3 j) de 20 mL de solution HN ou LN (§ 2.6). Au bout des 30 j, le système racinaire est extrait et excisé de la partie aérienne. Les racines sont délicatement lavées, photographiées et séchées (80°C, 7 j) puis pesées et réduites en poudre dans un mortier avant d'analyser leur composition ionique (C, N, K, P, Na, Ca, Mg, Mn, Fe, Cu et Zn).

Imagerie de l'architecture racinaire. Les racines sont lavées (5-6 fois) à l'eau et les particules de sol adhérentes ôtées. Le système racinaire est placé entre 2 feuilles de plastique transparentes et scanné (Epson Perfection V850 Pro Scanner 24-bits, 800 ppp). Les images ont été analysées par ImageJ et les outils IJ_Rhizo (Pierret *et al*., 2013). Voir Figure 2.5.

Détermination du carbone et de l'azote total. Les échantillons (1-2 g MS) sont analysés par spectrométrie de masse sur un Elementar Pyrocube analyzer (Elementar France Lyon France). Chaque valeur est la mesure de 5 réplicats.

Analyses de composition ionique. Les échantillons (10 mg MS) contenus dans des tubes TPE sont digérés sous hotte avec 750 µL d'acide nitrique à 65% et 250 µL d'H_2O_2 pendant 8 à 16H (jusqu'à disparition de la production de gaz) puis incubés à 85°C pendant 8H. Lorsque les tissus végétaux ne sont plus visibles dans la solution devenue jaune transparente, celle-ci est diluée par 4 mL d'eau distillée. Chaque tube

est alors repesé avant transfert de l'échantillon dans des tubes de l'automate (autosampler, tubes Agilent PPP) afin de corriger les données finales des éventuelles disparités durant la digestion. Chaque échantillon est analysé pour sa composition en P, K, Na, Ca, Mn, Fe, Mn, Zn et Cu en utilisant un couplage micro-onde-spectromètre à plasma atomique (MP-AES, Agilent). Chaque traitement est la moyenne de 5 réplicats.

2.8. Prélèvement des échantillons et analyse chimique des sols libanais

Les échantillons de sol ont été prélevés par Houssein Zhour (doctorant dans l'équipe) dans un champ de blé dur situé près du village de Zawtar Al-sharkiya proche de la ville de Nabatiyeh (Liban) (latitude 33° 19' 28.5" N et longitude 35° 28' 8.83" E, altitude 460 m) (Figure 2.6). Ces échantillons de sol ont été collectés dans 5 endroits du champ pris au hasard et regroupés ensemble par la suite. Ils correspondent au sol adhérent aux racines à une profondeur de 5 à 10 cm. Le sol est séché à 50°C pendant 5 J, broyé dans un mortier et tamisé (maillage de 12 mm). Le sol broyé est ensuite resuspendu dans de l'eau distillée (ratio sol-eau 1:4 p/v). L'analyse des paramètres physico-chimiques est fournie dans le Tableau 2.1. L'analyse texturale (sable, limon, argile) a été réalisée par hydrométrie. pH et conductivité électrique ont été déterminés par une électrode à pH et un conductimètre respectivement. La teneur en matière organique a été déterminée par la méthode de Walkley and Black (1934), celle de l'azote total par la méthode de Kjeldahl et celle du phosphate disponible par la méthode vanado-molybdate (Jackson, 1973) suivie par la digestion par HNO_3-$HClO_4$. Les teneurs en K, Fe, Mn, Zn et Cu ont été déterminées par spectrométrie d'absorption atomique (AAS).

2.9. Isolement des diazotrophes du sol libanais

Un échantillon de sol rhizosphérique (50 mg) est déposé directement à la surface d'un milieu semi-solide (5 mL/tube) dépourvu d'azote assimilable (milieu NFb : Nitrogen-Free bromothymol medium, Baldani *et al.*, 2014) contenant 10 $mg.L^{-1}$ de bleu de bromothymol (indicateur de pH) contenu dans un tube « vacuette® » dont le bouchon contient un septum en caoutchouc (pour l'introduction de gaz ou pour les prélèvements; *Cf*. Figure 2.7). Après 3j d'incubation à 28°C, une pellicule trouble typique de la croissance des diazotrophes apparait à la surface ou au voisinage de la surface. Cette pellicule est accompagnée par une dérive de la couleur du milieu de bleu à jaune-orange (pH plus acide). Un test ARA (réduction d'acétylène) permet de tester la capacité de la pellicule à fixer le diazote. Pour ce faire, de l'acétylène(C_2H_2) est injecté (10% v/v) dans la vacuette et la production d'éthylène (C_2H_4) est mesurée 24 h plus tard (voir ci-dessous). La pellicule est ensuite prélevée, homogénéisée et 50 µl de la suspension finale sont transférés sur un milieu neuf NFb en vacuette. Trois repiquages successifs sont généralement suffisants et lors du dernier, un nouveau test ARA est effectué (Figure 2.7). Au dernier repiquage, 1 mL de la pellicule est dilué dans 9 mL de PBS pour atteindre une concentration approximative de 10^{-6}. Cent µL de cette dilution sont étalés sur boite de Petri contenant du LB + agarose et incubé pendant 4j à 28°C. Les colonies développées permettent d'estimer la quantité de bactéries et leur diversité (forme et hauteur de la colonie, couleur,

forme de la marge, brillance…). Un repiquage en stries des morphotypes est effectué et les boites sont de nouveau incubées dans des conditions identiques. Une anse ronde est prélevée de chaque morphotype et resuspendue dans 1 mL de PBS stérile. Chaque resuspension est vortexée environ 1 min et centrifugée 10 min à 14000 rpm. Le culot est lavé 3 fois dans le PBS et 50 µL du dernier lavage est transféré dans une vacuette sur 5 ml de NFb. Après 3 j à 27°C, un nouveau test ARA est effectué et la pellicule est prélevée. Une fois homogénéisée, des aliquotes de 50 µl de pellicule sont mélangés à du glycérol pour faire un stock à 50% et stockées à -80°C.

Le test ARA est effectué selon Mirza *et al.*, 2001. L'acétylène (10% v/v) est injecté dans la vacuette (contrôle sans acétylène) et après 24h à 27°C, 10 ml de gaz sont prélevés à partir des vacuettes et analysés par chromatographie gazeuse afin de détecter la présence d'éthylène. Les résultats sont exprimés en nmol de C_2H_4 produits par tube et par jour.

2.10 Tests de solubilisation du phosphate et du potassium par les bactéries

La capacité des bactéries diazotrophes à utiliser une source de phosphate insoluble ($Ca_3(PO_4)_2$) a été testée sur les souches libanaises isolées. Chaque souche a été déposée (aliquote de 15 µL) sur un milieu Pikovskaya (PVK) (Pikovskayas *et al.*, 1984) contenant en $g.L^{-1}$ 10 glucose, 0,1 $(NH_4)_2SO_4$, 0,2 KCl, 0.25 $MgSO_4.7H_2O$, 5,0 $MgCl_2.6H_2O$ et 5 $Ca_3(PO_4)_2$ (tricalcium phosphate) et 12 agar, pH ajusté à 7 avec HCl 1 M. Avant étalement du milieu en boite de Petri, du violet de bromocrésol (150 µl d'une solution à 5 $g.L^{-1}$ de violet de bromocrésol (pKa 6,3) dans 0,2 N KOH pour 20 mL de PVK) est ajouté en tant qu'indicateur de pH. Les boites sont incubées 3 j à 27°C et la formation d'un halo jaune (pH < 5,8) autour du point d'inoculation est suivie (Figure 2.8). La taille du halo est corrélée au développement de la colonie acidifiant le milieu en utilisant la source de phosphate tricalcique. Les bactéries solubilisant les sources de phosphate insolubles sont nommées BSP (Bacteries solubilisant le phosphate).

En plus de la présence de phosphate insoluble comme seule source de phosphate, la faculté des bactéries à utiliser une source de K insoluble (aluminosilicate de potassium, $KAlSi_3O_8$ Potash Feldspar, Bath Potters' Supplies, Somerset, UK) a aussi été testée. Comme précédemment, chaque souche (15 µL) a été déposée sur un milieu Alexandrov (Rajawat *et al*., 2016) contenant en $g.L^{-1}$ 5 glucose, 2 Ca_3PO_4, 0,2 KCl, 0,05 $MgSO_4.7H2O$., 0,1 $CaCO_3$, 0,005 $FeCl_3$, 2 $KAlSi_3O_8$, 12 d'agar avec le pH de 7,2 ajusté avec HCl 1M. Avant étalement du milieu en boite de Petri, du bleu de bromothymol (75 µL d'une solution à 5 $g.L^{-1}$ de bleu de bromothymoll (pKa 7,1) dans 0,2 N KOH pour 20 mL de milieu) est ajouté en tant qu'indicateur de pH. Les boites sont incubées 3 j à 27°C et la formation d'un halo bleu/vert (pH < 7) ou jaune (pH<6,8) autour du point d'inoculation est suivi (Figure 2.8). Comme dans le cas du phosphate tricalcique, la taille du halo est enregistrée et reflète la capacité des bactéries à utiliser les sources insolubles de sels, dans notre cas, les bactéries sont nommées BSPK (bactéries solubilisant le phosphate et le potassium. Cette faculté

est quantifiée en utilisant l'index de solubilisation (SI) (Setiawati et Mutmainnah, 2016)

SI = Diamètre du halo / diamètre de la colonie

2.11. Souches et culture bactériennes

Les souches bactériennes utilisées sont listées dans le Tableau 2.2

2.11.1 Milieux de culture utilisés

(i) Bradyrhizobium japonicum strain ORS285 et *B. japonicum* strain ORS285*Δnif.* Ces 2 souches sont cultivées sur milieu YM (Vincent *et al.*, 1970) contenant en $g.L^{-1}$ 5 mannitol, 0,6 K_2HPO_4, 0,1 $MgSO_4.7H_2O$., 0,04 $CaCl_2.2H_2O$., 3 d'extrait de levure (yeast extract), et 12 d'agar, pH ajusté à 7 avec HCl 1 M.

(ii) Azospirillum lipoferum strain 4B, *Azospirillum brasilense* strain Sp245 et les bactéries isolées du Liban. Ces bactéries ont été cultivées sur milieu NFb modifié (à partir de Baldani *et al.*, 2014). Ce milieu contient en $g.L^{-1}$ 3,71 acide malique, 0,509 citrate de sodium, 0,53 fructose, 0,265 glucose, K_2HPO_4, 0,2 $MgSO_4.7H_2O$, 0,02 $CaCl_2.2H_2O$, 0,1 NaCl, 2,8 KOH, and 0,04 d'extrait de levure (yeast extract) et des micronutriments et vitamines comme suit:
- micronutriments en $mg.L^{-1}$: 2,8 H_3BO_3, 2,35 $MnSO_4.H_2O$, 2,0 $Na_2MoO_4.2H_2O$, 0,2 $CuSO_4.5H_2O$, 0,6 $ZnSO_4.7H_2O$ (ajoutés à partir d'une solution concentrée 500x) and 65,6 NaFeEDTA (stock ×250).
- vitamines: 0,1 biotin and 0,2 $pyridoxal_{HCl}$ (Stock ×1000).
Dans le cas d'un milieu gélosé classique, 12 $g.L^{-1}$ d'agarose sont ajoutés, dans le cas d'un milieu semi-gélosé l'extrait de levure et l'agarose sont remplacés 1,8 g de Bacto-Agar®. Si non indiqué, le pH final est ajusté à 7,5 avec HCL 1M.

(iii) Frankia. Frankia sp. R43 est cultivée sur mileu BAP sans N (N-free BAP liquid medium (Murry *et al.*,1984), contenant en $g.L^{-1}$ 0,5 NaPropionate, 0,95 KH_2PO_4, 0,6 K_2HPO_4, 0,025 $MgSO_4.7H_2O$, 0,003 $CaCl_2.2H_2O$, et en $mg.L^{-1}$ 0,45 Biotin, 7,5 $FeSO_4.7H_2O$, 5,6 $Na_2EDTA.2H_2O$. (stock x1000), 2,8 H_3BO_3, 1,8 $MnCl_2.4H_2O$, 0,1 $CuSO_4.5H_2O$, 0,2 $ZnSO_4.7H_2O$, 0,025 $Na_2MoO_4.2H_2O$ (stock micronutriments ×1000). Le pH final est ajusté à 6,4 avec 1 M HCl.

2.11.2 Cultures bactériennes

(i) Pour toutes les bactéries à l'exception de Frankia. Les cultures sont initiées à partir d'une seule colonie. Chaque colonie pousse dans 30 ml de milieu et est incubée à 30°C avec agitation (300 rpm), jusqu'à une DO à 600 nm (DO_{600}) de 1,0. La culture est alors centrifuge à 4,000 rpm pendant 20 min et le culot est lavé 3 fois dans du PBS (8 $g.L^{-1}$ NaCl, 0,2 $g.L^{-1}$ KCl, 0,24 $g.L^{-1}$ KH_2PO_4, and 1,44 $g.L^{-1}$ $Na_2HPO_4.2H_2O$, le pH est ajusté à 7 avec HCl 1 M). Les bactéries sont resuspendues dans du PBS pour atteindre une DO_{600} de 0,1.

(*ii) Frankia*. *Frankia* est incubée à 26°C à l'obscurité pendant 2 semaines. La culture est vortexée *ca.* 1 min puis centrifugée à 4,000 rpm pendant 20 min. Le culot (contenant les fragments d'hyphes) est resuspendu dans 20 ml de PBS stérile (*ca.* 1 min) puis de nouveau centrifugé à 4,000 rpm pendant 20 min. Les fragments d'hyphes sont lavés 3 fois dans le PBS stérile et resuspendu dans ce même tampon pour une DO_{600} finale de 0,1.

Les suspensions bactériennes sont utilisées pour inoculer des plantules de blé (5 plantules pour 20 ml de suspension ; voir § 2.2) ou un substrat artificiel stérilisé (20 ml par pot ; voir § 2.7)

2.12 Caractérisation moléculaire des souches bactériennes libanaises

Extraction d'ADN : L'ADN génomique est isolé après passage des bactéries à 94°C pendant 10 min dans de l'eau distillée puis la concentration est déterminée au spectrophotomètre Nanodrop (Nanodrop 1000, Thermo Scientific, ratio A260/A280), (Dashti *et al*., 2009).

Amplification de l'ARNr 16S. Les segments d'ARNr 16S sont amplifiés en utilisant les 2 amorces universelles 27F et 1525R (séquences des amorces: voir Tableau 2.3). L'amplification PCR est réalisée dans un volume final de 25 µl, en additionnant 1,0 µL d'ADN bactérien, 0,12 µL de 5,0 U μL^{-1} d'ADN polymerase *Taq*, 2,5 µL of 5× tampon *Taq*, 1,0 µl de 5 mM deoxynucleotide triphosphates (dNTPs), 2,0 µL de 25 mM $MgCl_2$ et 1,0 µL de chaque amorce (10 µM), ajusté à 25 µL par de l'eau distillée). Après l'étape de dénaturation initiale à 96°C pendant 5 min, la phase d'amplification comprend 35 cycles, chaque cycle comprend les étapes suivantes à savoir 96 °C durant 30s, 57°C durant 30s et 72°C durant 2 min, suivis d'une phase d'extension à 72°C pendant 10 min.

Amplification PCR du gène *nifH***.** L'amplification d'un fragment du gène *nifH* se déroule en 2 étapes. La première amplification se déroule en utilisant les amorces PolF et PolR, la seconde en utilisant les amorces PolF et AQER (séquences des amorces voir Tableau 2.3). Lors de la première amplification, (volume final 25 µL) 2 µL d'ADN bactérien sont ajoutés à 0,3 µL de 5,0 U μL^{-1} d'ADN polymerase *Taq*, 5 µL de 5× tampon *Taq*, 2 µL de 2,5 mM dNTPs, 0,5 µL de BSA (10 $mg.mL^{-1}$) et 0,625 µL de chaque amorce PolF et PolR (20 µM) et qsp 25 µL avec de l'eau distillée. Le protocole de la réaction est le suivant: dénaturation initiale à 94°C durant 5 min, puis 30 cycles comprenant les étapes suivantes : 94°C durant 1 min, 55°C durant 1 min, 72°C durant 1 min, et une extension finale à 72°C pendant 10 min. Lors de la seconde amplification, le volume réactionnel est toujours de 25 µL contenant 0,5 µL de produit PCR de l'étape 1, 0,2 µL de 5 U μL^{-1} d'ADN polymerase *Taq*, 5,0 µL de 5× tampon *Taq,* 2,0 µL de 2,5 mM dNTPs, 0,5 µL de BSA (10 $mg.mL^{-1}$) et 0,625 µl de chaque amorce PolF et AQER (20 µM) et qsp 25 µL avec de l'eau distillée.

Amplification PCR de la BOX-A1R. L'amplification de la *BOX-A1R* s'effectue avec une seule amorce puisque ces séquences sont répétées inversées (séquence voir tableau 2.3). Elles offrent une signature assez spécifique des souches. L'amplification PCR est réalisée dans un volume final de 25 µL en additionnant 2 µL

d'ADN bactérien, 0,3 µL de 5,0 U μL^{-1} d'ADN polymerase *Taq*, 5,0 µL de 5×tampon *Taq*, 2,0 µL de 2,5 mM deoxynucleotide triphosphates (dNTPs), 2,0 µL de 25 mM $MgCl_2$ et 1,25 µL de l'amorce *BOX-A1R* (20 µM), qsp 25 µL par de l'eau distillée. Après l'étape de dénaturation initiale à 95°C pendant 5 min, la phase d'amplification comprend 35 cycles, chaque cycle comprend les étapes suivantes à savoir 94°C durant 1 min, 48°C durant 1min et 72°C durant 1 min, suivis d'une phase d'extension à 72°C pendant 5 min.

Séquençage. Les produits PCR ont été séparés sur gel d'agarose (1,2%) et les acides nucléiques colorés au ClearSight DNA et visualisés avec Gel Doc™ EZ imager (Bio-Rad). Les produits PCR ont été élués du gel grâce à Wizard® SV Gel et PCR Clean-up System (Promega, USA). Les produits PCR purifiés ont été séquencés par Eurofins France.

Séquences et analyses phylogénétiques. L'analyse comparative des séquences a été réalisée grâce à EzBiocloud (https://www.ezbiocloud.net) et à BLAST (https://blast.ncbi. nlm.nih.gov/Blast.cgi). L'alignement des séquences a été effectué en utilisant Clustalx version 1.81. Les arbres phylogénétiques ont été construits via Neighbor-Joining method du logiciel MEGA version 7.

Chapitre 3 :

Isolement de bactéries diazotrophes du sol libanais et réponses du blé à certaines souches bactériennes

3.1. Introduction

De grandes quantités de composés organiques sont exsudées par les racines dans la rhizosphère et sont utilisés par les micro-organismes comme source de carbone. En contrepartie, les microorganismes bénéfiques peuvent engager des interactions symbiotiques avec les racines, ce qui améliore la croissance et la santé des plantes.

On peut supposer que, après la domestication du blé dans le Croissant Fertile, les migrations humaines qui ont élargi les zones de culture du blé ont contraint les blés à s'adapter à un microbiote différent. En outre, il est très probable que les programmes de sélection mis en œuvre après la seconde guerre mondiale, durant la Révolution verte et jusqu'à présent, sur la base de cycles de sélection de plantes sur des sols artificialisés par des apports élevés en fertilisation, ont affecté la capacité des systèmes racinaires à interagir avec des microorganismes bénéfiques du sol, ces interactions ayant un coût non négligeables (25% ou plus des photosynthétats transférés par la plante à des micro-organismes), ce qui a=peut avoir un impact sur le rendement des cultures dans les sols fortement fertilisés (Brown *et al.*, 2013). Il est clair que la promotion ou la restauration d'interactions bénéfiques entre les racines et les microorganismes du sol avec un équilibre maximisé avantages / coûts serait très

bénéfique pour les pratiques agricoles durables. L'objectif général de mes travaux de doctorat est de fournir des connaissances susceptibles de soutenir les progrès dans cette direction.

Dans ce cadre, j'ai effectué des expériences visant à isoler et à caractériser des souches bactériennes d'un échantillon de sol libanais, en me concentrant sur les bactéries fixatrices de N_2, et j'ai étudié les effets de ces souches et d'autres bactéries modèles diazotrophes (*Bradyrhizobium japonicum, Frankia* sp., *Azospirillum lipoferum*) sur la croissance des plantes dans le sol et le contenu en éléments nutritifs de la plante. Les résultats fournis par ces deux types d'expériences sont rapportés dans le présent chapitre.

3.2. Matériels et méthodes voir Chapitre 2

3.3. Résultats

3.3.1. Isolement des souches bactériennes fixant le N_2 du sol libanais

Une partie du travail visant à isoler les souches bactériennes d'un échantillon de sol préparé à partir de la rhizosphère de blés cultivés au Liban a été réalisée en collaboration avec Houssein Zhour, doctorant de notre groupe.

Un ensemble de colonies avec des phénotypes visuellement différents a été sélectionné et soumis à 2 cycles de croissance supplémentaires sur milieu NFb, suivis de tests ARA, comme décrit à la figure 2.7. Un total de 16 souches bactériennes ont ainsi été isolées à la fin du dernier cycle de sélection (6ème cycle sur NFb dans un tube vacuette®). Ces souches ont été nommées en fonction de la boîte de Petri dont elles ont été recueillies et de l'étape à laquelle elles ont été considérées comme purifiées. Les noms de ces 16 souches sont (par ordre alphabétique): A10, A11, A12, B1, B2, B3-1, B3-2, B4, C1, C2, H1, H2, H3, I1-1, I1-2 et I1-3.

Étant donné que toutes ces souches ont pu croître et former des colonies sur un milieu "sans N assimilable", on peut supposer qu'elles sont toutes dotées d'une capacité de fixation de N_2. Cette capacité devrait toutefois être très variable entre les 16 souches sélectionnées, car la sélection a été basée uniquement sur l'aspect visuel des colonies cultivées sur un milieu d'agar NFb dans des boîtes de Petri.Parc contret, les tests ARA effectués à la fin du 6ème cycle de culture (final) sur un milieu NFb ont fourni une estimation de l'activité de la nitrogénase qui variait de plus de 100 fois entre les différentes souches (Figure 3.3).

3.3.2. Caractérisation moléculaire et fonctionnelle des souches bactériennes isolées

Le métabarcodage est une méthode rapide d'évaluation de la biodiversité qui combine deux technologies: l'identification basée sur l'ADN et le séquençage d'ADN à haut débit. Il utilise des amorces de PCR universelles pour amplifier en masse des régions d'ADN précises retrouvées dans des embranchements ou des phylums (amplicons) à partir de collections massives d'organismes ou d'ADN

environnemental. Pour les bactéries diazotropes, l'ARN ribosomal 16S, le gène *nif* et les amorces *BOX-A1R* sont les amplicons les plus couramment utilisés. Premièrement, des expériences de PCR visant à caractériser les 16 souches sélectionnées au niveau moléculaire ont été réalisées à l'aide d'amorces ciblant l'ARN 16S (Figures 3.4). En accord avec le fait que la sélection des colonies bactériennes avait été réalisée après croissance sur un milieu exempt d'azote, les expériences de PCR ont révélé qu'un fragment d'ADN du gène *nifH* pouvait être amplifié dans chacune des 16 souches bactériennes sélectionnées (Figure 3.5). *nifH* code pour le composant protéique Fe de la nitrogénase, l'enzyme qui catalyse la fixation biologique de l'azote (réduction du diazote en ammonium). Finalement, l'amorce *BOX-A1R* a été utilisée pour caractériser davantage les souches bactériennes (Figures 3.6). Ensuite, les amplicons de l'ARN 16S ont été séquencés pour des analyses phylogénétiques.

Les arbres phylogénétiques obtenus indiquent que les rhizobiums sont les parents les plus proches des souches A10 et A12 (Figure 3.7). Les parents les plus proches de A11, B1, B2, C1 et H1 se sont avérés être des *Stenotrophomonas* (Figure 3.8). Les parents les plus proches de B3-2, B4, C2, H2, H3, I1-1 et I1-2 se sont révélés être des *Achromobacter* (Figure 3.9). Enfin, les parents les plus proches de B3 1 sont des *Paraburkholderia* (figure 3.10), et ceux de I1-3 sont des *Klebsiella* (Figure 3.11). Voir également le tableau 3.1.

Il convient de noter que les schémas d'amplification *BOX-A1R* obtenus pour B3-2, B4, C2, H2, H3, I1-1 et I1-2, identifiés comme proches parents d'Achromobacter par les analyses phylogénétiques décrites ci-dessus, sont apparus strictement similaires (Figure 3.6), ce qui suggère que ces souches pourraient correspondre à une seule espèce. Les 2 souches A10 et A12, identifiées comme des proches parents de *Rhizobia*, semblent également présenter un schéma d'amplification *BOX-A1R* similaire. Par contre, parmi les 5 souches identifiées comme étant des parents proches de *Stenotrophomonas*, A11, B1, B2, C1 et H1, seules B2 et C1 semblent partager le même schéma d'amplification *BOX-A1R* (Figure 3.6), ce qui suggère qu'au moins 4 génotypes distincts sont présents parmi ces 5 souches apparentées à Stenotrophomonas.

Enfin, la capacité des 16 souches bactériennes à utiliser des sources insolubles de Pi et de K + a été testée comme décrit au chapitre 2 (§ 2.10 et figures 2.9 et 2.10), et évaluée à l'aide des indices de solubilisation (SI). Des tests de croissance représentatifs sur des plaques de gélose en présence d'une source de Pi insoluble ou de sources insolubles de Pi et de K^+ sont présentés par les figures 3.12 et 3.13, respectivement. Toutes les souches, sauf la souche A11 liée à *Stenotrophomonas*, présentaient une activité solubilisante de phosphate. Le tableau 3.2 présente les valeurs SI dérivées de ces expériences. Des différences d'IS apparaissent entre les 15 souches pouvant utiliser une source insoluble de Pi, mais ces différences sont restées dans une gamme de variations assez étroite (inférieure à environ 3 fois) par rapport aux très grandes variations de l'activité de la nitrogénase, d'au moins 100 fois, telle qu'évaluée par les tests ARA (Figure 3.3).

L'aptitude à utiliser la source insoluble de K^+ (en présence d'une source insoluble de Pi) a été clairement démontrée par 2 souches, les souches C2 liées à Achromobacter et I1.3 liées à Klebsiella (Figure 3.13 et Tableau 3.2). Il convient de noter que ces deux souches ont également montré la plus grande capacité à utiliser la source insoluble de Pi (valeurs les plus élevées de SI dans le tableau 3.2).

Un résumé des résultats obtenus dans ces expériences concernant les relations phylogénétiques, les profils d'amplification *BOX-A1R*, l'activité de la nitrogénase (tests ARA), le SI pour la source insoluble de Pi ("SI pour Pi") et le SI pour la source insoluble de K^+ (en présence de la source insoluble de Pi) ("SI pour K") est donné dans le tableau 3.3.

Un examen détaillé de ce tableau révèle que des différences de "SI pour K", de "SI pour P" et / ou d'activité de la nitrogénase peuvent être observées entre les 7 souches identifiées par les analyses phylogénétiques comme étant liées au genre *Achromobacter* alors que les expériences de PCR ont identifié le même schéma d'amplification *BOX-A1R.* Cela indique que différents génotypes sont présents parmi ces 7 souches bien qu'elles présentent le même schéma d'amplification *BOX-A1R.* D'autre part, parmi les 5 souches liées à *Stenotrophomonas*, les 2 qui présentaient des schémas d'amplification *BOX-A1R* similaires affichaient également un SI similaire pour Pi (SI pour K étant "0" dans les deux cas) et une activité nitrogénase similaire. Les deux souches apparentées au *Rhizobium*, qui présentent des profils d'amplification *BOX -A1R* similaires, présentent également une activité nitrogénase et une SI similaires pour Pi (SI pour K étant égal à 0 dans les deux souches).

3.3.3. Effets des souches bactériennes sur la croissance des plantes

Cinq souches bactériennes classiques de laboratoire, *Bradyrhizobium japonicum* ORS285, *B. japonicum* ORS285Δ*nif*, *Frankia* sp. R43, *Azospirillium lipoferum* 4B et *A. brasilense* Sp245 connus pour être capables d'engager des interactions symbiotiques bénéfiques avec différentes espèces de plantes et 7 souches bactériennes isolées du sol libanais, A11 et B1 (apparentés à *Stenotrophomonas*), B3-1 (apparentée à *Parabulkholderia*), B3-2, H2 et I1-2 (lié à *Achromobacter*) et I1-3 (apparenté à *Kebsiella*) ont été sélectionnées pour une analyse de leurs effets sur la croissance du blé (*Triticum turgidum* spp. durum, cv. Oued Zenati) sur un sol artificiel (tourbe/sol/perlite, 1/1/1, v/v/v) pendant 30 jours dans une chambre de culture, comme décrit au chapitre 2 (§ 2.7). Une solution à faible teneur en azote (LN: 0,7 mM de N assimilable; voir le § 2.3) a été utilisée pour l'arrosage des plantes. Des plantes non inoculées arrosées avec une solution LN ou HN (5,2 mM de N assimilable; voir le § 2.3) ont été cultivées en parallèle et utilisées comme témoins. Les racines et les tiges ont été collectées, séchées et pesées (poids sec de la biomasse: DW).

On a constaté que plusieurs souches bactériennes augmentaient de manière significative la biomasse totale des racines, des tiges et/ou la biomasse totale (Figure 3.14). Les effets les plus prononcés sur la biomasse totale ont été observés avec B3-2, B1, *Azospirillium lipoferum* 4B, B3-1, A11 et I1-2. L'inoculation avec chacune

de ces souches a également entraîné une augmentation du rapport biomasse tiges / racines, indiquant que l'effet stimulant sur la croissance de la plante a été plus bénéfique pour les tiges que pour les racines. Une situation inverse a été observée dans le cas de l'inoculation de *Frankia*.

Sur la base de l'ensemble des résultats, nous avons sélectionné 6 souches bactériennes, *B. japonicum* ORS285 (abréviation: Brad), *Frankia* sp. R43 (abréviation: Frankia), *Azospirillium lipoferum* 4B (abréviation: Azo4B), B1 (apparenté à *Stenotrophomonas*), B3-2 (apparenté à *Achromobacter*) et I1-3 (apparenté à *Kebsiella*) pour d'autres analyses des réponses de la plante. B1 et B3-1 ont été sélectionnés en raison de leurs effets puissants sur la croissance des plantes (figure 3.14). L'effet de I1-3 sur la croissance des plantes était plus faible, mais cette souche a été choisie car elle s'est avérée la plus efficace pour utiliser des sources peu solubles de Pi et de K^+ (Tableau 3.3 et Figure 3.13). La figure 3.15 montre les mêmes données que celles présentées dans la figure 3.14 mais exprimées en % des valeurs correspondantes affichées par les plantes témoins non inoculées (arrosées avec une solution de LN).

Les contenus des racines et des tiges en C et N des plantes inoculées avec les 6 souches sélectionnées et des plantes témoins non inoculées ont été analysés par spectrométrie de masse. Les valeurs, déterminées, exprimées par plante, sont présentées à la figure 3.16. Dans l'ensemble, ces données ont indiqué que l'identité de la souche bactérienne inoculée affectait les quantités de C et de N présentes dans les tiges, les racines et les plantes entières (tiges + racines), ainsi que les teneurs en N/C.

Les données de contenu en C et en N présentées à la figure 3.16 ont ensuite été comparées aux valeurs de biomasse correspondantes et les ajustements linéaires ont été ajustés aux points expérimentaux (Figure 3.17). Une très forte corrélation est apparue entre les valeurs de contenu en C et de biomasse, aussi bien dans les racines que dans les tiges, avec une pente proche de 0,4 dans les deux cas (Figure 3.17, panneaux de gauche). Autrement dit, le C a toujours représenté environ 40% de la biomasse de blé, indépendamment de l'organe (racines ou tiges), du traitement (inoculation ou non) et de l'identité de la souche bactérienne inoculée. Des pourcentages similaires de teneur en C, près de 40%, ont été signalés dans diverses espèces de plantes et tissus (communication personnelle avec Pascal Tillard, Atelier des Isotopes Stables, BPMP, SupAgro Montpellier). En revanche, la corrélation entre la teneur en N et les valeurs de la biomasse était différente dans les racines et dans les tiges, les ajustements linéaires affichant une pente de 0,01 et 0,03, respectivement. Ainsi, par unité de biomasse, plus d'azote (environ 3 fois plus) a été utilisé (stocké dans des vacuoles ou métabolisé en composés organiques) pour la production de tiges par rapport à la production de racines par les semis de blé. De même, sur la figure 3.17, la corrélation des teneurs en C et en N avec la biomasse est apparue plus faible dans le cas des teneurs en N que dans celle des teneurs en C, en particulier dans les racines (R2 inférieur à 0,4). Cela suggérait que des différences significatives d'efficacité d'utilisation de l'azote, évaluées par le rapport

"biomasse sur teneur en azote" (Masclaux-Daubresse *et al.*, 2010), sont apparues entre les plantes, peut-être en fonction de l'identité de la souche inoculée.

Les valeurs de biomasse de racines, de tiges et de plantes entières ont ensuite été rapportées aux teneurs en N correspondantes (plante par plante), le rapport obtenu correspondant à l'indice dit d'efficacité de l'utilisation des éléments nutritifs (NUE) pour l'azote (Good *et al.*, 2004; Masclaux-Daubresse *et al.*, 2010). Les données sont présentées par la figure 3.18. Elles indiquent que la NUE a été réduite dans les plantes inoculées par rapport aux plantes contrôle LN non inoculées. Cela suggère que la croissance des plantes n'était pas limitée par la disponibilité de l'azote dans le cas des plantes Brundrett, mais était limitée par un autre facteur.

Le contenu des racines et des tiges en P, K, Ca, Mg, Mn, Fe, Cu, Zn et Na a ensuite été analysé. Les résultats ont été exprimés en unité de biomasse (mg DW) (Figure 3.19). Globalement, les données ont indiqué que l'inoculation et l'identité de la souche bactérienne inoculée peuvent affecter l'abondance relative des éléments nutritifs dans les racines et les tiges des plantes.

Chapitre 4 :

Développement de méthodologies pour le phénotypage des traits de poils racinaires

4.1. Introduction

Les interactions des racines avec les souches de PGPR peuvent avoir des effets bénéfiques très divers, allant d'une résistance accrue aux microbes pathogènes à une meilleure nutrition minérale des plantes. Nous nous intéressons aux mécanismes qui pourraient sous-tendre ce dernier effet.

Il a souvent été signalé que les PGPR peuvent à la fois favoriser la production et l'allongement des poils racinaires et affecter l'architecture du système racinaire en inhibant la croissance des racines primaires et en stimulant la production et l'allongement des racines secondaires. Notre hypothèse est que ces effets sur le développement du système racinaire et de la pilosité des racines, en augmentant le volume de sol exploité par la plante, peuvent améliorer l'acquisition des ions nutritifs et ainsi favoriser le développement et la croissance des plantes. Pour mémoire, nous avons présenté, dans le chapitre 1; les différents rôles des poils racinaires, au carrefour de la nutrition des plantes et de l'interaction avec les microorganismes du sol.

Dans le cadre de l'hypothèse ci-dessus, on peut présumer réciproquement que l'ampleur des effets d'une souche de PGPR donnée sur le développement de

l'architecture du système racinaire et l'élongation du poil racinaire chez une espèce / un cultivar donné est susceptible de refléter la capacité du couple plante/PGPR pour développer des interactions bénéfiques. Ainsi, le développement de procédures permettant de décrire quantitativement les réponses des racines aux souches de PGPR pourrait permettre, par exemple, de cribler des collections de souches bactériennes et/ou de cultivars de plantes, en tant que première étape de la recherche des couples les plus efficaces de partenaires en interaction dans des conditions environnementales données et d'identifier les mécanismes sous-jacents via des analyses GWAS.

Sur la base de ces considérations, nous avons cherché à développer des méthodologies permettant de décrire le développement des racines et poils absorbants avec des paramètres quantitatifs afin de "quantifier" les effets des conditions abiotiques et biotiques, en particulier de la réduction de la disponibilité en ions nutritifs et de la présence de souches PGPR, sur les racines.

4.2. La méthodologie de la "cuvette" pour phénotyper les traits des poils racinaires

4.2.1. Le montage expérimental

Le transfert d'échantillons de racines sur des lames de verre pour l'observation au microscope risquant d'endommager les poils absorbants, l'objectif était d'utiliser un dispositif de croissance des plantes permettant l'observation directe des zones de poils racinaires sans transfert sur une lame de verre. Plusieurs prototypes d'appareils faits maison ont été testés successivement. Ils ont été produits avec des imprimantes 3D. Leur conception impliquait l'intégration d'une lame de verre et d'une lamelle couvre-objet, avec un espace de 3 mm les unes des autres, formant une "fenêtre" à travers laquelle les racines pouvaient être vues et photographiées.

La forme générale de l'appareil est adaptée à la platine du microscope. Les dimensions et la conception des prototypes actuellement utilisés sont présentés sur la figure 4.2. La vue latérale du panneau C permet de voir la position de la lame de verre et de la lamelle couvre-objet dans l'appareil, ainsi que la manière dont elles peuvent être ajustées et fixées au dispositif en plastique à l'aide d'une colle à silicone dentaire. La racine principale d'une très jeune plantule est introduite dans un tunnel de 4 mm de diamètre qui permet à la racine en croissance d'atteindre la "fenêtre" à travers laquelle elle peut être photographiée au microscope (Figure 4.3). Un tunnel de 2 mm de diamètre présent dans la partie supérieure de l'appareil et un tunnel de 3 mm de diamètre dans la partie inférieure (Figure 4.2) permettent des mouvements d'air et d'eau à travers l'appareil, permettant ainsi un rééquilibre rapide de la pression hydrostatique et du niveau de solution à l'intérieur du dispositif lorsque le niveau de la solution à l'extérieur du dispositif est modifié afin d'oxygéner la solution à l'intérieur du dispositif.

La figure 4.3 illustre la position de la plantule et des racines en croissance dans le dispositif. Seule la lamelle a été adaptée à ce prototype, pas la lame de verre.

Une telle "cuvette", avec sa plante, est placée dans un récipient rempli de la solution nutritive à tester, comme le montre la figure 4.4, le plant ayant été inoculé ou non avant sa transplantation dans la cuvette. Dans la configuration expérimentale illustrée à la figure 4.4, la cuvette est inclinée d'environ 30 degrés par rapport à la direction verticale. Dans cette position, en raison du gravitropisme, les racines poussent préférentiellement le long de la surface de la face inférieure de la cuvette, sur laquelle la lamelle a été fixée. Dans cette expérience, la lame de verre correspondante n'était pas fixée à la face opposée (la face supérieure) de la cuvette.

La figure 4.6 fournit une photo de la plantule de blé et de ses racines dans un dispositif de cuvette (panneau A), le dispositif sur la lame de microscope (panneau B) et un segment de racine avec des poils racinaires sous le microscope (panneau C). Ces photos peuvent être analysées à l'aide du programme MRI RHT (développé par Volker Baecker,Montpellier Rio Imaging), décrit ci-dessous. Ce programme a également été appelé plus brièvement MRHT dans le texte suivant.

4.2.2. Description du programme IRM RHT développé pour le phénotypage automatique des traits racinaires

A l'aide du logiciel ImageJ, un programme dédié à l'analyse d'images telles que celles obtenues avec le dispositif "cuvette" (Figure 4.6) a été écrit pour le phénotypage automatique des traits racinaires par Volker Baecker (Analyste Bioimage, Montpellier Ressources Imagerie, CNRS-INSERM), en interaction avec nous. Ce programme a été nommé MRHT, pour Montpellier RIO Imaging_Root Hair Tool.

À partir de telles images, le programme MRHT peut fournir des estimations de la densité des poils racinaires, de leur longueur moyenne, de leur longueur maximale et de la surface totale (nombre de pixels) des poils absorbants. Le programme et son code sont disponibles sur: http://dev.mri.cnrs.fr/projects/imagej-macros/wiki/MRI_Root _Hair_Tools

La figure 4.7 fournit une description schématique du fonctionnement du programme. En résumé, la photo est nettoyée, segmentée et binarisée (pixels noirs pour les tissus racinaires et pixels blancs pour l'arrière-plan) (Figure 4.7, panneau A). Ensuite, deux lignes sont dessinées le long des frontières de la racine dans l'image, une ligne le long du côté supérieur et une ligne le long du côté inférieur de la racine dans le panneau B de la figure 4.7 (lignes dessinées en bleu sur la figure, mais en jaune le l'écran lorsque le programme est en cours d'exécution (voir plus loin, Figure 4. 10D). Ces lignes, qui seront utilisées pour "décrire" les traits des poils racinaires, sont nommées "lignes d'analyse" dans la figure 4.7. Chaque ligne est décalée de la surface de la racine, pixel par pixel, lui permettant de rester "parallèle" à la surface de la racine (Figure 4.7, Panneau C pour la ligne supérieure).

Ces déplacements successifs sont arrêtés dès que la ligne ne croise aucun pixel noir (c'est-à-dire ne croise aucun poil). Ensuite, la distance entre cette position de la ligne et la surface radiculaire fournit une estimation de la longueur du ou des poils racinaires les plus longs (Figure 4.7, Panneau C et Figure 4.8). En outre, à chaque

position de la ligne entre sa position initiale le long de la surface radiculaire et sa position finale à l'extrémité du ou des poils absorbants les plus longs, la ligne est "analysée" de gauche à droite par rapport à la "couleur" (blancs ou noirs) des pixels qu'elle traverse: une transition de gauche à droite d'un pixel blanc à un noir signifie que la ligne est entrée dans un nouveau poil racinaire, et que "+1" est ajouté à un compteur (Figure 4.7, Panneau D). Le nombre de poils racinaires que la ligne croise à chaque position à partir de la surface radiculaire est ainsi déterminé. La relation entre la distance x de la ligne à la surface de la racine et le nombre de poils absorbants n que la ligne a croisé lorsqu'elle est présente à cette distance de la surface racinaire permet de déterminer le nombre de poils absorbants ayant une longueur donnée (Figure 4.7, Panneau E et Figure 4.8) et, par conséquent, par exemple la longueur moyenne des poils absorbants. Le nombre de poils racinaires que la ligne croise lorsqu'il est proche de la surface radiculaire (Figure 4.8) fournit une estimation de la densité du poil racinaire à ce "côté" de la racine sur la photo. Enfin, cette procédure permet également de "compter" le nombre total de pixels "noirs" (poils absorbants) que les deux lignes ont croisés, et donc un paramètre reflétant la surface totale occupée par les poils absorbants de la photographie.

La figure 4.9 explique comment installer et utiliser l'outil MRHT dans le logiciel ImageJ, tandis que la figure 4.10 décrit le flux de travail du programme.

4.2.3. Test du programme MRHT

Afin de tester les résultats du programme MRHT par rapport à une analyse "manuelle" effectuée directement à l'aide du logiciel ImageJ, des photographies de zones racinaires ont été prises à l'aide du microscope Apotome à environ 1 cm de l'extrémité de la racine principale de plantules de blé dur cultivé dans des conditions différentes. Les valeurs de la longueur moyenne et de la longueur maximale des poils absorbants fournies par MRHT pour un ensemble de 23 images sont comparées sur les figures 4.11 et 4.12 aux valeurs correspondantes obtenues par analyse "manuelle". Prises dans leur ensemble, ces analyses indiquent que le programme MRHT peut être considéré comme suffisamment opérationnel et fiable pour la réalisation de nos analyses.

4.3. La méthodologie dite du "rhizobox" pour phénotyper les traits de poils racinaires à partir de systèmes racinaires entiers

4.3.1. Le montage expérimental

Différents prototypes de rhizobox ont été testés successivement. Ils différaient, par exemple, par le substrat, le sol artificiel, le papier filtre ou le tissu dans lequel - ou à la surface duquel – les racines pouvaient se développer. La croissance à la surface d'un morceau de tissu apparaissant comme la meilleure solution, différents types de tissu ont été testés (matériau et grosseur de maille différents). Ensuite, nous avons considéré qu'un substrat solide devait être introduit "derrière" le tissu, remplissant ainsi l'espace entre les deux plaques de verre de la rhizobox, afin de "tamponner" et

de contrôler le niveau d'humidité à la surface du tissu. Des essais réalisés avec des sols artificiels (sable, perlite, vermiculite et mélanges) ont révélé que la pression du substrat sur le tissu et la plaque de verre présentait de fortes hétérogénéités locales, probablement surtout lorsque le substrat était rendu humide par arrosage, et que de telles hétérogénéités affectaient profondément le développement final de l'architecture du système racine et la qualité de l'analyse (buée).

La solution à ce problème a été d'introduire un "panneau solide" en mousse de polyuréthane "derrière" le tissu. La mousse de polyuréthane a les dimensions d'une feuille de papier A4 (ou A3), puisque les rhizoboxes sont numérisées avec un scanner haute résolution A4/A3 et ont une épaisseur de 10 mm. En pratique, un morceau de tissu un peu plus grand que deux feuilles A4 est cousu pour former un sac de dimensions A4 dans lequel la mousse de polyuréthane est introduite. La rhizobox est ainsi rendu symétrique et des plantules peuvent être cultivées entre le tissu et la plaque de verre des deux côtés de la rhizobox.

La figure 4.13 fournit une description schématique des prototypes de rhizobox actuellement utilisés. Un système d'arrosage automatique des installations a été installé sur le dispositif expérimental, comme illustré à la figure 4.14. Des ensembles de rhizoboxes, partageant le même dispositif d'arrosage (et la même minuterie), sont installés dans des supports constitués de panneaux de polystyrène (Figure 4.15).

4.3.2. Description du programme ACRT développé pour l'analyse des systèmes racinaires de plantes cultivées dans des dispositifs à rhizobox

La figure 4.16 fournit un exemple des images obtenues à l'aide de la méthode de type rhizobox. Des parties de l'image ont été agrandies, ce qui montre que de grandes parties du système racinaire présentent des poils racinaires.

Le programme MRHT développé pour le phénotypage des traits de poils racinaires (densité, longueur…; voir ci-dessus) à partir de photos obtenues à l'aide de la méthode "cuvette" ne semblait pas réellement adapté à l'analyse d'images de systèmes racinaires entiers telles que celles fournies par la méthodologie rhizobox. Nous testons actuellement le logiciel WINRHIZO^{TM} disponible dans le commerce (voir chapitre 5), mais nous avons également commencé à définir une stratégie permettant de caractériser à partir de telles images les traits racinaires (poils) susceptibles d'être utiles pour l'exploration racinaire et l'acquisition d'éléments nutritifs.

Des images telles que celle présentée à la figure 4.16 montrent clairement que le développement des poils absorbants entraîne une très forte augmentation de la surface absorbante du système racinaire. Nous avons choisi d'évaluer la surface racinaire totale (en 2D) à partir de telles photos parce qu'il est raisonnable d'imaginer que cette surface est un déterminant majeur de:

- la contribution du développement des poils racinaires à la surface absorbante des racines

- la capacité du système racinaire à explorer et à exploiter le sol.

Pour évaluer cette surface (en réalité sa projection 2D), le programme développé compte le nombre de pixels appartenant au système racinaire, et l'exprime soit en fonction de la distance à la surface "du sol" - c'est-à-dire la "profondeur dans le rhizobox" – soit en fonction de la distance au grain germé.

Ce programme, qui a été écrit par Volker Baecker (Imagerie CNRS-INSERM Montpellier Ressources) à l'instar du programme MRHT, a été nommé ACRT (Outil d'analyse du système racinaire complexe). Le menu Jeu d'outils dans ImageJ et le schéma de travail de ce programme sont décrits sur les figures 4.17 et 4.18.

Le programme est disponible à l'adresse suivante:

https://github.com/MontpellierRessourcesImagerie/imagej_macros_and_scripts/wiki/Analyze_Complex_Roots_Tool

Les premières analyses à l'aide du programme d'images ACRT fournies par la méthodologie rhizobox sont rapportées au chapitre 5.

Chapitre 5 : Réponses du développement racinaire aux conditions biotiques et abiotiques: effets des souches bactériennes et réduction de la disponibilité de Pi

Tout en développant des procédures de phénotypage des réponses du système racinaire aux conditions biotiques et abiotiques, mon travail de doctorat a été entrecoupé de diverses expériences conduites dans différentes conditions environnementales afin de tester les effets de carences en nutriments ou d'inoculation avec des souches bactériennes à l'aide de prototypes qui étaient en cours de développement. Une grande partie de ces expériences, qui ont conduit à l'adaptation de protocoles ou à des modifications de la conception des prototypes, n'ont pas été réalisées dans le but de fournir des informations scientifiques publiables. Ces expériences ne figureront donc pas dans le présent manuscrit.

Ci-dessous, je présente 4 expériences récentes réalisées en cultivant des plantes inoculées ou non dans des conditions de sol, ou sur des plaques de gélose, ou en culture hydroponique dans des dispositifs de cuvette ou des dispositifs de rhizobox. Dans l'ensemble, les résultats de ces expériences permettent à la fois de répondre à des questions méthodologiques et de fournir des informations scientifiques.

5.1. Réponses du système racinaire à l'inoculation chez des plantes cultivées dans le sol pendant 30 jours.

L'inoculation avec plusieurs souches bactériennes testées au chapitre 3 s'est avérée conduire à une augmentation de la production de biomasse et à une incidence sur la teneur en éléments nutritifs. Une hypothèse de travail était que ces effets impliquaient des changements dans le développement des racines. Avant d'être pesés pour les dosages des contenus en éléments nutritifs, les systèmes racinaires de ces plantes avaient été soigneusement lavés afin d'éliminer les particules de sol adhérentes, puis photographiés. Des photographies représentatives sont fournies à la figure 5.1. Les souches bactériennes testées (6 au total) étaient la souche ORS285 de *B. japonicum*, *Frankia* sp. R43, souche 4B d'*Azospirillum lipoferum* et les isolats Libanais B1, B3-2 et I1-3.

De nombreux poils absorbants ont probablement été endommagés par l'isolement et le processus de lavage du système racinaire, ou ont été "pliés" le long des racines et ne sont donc plus visibles. Il convient toutefois de noter que des examens minutieux ont permis la détection de poils racinaires dans certaines zones (voir l'agrandissement à la figure 5.1), ce qui indique que les racines présentaient des poils absorbants dans les conditions expérimentales que nous avons utilisées. Cependant, les poils racinaires visibles étaient toujours difficilement détectables et n'étaient pas pris en compte dans notre analyse des photos.

Les photos ont été analysées à l'aide d'IJ Rhizo pour obtenir des estimations de la longueur totale et de la surface totale des racines de chaque système racinaire (Figure 5.2). Par rapport aux plantes témoins, une augmentation statistiquement significative de ces paramètres descriptifs n'a été observée que dans le cas d'inoculation de racines avec la souche B3-2 libanaise. Il est intéressant de noter que cette souche était auparavant la seule, parmi les 6 souches testées, à induire une augmentation statistiquement significative de la biomasse racinaire (voir Chapitre 3, Figures 3.14 et 3.15).

Les données de longueur totale et de surface racinaire totale ont ensuite été comparées à la biomasse racinaire (déterminée auparavant dans l'expérience décrite à la figure 3.14). Les courbes résultantes sont représentées par les figures 5.3A et B. Une assez bonne corrélation a été observée entre la surface racinaire et la biomasse racinaire (panneau A). La corrélation semblait plus faible entre la longueur des racines et la biomasse des racines. Les données de "surface racinaire" ont ensuite été divisées par les données de "longueur de racine" correspondantes, afin d'obtenir un paramètre reflétant un "diamètre de racine moyen". Les rapports étaient faiblement variables entre les différentes plantes, non inoculés ou inoculés, y compris l'inoculation avec l'isolat Libanais B3-2 et aucune corrélation n'apparaissait avec la biomasse racinaire. Globalement, ces résultats suggèrent que l'inoculation avec B3-2, qui entraîne une augmentation de la biomasse racinaire et de la surface racinaire accrue, affecte faiblement la croissance radiale des racines.

5.2. Effet de l'inoculation avec des souches bactériennes sur l'élongation des poils racinaires chez de jeunes plantules cultivées sur milieu gélosé

L'inoculation des plantules germées et des boîtes de gélose a été effectuée comme décrit au chapitre 2, paragraphes 2.2 à 2.4. Six souches bactériennes ont été testées, la souche ORS285 de *B. japonicum*, *Frankia* sp. R43, la souche 4B d'*Azospirillum lipoferum* et les isolats libanais B1, B3-2 et I1-3, constituant ainsi le même ensemble de souches que celui utilisé dans l'expérience décrite ci-dessus. Les semis se sont développés pendant 3 jours dans des conditions d'agar LN. Des images représentatives de poils absorbants, prises à environ 1,5 cm de l'extrémité de la racine, sont présentées à la figure 5.4. Les résultats de l'analyse de la longueur des poils absorbants sont présentés sur la figure 5.5. Les deux côtés de chaque zone racinaire sur les photos ont été analysés séparément (Figure 5.5A), ce qui a donné des données très similaires, ce qui constitue une validation de la procédure de mesure (réalisée avec ImageJ).

Chacune des 6 souches bactériennes a induit une augmentation de la longueur du poil racinaire d'environ 25% à 45% exprimés en% de la longueur du poil chez les plantes témoins non inoculées. L'augmentation était statistiquement significative dans le cas de *B. japonicum, Frankia*, B3-2 et I1-3 (augmentation de la longueur des poils racinaires de 35%, 29%, 34% et 43%, respectivement).

5.3. Effet de *Bradyrhizobium japonicum* sur l'élongation des poils absorbants chez les plantes cultivées en culture hydroponique dans des dispositifs de "cuvette"

Les semis inoculés avec *B. japonicum* ont été cultivés en culture hydroponique dans une solution de LN pendant 4 jours dans des dispositifs à "cuvettes" (Chapitre 4, § 4.2 et Figures 4.2 à 4.6). Des photos ont été prises de la région située à environ 1,5 cm de la racine. Des images représentatives sont fournies à la figure 5.6A. Le phénotypage du développement des poils absorbants au moyen du programme MRHT a révélé que l'inoculation avec *B. japonicum* entraînait des augmentations statistiquement significatives de la densité des poils absorbants (d'environ 8%), de la longueur moyenne des poils absorbants (d'environ 26%) et de la longueur maximale des poils de 22%) (Figure 5.6B) par rapport aux plantes témoins non inoculées. Ainsi, l'augmentation de la longueur moyenne des poils racinaires (environ 26%) dans ces conditions expérimentales était proche de celle induite par la même souche bactérienne dans l'expérience réalisée sur des plaques de gélose (35%; Figure 5.5B).

5.4. Effets de *B. japonicum* et d'une faible disponibilité en éléments nutritifs (N et P) sur le développement racinaire dans des dispositifs rhizobox

Les plantes inoculées avec *B. japonicum* ou non inoculées ont été cultivées dans des dispositifs rhizobox pendant 12 jours, comme décrit au § 2.6 (Chapitre 2). L'inoculation a été réalisée comme décrit au § 2.2. Les plantes non inoculées ont été

arrosées avec une solution LN ou LP ("Low N" or "Low Pi" availability). Les plantes inoculées ont été arrosées avec une solution LN.

La solution LN (composition détaillée fournie au § 2.3) contenait 0,7 mM d'azote assimilable (0,1 mM de NH_4NO_3 et 0,5 mM de KNO_3) et 1 mM de Pi (introduit sous la forme de KH_2PO_4). La solution LP contenait 5,2 mM d'azote assimilable (0,1 mM de NH_4NO_3 et 5 mM de KNO_3, semblable à une solution de HN: voir § 2.3) et 0,1 mM de Pi (fourni sous forme de KH_2PO_4). Les autres macro-éléments et les micro-éléments étaient les mêmes dans les solutions LN et LP.

Les figures 5.7, 5.8 et 5.9 fournissent des images des systèmes racinaires de (i) plantes non inoculées cultivées dans des conditions LN, (ii) plantes inoculées cultivées dans des conditions LN, et (iii) plantes non inoculées cultivées dans des conditions de LP, respectivement (10 plantes dans chaque cas). Comme indiqué précédemment à la figure 4.16 et encore illustré par la présence sur chacune de ces figures d'un panneau présentant un agrandissement d'une région racinaire, de grandes parties du système racinaire sont recouvertes de poils racinaires denses et longs dans ces conditions expérimentales.

Les images ont été analysées à l'aide du programme ACRT (plug-in d'ImageJ développé par Volker Baecker; voir le § 4.3.2 et les figures 4.17 et 4.18), ainsi que du logiciel WINRHIZO™ disponible dans le commerce (Regent Instruments Inc., Canada). Les deux procédures tiennent compte de la présence de poils absorbants, mais de manière différente.

Le programme ACRT trie les pixels de l'image en deux catégories, «pixels d'arrière-plan» ou «pixels racine». En ce qui concerne les pixels de racine, le programme ne fait pas la distinction entre les pixels correspondant aux poils racinaires et ceux correspondant aux racines à partir desquelles les poils ont été émis, mais regroupe tous ces pixels ensemble et détermine la zone que ces pixels couvrent, prise comme une estimation de la surface racinaire en 2D. Ensuite, le programme exprime la surface racinaire en fonction de la "distance" à la graine germée, ou en fonction de la "profondeur" dans la rhizobox, c'est-à-dire la distance à la ligne horizontale du sommet de la rhizobox où la graine germée a été déposée. La figure 5.10 fournit les graphiques décrivant la relation entre la surface racinaire et la distance par rapport à la graine (panneau de gauche) ou la profondeur par rapport à la "surface" du rhizobox (ligne horizontale passant par la graine initiale) (panneau de droite) dans le cas des racines non inoculées cultivées dans des conditions LN (symboles ouvert) et les racines inoculées par *B. japonicum* souche ORS285 cultivées dans des conditions LN (symboles noirs). La figure 5.11 permet de comparer de manière similaire le développement de racines non inoculées cultivées dans des conditions LN (symboles ouverts) ou LP (symboles noirs").

Le logiciel WINRHIZO™ a été développé (comme indiqué sur le site Web de la société Regent Instruments Inc.: http://regent.qc.ca/assets/winrhizo_software.html) pour "Analyse des systèmes de racines lavées". Il fournit "des mesures globales telles que le diamètre moyen des racines, la longueur totale des racines, la surface,

le volume et le nombre de cônes… la mesure de la morphologie des racines en fonction des classes de diamètre définissables par l'utilisateur ...". La figure 5.12 fournit les valeurs de "Longueur totale de la racine" (panneau A de cette figure), "Surface totale de la racine" (panneau B), "Longueur totale de la racine" par classe de diamètre de la racine (panneau C) et "Surface totale de la racine" par classe de diamètre de racine (panneau D) obtenu par WINRHIZO™ pour les images des systèmes racinaires illustrées aux figures 5.7, 5.8 et 5.9 afin de comparer les racines non inoculées en condition LN, les racines inoculées avec *B. japonicum* et arrosées avec LN, et les racines non inoculées en condition LP. Dans cette analyse, nous avons défini dans l'interface WINRHIZO les paramètres de "classe de diamètre" de manière à ce que les poils racinaires soient considérés comme des "racines de diamètre très fin" (le diamètre le plus fin est compris entre 0 et 0,2 mm).

Pris dans leur ensemble, les analyses effectuées avec ACRT et WINRHIZO™ prouvent que, par rapport aux plantes non inoculées cultivées dans des conditions LN, le développement racinaire a été altéré dans les plantes inoculées et dans les plantes cultivées en conditions LP. Par exemple, l'inoculation a entraîné une augmentation de la longueur totale des poils racinaires (comparez les deux premières barres de l'histogramme de la figure 5.12C) et une augmentation de la surface racinaire détectée dans la moitié supérieure des dispositifs de rhizobox (Figure 5.10B). La croissance en condition LP a entraîné une diminution de la surface racinaire détectée dans la partie supérieure des rhizobox de 25%, puis une augmentation de 75% de la surface des racines dans la partie inférieure des dispositifs. Cela a également entraîné une augmentation de la longueur totale des poils racinaires (comparez les premières et troisièmes barres de l'histogramme de la figure 5.12C).

Ces résultats sont examinés plus en détail dans le chapitre suivant (Chapitre 6: "Discussion et perspectives").

Chapitre 6 :

Discussion et perspectives

L'objectif général de mon travail de doctorat est de contribuer aux efforts de recherche visant à acquérir des connaissances permettant à l'agriculture de progresser vers une intensification écologique. Dans cette perspective, la réduction des intrants de fertilisation, ainsi que de leurs coûts et dommages écologiques, apparaît comme l'un des défis majeurs. Dans ce cadre, j'ai axé mon projet de recherche sur le développement des racines et les fonctions physiologiques contribuant à la nutrition minérale des plantes, y compris les interactions avec des microbes bénéfiques du sol, car il est prouvé que ces interactions peuvent être d'une importance cruciale pour l'acquisition d'éléments nutritifs. J'ai choisi de travailler sur le blé, car il s'agit d'une céréale d'une grande importance agronomique et d'étudier

ses interactions avec des bactéries du sol susceptibles de se comporter comme des rhizobactéries promotrices de la croissance des plantes (PGPR).

Différents types de mécanismes peuvent être à la base des effets bénéfiques des PGPR sur la croissance des plantes, notamment la stimulation du développement des racines et la production et l'allongement des poils racinaires. J'ai isolé des souches bactériennes susceptibles d'interagir avec les racines du blé, puis j'ai développé des procédures méthodologiques permettant de phénotyper les réponses des racines aux conditions abiotiques et biotiques.

6.1. Caractérisation de souches de rhizobactéries capables d'interagir avec le blé

6.1.1. Diversité dans le panel d'isolats bactériens obtenus à partir de la rhizosphère de blé du Liban

L'ensemble des 16 isolats bactériens purifiés à partir du sol rhizosphérique de plants de blé cultivés dans un champ au Liban peut être répartis, au niveau des genres (Tableau 3.1), avec 7 *Achromobacter* (B3-2, B4, C2, H2, H3, I1-1 et I1-2), 5 *Stenotrophomonas* (A11, B1, B2, C1 et H1), 2 *Rhizobia* (A10 et A12), 1 *Paraburkholderia* (B3-1) et 1 *Klebsiella* (I1-3).

Sur le site Web de PUBMED, en octobre 2019, les termes "PGPR" associés à "*Achromobacter*", "*Stenotrophomonas", "Paraburkholderia*" ou "*Klebsiella*" permettaient de récupérer 5 références *Achromobacter* (la première étant publiée en 2014), 17 références *Stenotrophomonas* (première en 2012), 3 références *Paraburkholderia* (première en 2016) et 15 références *Klebsiella* (première en 2013). Davantage de références ont été obtenues pour PGPR et "*Rhizobium*" (66 publications, la première publiée en 1995) ou "*Azospirillum*" (51 références ; la première en 1999). Ainsi, ce type de recensement de la littérature indique que les connaissances concernant les activités de type PGPR sont moins développées dans les genres *Achromobacter, Paraburkholderia, Stenotophomonas* et *Klebsiella* que dans *Azospirillum* ou *Rhizobium*. *Azospirillum brasiliense* apparaît comme une espèce modèle de PGPR.

Les Achromobacter (classe: Betaproteobacteria) sont des bâtonnets Gram négatif, mobiles utilisant de un à 20 flagelles péritriches. Ils sont strictement aérobies et se retrouvent dans l'eau et les sols (Garrity *et al.*, 2005).

Il a été montré que la souche d'*Achromobacter atchhaudii* ARV8 présentait une activité PGPR chez la tomate et le poivron cultivés dans des conditions biotiques difficiles (sécheresse et / ou stress salin) (Mayak *et al*., 2004). Il a également été montré que l'inoculation du colza avec *Achromobacter sp*. souche U80417 a entraîné une augmentation de la production de biomasse, une stimulation de l'influx net de NO_3^- et de K^+ par unité de surface racinaire et une promotion du développement des poils absorbants (Bertrand *et al*., 2000). Une souche d'*Achromobacter xylosoxidans*, dotée de la capacité de produire de l'acide indole acétique (IAA), de solubiliser le phosphate inorganique et d'accroitre la longeur des racines chez *Brassica juncea*,

s’est révélée améliorer significativement l’absorption de Cu chez cette espèce (Ma *et al.*, 2009). La souche WM234 C d'*Achromobacter xylosoxidans*, initialement isolée en tant qu'endophyte dans les racines de blé, s'est avérée favoriser la production de biomasse (poids frais) et augmenter la teneur en chlorophylle du riz (Jha et Kumar, 2009).

Stenotrophomonas (Classe: Gammaproteobacteria) est un genre de bactérie Gram négatif, comprenant au moins dix espèces (Palleroni et Bradbury, 1993; Ryan *et al.*, 2009). Les principaux réservoirs de *Stenotrophomonas* sont le sol et les plantes. Les espèces de *Stenotrophomonas* vont d'organismes courants du sol (*S. nitritireducens*) à des agents pathogènes humains opportunistes (*S. maltophilia). Stenotrophomonas rhizophila sp. nov.* a été caractérisée comme une bactérie capable d'interagir avec des plantes et dotée d'une activité antifongique contre les champignons phytopathogènes (Wolf *et al.*, 2002). Il a été démontré que l'inoculation de *Stenotrophomonas maltophilia* SBP-9 sur racines du blé entraînait une augmentation de la croissance des plantes et une augmentation de leur teneur en chlorophylle (Singh et Jha, 2017). L'inoculation avec cette souche bactérienne a également conduit à une meilleure adaptation au déficit en azote chez *Arachis hypogea* (Alexander *et al.*, 2019).

Les *Paraburkholderia* (classe: Betaproteobacteria) sont des bâtonnets Gram négatif légèrement incurvés qui sont mobiles au moyen de flagelles. Des membres de ce genre ont été trouvés dans des nodules de légumineuses fixant l'azote (par exemple, chez le *Mimosa*, *Lebeckia ambigua et Hypocalyptus sophoroides, les souches trouvées sont Paraburkholderia diazotrophica, Paraburkholderia dilworthii*, *Paraburkholderia strydomiana sp. Nov*. et *Paraburkholderia steynii*; Meyer *et al.*, 2013; Beukes *et al.*, 2019). *Paraburkholderia phytofirmans* PsJN s'est comporté comme une PGPR lors de son interaction avec Arabidopsis, augmentant la tolérance de la plante à la salinité (Ledger *et al.*, 2016) et offrant une protection contre une souche virulente de *Pseudomonas syringae* par activation de la résistance induite (Timmermann *et al*., 2017).

Les *Klebsiella* (gammaprotéobactéries) sont des bactéries gram négatif et généralement non motiles (dépourvues de flagelle). Elles se présentent généralement sous la forme de tiges droites aux extrémités arrondies ou légèrement pointues. Les membres du genre *Klebsiella* font partie de la flore normale du nez, de la bouche et des intestins de l'homme et de l'animal. *Klebsiella* peut être trouvé dans une variété d'hôtes chez les plantes. *K. pneumoniae* et *K. oxytoca* sont capables de fixer l'azote atmosphérique sous une forme utilisable par les plantes (Cakmaki *et al*., 1981). Il a été démontré que l'inoculation avec *Klebsiella pneumoniae* 342 conduisait à une productivité accrue du maïs sur le terrain (Riggs *et al*., 2001). Chez le blé, il a été démontré que cette souche atténuait les symptômes de carence en azote (N) et augmentait la concentration totale en N et d’azote dans la plante (Iniguez *et al.*, 2004). Il convient de noter que ce phénotype de fixation de l'azote apparaît comme spécifique à un cultivar de blé (Trenton) puisqu'il n'a pas été observé avec deux autres cultivars. De plus, il a été démontré que la tolérance du blé à la salinité était

accrue par l'inoculation de *Klebsiella sp.* SBP-8 (Singh *et al.*, 2015). La promotion de la croissance des plantes et l'abaissement de la toxicité du Cd_2^+ ont été rapportés chez *Vigna mungo* lors de l'inoculation avec la souche *Klebsiella pneumoniae* HR1 (Dutta *et al.*, 2018).

6.1.2. Caractérisation de la capacité des isolats libanais à se comporter comme des PGPR

Les 16 isolats bactériens que nous avons obtenus sont tous des espèces diazotrophes puisqu'ils ont été sélectionnés après 6 cycles de croissance successifs sur un milieu "sans azote". De plus, des tests de croissance en présence d'une source de phosphate peu soluble indiquent que ces 16 isolats sont dotés d'une capacité de solubilisation de Pi. Deux d'entre eux, C2 et I1-3, ont également affiché une croissance significative en présence de sources peu solubles à la fois de Pi et de K^+ (Figure 3.13 et Tableau 3.2).

Parmi ces 16 isolats, les 7 souches sélectionnées (basées sur le fait que leurs colonies diffèrent par leur aspect visuel) et testées pour leurs effets sur la croissance du blé ont toutes entraîné une augmentation de la production de biomasse par rapport aux variétés contrôle non inoculées (Figure 3.14). De plus, pour 5 des 7 souches, une augmentation statistiquement significative de la production de biomasse a également été observée par rapport aux souches contrôles *Bradyrhizobium japonicum* et *Frankia* (Figure 3.14). Enfin, par comparaison avec les 2 souches de contrôle qui ont provoqué la plus forte augmentation de croissance des plantes*, Azospirillum lipoferum* 4B et *Azospirillium brasilense* Sp245, les 4 souches libanaises ont entraîné une augmentation statistiquement similaire de la biomasse et une, B3-2, une augmentation encore plus importante de la croissance des plantes (Figure 3.14). Globalement, ces résultats fournissent la preuve qu'au moins 4 ou 5 des souches libanaises testées sont effectivement dotées d'une activité PGPR; à savoir d'une capacité de "Promotion de la croissance des plantes". Il convient de noter que l'évaluation de l'efficacité d'utilisation de l'azote des plantes chez 3 de ces souches libanaises, B1, B3-2 et I1-3, et chez les 3 souches de contrôle, *Bradyrhizobium japonicum* ORS285, *Frankia* sp. R43 et *Azospirillum lipoferum* 4B ont révélé que la promotion de la croissance des plantes s'accompagnait d'une diminution de "l'efficacité de l'utilisation de l'azote", ce qui suggère que la disponibilité d'azote assimilable n'était pas le principal facteur limitant la croissance des plantes dans ces conditions expérimentales (Figure 3.18). Les dosages des teneurs en éléments nutritifs (Figure 3.19) ont révélé que l'inoculation avec différentes souches bactériennes entraînait des différences dans les teneurs en éléments nutritifs, par exemple en P, K ou Fe, mais n'ont fourni aucune hypothèse simple sur l'origine de l'augmentation de la croissance des plantes. La sécrétion de phytohormones stimulantes aurait pu jouer un rôle, avec d'autres processus, dans la promotion de la croissance des plantes.

6.2. Phénotypage du développement racinaire et des réponses aux conditions abiotiques et biotiques: problèmes méthodologiques

6.2.1 Méthodologie

Un processus susceptible de contribuer à la promotion de la croissance des plantes par les souches de PGPR est la stimulation de la croissance des racines et le développement des poils racinaires. Les effets fréquemment observés avec des souches PGPR sont l'inhibition de la croissance des racines principales, la stimulation de la croissance des racines secondaires et la promotion de la production et de l'allongement des poils racinaires (Vacheron *et al.*, 2013; Poitout *et al.*, 2016).

Les analyses quantitatives de ces effets caractéristiques des PGPR sur le développement des racines et des poils ont été principalement effectuées sur des plantes cultivées sur des plaques de gélose, et le plus souvent sur *Arabidopsis thaliana* (Poitout *et al.*, 2016).

Je me suis attaché à analyser les effets des souches de PGPR sur le développement des poils racinaires chez les plants de blé cultivés (i) en gélose,(ii) en conditions hydroponiques, (iii) dans des rhizobox modifiés fournissant des conditions "aéroponiques" à la surface d'un tissu de polyester humide, et (iv) dans le sol. Les expériences menées sur des plantes cultivées dans le sol ne visaient pas à prendre en compte le développement des poils absorbants. Ces cellules étaient très difficilement visibles et probablement souvent endommagées lors de la récupération du système racinaire dans le sol, car les longs poils racinaires sont fragiles (Figure 4.1). Concernant la culture en sol, les analyses d'images de systèmes racinaires inoculés avec différentes souches de PGPR ont révélé des différences, en termes de longueur totale de racine et de surface de racine totale, en fonction de la souche inoculée, mais ces différences n'étaient pas statistiquement significatives, sauf dans un cas, l'inoculation avec l'isolat libanais B3 2, qui a conduit à une augmentation de ~120% de la surface totale des racines (Figure 5.2). On peut considérer que de telles analyses sont biaisées car elles ne tiennent pas compte de la surface des poils absorbants, alors que, dans l'ensemble, mes expériences démontrent que le blé peut produire des poils racinaires denses et longs augmentant fortement la surface de l'interface racine-sol (Figure 1.1; voir aussi ci-dessous). D'autre part, les images de jeunes plantules cultivées sur milieu gélosé ont révélé que l'inoculation de diverses souches bactériennes entraînait une augmentation statistiquement significative de l'élongation des poils racinaires, de plus de 30% dans le cas des souches libanaises B3-2 et I1-3 (Figure 5.5).

La culture de plantes dans nos rhizobox permet clairement d'obtenir des images de haute qualité de tout le système racinaire, à partir de plantules âgées de 2 semaines environ. La croissance se produit dans "l'air ambiant" à la surface d'un tissu maintenu humide par l'arrosage automatique d'une mousse de polyuréthane ajustée "derrière" le tissu. De telles conditions sont susceptibles de mimer la croissance des racines dans certaines conditions de sol, lorsque la croissance se produit le long des particules de sol dans les pores du sol présentant une atmosphère similaire à celle

située au-dessus du sol (en termes de disponibilité en O_2) mais plus humide. Des exemples d'images de systèmes racinaires cultivés dans de telles conditions (Figures 1.1, 5.7 à 5.9) montrent que les poils racinaires denses et longs peuvent couvrir de grandes parties de l'ensemble du système racinaire. De toute évidence, il est difficile d'obtenir des estimations de paramètres tels que "densité des poils racinaires" ou "longueur moyenne des poils racinaires". En revanche, l'analyse de petites régions racinaires telles que celles agrandies dans les panneaux de la figure 1.1 indique que la surface totale des poils racinaires peut être environ 10 fois supérieure à celle du segment racinaire correspondant qui serait "exempt de poils racinaires" (Tableau 6.1).

Notre hypothèse de travail pour décrire les images du système racinaire complexe obtenues à l'aide des rhizobox a été que la courbe décrivant l'évolution de la surface racinaire en fonction de la distance par rapport à la graine germée (ou en fonction de la profondeur dans le rhizobox, c'est-à-dire la distance à la ligne horizontale passant par le "point" à la surface du rhizobox où la graine germée a été déposée) pourrait servir de support aux premières analyses quantitatives des effets de conditions biotiques et abiotiques sur le développement du système racinaire. Un programme (plugin d'ImageJ) nommé ACRT a été développé (par Volker Baecker, MRI, Montpellier) dans cette perspective. J'ai ensuite effectué deux expériences différentes pour comparer les effets de la condition de faible P (LP) par rapport à la condition de faible N (LN) et l'effet de l'inoculation des racines avec *Bradyrhizobium japonicum*, par rapport à l'absence d'inoculation, sur le développement des racines.

6.2.2. Effet des conditions LP et de l'inoculation avec B. japonicum sur le développement des racines

Comparaison entre les plantes non inoculées et inoculées. La figure 5.10 (comme la figure 6.4) indique que l'inoculation avec *B. japonicum* a entraîné une augmentation de la surface totale des racines. Cette conclusion est également corroborée par les résultats des analyses de la surface racinaire réalisées avec WINRHIZO™ et présentées à la figure 5.12. Il est intéressant de noter que l'augmentation de la surface racinaire due à l'inoculation de la plante apparaît principalement en profondeur, par rapport à la position de la graine germée, entre env. 5 cm et 14 cm (Figure 5.10B) (distance à la graine germée comprise entre 6 et 15 cm environ; Figure 5.10A), au-dessus ou au-dessous de cette région, la surface racinaire apparaît comme strictement similaire dans la racine inoculée ou non inoculée.

Dans les systèmes racinaires inoculés et non inoculés, la plus grande surface racinaire se situe dans cette plage de 5 à 15 cm à la graine germée. L'observation visuelle des images initiales (Figures 5.7 et 5.8) révèle que cette région dans le rhizobox est colonisée par des racines secondaires bien développées. Les données présentées à la figure 5.12 (analyses WINRHIZO™) suggèrent que l'augmentation de la surface racinaire dans cette région due à l'inoculation résulte principalement d'une augmentation de la surface des poils absorbants, plutôt que d'une augmentation de la croissance des racines (longueur) dans cette région (comparez les barres blanches et noires de la figure 5.12).

Comparaison entre les systèmes racinaires développés en conditions LN ou LP. La figure 5.11 (comme la figure 6.5) révèle les différences de développement du système racinaire entre les plantes traitées LN et les plantes traitées LP. Les analyses avec WINRHIZO™ (Figure 5.12) montrent que les différences résultent d'une augmentation de la surface totale des racines, due à la fois à une augmentation significative de la croissance des racines (longueur) et du développement des poils des racines (Figure 5.12, comparer les barres noires et grises). Il convient toutefois de noter que, dans les 5 à 6 premiers centimètres, la surface totale des racines était nettement plus importante dans le cas du traitement LN que dans celui du traitement LP. Au-delà de cette distance, la situation inverse a été observée et une plus grande surface racinaire a été systématiquement observée chez les plantes traitées LP. Ceci suggère probablement que la croissance des racines dans les 5-6 premiers cm supérieurs des rhizoboxes est survenue avec une production de racines secondaires et un allongement moins important dans les conditions LP que dans les conditions LN. Au-delà de cette distance, la situation inverse se produirait. Une telle différence dans le développement de l'architecture racinaire n'a pas été observée dans la comparaison entre les plantes inoculées et les plantes non inoculées (paragraphe ci-dessus).

6.3. Conclusions et perspectives

Les résultats que j'ai obtenus indiquent que la souche de *Bradyrhizobium japonicum* que j'ai testée, ORS285, peut interagir avec le cultivar de blé que j'ai utilisé, Oued Zenati, car elle affecte le développement des racines (Figures 5.10 et 6.4; voir ci-dessus), mais est peu active en termes promotion de la croissance des plantes, du moins dans les conditions expérimentales que nous avons utilisées (Figures 3.14 et 3.15). Il est toutefois important de noter qu'il est prouvé que les interactions bénéfiques entre les racines et les microbes du sol peuvent afficher un niveau élevé de spécificité. Par exemple, comme indiqué ci-dessus, l'inoculation de *Klebsiella pneumoniae* 342 s'est avérée soulager les symptômes de la carence en azote chez un seul cultivar de blé, sur les 3 cultivars testés (Iniguez *et al.*, 2004). Ainsi, il peut être intéressant d'évaluer les effets d'autres souches de *B. japonicum* sur la croissance du blé et le développement du système racinaire, ainsi que de tester les réponses correspondantes avec d'autres cultivars de blé.

Deux méthodologies ont été développées au cours de ce travail afin de phénotyper le développement des racines et des poils racinaires. En ce qui concerne les protocoles actuels et les prototypes d'appareils, je pense que la méthodologie «rhizobox» est la plus intéressante, car les conditions de croissance sont plus pertinentes sur le plan physiologique et que l'on peut obtenir des images de systèmes racinaires entiers, y compris les poils absorbants.

En aval de ce travail, il serait certainement utile d'améliorer le programme ACRT mis au point pour l'analyse automatique des images de racines obtenues à l'aide du dispositif "rhizobox", et de développer des stratégies permettant de compléter/associer les services et informations fournis par ce programme avec ceux fournis par WINRHIZO™. Une première étape consisterait à "ajuster" les paramètres

internes de ces programmes afin qu'ils fournissent des analyses très similaires, par exemple en termes de surface totale des racines. Certaines divergences concernant ce résultat ont en effet été observées entre les deux programmes, ce qui pourrait être dû au "nettoyage" initial, à la segmentation et à la binarisation des images. Probablement plus important encore, il serait très intéressant d'optimiser les complémentarités possibles entre les deux programmes. Par exemple, je pense qu'une première description des images de racines pourrait être fournie par WINRHIZO™, en ne tenant compte que des poils absorbants (identifiés par ce logiciel comme étant les "éléments du système racinaire" ayant le diamètre le plus mince), puis analysés avec ACRT afin de décrire la capacité du système racinaire à explorer et à pénétrer le "sol" à différentes profondeurs / distances de la graine germée, et la contribution des poils absorbants à l'augmentation de l'interface "sol-racine" en fonction des conditions de disponibilité des éléments nutritifs.

Outre ces objectifs, j'estime que la méthodologie des "rhizobox" pourrait maintenant permettre de cribler des collections de bactéries, y compris les isolats libanais que j'ai obtenus (Chapitre 3), afin d'identifier des souches très efficaces en termes d'impact sur le développement du système racinaire. L'hypothèse de travail qui sous-tend cet objectif est que les souches bactériennes identifiées comme ayant une forte capacité à stimuler le développement des racines (y compris les poils absorbants) sont susceptibles d'être efficaces pour améliorer la nutrition des plantes. Dans un deuxième temps, il faudrait bien entendu vérifier les effets de telles souches sur le développement des racines et la croissance des plantes dans des conditions réelles de sol. Inversement, des analyses GWAS pourraient être développées, en testant une collection d'accessions de blé, par exemple une série de génotypes qui récapituleraient la domestication du blé, contre une souche bactérienne (auparavant reconnue pour sa capacité à interagir efficacement avec au moins un des membres de la collection de blé testée) afin d'identifier les gènes et les mécanismes impliqués dans l'interaction et son impact sur le développement des racines et la nutrition des plantes. L'objectif général de toutes ces recherches est d'acquérir des connaissances sur les PGPR afin d'utiliser des bactéries comme biofertilisants favorisant le développement de pratiques agricoles durables.

Chapter 1: Literature survey

Root hairs at the crossroad of plant nutrition and interactions with beneficial soil microbes: perspectives in plant breeding

1.1. Introduction

One of the major challenge of the incoming second green revolution is to reduce the fertilization and irrigation levels and their ecological costs (Lynch, 2007) while coping with the sharp increase in world population. Strong research efforts aiming at better understanding the functioning of root systems are required to develop new crop cultivars with enhanced capacity for soil resource acquisition and to better exploit the genetic variation in productivity of crops in poorly fertile soils (Brown *et al.*, 2013). Root system architecture and, at the root soil interface, production and elongation of root hairs (RH), are major determinant of the volume and location of explored and exploited soil. It is also known that i) root secretion of protons, organic acids and enzymes, allowing mobilization of nutrients from soil particles and from organic matter, ii) transfer of carbohydrates to feed root symbionts and beneficial microbes in the rhizosphere are functions of major importance for plant nutrient acquisition and, finally, plant development.

The present review is focused on root hairs (RH). It has been reported that a single rye plant can develop more than 10 billions RH, representing an underground interface of about 400 m^2, much larger than that of the aerial parts of the plant (Dittmer, 1937). Figure 1.1 shows 2-week old wheat seedling displaying dense and long root hairs over almost the whole root system. The diameter of the root hair cylinder in the enlargements displayed by the panel D, E and F of Figure 1.1 is about 10 times larger than that of the root itself, and thus the volume of the root hair cylinder is *ca.*100 times larger than that of the root. Furthermore, for mobile ions that would display quasi-Brownian diffusion in soil solution close to such root regions, the probability of reaching the cell membrane of a root hair would be much higher than reaching the surface of the root cylinder. Here we review some major functions of root hairs, with respect to plant mineral nutrition in a broad sense, and take stock of the attempts to use root hair traits in plant breeding programs. The signaling processes and molecular mechanisms underlying the roles of root hairs in plant interactions with beneficial soil microbes, *e.g.*, in rhizobial symbiosis (Ibañez *et al.*, 2017; Zipfel and Oldroyd, 2017), are not reviewed in the present literature survey.

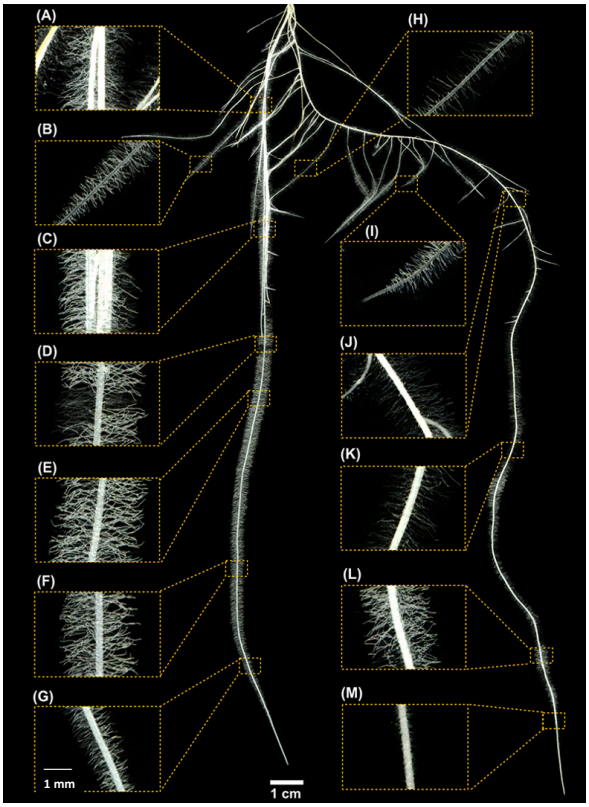

Figure 1.1. 2-week old wheat seedling grown in rhizobox in the lab.

1.2. Adhesion to soil particle, soil penetration and rhizosheat formation

Root hair adhesion to soil particle is of crucial importance for root tip anchorage, soil penetration and rhizosheath (see below) formation.

Rapid evocation of the role of root hairs in "plant anchoring", as often found in papers on root hair development, may be perceived in a confusing way. When the resistance to vertical uprooting forces is compared between Arabidopsis wild type plants and mutant plants impaired in root hair development or lateral root production, the conclusion is that root hairs do not contribute to whole plant anchoring in this operational definition (Bailey *et al.*, 2002). On the other hand, clear evidence is available that root hairs provide grip for root tip penetration in soil. For instance, about 80% of wild type barley roots growing from a loose layer of soil over a more compacted layer were found to be able to penetrate the compacted soil while the corresponding percentage was only 1% in the case of hairless mutant roots (Haling *et al.*, 2013). Similarly, in maize during germination on a soil displaying a moderate penetrometer resistance, wild-type seedlings took about 16 h to anchor themselves to the soil, compared with more than 30 h for hairless mutant seedlings, which most often did not

become anchored securely (Bengough *et al.,* 2016). The anchorage forces were up to 5 times weaker in the hairless mutant than in wild-type roots.

The strength of the grip provided by root hairs to growing root tips depends on both the microstructure of the rhizosphere and the root hair size, which together determine the depth to which root hairs can penetrate within the soil matrix and micropores. It is tempting to assume that, at least in some species, the strength of the grip is also dependent on secretion of adhering molecules, as performed by hausterial hairs of parasitic plants (Baird and Riopel, 1983; Cui *et al.*, 2016) and specialized root hairs from clinging-climbers like English ivy (Huang *et al.*, 2016) and *Syngonium podophyllum* (Yang and Deng, 2017).

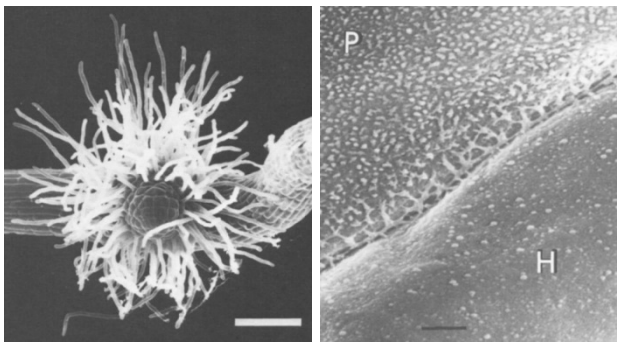

Figure 1.2. 48H-old haustorium (x150, bar represents 100 µm) and interface between haustorial hair (P) and host root surface (H) where secreted compounds (likely exopolysaccharides) have coalesced at the contact region (x10,000). Adapted from Baird and Riopel (1983).

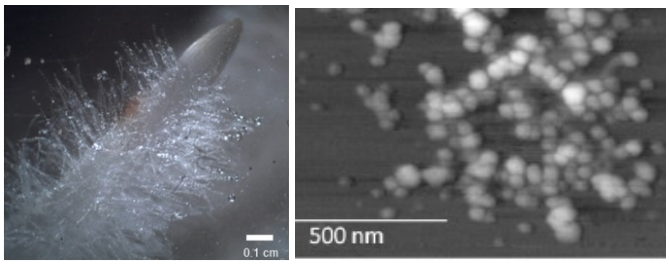

Figure 1.3. Root hair secretion in H. helix. Release of adhesive at the tip of root hairs (left), note that adhesive droplets from contiguous root hairs can fused to form larger droplets. Nanoparticules imaged by atomic force microscopy after purification (right). Adapted from Burris *et al.* (2012) and Burris (2016).

In ivy (*Hedera helix)*, it has been shown that root hairs present on adventitious roots produce specific secretion containing oligosaccharides and spherical nanoparticles, 60–85 nm in diameter, which give grip to the stem. The nanoparticules are predominantly composed of hydroxyproline-rich arabinogalactan proteins, which have been identified as key components of the ivy root hair high-strength adhesive (Huang *et al.*, 2016).

The adhesive properties may be reinforced via a calcium-mediated cross-linking with pectin in the secreted mucilage (Huang *et al.*, 2016) and a putative cross-linking with the matrix. Moreover, microfibril deposition via a specific angle in English ivy root hair combined with the dessication/squeezing of root hair in the gaps of the substrate and at last stage of their development a lignification may also contribute to structural and functional aspects of the high strength adhesion of *H. helix* adventitious roots (Melzer, 2010).

Mechanisms through which root hair contribute to soil penetration are also likely to play a major role in rhizosheath formation. Rhizosheaths have been initially described as "peculiar sheaths" composed of agglutinated particles of sand (Volkens, 1887). Operational descriptions are now proposed from the weight of soil that adheres to roots that have been freshly excavated and submitted to a soil removal treatment (*e.g.* hand shaking or sonication in water) of standardized vigor (McCully, 1999; George *et al.,* 2014; Brown *et al.,* 2017; Pang *et al.,* 2017). Evidence is available that the presence of root hairs that enmesh soil particles is required for formation of rhizosheaths (Moreno-Espindola *et al.,* 2007; Shane *et al.,* 2011). Hence, rhizosheath refers to the soil that physically adheres to the root system, while rhizosphere refers to the soil influenced by the root, beyond the "cylinder" of the rhizosheath (Hinsinger *et al*., 2009: York *et al.,* 2016). A strong correlation has been found between root hair length and rhizosheath weight in wheat (Delhaize *et al.,* 2012). The correlation is weaker in barley (George *et al.,* 2014), and no significant correlation has been observed in 58 other species except when root hairs were extremely short (Brown *et al.,* 2017). It is possible that rhizosheaths surrounding roots that possess long root hairs are unstable and prone to disintegrating during measurements resulting in a poor correlation. It has also been proposed that, when root hair length exceeds about 300 µm, other factors have increasing importance in rhizosheath formation, size and stability, among which probably root hair density and root hair morphology, *e.g.*, bent or hooked forms that would trap more soil, and root and microbial mucilage (McCully, 1999; Brown *et al.,* 2017).

The presence of rhizosheaths can play a major role in many physiological functions and plant adaptation to abiotic and biotic conditions, as prevention of water loss, nutrient and water acquisition, recycling of nutrients, provision of a mechanical defense against herbivorous and plant parasites (Striga, Orobanches…) and formation of a growth-promoting niche for beneficial microbes (Shane *et al.,* 2011). Rhizosheaths have also been shown to host diazotrophic bacteria (Wullstein *et al.,* 1979; Othman *et al.,* 2004) and to harbor nitrogenase activity (Wullstein *et al.,* 1979).

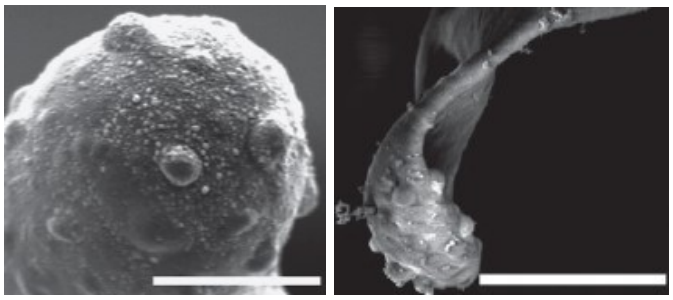

Figure 1.4. Developmental stages of ivy root hairs. Protuberances are present at the tip of root hairs and may represent the location of adhesive excretion. Later, root hairs dessicate, squeeze and lignify looking as curled ribbon (left panel scale bar, 5 mm, right panel scale bar, 10 mm). (Adapted from Melzer *et al.,* 2010).

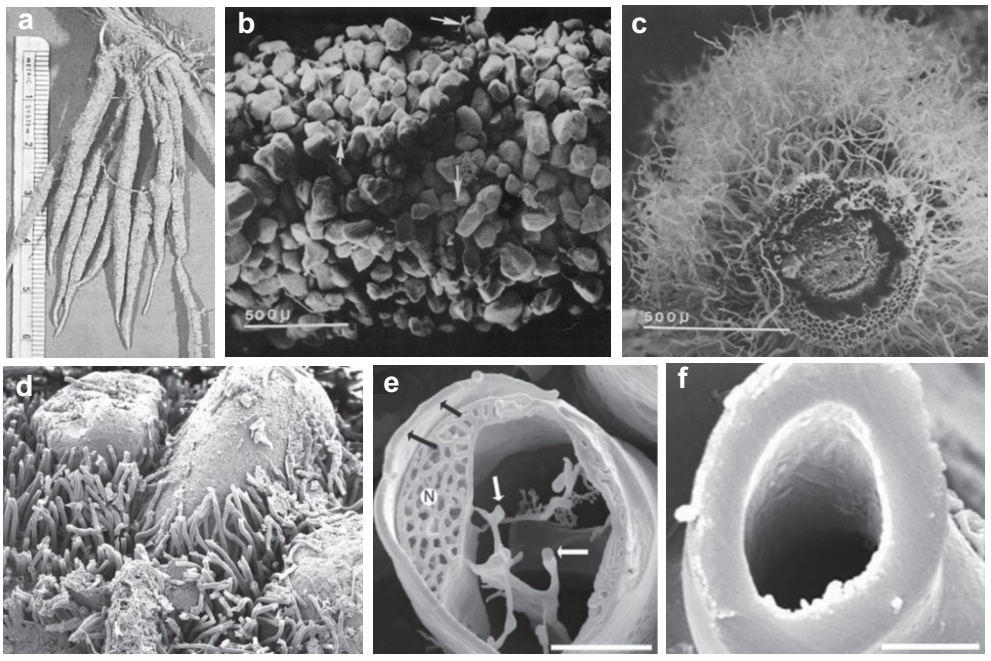

Figure 1.5. Rhizosheaths: a) Rhizosheaths of *Agropyron dasystachyum* b) external view of a rhizosheath of Oryzopsis hymenoides embedded in sand grains, c) Rhizosheath cross section after sand removal, d) root hairs entraping sand on rhizosheath of *Lyginia barbata* e) cross section of a living root hair close to the root tip of *L. barbata*. Note the thin wall (black arrow), the nucleus (N) and vacuolar vesicles (white arrows) d) cross section of an old root hair with a very thick wall. From Shane *et al.* (2011); shane *et al.* (2005); Wullstein *et al.* (1979) and Wullstein and Pratt (1981)

Figure 1.6 Dauciform roots: Dauciform roots in the *Schoenus unispiculatus* (Cyperaceae). (Shane *et al.,* 2005)

Thus, QTL (quantitative trait loci) for rhizosheath size, taken as surrogate of root hair length or, in a broader sense, of a root trait likely to contribute to improved soil foraging and hydromineral nutrition, resulting in increased biomass production and yield in crop plants grown in low fertility soils are actively looked for (Delhaize *et al.,* 2015; Horn *et al.,* 2016; James *et al.,* 2016; Liu *et al.,* 2017; Gong and McDonald, 2017; see below). Closely related to rhizosheaths, dauciform roots clusters are specialized root structure developed in monocotyledonous sedges. Their development occurred only in particular genera of Cyperaceae when grown at low P and N supply. These clusters of short carrot shaped lateral root harbor remarkably dense and long root hairs (Davies *et al.,* 1973; Lamont, 1974; Shane *et al.,* 2006). In conclusion, rhizosheaths and dauciform roots present in old landscape are structurally different from cluster/proteoid roots since they do not form abundant determinate rootlets but are functionally similar to them (Shane *et al.,* 2006) in terms of their abundance of fine root hairs and the release of organic anions that enhance mineral and water uptake from P-impoverished soils. (Albalasmeh and Ghezzehei, 2014).

1.3. Soil foraging for nutrient and water acquisition

Very numerous studies have provided indirect or direct evidence that root hairs significantly contribute to nutrient ion acquisition from the soil and plant mineral nutrition. Major lines of evidence can be sorted as follows. (i) Nutrient starvation results in increased root hair density and length (Bates and Lynch, 1996; Ma *et al.,* 2001; Schmidt and Shikora, 2001; Stettler *et al.,* 2015; Zygalakis *et al.,* 2011; Janes *et al.,* 2018). (ii) Mutant plants displaying impaired root hair growth are affected in nutrient ion uptake and biomass production, and nutrient (P) accumulation is positively correlated with root hair length under nutrient-deficient conditions (Brown *et al.,* 2013; Ahn *et al.,* 2004; Haling *et al.,* 2014; Tanaka *et al.,* 2014; Canales e*t al.,* 2017). (iii) Genotypes with longer root hairs have been shown in barley and wheat to be better adapted to low nutrient soil (Gahoonia and Nielsen, 2004; Han *et al.,* 2016; Klinsawang *et al.,* 2018). (iv) Finally, evidence that root hairs directly contribute to nutrient uptake has been obtained by various electrophysiological approaches (see below) or by using

dedicated growth devices ensuring that only root hairs have access to the nutrient source (Gahoonia and Nielsen, 1998).

Increase in root hair length and density upon nutrient deprivation has very often been reported for poorly soluble ions, such as phosphate, potassium, iron and manganese, which can be strongly bound to soil minerals and thus poorly mobile in the soil solution (low diffusion capacity) when compared to NO_3^- (Marschner, 1995). Also, the influence of root hairs on the rate of nutrient uptake is much more important in soil than solution culture (Leitner *et al.,* 2010). Such observations are in line with the widely accepted hypothesis that the increase in the area of the soil-root interface resulting from production of root hairs strongly underlies the contribution of these cells to the acquisition of poorly mobile nutrient ions. In other words, root hairs allow the root to increase the volume of soil from which nutrients can be taken up (see Figure 1.1). It should be noted that physical and mathematical analyses predict that increases in root hair length give greater increases in nutrient uptake than increases in hair density (Zygalakis *et al.,* 2011).

Root hair elongation can also facilitate water uptake (Segal *et al.,* 2008; Comas *et al.,* 2013; Ahmed *et al.,* 2018). Indeed, using a root pressure chamber derived approach to analyze the relationship between transpiration rate and xylem suction in wild-type and hairless mutant plants (barley), it has been recently demonstrated that root hairs contribute to water uptake in drying soils in rapidly transpiring plants by increasing the soil-root interface and thereby reducing the drop in matric potential at the interface between root and soil (Carminati *et al*., 2017). It has also been shown that absence of root hairs in Arabidopsis can significantly affect water absorption and drought tolerance (Tanaka *et al.,* 2014). The conditions in which increased root hair length can contribute to plant adaptation to low water availability and drought are however still unclear since rhizogenesis during progressive drought stress gives rise to short hairless roots, this adaptive response being under control of the stress hormone ABA (Vartanian, 1981; Vartanian *et al*., 1994; Schnall and Quatrano, 1992). Reducing the interface with the external medium is an efficient strategy when water availability is very low. Thus, the plant would cope, under different environmental conditions, in dependency of the gradient of water potential and water availability, with the conflicting needs of increasing the area of its interface with the soil in order to facilitate water uptake, or of decreasing this area in order to prevent desiccation. Finally, the involvement of root hairs in the formation of rhizosheaths, which are a classical feature of xerophytic grasses and are more developed on mesophytic grasses in drier conditions, also suggests that control of root hair development is an adaptive response to drought stress.

1.4. Ion transport systems at the root hair plasma membrane: a conserved panoply amongst plant species

Ion exchanges between root hair cells and the external medium have been evidenced by different approaches, ion-selective vibrating microelectrodes at the vicinity of root

hairs to determine net fluxes from local concentration gradients (Jones *et al.,* 1995; Felle *et al.,* 1998; Lew, 1998; Babourina *et al.,* 2001), recording of resting membrane potential variations in response to changes in ionic composition of the external medium (Meharg and Blatt, 1995) as well as monitoring of ion accumulation in root hair cytosol via fluorescence imaging or cytosolically-positioned ion-selective microelectrodes (Bibikova *et al.,* 1997; Felle and Kepler, 1997; Felle *et al.,* 1999; Halperin and Lynch, 2003; Bai *et al.,* 2014). These studies have been carried out in only 3 plant species (Arabidopsis, alfalfa, and the aquatic pondweed *Limnobium stoloniferum*) and were not generalized to a wide range of ions. They however could evidence root hair nutritional uptake of major ions: K^+ (uptake either coupled or not to H^+ efflux), NO_3^- (coupled to H^+ influx), Ca^{2+} and Na^+ (at high concentrations). In addition, imaging and ion-selective microelectrode studies revealed differences in ion transport properties in dependency of the root hair developmental stage as well as polarized transport of ions (Ca^{2+}, H^+) along growing root hairs, including a tip-localized Ca^{2+} influx determinant for tip growth (Bibikova *et al.,* 1997; Felle and Kepler, 1997; Felle *et al.,* 1999; Jones *et al.,* 1995; Bai *et al.,* 2014; see below). Such analyzes have also evidenced signaling ion fluxes, *e.g.*, in alfalfa in response to Nod factors, involving H^+, Cl^-, Ca^{2+} and K^+ (root hair signaling responses are not reviewed in the present article).

Patch-clamp and voltage-clamp investigations have provided further information on root hair membrane conductances responsible for inwardly and outwardly-directed ionic fluxes. An inwardly rectifying Shaker-type (see below) K^+ conductance (Véry and Sentenac, 2003) was ubiquitously reported (*i.e.*, in Arabidopsis, carrot, different legumes and cereals; Gassmann and Schroeder, 1994; Bouteau *et al.,* 1999; Downey *et al.,* 2000; Dauphin *et al.,* 2001; Ivashikina *et al.,* 2001; Reintanz *et al.,* 2002; Li *et al.,* 2012; Wang *et al.,* 2019). In *Arabidopsis*, reverse genetics analyzes coupled to patch-clamp studies have shown that two Shaker subunits, AKT1 and AtKC1, contribute to the inward K^+ conductance by forming homomeric (AKT1) or heteromeric (AKT1-AtKC1) channels (Reintanz *et al.*, 2002). Besides in Arabidopsis, this root hair inwardly-rectifying K^+ conductance was functionally characterized in some details in 2 other species, *Medicago* and wheat, allowing to confirm conservation of basic properties (selectivity for K^+, low affinity, voltage gating; Véry *et al.,* 2014). Another Shaker-like conductance devoted to K^+ effluxes (secretion: Véry and Sentenac, 2002) as well as a S-type anionic conductance have also been quite frequently reported, *i.e.*, in Arabidopsis, legume species, and (for the K^+ one) rice (Bouteau *et al.,* 1999; Dauphin *et al.,* 2001; Ivashikina *et al.,* 2001; Li *et al.,* 2012; Wang *et al.,* 2019). Comparison of basic functional properties of the *Arabidopsis* and *Medicago* K^+ outward conductance revealed also conservation of K^+ selectivity and gating properties (voltage dependent gating controlled by external K^+). On the other hand, for the S-type anionic conductance, the presently available information is not sufficient to allow comparison of ionic selectivity and gating between species. Besides these commonly reported conductances, an inwardly-rectifying Ca^{2+}-permeable cationic conductance has been characterized in Arabidopsis and thereafter reported in rice (Véry and Davies, 2000; Li *et al.,* 2014). Finally, it should be noted that several other plasma membrane conductances that have been described so far in root hairs from a single species, Arabidopsis, *Medicago* or white mustard, including 2

cationic conductances permeable to Ca^{2+}, an anionic conductance, and H^+-NO_3^- and H^+-Cl^- symports (Felle, 1994; Meharg and Blatt, 1995; Miedema *et al.,* 2008; Wang *et al.,* 2019) have probably not been looked for so far in other species.

Molecular analyses including reverse genetics approaches, most often carried out in Arabidopsis and, to a lower level, in rice, have provided valuable information on the genes and proteins involved in nutrient ion acquisition by roots and root hairs. With respect to root acquisition of K, N, P and S, the present knowledge in *Arabidopsis* can be summarized as follows (Figure 1.7). K^+ uptake from the soil is essentially mediated by the high affinity K^+ transporter AtHAK5, whose expression is increased upon K^+ starvation, and by the Shaker channel AtAKT1, whose voltage sensitivity (and thus activity) is regulated by the Shaker regulatory subunit AtKC1, able to form heteromeric channels with AKT1 (Véry *et al.*, 2014). Evidence is available that these 3 K^+ transport systems are expressed in Arabidopsis root hairs (Reintanz *et al.,* 2002; Ahn *et al.,* 2004). Membrane transport systems that have been shown to contribute to the uptake of NO_3^- in Arabidopsis belong to 3 different families, named NPF (Nitrate transporter 1/Peptide transporter Family; Léran *et al.,* 2014), NRT2 (Orsel *et al.,* 2002) and NRT3 (also named NAR for "Nitrate Assimilation Related family") (Okamoto *et al.,* 2006). The NPF family comprises the extensively studied “transceptor” NPF6.3, initially named AtNRT1.1 or CHL1, which behaves both as a dual affinity bidirectional NO_3^- transporter (Liu *et al.,* 1999; Léran *et al.,* 2013) and as a NO_3^- sensor mediating NO_3^- regulated auxin transport, thereby playing an important role in root development (Krouk *et al.,* 2010). Transcriptome data provide evidence that *NPF6.3/AtNRT1.1* transcripts are expressed in Arabidopsis root hairs (Huang *et al.,* 2017) like its counterpart in tomato (Lauter *et al.,* 1996). Some other members from the NPF family are likely to contribute to NO_3^- acquisition from the soil, like AtNPF4.6 (also named AtNRT1.2), which is expressed in root hairs and able to mediate NO_3^- uptake besides ABA transport (Huang *et al.,* 1999; Kanno *et al.,* 2013; Huang *et al.*, 2017). The Arabidopsis NRT2 family comprises AtNRT2.1 and AtNRT2.2, which play a major role in high affinity nitrate uptake by roots (Li *et a*l., 2007; Remans *et al.,* 2006). These membrane transport systems physically interact with a member of the NRT3 family, AtNRT3.1 (also named *AtNAR2.1*) to form heteromeric structures. The AtNRT2.1-AtNRT3.1 complex provides the major contribution to high affinity NO_3^- uptake from the soil solution (Yong *et al.,* 2010; Li *et al.,* 2007). Reporter gene experiments have revealed expression of *AtNRT2.1* (*At1g08090*) in root hairs (Nazoa *et al.,* 2003; Wirth *et al.,* 2007) and transcriptome data provide evidence that *AtNRT3.1* is expressed in this cell type too (Huang *et al.,* 2017). Finally, transcriptome data also provide evidence that root hairs express members of the AMT, PHT and Sultr families (Huang *et al.,* 2017), involved in ammonium, phosphate and sulfate uptake, respectively, in Arabidopsis as well as in several other species (Huang *et al.,* 2017).

It is worth to note that transcripts from several Arabidopsis transporter genes known to be repressed in media displaying high concentrations of nutrient are not present in root hair transcriptome data from plants grown on highly concentrated media like the Murashige and Skoog one. This is the case for instance of the Arabidopsis K^+ transporter gene AtHAK5, whose expression is induced by K^+ deficiency (Gierth *et al.,*

2005). No *AtHAK5* transcripts (*At4g13420*) can be detected in the root hair transcriptome from plants grown on the Murashige and Skoog (20 mM K^+) medium (Huang *et al.,* 2017) but expression of this gene has been observed in root hairs from plants grown on a medium containing a lower (1.7 mM) K^+ concentration (Ahn *et al.,* 2004). A similar assumption can be proposed to explain the absence of *AtNRT2.1* transcript in root hair transcriptomes from Arabidopsis plants grown on Murashige and Skoog medium, while this gene has been shown to be expressed in Arabidopsis root hairs in other experimental conditions (Nazoa *et al.,* 2003; Wirth *et al.,* 2007). Indeed, NRT2.1 expression is strongly dependent on the external availability of NO_3^- and on the plant nitrogen status, with a severe inhibition by NH_4^+ (Lejay *et al.,* 1999; Cerezo *et al.,* 2001), and both NO_3^- and NH_4^+ are present at high concentrations (20 mM) in Murashige and Skoog medium. In contrast, focusing on membrane transport systems, analyses of root hair transcriptomes from *Medicago truncatula* seedlings grown on Farhaeus medium, a nitrogen-free and rather diluted medium indicate that members from the Shaker K^+ channel family, the HAK K^+ transporter family, the NPF, NRT2 and NRT3 NO_3^- transporter families, and the ammonium; phosphate and sulfate transporter families AMT, HPT and Sultr, and very close homologs of all the cited channels and transporters, *AtAKT1, AtKC1, AtHAK5, NPF6.3, AtNPF4.6, AtNRT2.1 and AtNRT3.1*, display expression in root hairs (Damiani *et al.,* 2016).

It is worth to note that members from the Shaker channel family and from the HAK, NRT2, NRT3, AMT, PHT and Sultr transporter families are also present in the moss *Physcomitrella patens* (Garciadeblas *et al.*, 2007; Tsujimoto *et al.*, 2007; De Michele *et al.*, 2012; Takahashi *et al.,* 2012; https://phytozome.jgi.doe.gov/pz/portal.html#!info?alias=Org_Ppatens). Together with the conservation of the major ionic conductances that dominate the electrical properties of the plasma membrane of root hair cells, as revealed by patch-clamp analyzes, and the conservation of the transport systems ensuring macronutrient ion uptake, this suggests that major components of the root hair equipment involved in plant mineral nutrition have been acquired very early during plant evolution.

1.5. Root hairs and mycorrhizal symbiosis contributions to soil foraging

It is well known that symbiotic association with mycorrhizal fungi can also allow the plant to increase the volume of exploited soil. It has been proposed that plant species with a coarse root architecture, characterized by relatively large diameter roots, low root hair density and short root hairs, and thus a limited intrinsic capacity to take up soil nutrients, derive the greatest growth benefit from arbuscular mycorrhizal (AM) symbiosis (Baylis, 1970; Brundrett, 2002; Smith and Read, 2008). A recent meta-analysis indicates however that mycorrhizal growth response is not correlated with root diameter, root hair length and root hair density. In other words, possessing coarse roots cannot be considered as a predictor of plant growth response to AM fungal colonization (Maherali, 2014).

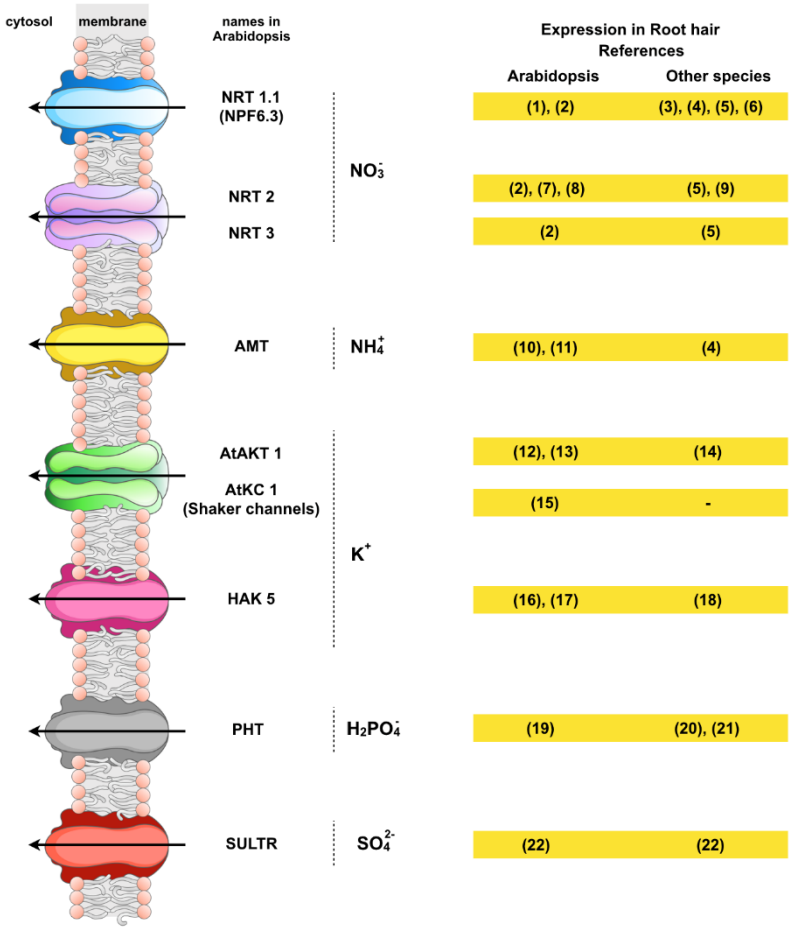

Figure 1.7. Ion channels and transporters involved in nutrient ion uptake and displaying expression in root hair in *Arabidopsis* and other species. References: (1) Krouk *et al.* (2010), (2) Krapp *et al.* (2014), (3) Lin *et al.* (2000), (4) Lauter *et al.* (1996), (5) Pellizzaro *et al.* (2015), (6) Huang *et al.* (2017), (7) Li *et al.* (2007), (8) Romans *et al.* (2006), (9) Feng *et al.* (2011); Luo *et al.* (2018), (10) Yuan *et al.* (2007), (11) Ludewing *et al.* (2007), (12) Hisrch *et al.* (1998), (13) Lagarde *et al.* (1996), (14) Ahmad *et al.* (2016), (15) Reintanz *et al.* (1996), (16) Gierth *et al.* (2005), (17) Nieves-Cordones *et al.* (2010), (18) Yang *et al.* (2014); Chen *et al.* (2015), (19) Shin *et al.* (2004), (20) Wang *et al.* (2018), (21) Chang *et al.* (2019) and (22) Takahashi (2019).

Investment of photosynthates in increased root hair production and in engagement in mycorrhizal symbiosis can be considered as complementary strategies to improve nutrient acquisition. It is worth to note however that mature ectomycorrhizae do not display root hairs (Peterson and Farquhar, 1996). This absence is likely to involve root hair incorporation into the fungal mantle. Upon incorporation, root hairs would collapse due to mechanical pressure of the hyphae (Brown and Sinclair, 1981; Thomson *et al.,* 1989). However, evidence has also been provided that fungal secretion of the auxin antagonist hypaphorin can contribute to the absence of root hairs in ectomycorrhizae by directly inhibiting root hair elongation (Ditengou *et al.,* 2000 and 2003; Rigas *et al.,* 2013). The relationship between arbuscular endomycorrhizal colonization (AM) and root hair development is complex. Evidence is available that AM can be associated to either a decrease or an increase in root hair density and length (Orfanoudakis *et al.,* 2010; Sun and Tang, 2013; Wu *et al.,* 2015). Reduction in root

hair development might result from changes in the root metabolic status and competition for available photosynthates between root hair production and the fungus (Orfanoudakis *et al.,* 2010). It has also been reported in trifoliate orange that the effects of AM on root hair development are associated with changes in the expression of auxin metabolism and transport genes and in *expansins* (Liu *et al.,* 2018), which is likely to impact root hair development (see below).

Fossil records provide evidence that fungal organisms that entered into mycorrhizal-like symbioses existed before the appearance of true roots (Bonfonte and Genre, 2008). Because fungal hyphae have a smaller diameter than root hairs, allowing exploration of smaller soil pores, and that they can extend far beyond the limits of the root hair cylinder, plant engagement in mycorrhizal symbiosis may be hypothesized to be more efficient than promotion of root hair elongation and density. This question has been investigated in barley by comparing the responses (biomass production and Pi contents) of wild-type and hairless mutant plants (*brb*) grown at different soil P levels in association with mycorrhizal fungi (co-inoculation with 2 *Glomus* species) or not. Mycorrhizas were found to effectively substitute root hairs in P uptake, but the additional P was most often used less effectively, in terms of plant growth, than P provided by root hairs (Jakobsen *et al.,* 2005). In similar experiments, in which several barley mutant lines affected in root hair development (hairless, short or intermediate root hair length phenotype) and wild type plants were colonized naturally by a live community present in the soil, endomycorrhizal symbiosis was found to not fully compensate for the absence of root hairs, with respect to both P acquisition and biomass production (Brown *et al.,* 2013). A third series of similar experiments, using the same hairless barley mutant (*brb*) and the corresponding wild type genotype but grown under well-watered or drought conditions led to the conclusion that, with respect to biomass production, endomycorrhizal symbiosis (following inoculation with *R. intraradices*) did not compensate for the absence of root hairs in the former conditions but compensate in the drought conditions (Li *et al.,* 2014). Altogether, these reports indicate that AM associations can be less effective in P-acquisition and biomass production than root hairs in barley in some environmental conditions. It has been evoked that this could be a consequence of generations of selective barley breeding for increased yields in artificialized soil conditions (Brown *et al.,* 2013).

1.6. Root hairs interactions with plant growth-promoting rhizobacteria (PGPR)

The microbial community thriving in the rhizosphere at the root surface and named rhizo-microbiota (Chaparro *et al.,* 2013; Bulgarelli *et al.,* 2013) is extremely rich. It can include up to 10^{10} bacteria per gram of soil (Gans *et al.,* 2005; Roesch *et al.,* 2007), representing a large diversity of taxa (Kyselková *et al.,* 2009; Gomes *et al.,* 2010; Robertson-Albertyn *et al.,* 2017). Within this population, bacteria generically named Plant Growth-Promoting Rhizobacteria (PGPR) can be recruited by roots to engage in beneficial interactions (associative symbiosis). In comparison to mutualistic symbionts (*e.g.*, nitrogen-fixing symbiosis in legumes), PGPR interact with a large range of host plant species and this generic appellation encompasses an important taxonomic

diversity, especially within the Firmicutes and Proteobacteria phyla (Lugtenberg and Kamilova, 2009; Drogue *et al.,* 2012; Yeoh *et al.,* 2017; Garrido-Oter *et al.,* 2018). PGPR promote plant growth via very diverse mechanisms, such as improved plant mineral nutrition resulting for instance from solubilization of poorly soluble sources of phosphate or other nutrients, phytosiderophore secretion, production of phytohormones that affect root development, facilitated establishment of rhizobial or mycorrhizal symbioses, protection against phytoparasites based on antagonism or competition mechanisms and/or on elicitation of plant defenses such as induced systemic resistance (Bashan and de-Bashan, 2010; Vacheron *et al.,* 2013). A shift in root surface pH towards more acidic values has also been reported (Poitout *et al.,* 2017), suggesting an increase in the rate of H^+ excretion by the plasmalemma proton pumps and thereby in the H^+ electrochemical potential that energizes the cell membrane and nutrient uptake (Sentenac and Grignon, 1987; Thibaud *et al.,* 1988).

Promotion of root hair development, likely to result in improved nutrient acquisition from the soil, has been reported in response to diverse PGPR and in different plant species, from Arabidopsis to Poaceae (Jain *et al.,* 1984; Dobbelaere *et al.,* 1999; Ribaudo *et al.,* 2006; Lopez-Bucio *et al.,* 2007; Contesto *et al.,* 2008; Galland *et al.,* 2012; Zamioudis *et al.,* 2013; Poitout *et al.,* 2017; Vacheron *et al.,* 2018). The increase in root hair length can be very important, by more than 100% (Contesto *et al.,* 2008; Poitout *et al.,* 2017), making this response to the bacterial inoculation the easiest one to detect, and thus the most straightforward way in laboratory experiments to check whether a given plant species can interact with a given PGPR.

Differences in the capacity to promote root hair elongation have been observed between PGPR strains (Contesto *et al.,* 2008). This raises the question, regarding strategies of (pre)selection of improved bacterial strains for field applications (Orozco-Finkel *et al.,* 2017; Mosqueda *et al.,* 2018) of whether such differences might be correlated to the studied PGPR capacity to promote plant growth, and be indicative of symbiosis efficiency. It should however be noted, with respect to this question, that pathogenic strains of the bacterial species *Pseudomonas syringae* have been shown to promote root hair elongation in Arabidopsis like beneficial *Pseudomonas* spp. bacteria (Pečenková *et al.,* 2017).

Root hair development phenotyping has also allowed to reveal differences between mutant plants and/or mutant bacterial strains, affected for instance in phytohormone metabolism, perception or transport, and to check the effects of molecules interfering with phytohormone pathways. Such analyses have provided information about molecular mechanisms underlying the promotion of root hair elongation (Ribaudo *et al.,* 2006; Lopez-Bucio *et al.,* 2007; Contesto *et al.,* 2008; Galland *et al.,* 2012; Poupin *et al.,* 2016; Zhao *et al.,* 2017; Vacheron *et al.,* 2018). They have also contributed to highlight how PGPR alter root development (they most often induce an inhibition of primary root elongation, a promotion of lateral root formation and a stimulation of root hair development; same references as above) by interfering with endogenous host mechanisms controlling post-embryonic root

development (Verbon and Liberman, 2018; Figure 1.3. It is not known whether PGPR-induced alterations in root development are beneficial to the bacteria by leading to qualitative or quantitative changes in root exudation of biomolecules.

Plant exude large amounts of biomolecules into the soil, that can represent more than 20% of fixed carbon, rendering the rhizosphere a carbon-rich niche for the development of microbial communities (Clarkson, 1985; Marschner, 1995; Haichar *et al.,* 2016; Venturi and Keel, 2016). Root exudation has been compared in wild-type and hairless mutant barley plants, revealing that the amounts of exsuded carbon was three times larger in wild type plants compared to the hairless mutant (Holz *et al.,* 2018). Such important contributions of root hairs to root exudation can be predicted to affect the microbial population. Regarding the impact on the composition of the microbial population, experiments carried out with wild-type and hairless mutant barley plants have provided direct evidence of a root hair-dependent diversification of the rhizosphere microbiota, the absence of root hairs resulting in a significant reduction in the diversity and complexity of the bacterial community (Robertson-Albertyn *et al.,* 2017). Evidence is available that the plant species, together with the soil type, shape the rhizosphere microbiota (Berg and Smalla, 2009; Yuan *et al.,* 2015; Sasse *et al.,* 2018). Bacterial attraction by root exudates probably involves selective chemotaxis processes (Drogue *et al.,* 2012; Bulgarelli *et al.,* 2013).

1.7. Plasticity of root hair development and adaptation to low nutrient availability and environmental conditions

The distribution of root hairs in the root epidermis varies amongst species, and 3 types of patterns can be distinguished. In species exhibiting a type I pattern, like rice or tomato for example, root hairs develop in a random pattern. In the type II pattern, displayed by grasses like *Brachypodium*, hair cells develop from smaller cells derived from an asymmetric cell division, the larger cells entering a non-hair cell fate. In the third type, which is displayed by Brassicaceae, like Arabidopsis, and some of their sister families, cell files are arranged longitudinally such that hair-forming hair cell files alternate with hairless cell files.

Most of the present knowledge about the genetically-fixed developmental mechanisms governing epidermal cell fate has been gained in *Arabidopsis*. In this model, the default fate for an epidermal cell is a root hair cell, and entry in the non-hair cell developmental program involves expression of a transcription factor (TF) named GL2 (GABRA2), which ultimately blocks the hair pathway. In a given epidermal cell, the level of *GL2* expression, and thereby the cell fate, is determined by the relative position of this cell with respect to the underlying cortical cells. An epidermal cell in contact with two cortical cells, a position which is named "H" (for "Hair"), develops into a root hair cell, whereas a cell in contact with a single cortical cell, a position named "N" (for Non hair), enters the non-hair cell developmental program (Figure 1.7). Evidence is available that signals leading to this differentiation pattern are emitted by

the cortical cell layer, but the present knowledge about the nature and pathways of these signals is still limited.

It is however known that JACKDAW (JKD), a zinc finger protein expressed in cortical cells, plays a role in the production process of a signal (Hassan *et al.,* 2010) whose perception by epidermal cells involves a plasmalemma leucine-rich repeat receptor-like kinase named SCRAMBLED (SCM) (Kwak *et al.,* 2005). Perception of this signal, thought to be stronger (or at least different) in H cells than in N cells, contributes to tune the relative activity of two competing transcription factors complexes, the first one including WEREWOLF (WER), or its partly redundant functional paralog MYB23, and the second one including CAPRICE (CPC), or one of its partly redundant functional paralogs, TRIPTYCHON and ENHANCER OF TRY AND CPC1 (TRY and ETC1). Besides WER or CPC, both complexes comprise GLABRA 3 (GL3) or its paralog ENHANCER OF GLABRA 3 (EGL3), and TRANSPARENT TESTA GLABRA 1 (TTG1). The WER-GL3/EGL3-TTG1 complex has the capacity to activate the expression of GL2 (Figure 1.8B), the blocker of the hair fate, and CPC inhibits the function of the WER-GL3/EGL3-TTG1 complex by interfering with WER binding to GL3/EGL3 in a competitive manner, leading to an inactive complex with respect to *GL2* expression (Figure 1.8B and C).

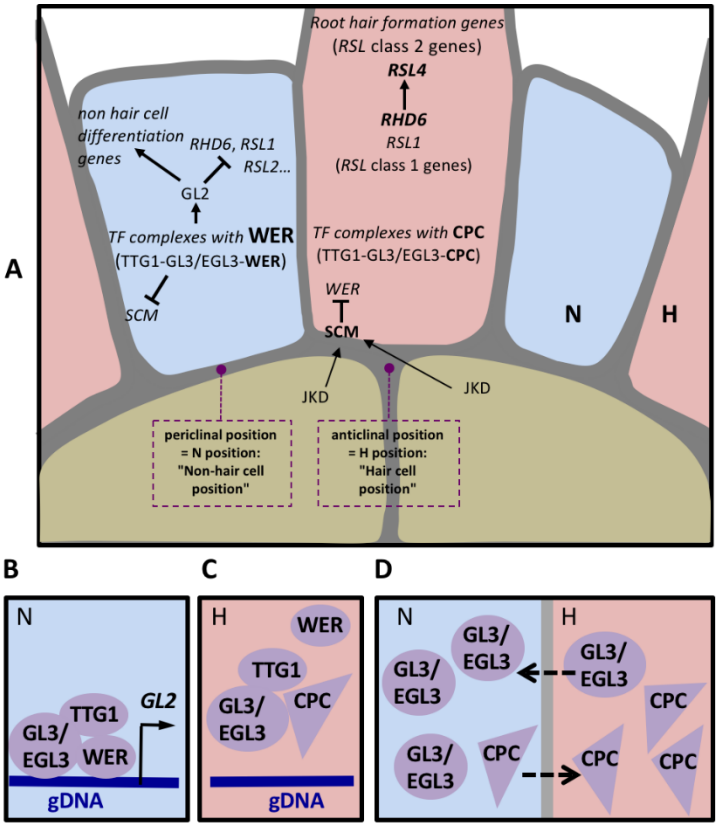

Figure 1.8. Trichoblast formation in *Arabidopsis* and complexes involved in formation or regulation of root hair formation.

A highly diversified series of processes (Reviews: Grierson *et al.,* 2014; Salazar-Henao *et al.,* 2016; Cui *et al.,* 2017), including epigenetic mechanisms as well as migration of CPC from N-position epidermal cells to their neighboring H-position cells, migration of GL3/EGL3 in the opposite direction (Bernhardt *et al.,* 2005) (Figure 1.8D) and transcriptional positive or negative feedback loops, results in a differential distribution of the WER and CPC complexes, the WER complex being present and active in N-position cells and the CPC complex in H-position cells. In the former cells, GL2 (whose expression is stimulated by the WER complex) inhibits the expression of genes encoding transcription factors (TF) required for root hair formation. In H-position cells, absence of GL2 block (Lin *et al.,* 2015) allows expression of ROOT HAIR DEFECTIVE 6 (RHD6), which plays a major role in root hair initiation and elongation, and of other TFs, amongst which ROOT HAIR DEFECTIVE 6-LIKE #1 and #2 (RSL1 and RSL2). Arabidopsis mutants harboring KO mutations in both RHD6 and RSL1 do not develop root hairs (Menand *et al.,* 2007). After root hair initiation (bulge formation), which involves integration of multiple mechanisms, elongation (tip growth) requires reorganization of organelle (nucleus, vacuole) position, polarized ion transport across the cell membrane and Ca^{2+} gradients, a special cytoskeletal organization, endomembrane trafficking, cell secretion, spatially distinct regulation of reactive oxygen species (ROS) production and distribution, cell wall production and modifications (Grierson *et al.,* 2014; Franciosini *et al.,* 2017). ROOT HAIR DEFECTIVE 6-LIKE 4 (RSL4), which is one of the direct targets of RHD6, is a major contributor to the expression of root hair cell-specific genes involved in root hair elongation. Positive regulation of root hair elongation by RSL4 involves stimulated transcription of genes playing a role in cell wall synthesis and modification, endomembrane transport and cell signaling (Yi *et al.,* 2010; Datta *et al.,* 2015; Shibata *et al.,* 2018).

Pharmacological and genetic approaches have provided evidence that plant hormones play a role in the control of epidermal cell differentiation and root hair development (Review: Cui *et al.*, 2017), and that auxin and ethylene, and their crosstalk, are major regulators of these processes (Bruex *et al.,* 2012; Zhang *et al.,* 2016). Evidence has also been obtained that jasmonic acid, strigolactone and cytokinine are positive regulators of root hair growth, whereas brassinosteroid and abscisic acid are negative regulators. Proper auxin distribution is required for correct cell fate assignment and root hair formation (both initiation site selection and tip growth). Auxin regulates root hair formation by acting downstream of *RHD6*, and probably primarily via *RSL4* (Masucci and Schiefelbein, 1996; Yi *et al.,* 2010). It is also worth to note that, as a consequence of its role in root hair tip growth, auxin is also involved in cessation of tip growth, and thereby in control of the final root hair length. The present model is that auxin is supplied to young hair cells by neighboring non-hair cells that transport auxin through the epidermis from the root tip toward the shoot. As the root tip grows away, maturing root hair cells receive less and less auxin, until the auxin supply is limiting and growth stops (Jones *et al.*, 2009). Ethylene acts on root hair formation at the same stage as auxin, downstream of *RHD6* (Masucci and Schiefelbein, 1996). The large overlap of ethylene- and auxin-induced genes (Bruex

et al., 2012) suggests that the pathways allowing these two hormones to affect root hair formation are significantly congruent.

Analyses of this highly complex network of developmental processes in Arabidopsis provide information on how external biotic or abiotic conditions, such as presence of PGPR strains promoting root hair development or low availability of nutrient ions, are integrated into the intrinsic genetic programs and hormonal controls to impact epidermal cell differentiation and root hair morphogenesis. ROS homeostasis and hormones have been shown to play crucial roles in integration of environmental cues (Zhang *et al.,* 2016; Camacho-Cristobal *et al.,* 2015). Auxin and ethylene again appear as the major integrators of these external cues, but other hormones also contribute to this process (López-Bucio *et al*., 2007; Lee and Chao, 2013; Poupin *et al.,* 2016; Cui *et al.,* 2017). For instance, the widely reported increase in root hair density and length in response to low Pi (Bates and Lynch, 1996; Ma *et al.,* 2001; Janes *et al.,* 2018) involves CAPRICE and its partly redundant functional paralogs, TRY and ETC1 (see above) (Chen and Schmidt, 2015), as well as enhanced synthesis and increased half-life of *RSL4* (Datta *et al.,* 2015) and induction of root hair expressed auxin-inducible transcription factors, including RSL2 and RSL4 (Bhosale *et al.,* 2018). Also, promotion of root hair development by PGPR species has been shown to involve auxin (Zamioudis *et al.,* 2013), ethylene (Ribaudo *et al.,* 2006; Galland *et al.,* 2012), as well as complex interplay of auxin and ethylene signaling pathways (Poupin *et al.,* 2016). It should however be noted that a PGPR-induced promotion of root hair elongation that was poorly dependent on auxin and ethylene signaling mechanisms has also been reported in Arabidopsis (López-Bucio *et al.,* 2007).

The mechanisms involved in root hair cell specification and development are still insufficiently characterized in species displaying type 1 or type 2 epidermal patterning, *e.g.* in cereals (Marzec *et al.,* 2015; Dolan *et al.,* 2017; Huang *et al.,* 2017). It should however be noted that comparative transcriptomic analyses of root hair development genes from Arabidopsis and 6 other vascular plants, including eudicots and monocots (tomato, cucumber, soybean, rice, maize, all these species displaying type 1 epidermal patterning) and a lycophyte (*Selaginella moellendorffii*), have revealed substantial divergence in the structure and expression of genes used for root hair patterning in Arabidopsis, which led to conclude that the Arabidopsis WER/CPC patterning process is not shared by other species (Huang *et al.,* 2017). In contrast, root hair initiation and elongation (bulge initiation and tip growth) involves a widely conserved core set of root hair genes, probably derived from an ancient program for unidirectional cell growth and coopted during vascular plant evolution (Menand *et al*., 2007; Huang *et al.,* 2017). Indeed, close homologs of *AtRHD6* and of its partly redundant paralog *AtRSL1*, which both identify (based on sequence similarities) the so-called *RSL* class 1 (*RSL* class 2 comprising *RSL4* and its homologs), appear to be present in every land plant, mosses, lycophytes, eudicots and monocots, and to function similarly in divergent species (Menand *et al.,* 2007; Pires *et al.,* 2013). Altogether, these results suggest that *RSL* class 1 genes would play a role in root hair initiation and growth in type 1 and type 2 epidermal patterning similar to the one played

by *RHD6* in the patterning displayed by *Arabidopsis*, but that the mechanisms controlling the expression of these *RHD6* counterparts would be different from the *Arabidopsis* WER/CPC system.

Finally, it is important to note that control of root hair longevity could be of major importance in root system adaptation to soil abiotic and biotic factors. Root hair longevity is still poorly documented. Reported values in a given species, barley, varies from few days to 2-3 weeks (McElgunn and Harrisson, 1969; Holden, 1975; Henry and Deacon, 1981). The wheat seedling shown in Figure 1.1 was 2-week old. Evidence has been obtained that apoptose-like programmed cell death (AL-PCD), characterized by protoplast retraction, nuclear DNA fragmentation and sensitivity to inhibitors of caspase-3-like activity, occurs in Arabidopsis root hairs in response to heat shock, salt stress and ROS (H_2O_2) treatment (Hogg *et al.,* 2011; Tan *et al.,* 2016). Basal AL-PCD rates ranging from *ca.* 5% to 15% have been monitored in *Arabidopsis* seedlings classically grown on agar plates (Tan *et al.,* 2016). Thus, the presence of root hair zones (in broad sense) and root hair density might be regulated by AL-PCD in response to local environmental conditions.

1.8. QTL of root hair development and relation with plant yield

Different studies carried out in cereals, essentially in barley, wheat or maize, aim at assessing the possibility to exploit the natural variation in root hair length in order to develop improved cultivars allowing sustainable yields under low input (fertilization and irrigation) conditions. In barley, for example, a founding and reference work in this domain has explored the biological diversity within 38 cultivars, revealing a *ca.* 4 fold variations in root hair length, from about 0.4 mm to more than 1.3 mm, in hydroponically grown plants, consistent with variations thereafter observed in control experiments carried out in field conditions (Gahoonia and Nielsen, 2004). Then, a set of 10 representative cultivars was tested in field experiments, with different levels of soil P availability/fertilization. The whole set of results indicated that barley genotypes with long root hairs displayed higher tolerance to low P conditions and expressed higher yield potentials both in low and high P soils. Similarly, characterization of barley mutant lines with various root hair phenotypes, screened from an ethylmethane sulfonate (EMS) mutagenized population showed that root hair length was important for shoot P accumulation and biomass production, especially when the plants were grown under combined water and phosphorus stress (Brown *et al.,* 2012). For grain yield, however only the presence of root hairs, and not root hair length, was critical. It is however worth to note that the difference in root hair length between the genotypes classified as “Short Root Hair” and “Long Root Hair” (0.543 mm against 0.69 mm) in these experiments was rather small when compared with the differences observed within the set of barley cultivars previously used by Gahoonia and Nielsen (2004). Evidence that plant biomass production can be positively correlated to root hair length in barley has also been provided by phenotyping 175 lines from a doubled-haploid (DH) population, using rhizosheath size as a reliable surrogate for root hair length and NDVI (normalized difference vegetation index) as a surrogate for crop biomass, which revealed that

major QTLs (quantitative trait loci) for root rhizosheath size were associated with NDVI-estimated mass (Gong and McDonald, 2017). None of the QTLs for rhizosheath size and grain yield however overlapped or were collocated. The fact that higher biomass production did not translate into greater grain yields in these experiments might have resulted from the complex link between vegetative growth and grain yield in rainfed systems (Ahmed *et al.,* 2018).

Analyses of several populations have also identified QTLs of root hair length in maize (Zhu *et al.,* 2005) and wheat (Delhaize *et al.,* 2015; Horn *et al.,* 2016; James *et al.,* 2016; Liu *et al.,* 2017). It has also been shown that large rhizosheaths, compared with small rhizosheaths, can increase shoot biomass due to improved P nutrition (Zhu *et al.,* 2005; James *et al.,* 2016). QTLs for root hair length have been found to collocate with QTL for yield components in wheat (Horn *et al.,* 2016) but further work is still required to investigate whether, and in what environmental conditions longer root hairs actually benefit to grain yields.

* *

*

In summary, the objective of reducing fertilization and irrigation inputs in order to progress towards more sustainable agricultural practices has resulted in increased efforts of research on plant roots and their interactions with beneficial soil microbes (Lynch, 2007). Evidence is clearly available now that, in the rhizosphere, root hairs play major roles in both nutrient uptake and interactions with beneficial microbes. However, many major questions regarding root hair development and functions have to be further investigated, like for instance the mechanisms involved in epidermal cell fate in species different from Arabidopsis and displaying a root hair patterning corresponding to the so-called type 1 or type 2, or the environmental and internal determinants of root hair longevity and apoptose-like programmed cell death. Also, at a more applied level, regarding crop breeding and agricultural practices, the impact of selection procedures in artificialized soil conditions on root hair ability in elite varieties to engage beneficial interactions with soil microbes at the cost of intense exudation of photosynthates and organic compounds into the rhizosphere deserves to be thoroughly investigated.

A major difficulty in investigating the effects of biotic and abiotic environmental factors on root hair development and activity is that this cell type is not straightforwardly amenable to experimental studies except when seedlings can be grown on agar plates for few days, like in the case of *Arabidopsis*. This has probably contributed to the fact that the present knowledge at the molecular level about root hair development and functions has been mainly gained in this species. Furthermore, very few methods have been developed allowing to phenotype root hair development in conditions other than growth on agar plates.

Objectives of thesis

My PhD project has been aimed at identifying bacterial strains from a soil located in Lebanon (part of the *Fertile Crescent* where wheat domestication occurred), at investigating the effects of isolated strains on wheat growth and nutrient element contents, and at developing procedures for phenotyping root hair development and responses to environmental conditions in this species.

Chapter 2

Material and methods

2.1. Wheat seed sterilization

Seeds of *Triticum turgidum* spp. durum (cv. Oued Zenati) were immersed in *ca.* 15 mL of calcium hypochlorite solution (40 $g.L^{-1}$) contained in a 35 ml pot that was then transferred under the vacuum (*ca.*15 minutes; shaking after 7 minutes) to allow the solution to completely penetrate the seed surface after elimination of air bubbles. The pot was then transferred in sterile atmosphere (in a laminar flow hood) and the seeds were washed 5 times with sterile water at room temperature. After the 5^{th} wash, the seeds were transferred into a pot containing sterile "hot" water (at about 40°C, with a ratio of *ca.* 1 seed per ml) extemporaneously prepared by mixing 4 volumes of room temperature water with 1 volume of boiling water. This treatment (traditionally used by Vietnamese farmers for rice seeds) stimulate germination. The pot was then transferred into a culture chamber at 26˚C in the dark, for at least one night.

2.2. Seed germination and pretreatment

Under laminar flow, the sterilized seeds were transferred onto a piece of filter paper soaked with sterile water in a Petri dish (120 mm × 120 mm × 15 mm; nine seeds per Petri dish; Figure 2.1, panel A). Seeds were germinated in the dark at 26°C for at least 2-3 days.

Selected seedlings displaying 3-4 cm-long roots and a visible hypocotyl (Figure 2.1, panel B) were transferred to new Petri dishes containing 20 ml of PBS solution, the roots being immerged in the solution but not the shoots (Figure 2.1, panel C). The solution had been added or not with a selected bacterial strain, allowing to get inoculated or non-inoculated plants, respectively. For the inoculation treatment, the bacterial suspension in PBS had been prepared by mixing 19 ml of sterile PBS solution with 1 ml of bacterial suspension (OD_{600} of the suspension: 0.1) prepared in PBS.

A treatment with a sulfur suspension was then applied to the seedling grains to avoid fungal contamination in rhizoboxes. The grains were "painted" with the sulfur suspension (prepared with *ca.* 640 mg of micronized sulfur, Neudorff, per ml of water). After the sulfur coat had dried, the grains were "painted" again. Three successive coats were thereby applied before the seedling was used for experiments (see below).

2.3. Nutrient solution

Various nutrient solutions were used, all derived from the Hoagland solution, but differing in their contents in the macro-nutrients N and P. Their composition is provided in the legend or text accompanying the corresponding figures.

The most often used solutions differ in their total N concentration.

The low N solution (LN) contained 0.1 mM NH_4NO_3, 0.5 mM KNO_3, 2.0 mM $CaCl_2$, 2.0 mM $MgSO_4$, 1.0 mM KH_2PO_4, 0.5 mM Na_2SiO_3, 0.1 mM NaFe (III) EDTA, 0.0125 mM H_3BO_3, 0.002 mM $MnCl_2$, 0.003 mM $ZnSO_4$, 0.0005 mM $CuSO_4$, 0.0001 mM Na_2MoO_4, 0.0001 mM $NiSO_4$ and 0.025 mM KCl.

The corresponding high N (HN) solution had the same composition except that KNO_3 was added at 5 mM instead of 0.5 mM. Thus the total N concentration in the LN and HN solutions were 0.7 and 5.2 mM, respectively.

When compared with HN solution, LN solution displays a decrease in the concentrations of both NO_3^- and K^+ due to the reduction in KNO_3 concentration from 5 mM to 0.5 mM. We however considered that the concentration of K^+ in LN solution was high enough due to the presence of 1 mM KH_2PO_4 and that K^+ was therefore not likely to be a limiting nutrient in LN solution.

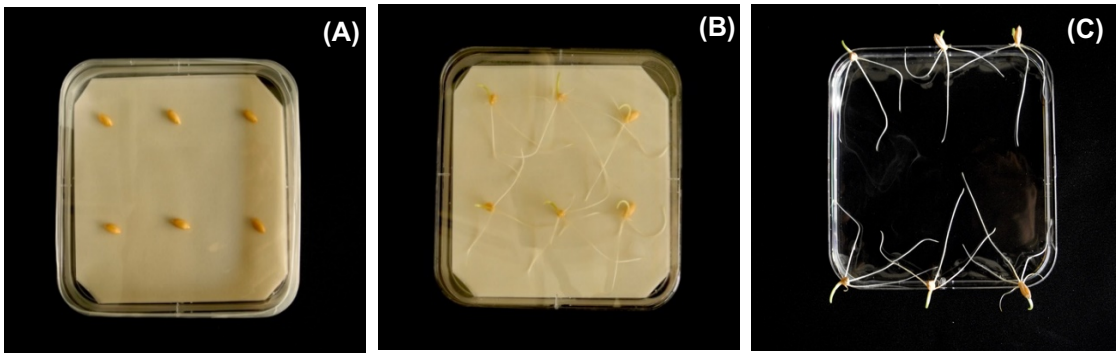

Figure 2.1. Wheat seed germination. After the sterilization treatment (with calcium hypochlorite solution; see main text), the seeds were transferred onto a piece of sterilized filter paper soaked in 15 mL of sterilized water in a Petri dish (Panel A). They were then kept in dark conditions at 26 ˚C for at least 2 or 3 days until they displayed 3-4 cm-long roots and a visible hypocotyl (Panel B). Selected seedlings were then transferred onto a new Petri dish filled with 20 ml of PBS solution for 90 min in presence (inoculation) or absence of the tested bacterial strain (Panel C). Before seedling transfer to the rhizobox or cuvette devices, the grains were painted (3 coats) with of a suspension of sulfur (about 480 mg of micronized sulfur, Neudorff, per ml of water. This treatment prevented grain fungal contamination (leading to root contamination) during growth.

2.4. Growth on agar plates for root hair phenotyping

Germinated seedlings were transferred onto agar plates (half-strength derived Hoagland medium unless otherwise indicated, and 12 $g.L^{-1}$ agar), one plant per Petri dish as described in Figure 2.3. Inoculated medium was obtained by mixing 100 µL of bacterial suspension (OD_{600} = 0.1) in 30 ml agar medium before pouring into the Petri dish. The Petri dish was ¾ wrapped with black plastic (ensuring root protection against light) before being transferred into an Aralab growth chamber: day/night photoperiod 8/16 hours, day/night temperature 23/20°C and 70% air humidity. It was placed in a quasi-vertical position (angle of around 85°) so that roots preferentially grew at the agar surface (and not in the atmosphere of the dish above the agar). Growth took place for 72 h in these conditions. The seminal roots displayed root hairs developed on the surface of agar medium (Figure 2.3).

Photos of the roots were taken at 1 cm from the root tip unless otherwise stated using an Olympus binocular (bright field mode). After contrast adjustment, the images were analyzed (essentially root hair length measurements) using ImageJ.

2.5. Plant growth in "cuvette" devices for root hair phenotyping under microscope

Seedlings (the grain of which had been pretreated with the sulfur suspension; see above) were then transferred to acrylic devices called “cuvettes”, built using a 3D printer (Figure 2.2A). The device was designed to allow precise observation of root hairs from the plant under microscope and to try to avoid any root hair damage that could result from sample preparation and transfer onto a microscope glass slide. A detailed description of the "cuvette" device is provided in Chapter 4.

Each cuvette was designed to receive one seedling. The transfer was done under laminar flow with the aim of avoiding possible contamination at this stage. The main seedling root was slipped into a pipe connecting the upper inner part of the cuvette to its lower inner part. The seed was placed on the upper part of the device. Subsequently, the pipe was sealed close to the seed using a moulting material (Coltène President microSystem, light body, Coltène/Whaledent AG, Altstätten, Switzerland). The cuvette was then placed into a container filled with nutrient solution, the seed grain being at about 1 cm of the level of the solution. A device allowing to pump out the solution and to recirculate it in order to refill the container was set up, allowing re-oxygenation of the solution within the cuvette and thereby of the developing roots (see Chapter 4).

Plant growth took place for *ca*. 3 days in a growth chamber: 16 h photoperiod, day/night temperature 22/20˚C, 150 µE light intensity, and 70% air humidity. The cuvettes were warily taken out of the hydroponic solution in order to avoid damage to root hairs, gently dried with a piece of tissue paper, and horizontally placed so that the roots laid on the glass coverslip. Droplets of LN solution were deposed onto the root until the main root was covered (see later, Figure 4.6). Images were taken at a given

distance from the root tip (1 cm or otherwise indicated in the corresponding figure legends) with a Zeiss Apotome device at x5 magnification (Microscope Zeiss Apotome, Bright field, Z-stacks mode).

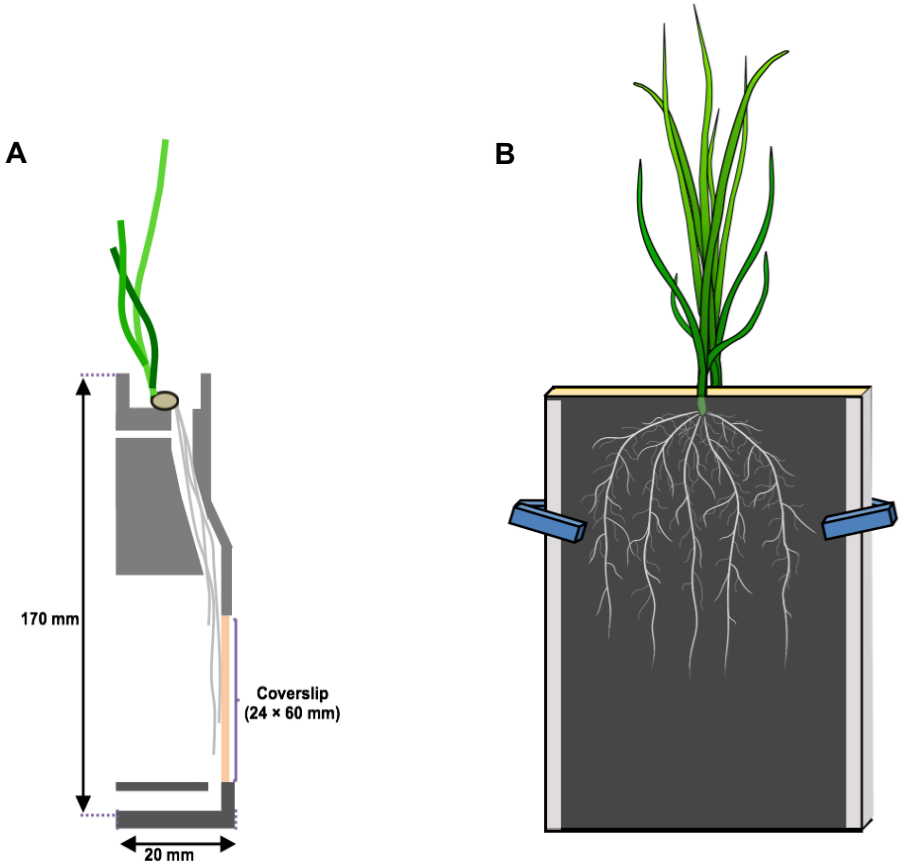

Figure 2.2. The cuvette and rhizobox prototypes currently used for root hair trait phenotyping:

(A) Cuvette. See also Figures 4.2 to 4.6.
(B) Rhizobox. See also Figures 4.13 to 4.15.

Figure 2.3. Plant growth on agar plate for root hair phenotyping. See main text.

2.6. Plant growth in rhizoboxes for root system and root hair phenotyping

A detailed description of the glass-wall rhizobox device we have developed in Chapter 4. Two seedlings were set per rhizobox, one on each side of the rhizobox. The roots grew between the plexiglass plate and a polyester dark tissue covering a thin board of polyurethane foam, that was periodically watered, in the center of the rhizobox (Figure 2.2B). In order to prevent light to reach the root system, the rhizobox sides and top were covered with a light-protecting structure (made of a thin polystyrene board covered with an aluminium foil). The rhizoboxes were set on a support system that allowed to stack together 6 rhizoboxes per experiment/treatment (12 plants per treatment). The supporting system also permitted the set-up of an automatic irrigation device on the top of the rhizoboxes (see Chapter 4, Figures 4.14 and 4.15). Plant growth took place for *ca*. 12 days in a growth chamber (16 h photoperiod, day/night temperature 22/20˚C, 150 µE light intensity, and 70% air humidity, as in the case of plants grown in "cuvettes", see above). High definition image (48-bits, 1,200 ppp) of root systems from plants grown for 12 days in rhizoboxes were taken using an Epson Perfection V850 Pro Scanner.

2.7. Growth in growth chamber on artificial soil for phenotyping biomass production, nutrient element contents and root system development

This experiment was aimed at investigating the effects of various diazotroph strains on wheat growth in "artificial soil" in a growth chamber. Durum wheat seedlings (Oued Zenati cultivar) were grown in pots in the presence of a high or low concentration of NO_3^- (in the watering solution) and presence or absence of different diazotrophs strains. Twelve strains of diazotroph bacteria were checked: (i) the *Bradyrhizobium japonicum* strain ORS285 and *B.* strain ORS285Δ*nif* (abbreviation: Brad and BradΔ*nif*)

strains, obtained from Dr. Nico Nouwen (IRD Montpellier), (ii) *Frankia* sp. R43 (abbreviation: Frankia) strain, obtained from Prof. Philippe Normand, Université de Lyon, (iii) *Azospirillium lipoferum* 4B (abbreviation: Azo4B) strain and *Azospirillium brasilense* Sp245 (abbreviation: AzoSp245) strain obtained from Prof. Guilhem Desbrosses, Université de Montpellier and (iii) the Lebanese A10, B1, B3-1 B-3-2,H2, I1-2 and I1-3 (abbreviation: A10, B1, B3-1, B3-2, H2, I1-2 and I1-3) stains that we directly isolated from wheat rhizosphere from Lebanon soil samples (see Chapter 3).

Peat moss/sand/perlite (1/1/1, v/v/v) was sterilized in an autoclave, dispatched into pots (about 170 g of substrate per pot) and inoculated or not inoculated (control plants) with a selected bacterial strain. In the former case, inoculation was achieved by watering the substrate with 20 mL of bacterial suspension per pot. The bacterial suspension was prepared by mixing 19 volumes of sterile PBS solution to 1 volume of bacterial suspension (in PBS) displaying an O.D. at 600 nm of 0.1.

Durum wheat seedlings (3-day-old), with root length of about 2-3 cm, obtained as described in § 2 and Figure 2.1 (except that the grain was not treated with sulfur suspension), pre-inoculated with the tested bacterial strain or not inoculated (control plants), were transferred to pots, one seedling per pot. Every pot was covered with plastic film for preventing contamination by other microbial strains during the growth period.

The plants were grown for 30 days in a growth chamber (16 h photoperiod, day/night temperature 22/20˚C, 150 µE light intensity, and 70% air humidity) before being sampled for phenotyping (visual aspect of the plants before harvest: see Figure 2.4). During the 30 d growth period, the plants were periodically watered with HN or LN solution (composition: see § 2.6), every 3 days with 20 mL of solution per pot.

Plants were sampled at the end of the 30-day growth period. The root systems were excised from the shoots and carefully washed in order to take photographs of root system architecture. Root and shoots were dried (80°C, 7 days), weighted (DW biomass), and crushed into powder using a porcelain mortar and pestle before assaying their contents in C, N, K, P, Na, Ca, Mg, Mn, Fe, Cu and Zn.

Root architecture imaging. Roots were separated from the artificial soil by washing (5 to 6 times) unit the soil particles were completely removed before imaging. The root system immerged in water in a transparent tray was transferred onto a scanner (Epson Perfection V850 Pro Scanner) for imaging (24-bits, 800 ppp). Images were prepared using *ImageJ* facilities (image > adjust > threshold > B&W) and then analyzed with the IJ Rhizo tool (Pierret *et al.,* 2013). See Figure 2.5.

Carbon and Nitrogen content measurements. Samples (1 to 2 mg DW) were analyzed for total carbon and nitrogen by Elementar Pyrocube analyzer (Elementar France Lyon France). Each value is the mean of 4 technical replicates.

Macro- and micro- element assay. Samples (10 mg DW) in TPE tubes were digested under fume-hood with 750 µl of 65% nitric acid and 250 µl of 30% H_2O_2 for 8 to 16 hours (until gas production could not been observed), and then treated at 85°C

for 8 hours. When plant tissue particles could no longer be distinguished in the digestion solution, which then displayed a transparent yellowish color, the solutions were diluted by addition of 4 mL of miliQ water. Weighted samples of extraction liquids were then transferred into tubes adapted to an autosampler (Agilent PPP tube). Each sample was analyzed for P, K, Na, Ca, Mn, Fe, Mn, Zn and Cu using a microwave-plasma atomic emission spectrometer (MP-AES, Agilent. Each treatment is the mean of 5 biological replicates.

2.8. Location of the Lebanon soil sampled for isolating N_2-fixing bacteria and soil analyses

Soil samples were taken by Houssein Zhour (PhD student in our group) from a *durum* wheat field in Zawtar Al-sharkiya village, Nabatiyeh city, Lebanon. The site is situated at latitude 33° 19' 28.5" N and longitude 35° 28' 8.83" E, at the altitude of 460 meter above sea level (Figure 2.6). Soil samples were randomly collected from rhizosphere adhering to roots harvested at a depth of 5 to 10 cm at 5 locations in the field and mixed together to get a composite soil sample.

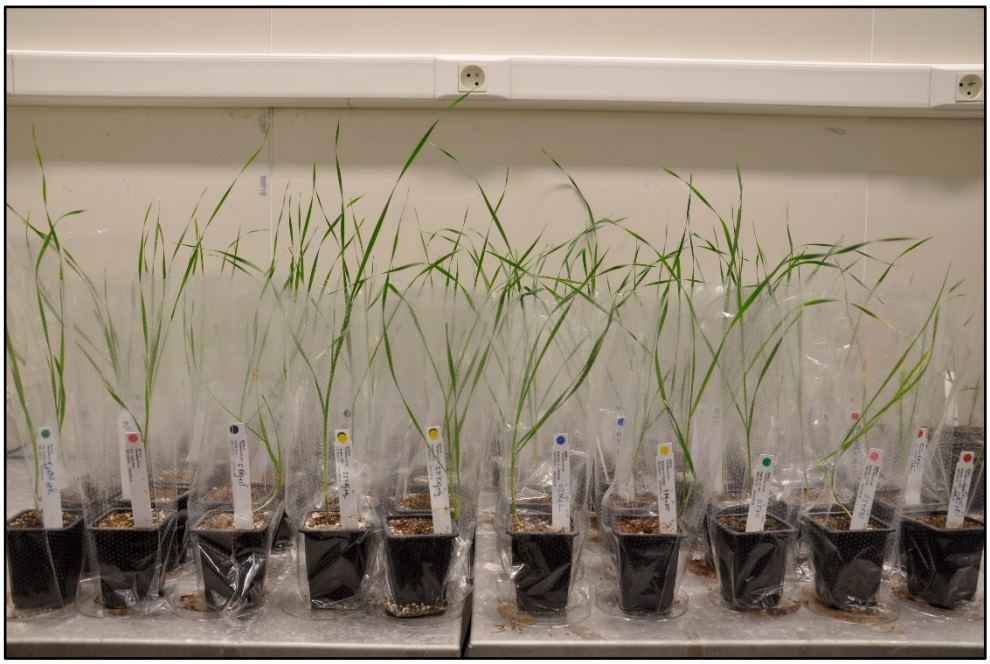

Figure 2.4. Visual aspect of the *durum* wheat plants at the end of the 30-day growth in growth chamber.

The soil sample was dried at 50°C (5 days) ground using a mortar and pestle and sieved (12 mm. mesh siever). Samples were suspended in distilled water (1:4 w:v). Analysis of soil physico-chemical parameters was carried out (Table 2.1) after large particles had settled down.

The percentages of sand, silt and clay (soil texture analysis) in soil samples were determined using the hydrometer method. The pH of the suspension was determined using a pH electrode. Electrical conductivity of the soil was determined in the filtrate of the water extract using a conductivity meter. Organic matter (OM) was determined using the protocol described by Walkley and Black (1934). Total nitrogen was estimated by the Kjeldahl method, and available phosphorus by the vanado-molybdate method (Jackson, 1973) following digestion with HNO_3-$HClO_4$. Available potassium, exchangeable calcium, exchangeable magnesium, exchangeable sodium, exchangeable iron, manganese, exchangeable zinc and exchangeable cupper contents were measured by the Atomic Absorption Spectrometry (AAS) (Table 2.1).

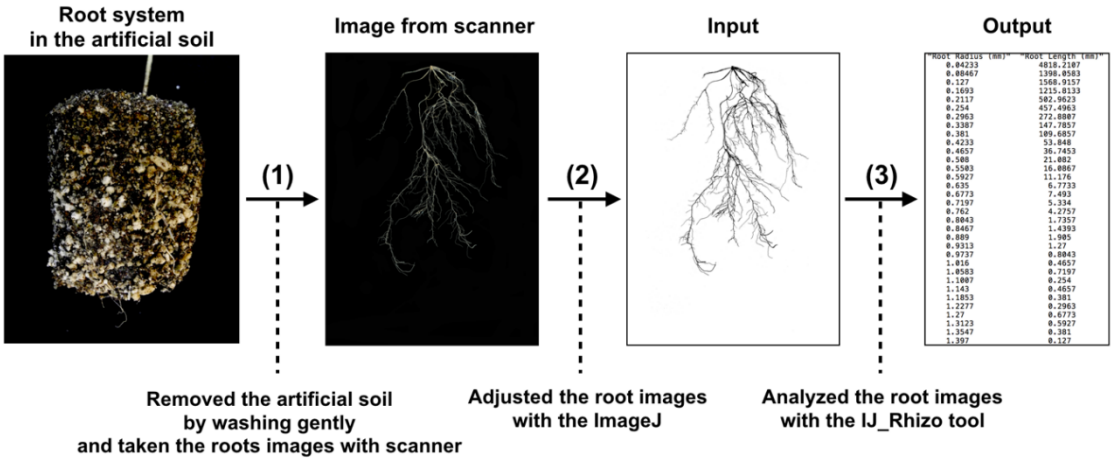

Figure 2.5. Imaging root systems from plants grown in artificial soil for 30 days.

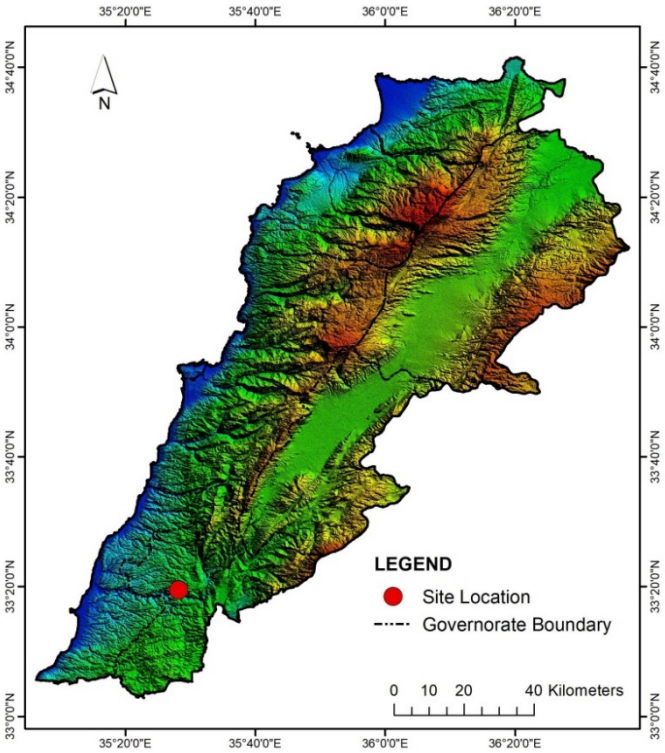

Figure 2.6. Bacterial strain collection site in Zawtar Al-sharkiya village, Nabatiyeh city, Labanon. Soil samples prepared from wheat root rhizosphere were collected by Houssein Zhour, PhD student in our group.

Table 2.1. Physio-chemical properties of the soil at the collection site in Zawtar Al-sharkiya village.

Parameters	Value	Remarks
Physical properties		
Soil textural class	Silt	-
Sand (%)	5.01	-
Silt (%)	92.06	-
Clay (%)	2.93	-
Chemical properties		
pH (H_2O)	5.78	Moderately acidic
EC ($ds.m^{-1}$)	0.12	-
Organic matter (%)	2.267	High
Total N (%)	0.155	Low
Available P (ppm)	166.4	High
Available K (ppm)	701.3	High
Exchangeable Ca (ppm)	7,289.7	High
Exchangeable Mg (ppm)	227.3	High
Exchangeable Na (ppm)	32.4	Optimum
Exchangeable Fe (ppm)	18.5	Low
Exchangeable Mn (ppm)	48.9	Medium
Exchangeable Zn (ppm)	9.2	Optimum
Exchangeable Cu (ppm)	12.2	High

2.9. Isolation of N_2-fixing bacteria from soil samples

Rhizosphere soil (50 mg) was directly transferred onto the surface of semi-solid nitrogen-free NFb medium containing 10 $mg.L^{-1}$ of the pH indicator bromothymol blue (NFb: Nitrogen Fixation Bromothymol medium; Baldani *et al.,* 2014) in a vacuette® tube closed with a rubber septum cap (5 mL of NFb per vacuette®) (Figure 2.7). After incubation of 3 days at 28°C, a typical diazotrophic bacterial pellicle could be seen at the surface/subsurface of the medium, with a yellowish orange color, due to the shift in color of the bromothymol blue pH indicator (Figure 2.8). An ARA test (Acetylene Reduction Assay) was performed to assess bacterial N_2 fixation ability at this stage. This was achieved by injecting C_2H_2 into the vacuette® tube and assaying C_2H_4 24 h later (see below). Then, 50 µL of the diazotrophic bacterial pellicle was transferred into a new vacuette® tube for a new round of selection of N_2 fixing bacteria on NFb medium. Four rounds of selection/purification were performed in total (Figure 2.7). At the end of the 4^{th} round, one ml of bacterial pellicle was diluted (10^{-6}) and 0.1 mL of the resulting bacterial suspension was spread onto a LB agar plate, allowing to count the number of bacteria and to assess the diversity of colony morphology after incubation for 4 days at 28°C. Morphology of randomly chosen colonies was visually characterized, in terms of form, height, color and margin aspect. Different types of colonies were then picked up and streaked onto NFb agar plates, which were incubated at 28°C for 4 days. One loopfull of bacteria was then transferred into 1 mL of sterile PBS buffer. Each suspension was homogenized *ca.* 1 min on a vortex mixer and then centrifuged at

14,000 rpm for 10 min. The supernatant was discarded and the pellet was washed 3 times in same buffer. Then, 50 μL of each suspension was inoculated onto 5 ml of semi-solid NFb medium in a vacuette® tube and incubated at 27°C for 3 days (Round 5). A 6th and last selection round was then performed, and N_2 fixation ability confirmed (Figure 2.7), before bacteria were resuspended in 50% glycerol solution and stocked at -80 °C.

ARA tests were performed as described by Mirza *et al.* (2001). Acetylene (10% v/v) was injected to the vacuette® tube, whereas tubes without acetylene were used as the controls. After 24 hours at 27°C, 10 ml of gas samples were taken from each tube for C_2H_4 assay using a gas chromatography (GC) analyzer. The results were expressed in nmol of C_2H_4 produced per tube and per day.

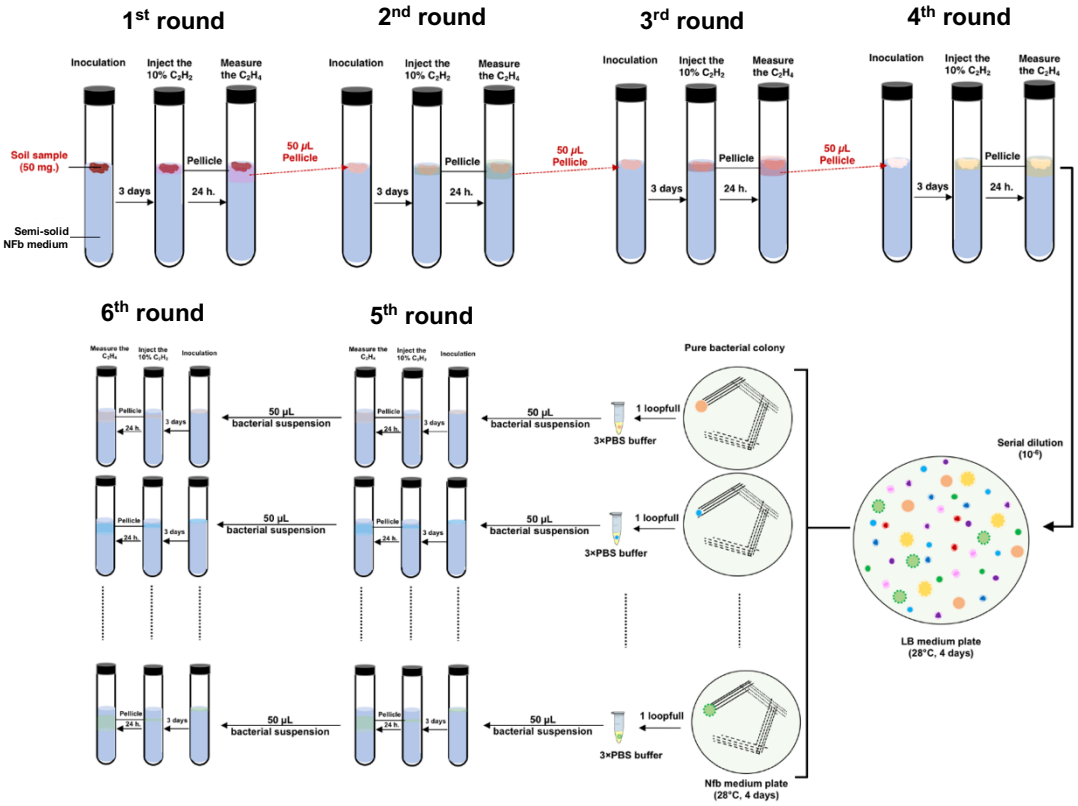

Figure 2.7. Diagram showing all the steps applied to count and isolate the diazotrophic bacteria from the rhizospheric soil.

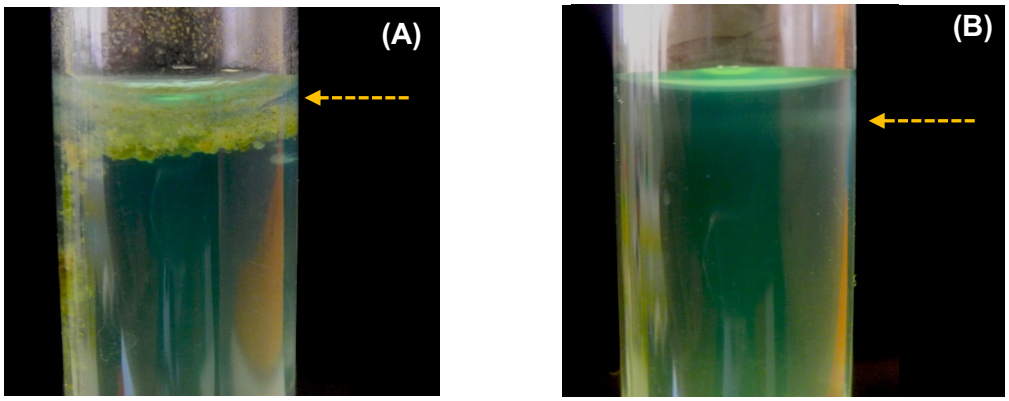

Figure 2.8. Surface/subsurface pellicle formed 3 days of 1st round (A) and 4th round after inoculation. The orange arrows in the figures indicate the pellicle of the diazotrophic bacterial during growth in the semi-solid NFb medium.

2.10. Tests of bacterial ability to use insoluble sources of phosphate and potassium

Bacterial ability to use insoluble sources of P was assessed by introducing an insoluble phosphate salt, tricalcium phosphate, as the only source of P in the growth medium. Each bacterial suspension (15 μL) was spot inoculated on Pikovskaya's (PVK) medium plates (Pikovskaya, 1984) containing ($g.L^{-1}$) 10 glucose, 0.1 $(NH_4)_2SO_4$, 0.2 KCl, 0.25 $MgSO_4.7H_2O$, 5 $MgCl_2.6H_2O$ and 5 $Ca_3(PO_4)_2$ (tricalcium phosphate) and 12 $g.L^{-1}$ agar, pH adjusted to 7 with 1 M HCl. Before pouring into Petri dishes, the medium was supplemented with bromocresol purple as a pH indicator (150 μL of 5 $g.L^{-1}$ bromocresol purple in 0.2 N KOH per 20 ml of PVK medium). The plates were incubated at 27°C for 3 days and then observed for the formation of yellowish halo zone around the inoculation spot (Figure 2.9). The pH indicator bromocresol purple (pKa value of 6.3) is violet above pH 6.8 and turns to yellow below pH 5.8. Hence, the color of the inoculated medium turns from a purple-blue color to yellow if the external pH is decreased due to bacterial development and the resulting release of CO_2 and H^+. Thus the color and size of the halo zone around the spotted bacteria reflect bacterial development, and are thus indicative of the ability of the tested bacteria to use the insoluble phosphate salt as a source of P. Bacteria endowed with efficient ability to use insoluble sources of P are generically named PSB for Phosphate Solubilizing Bacteria.

Still in presence of tricalcium phosphate as the single P source, the bacterial ability to also use insoluble sources of K^+ was assessed by introducing an insoluble potassium

salt, potassium aluminosilicate, as the only source of K^+ in the growth medium. Fifteen microliters of each bacterial suspension was spot inoculated on modified Alexandrov medium (Rajawat *et al.,* 2016) containing ($g.L^{-1}$) 5 glucose, 2 Ca_3PO_4, 0.2 KCl, 0.05 $MgSO_4.7H_2O$, 0.1 $CaCO_3$, 0.005 $FeCl_3$, 2 $KAlSi_3O_8$ (potassium aluminosilicate: Potash Feldspar, Bath Potters' Supplies, Somerset, UK) as insoluble potassium source, and 12 $g.L^{-1}$ agar, the final pH being adjusted to 7.2 with 1 M HCl. Before pouring into Petri dishes, the medium was supplemented with the pH indicator bromothymol blue (75 µl of 5 $g.L^{-1}$ bromothymol blue in 0.2 N KOH added per 20 ml of medium). The plates were incubated at 27°C for 3 days and observed for the formation of yellowish halo zone around the inoculation spot (Figure 2.10). The pH indicator bromothymol blue (pKa value of 7.1) is blue above pH 7.6, greenish-blue at pH 7, and yellow below pH 6.8. Thus, like in the above described test, the color and size of the halo zone around the spotted bacteria reflect bacterial development, and are thus indicative of the ability of the tested bacteria to use the insoluble K^+ salt as a source of potassium. Bacteria endowed with efficient ability to use insoluble sources of K^+ are generically named KSB for K^+ Solubilizing Bacteria.

The ability of phosphate solubilizing bacteria (PSB) to use insoluble Pi source and of K^+ solubilizing bacteria (KSB) to use insoluble potassium source (in presence of insoluble P source in our tests) was quantified using a so-called "*Solubilizing Index*", *SI*, as follows (Setiawati and Mutmainnah, 2016):

$$SI = \text{Halo zone diameter / colony diameter}$$

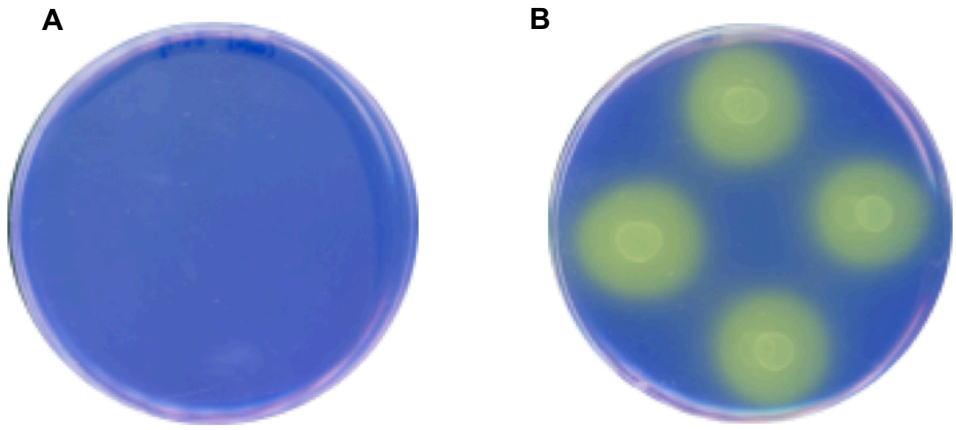

Figure 2.9. The Pikovskaya's medium plate containing bromocresol purple (A) and the appropriate nutrient medium inoculated with phosphate solubilizing bacteria (B).

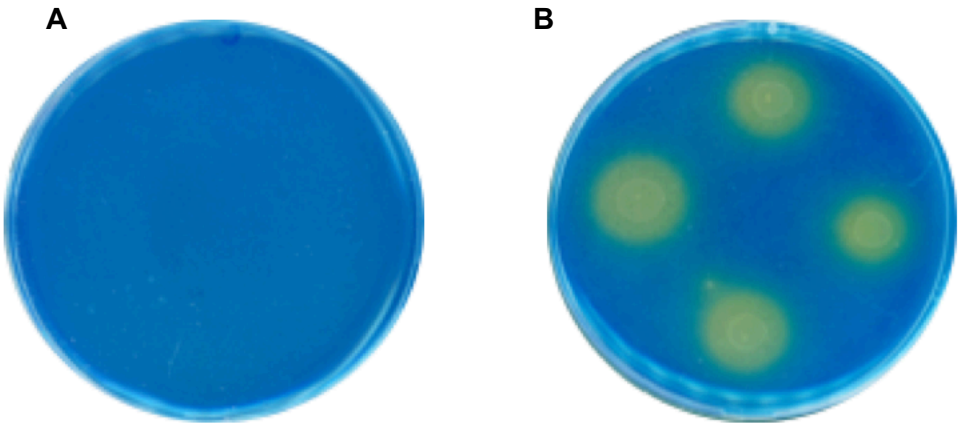

Figure 2.10. The modified Alexandrov medium plate containing bromothymol blue and medium plate inoculated with potassium solubilizing bacteria (B).

2.11. Bacterial cultures

The different bacterial strains that have been tested are listed in Table 2.2.

2.11.1. Growth media

(i) Bradyrhizobium japonicum ORS285 and *B. japonicum* ORS285*Δnif.* These bacteria were grown in YM medium (Vincent, 1970) which contains 5 $g.L^{-1}$ mannitol, 0.6 $g.L^{-1}$ K_2HPO_4, 0.1 $g.L^{-1}$ $MgSO_4.7H_2O$, 0.04 $g.L^{-1}$ $CaCl_2.2H_2O$, 3 $g.L^{-1}$ yeast extract, and 12 $g.L^{-1}$ agar, pH adjusted to 7 with 1 M HCl.

(ii) Azospirillum lipoferum strain 4B, *Azospirillum brasilense* strain Sp245, and rhizospheric bacteria isolated from Lebanese soil. These bacteria were grown in a modified NFb medium (modified from Baldani *et al.,* 2014). This medium contained 3.71 $g.L^{-1}$ malic acid, 0.509 $g.L^{-1}$ citric acid-Na_3, 0.53 $g.L^{-1}$ fructose, 0.265 $g.L^{-1}$ glucose, 0.5 $g.L^{-1}$ K_2HPO_4, 0.2 $g.L^{-1}$ $MgSO_4.7H_2O$, 0.02 $g.L^{-1}$ $CaCl_2.2H_2O$, 0.1 $g.L^{-1}$ NaCl, 2.8 $g.L^{-1}$ KOH, and 0.04 $g.L^{-1}$ yeast extract and micronutrients and vitamins as follows:
- micronutrients: 2.8 $mg.L^{-1}$ H_3BO_3, 2.35 $mg.L^{-1}$ $MnSO_4.H_2O$, 2.0 $mg.L^{-1}$ $Na_2MoO_4.2H_2O$, 0.2 $mg.L^{-1}$ $CuSO_4.5H_2O$, 0.6 $mg.L^{-1}$ $ZnSO_4.7H_2O$ (all the previous micronutrients being added from a 500x stock solution) and 65.6 $mg.L^{-1}$ NaFeEDTA (added from a 250x stock solution).
- vitamins: 0.1 $mg.L^{-1}$ biotin and 0.2 $mg.L^{-1}$ $pyridoxal_{HCl}$ (added from a 1000x stock solution).

Solid medium was obtained by adding 12 $g.L^{-1}$ agar in the above described solution, Semi-solid medium was obtained by replacing yeast extract and agar in the above described solid medium by 1.8 g of Bacto-Agar®. Unless otherwise stated, the final pH was adjusted to 7.5 with 1 M KOH.

For some experiments, the above described solid and semi-solid media were added with a pH indicator, bromothymol blue. This was achieved by introducing

(iii) Frankia. Frankia sp. R43 was grown in N-free BAP liquid medium (Murry *et al.,*1984), which contains 0.5 $g.L^{-1}$ NaPropionate, 0.95 $g.L^{-1}$ KH_2PO_4, 0.6 $g.L^{-1}$ K_2HPO_4, 0.025 $g.L^{-1}$ $MgSO_4.7H_2O$, 0.003 $g.L^{-1}$ $CaCl_2.2H_2O$, 0.45 $mg.L^{-1}$ Biotin, 7.5 $mg.L^{-1}$ $FeSO_4.7H_2O$, 5.6 $mg.L^{-1}$ $Na_2EDTA.2H_2O$ (added from a 1000x iron stock solution), 2.8 $mg.L^{-1}$ H_3BO_3, 1.8 $mg.L^{-1}$ $MnCl_2.4H_2O$, 0.1 $mg.L^{-1}$ $CuSO_4.5H_2O$, 0.2 $mg.L^{-1}$ $ZnSO_4.7H_2O$, 0.025 $mg.L^{-1}$ $Na_2MoO_4.2H_2O$ (micronutrients added from a 1000x stock solution). The final pH was adjusted to 6.4 with 1 M HCl.

2.11.2. Culture

*(i) All bacteria except Frankia. C*ultures were started from fresh single colonies. Each single colony was grown in 30 ml of nutrient medium at 30 °C on a rotary shaker at 300 rpm, until an optical density at 600 nm (OD_{600}) of 0.5 was reached. Then, the nutrient medium was centrifuged at 4,000 rpm for 20 min and pellets were washed three times in sterile PBS buffer (8 $g.L^{-1}$ NaCl, 0.2 $g.L^{-1}$ KCl, 0.24 $g.L^{-1}$ KH_2PO_4, and 1.44 $g.L^{-1}$ $Na_2HPO_4.2H_2O$, pH adjusted to 7 with 1 M HCl). Then, the cells were re-suspended in PBS, the final DO_{600} of the suspension for inoculation being adjusted to 0.1.

Table 2.2. Bacterial strains used in this study.

Bacterial strains	Sources
Bradyrhizobium japonicum ORS285	Dr.Nico Nouwen, IRD Montpellier
Bradyrhizobium japonicum ORS285 Δ*nif*	Dr.Nico Nouwen, IRD Montpellier
Frankia sp. R43	Pr. Philippe Normand, Université de Lyon
Azospirillium lipoferum 4B	Pr. Guilhem Desbrosses, Université de Montpellier
Azospirillium brasilense Sp245	Pr. Guilhem Desbrosses, Université de Montpellier
Lebanese A11 (*Stenotrophomonas* sp.)	This study
Lebanese B1(*Stenotrophomonas* sp.)	This study
Lebanese B3-1 (*Paraburkholderia* sp.)	This study
Lebanese B3-2 (*Achromobacter* sp.)	This study
Lebanese H2 (*Achromobacter* sp.)	This study
Lebanese I1-2 (*Achromobacter* sp.)	This study
Lebanese I1-3 (*Klebsiella* sp.)	This study

(ii) Frankia. *Frankia* was grown at 26°C in dark conditions for 2 weeks. The culture was homogenized for *ca.* 1 min on a vortex mixer and then centrifuged at 4,000 rpm for 20 min. The supernatant was discarded. The pellet (containing the so-called "hyphal" fragments) was mixed with 20 ml of sterile PBS buffer on a vortex mixer (*ca.* 1 min). The suspension was then centrifuged at 4,000 rpm for 20 min. The hyphal fragments were washed three times in sterile PBS buffer and finally resuspended in sterile PBS buffer (final OD_{600} close to 0.1). Bacterial suspensions were used to inoculate wheat seedling (5 wheat seedling per 20 mL of bacterial suspensions; see § 2.2) and sterilized artificial soil (170 g per pot; see § 2.7).

2.12. Molecular characterization of bacterial strains isolated from Libanese soil

DNA extraction. Genomic DNA was isolated from bacteria in hot (94 °C) sterilize miliQ water as described by Dashti *et al*. (2009). DNA concentration in the extraction solution was assayed using a nanodrop spectrophotometer (Nanodrop 1000, Thermo Scientific).

16S rRNA amplification. 16S rRNA segments were amplified using the two universal primers 27F and 1525R (primer sequences: see Table 2.3). PCR amplification was performed in a 25 µL reaction volume, prepared by mixing 1 µL of the tested bacterial DNA extract, 0.12 µL of 5 U μL^{-1} *Taq* DNA polymerase, 2.5 µL of 5×*Taq* polymerase buffer, 1 µL of 5 mM deoxynucleotide triphosphates (dNTPs), 2 µL of 25 mM $MgCl_2$ and 1 µL of each 10 µM forward 27F and reverse 1525R primer solutions, the final volume of the reaction mix being adjusted to 25 µl with water). After the initial denaturation, performed at 96°C for 5 min, the amplification phase comprised 35 cycles of 96 °C for 30 second, 57°C for 30 second and 72°C for 2 min, and final extension at 72°C for 10 min.

PCR amplification of nifH genes. Amplification of *nifH* gene fragment was achieved in 2 steps. The first round of amplification was carried out using the forward and reverse primers PolF and PolR, and the second round using the forward PolF and the reverse AQER primers (primer sequence: see Table 2.3).

For the first amplification round, the reaction medium (final volume 25 µL) was prepared by mixing 2 µL of bacterial DNA extract, 0.3 µL of 5 U μL^{-1} *Taq* DNA polymerase, 5 µL of 5×*Taq* polymerase buffer, 2 µL of 2.5 mM dNTPs, 0.5 µL of BSA (10 $mg.mL^{-1}$) and 0.625 µL of each 20 µM PolF and PolR primer solution (the final volume of the reaction mix being adjusted to 25 µL with water). The PCR reaction protocol was as follows: initial denaturation at 94°C for 5 min, then 30 cycles of 94°C for 1 min, 55°C for 1 min, 72°C for 1 min, and final extension at 72°C for 10 min.

For the second amplification round, the reaction mixture (25 µL) contained 0.5 µL of the PCR product obtained at the end of the first amplification round, 0.2 µL of 5 U μL^{-1} *Taq* DNA polymerase, 5 µL of 5×*Taq* polymerase buffer, 2 µL of 2.5 mM dNTPs, 0.5 µL of BSA (10 $mg.mL^{-1}$) and 0.625 µL of 20 µM PolF and AQER solutions (final

volume adjusted to 25 µL with water). The PCR protocol was the same as the one used for the first amplification round.

PCR amplification of BOX-A1R. The amplification reaction was carried out using the *BOX-A1R* primer (sequence: see Table 2.3). The amplification mixture contained 2 µL of bacterial DNA extract, 0.3 µL of 5 U μL^{-1} *Taq* DNA polymerase, 5 µL of 5× *Taq* polymerase buffer, 2 µL of 2.5 mM dNTPs, 2 µL of 25 mM $MgCl_2$ and 1.25 µL of 20 µM of *BOX-A1R* primer solution (the final volume of the reaction mix being adjusted to 25 µl with water). The PCR reaction protocol was as follows: denaturation at 95°C for 5 min, followed by 35 cycles of 94°C for 1 min, 48°C for 1 min and 72°C for 1 min, and final extension at 72°C for 5 min.

Sequencing. Amplified PCR products of different size were separated by electrophoresis in 1.2% agarose gel and stained with ClearSight DNA (ref). Gels were examined and images were taken under Gel Doc™ EZ imager (Bio-Rad). The PCR products were eluted from the agarose gels using the Wizard® SV Gel and PCR Clean-up System (Promega, USA). The purified PCR products were sent to the Eurofins company (Germany) to be sequenced.

***Sequence and phylogenetic analyses*.** Sequence similarity searches were performed using the EzBiocloud (https://www.ezbiocloud.net) and BLAST (https://blast.ncbi.nlm.nih.gov/ Blast. cgi) databases. Nucleotide sequences were aligned using Clustalx version 1.81. Phylogenetic trees were constructed via the Neighbor-Joining method in the MEGA version 7 software.

Table 2.3. Oligonucleotide primers used for amplification of 16S *rRNA*, *nifH*, *AQER* and *BOX-PCR* in this study.

Targeted sequence	Primer name	Primer sequence	Reference
16s *rRNA*	27F	5'-GAGAGTTTGATCCTGGCTCAG-3'	Pascual *et al.* (1995)
	1525R	5'-AAGGAGGTGATCCAGCC-3'	Pascual *et al.* (1995)
nifH	Pol F	5'-TGCGAYCCSAARGCBGACTC-3'	Poly *et al.* (2001)
	PolR	5'-ATSGCCATCATYTCRCCGGA-3'	Poly *et al.* (2001)
	AQER	5'-GACGATGTAGATYTCCTG-3'	Poly *et al.* (2001)
BOX-PCR	BOX-A1R	5'-CTACGGCAAGGCGACGCTGACG-3'	Brusetti *et al.* (2008)

Chapter 3

Isolation of N_2-fixing bacteria from Lebanon soil and wheat responses to selected bacterial strains

3.1. Introduction

Large amounts of organic compounds are exudated by roots into the rhizosphere, feeding micro-organisms. In return, beneficial microorganisms can engage symbiotic interactions with roots, resulting in increased plant fitness and growth.

It may be assumed that, after wheat domestication in the so-called *Fertile Crescent*, human migrations that widened the areas of wheat cultivation have altered the initial root microbiote. Furthermore, it is very likely that breeding programs carried out after the second world war; during the so-called *Green Revolution*, and up to now, based on plant selection cycles on soils that were artificialized by high fertilization inputs, have counter-selected the ability of root systems to interact with beneficial soil microorganisms because these interactions have a significant cost in terms of photosynthetates transferred by the plant to microorganisms and thus can impact crop yield in highly fertilized soils (Brown et al., 2013). It is clear that promoting or restoring beneficial interactions between roots and soil microorganisms with a maximized benefit/cost balance would be highly beneficial to sustainable agricultural practices. The general objective of my PhD research work is to provide knowledge likely to support progress in this direction.

In this framework, I have carried out experiments aiming at isolating and characterizing bacterial strains from a sample of Lebanon soil, focusing on N_2-fixing bacteria, and I have investigated the effects of theses strains and of other N_2-fixing model bacteria *(Bradyrhizobium japonicum*, *Frankia sp*., *Azospirillum lipoferum*) on plant growth in soil and plant nutrient element contents. The results provided by these two lines of experiments are reported in the present chapter.

3.2. Material and methods

Information has been provided in Chapter 2 on bacterial strains used in this work (Table 2.2), the origin and characteristics of the Lebanon soil sample (Figure 2.6 and Table 2.1), the procedure we have used to isolate N_2-fixing bacteria from soil samples (§ 2.9, and Figures 2.7 and 2.8), the PCR-based methodology carried out to characterize bacterial strains at the molecular level (§ 2.12) and the operational protocol allowing to test bacterial ability to use insoluble sources of phosphate and potassium (Figure 2.9 and 2.10, and § 2.10).

The protocols we have used for investigating the effects of bacterial strains on plant growth and nutrient element contents have also been described in Chapter 2 (see § 2.7).

3.3. Results

3.3.1. Isolation N_2-fixing bacterial strains from Lebanon soil

Part of the work aimed at isolating bacterial strains from a soil sample prepared from the rhizosphere of wheat plants grown in Lebanon has been carried out in collaboration with Houssein Zhour, PhD student in our group.

Based on the assumption that the relative abundancy of the bacterial strains that would be able to engage interactions with wheat roots might be increased in rhizosphere of growing wheat plants, we introduced a preliminary step in the process of bacterial strain isolation. The soil sample was ground using a mortar and pestle and sieved (12 mm mesh siever). The collected soil particles were either i) directly used to inoculate the NFb medium or ii) mixed with sterilized perlite (soil/perlite 1/8, v/v) and the mix (final volume: ca. 500 ml) was transferred into a pot where wheat seedlings (*Triticum turgidum* spp. durum cv. Oued Zenati) (1 seedling in the pot) where grown for 30 days in a growth chamber, the plant being watered with MilliQ water every 3 days (Figure 3.1). The root systems were then collected with adhering soil particles. A 50 mg sample (piece of root + adhering soil) was then used to isolate bacterial strains according to the protocol described in chapter 2 (§ 2.9, and Figures 2.7 and 2.8). In both procedures, bacterial aliquots were successively transferred onto a nitrogen-free medium (NFb medium, see § 2.9) ensuring selection of N_2-fixing strains. Both procedures have led to the isolation of bacterial strains but only strains obtained from direct soil inoculation have been characterized.

Figure 3.2 shows the increase in N_2-fixing capacity (assessed by ARA tests) of the microbial population developed at the surface of the NFb medium at the end of the 1st, 3rd and 4th passages ("rounds" of selection). After the 4th round of selection, the bacterial population present in the pellicle at the surface/interface of the NFb medium was spread (after successive dilutions) onto NFb medium in Petri dishes, in order to count the number of bacterial colonies and to determine the "morphotype" of different colonies, in terms of color, shape, height, margins… A set of colonies with visually different phenotypes were selected and submitted to 2 further rounds of growth on NFb medium followed by ARA assays, as described in Figure 2.7. A total of 16 bacterial strains were thereby isolated at the end of the final round of selection (6th round on NFb in vacuette® tube). These strains were named according to the Petri dish they were collected from and the step at which they were considered as purified. The names of these 16 strains are (by alphabetical order): A10, A11, A12, B1, B2, B3-1, B3-2, B4, C1, C2, H1, H2, H3, I1-1, I1-2 and I1-3.

Since all these strains have been able to grow and form colonies on "N-free" medium, one may assume that they are all endowed with N_2-fixation capacity. This

capacity is however likely to be highly variable between the 16 selected strains since the selection was based on the visual aspect of the colonies, when grown on NFb agar medium in Petri dishes. Indeed, the ARA tests performed at the end of the (final) 6th round of culture on NFb medium provided estimation of nitrogenase activity that varied by more than 10^3 times between the different strains (Figure 3.3).

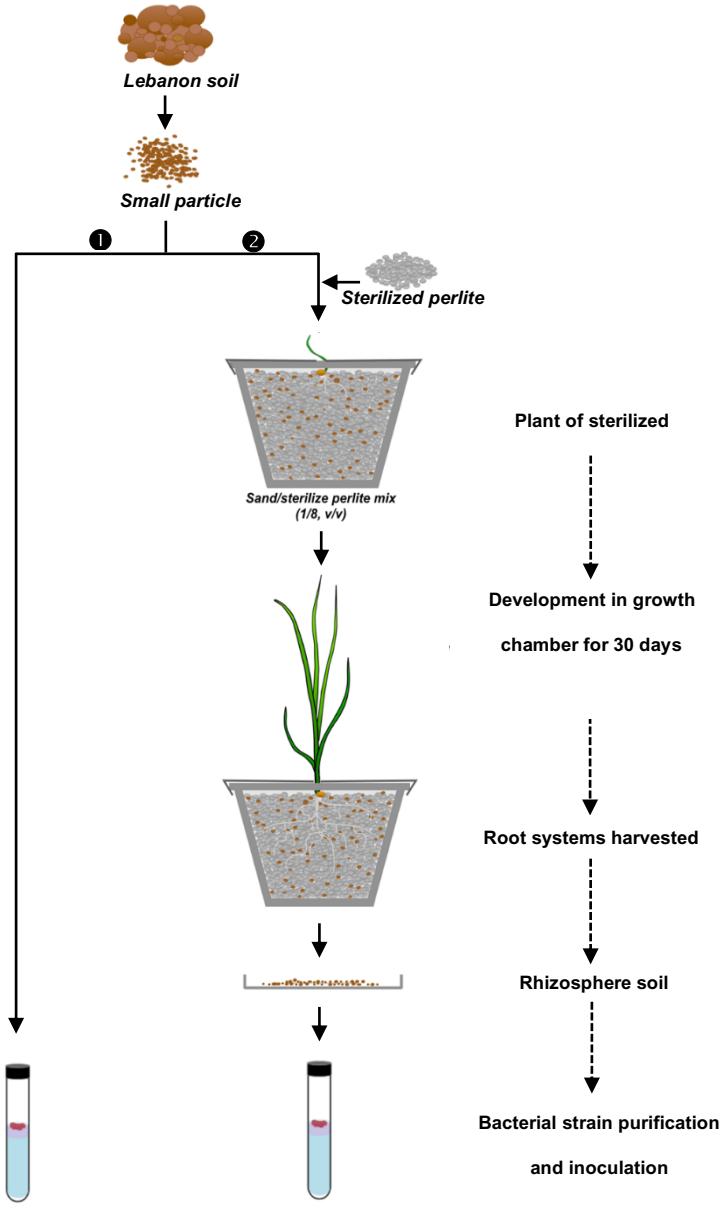

Figure 3.1. Isolation of bacterial strains from Lebanon soil: obtaining a rhizosheat sample from wheat seedlings grown in soil-perlite mix as a preliminary step in the isolation of Lebanese bacterial strains likely to interact with wheat root.

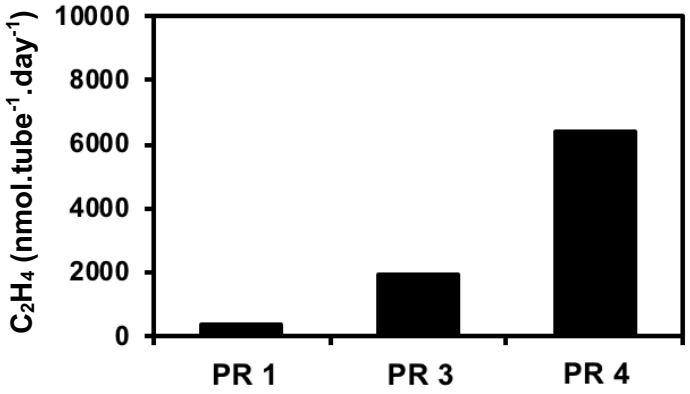

Figure 3.2. Increase in global nitrogenase activity of the bacterial population during the purification protocol using nitrogen-free medium. Nitrogenase activity of sub-surface bacterial pellicles growing in N free semi-solid Nfb medium was assessed by the acetylene reduction assay (ARA) at the end of the 1st (PR 1), 3rd (PR 3) and 4th (PR 4) purification rounds. Acetylene (10%) was provided after 3 days of growth and ARA was measured 24 h later. Four consecutive purification rounds were performed but results are only given for PR1, PR3 and PR4. Purification rounds and protocol: see Chapter 2, Figure 2.7.

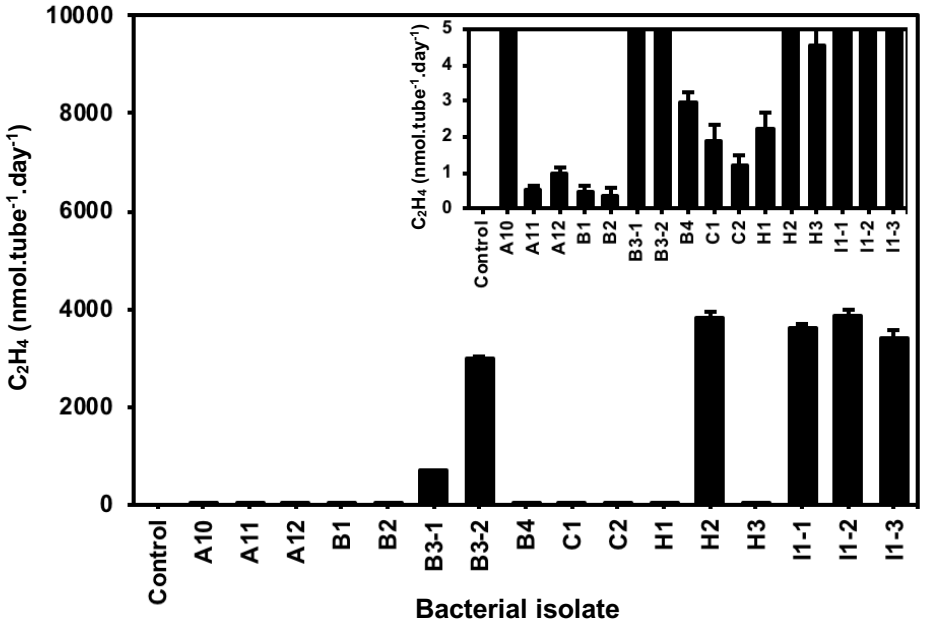

Figure 3.3. Nitrogenase activity of the 16 bacterial strains at the end of the 6th purification round. Insert: scale enlargement. Nitrogenase activity was assessed by the acetylene reduction assay (ARA). Acetylene (10%) was provided to the bacteria after 3 days of growth at the sub-surface of N free semi-solid NFb medium, and ARA was measured 24h later. Means ± SE, n = 3. Purification rounds and protocol: see Chapter 2, Figure 2.7.

3.3.2. Molecular and functional characterization of the isolated bacterial strains

Metabarcoding is a rapid method of biodiversity assessment that combines two technologies: DNA based identification and high-throughput DNA sequencing. It uses universal PCR primers to mass-amplify DNA barcodes from mass collections of organisms or from environmental DNA. For diazotroph bacteria, 16S ribosomal RNA, *nif* gene and BOX-A1R primers are the most commonly used amplicons. First, PCR experiments aiming at characterizing the selected 16 strains at a molecular level were carried out using primers targeting *16S RNA* (Figures 3.4). In agreement with the fact that selection of the bacterial colonies had been achieved after growth on N-free medium, PCR experiments revealed that a *nifH* gene DNA fragment could be amplified in each of the 16 selected bacterial strains (Figure 3.5). *nifH* encodes the Fe protein component of nitrogenase, the enzyme that catalyzes biological nitrogen fixation (dinitrogen reduction to ammonium). *BOX-A1R* primer was used to further characterized the bacterial strains (Figures 3.6). Then the amplicons for the 16S RNA were sequenced for phylogenetic analyses.

Phylogenetic trees that were obtained indicated that the closest relatives of strains A10 and A12 were rhizobia (Figure 3.7). The closest relatives of A11, B1, B2, C1 and H1 were found to be *Stenotrophomonas* species (Figure 3.8). The closest relatives of B3-2, B4, C2, H2, H3, I1-1 and I1-2 were found to be *Achromobacter* species (Figure 3.9). Finally, the closest relatives of B3-1 were found to be *Paraburkholderia* species (Figure 3.10), and those of I1-3 were *Klebsiella* species (Figure 3.11). See also Table 3.1.

It is worth to note that the *BOX-A1R* amplification patterns obtained for B3-2, B4, C2, H2, H3, I1-1 and I1-2, which were identified as close relatives of *Achromobacter* species by the above described phylogenetic analyses, appeared as strictly similar (Figure 3.6), suggesting that these strains might correspond to a single species. The 2 strains A10 and A12, identified as close relative of *Rhizobia*, seem also to display a similar *BOX-A1R* amplification pattern. On the other hand, from the 5 strains identified as close relatives of *Stenotrophomonas*, A11, B1, B2, C1 and H1, only B2 and C1, appear to share the same *BOX-A1R* amplification pattern (Figure 3.6), suggesting that at least 4 distinct genotypes are present amongst these 5 *Stenotrophomonas*-related strains.

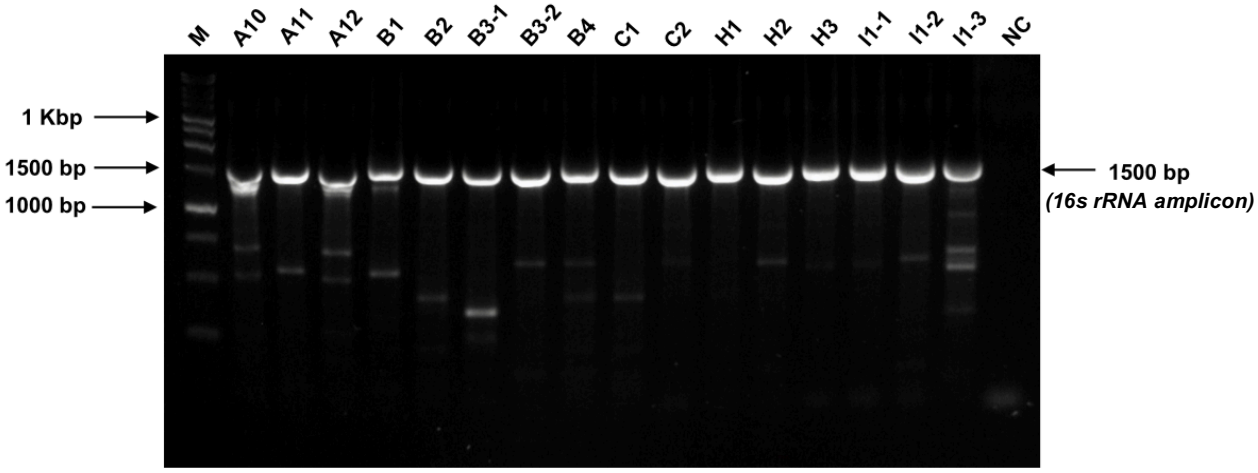

Figure 3.4. Molecular characterization of the 16 bacterial strains isolated from wheat rhizosphere from Lebanon soil: agarose resolution (1.2%) of 16S rRNA amplicons. Primer sequences: see table 2.3. PCR protocols: see § 2.12.

Lane M:	Molecular length marker (1 kb DNA ladder, Promega, USA)
Lane 1:	Isolate Lebanese A10
Lane 2:	Isolate Lebanese A11
Lane 3:	Isolate Lebanese A12
Lane 4:	Isolate Lebanese B1
Lane 5:	Isolate Lebanese B2
Lane 6:	Isolate Lebanese B3-1
Lane 7:	Isolate Lebanese B3-2
Lane 8:	Isolate Lebanese B4
Lane 9:	Isolate Lebanese C1
Lane 10:	Isolate Lebanese C2
Lane 11:	Isolate Lebanese H1
Lane 12:	Isolate Lebanese H2
Lane 13:	Isolate Lebanese H3
Lane 14:	Isolate Lebanese I1-1
Lane 15:	Isolate Lebanese I1-2
Lane 16:	Isolate Lebanese I1-3
Lane 17:	Negative control

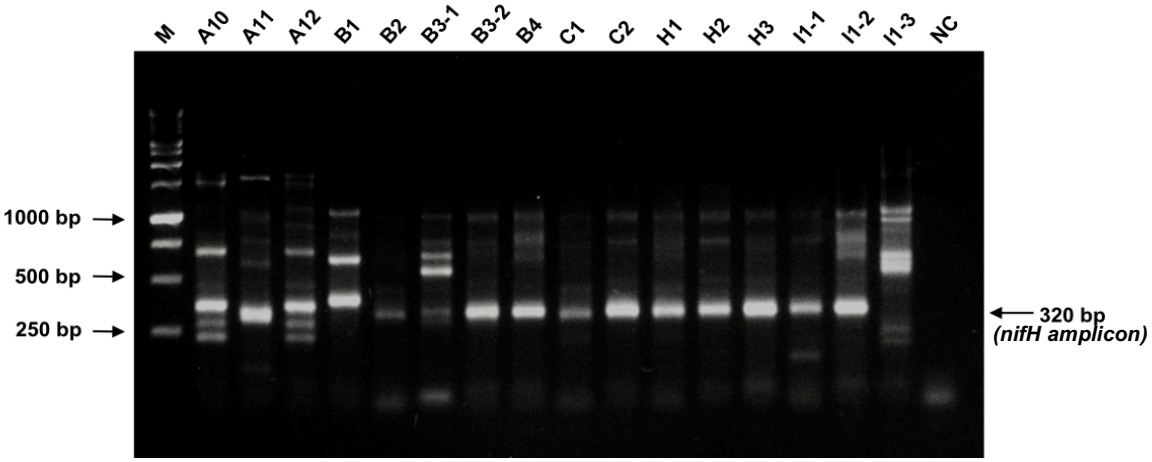

Figure 3.5. Molecular characterization of the 16 bacterial strains isolated from wheat rhizosphere from Lebanon soil: agarose resolution (1.2%) of partial *nifH* amplicons (PolF/AQER). A first amplification step was performed using the PolF-PolR primer pair, and then a second step using the PolF-AQER pair on an aliquot from the first amplification. Primer sequences: see table 2.3. PCR protocols: see § 2.12

Lane M:	Molecular length marker (1 kb DNA ladder, Promega, USA)
Lane 1:	Isolate Lebanese A10
Lane 2:	Isolate Lebanese A11
Lane 3:	Isolate Lebanese A12
Lane 4:	Isolate Lebanese B1
Lane 5:	Isolate Lebanese B2
Lane 6:	Isolate Lebanese B3-1
Lane 7:	Isolate Lebanese B3-2
Lane 8:	Isolate Lebanese B4
Lane 9:	Isolate Lebanese C1
Lane 10:	Isolate Lebanese C2
Lane 11:	Isolate Lebanese H1
Lane 12:	Isolate Lebanese H2
Lane 13:	Isolate Lebanese H3
Lane 14:	Isolate Lebanese I1-1
Lane 15:	Isolate Lebanese I1-2
Lane 16:	Isolate Lebanese I1-3
Lane 17:	Negative control

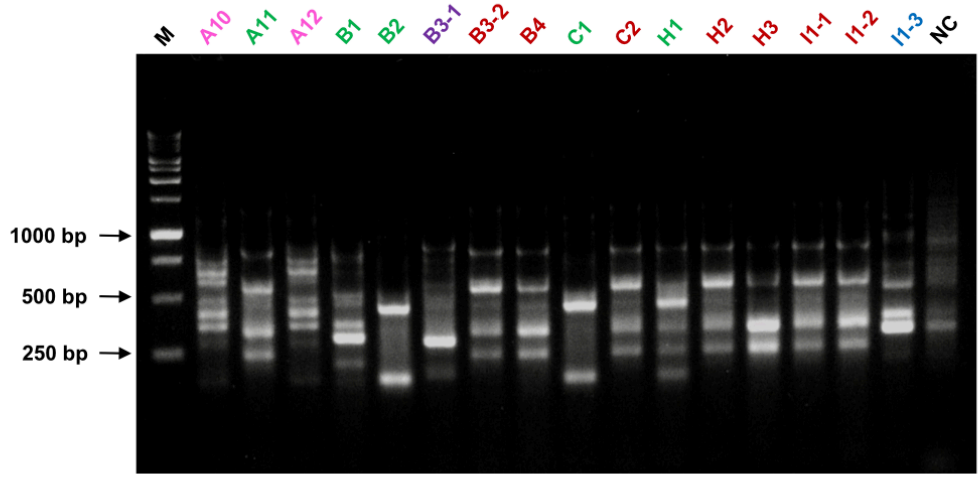

Figure 3.6. Molecular characterization of the 16 bacterial strains isolated from wheat rhizosphere from Lebanon soil: agarose resolution (1.2%) of *BOX-A1R* amplicons. Primer sequence: see table 2.3. PCR protocols: see § 2.12.

Lane M:	Molecular length marker (1 kb DNA ladder, Promega, USA)
Lane 1:	Isolate Lebanese A10
Lane 2:	Isolate Lebanese A11
Lane 3:	Isolate Lebanese A12
Lane 4:	Isolate Lebanese B1
Lane 5:	Isolate Lebanese B2
Lane 6:	Isolate Lebanese B3-1
Lane 7:	Isolate Lebanese B3-2
Lane 8:	Isolate Lebanese B4
Lane 9:	Isolate Lebanese C1
Lane 10:	Isolate Lebanese C2
Lane 11:	Isolate Lebanese H1
Lane 12:	Isolate Lebanese H2
Lane 13:	Isolate Lebanese H3
Lane 14:	Isolate Lebanese I1-1
Lane 15:	Isolate Lebanese I1-2
Lane 16:	Isolate Lebanese I1-3
Lane 17:	Negative control

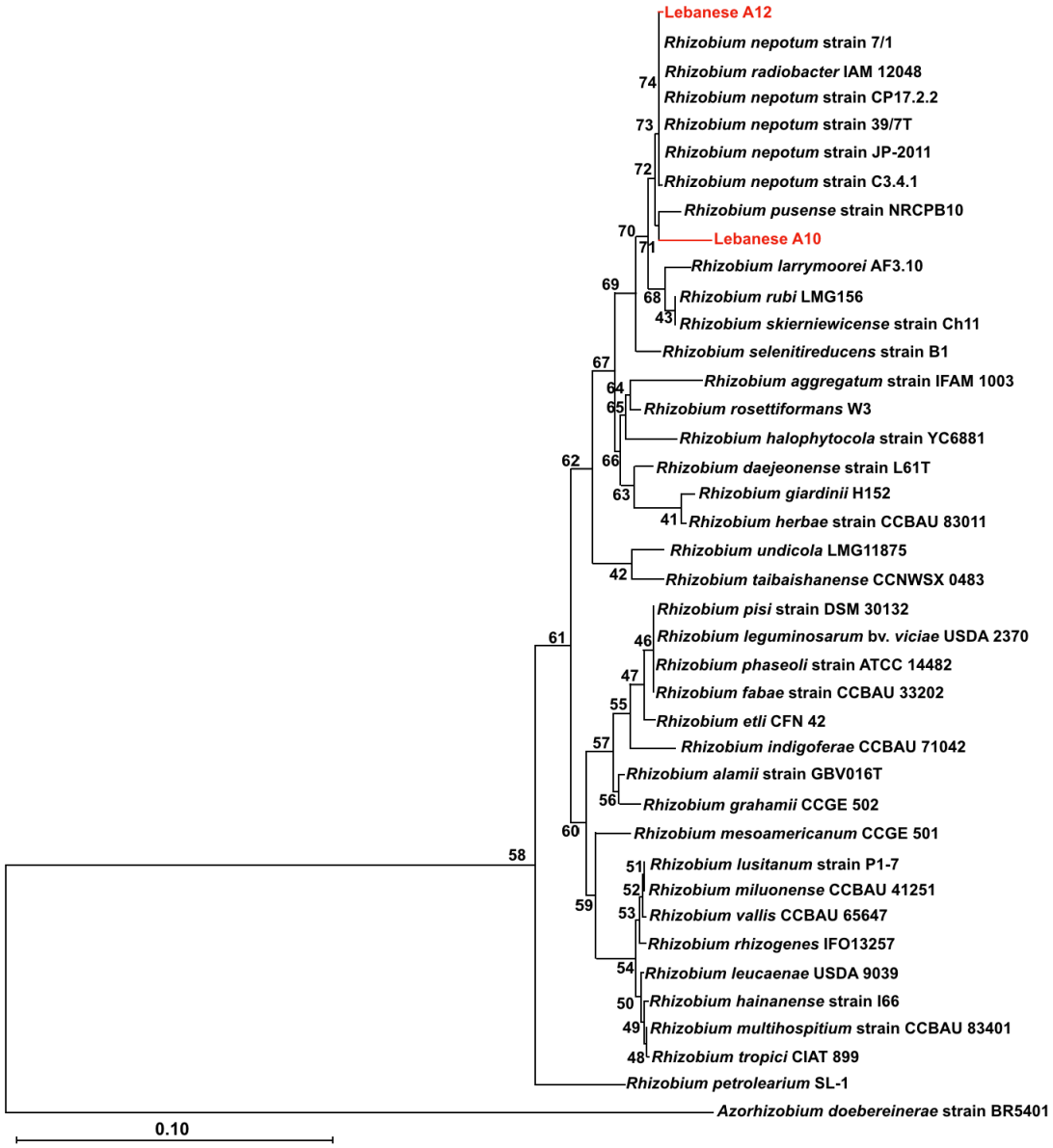

Figure 3.7. Phylogenetic tree showing the relationship of Lebanese A10 and Lebanese A12 with *Rhizobium* species based on 16S rRNA sequence. The neighbor-joining tree was rooted by a sequence of *Azorhizobium doebereinerae* as the outgroup. Bootstrap values (1000 replicates) are indicated. The scale bar represents 10% nucleotide substitutions.

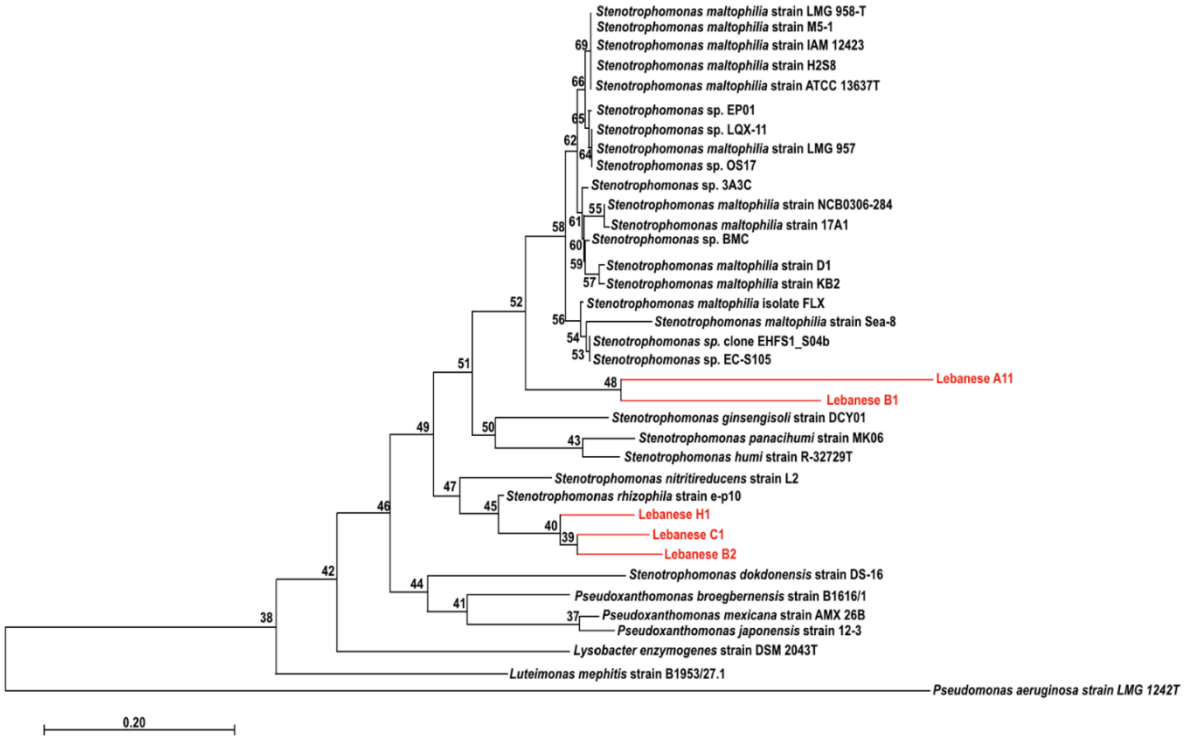

Figure 3.8. Phylogenetic tree showing the relationships of Lebanese A11, Lebanese B1, Lebanese B2, Lebanese C1 and Lebanese H1 with *Stenotrophomonas* species based on 16S rRNA sequence. The neighbor-joining tree was rooted by a sequence of *Pseudomonas aeruginosa strain LMG 1241T* as the outgroup. Bootstrap values (1000 replicates) are indicated. The scale bar represents 20% nucleotide substitutions.

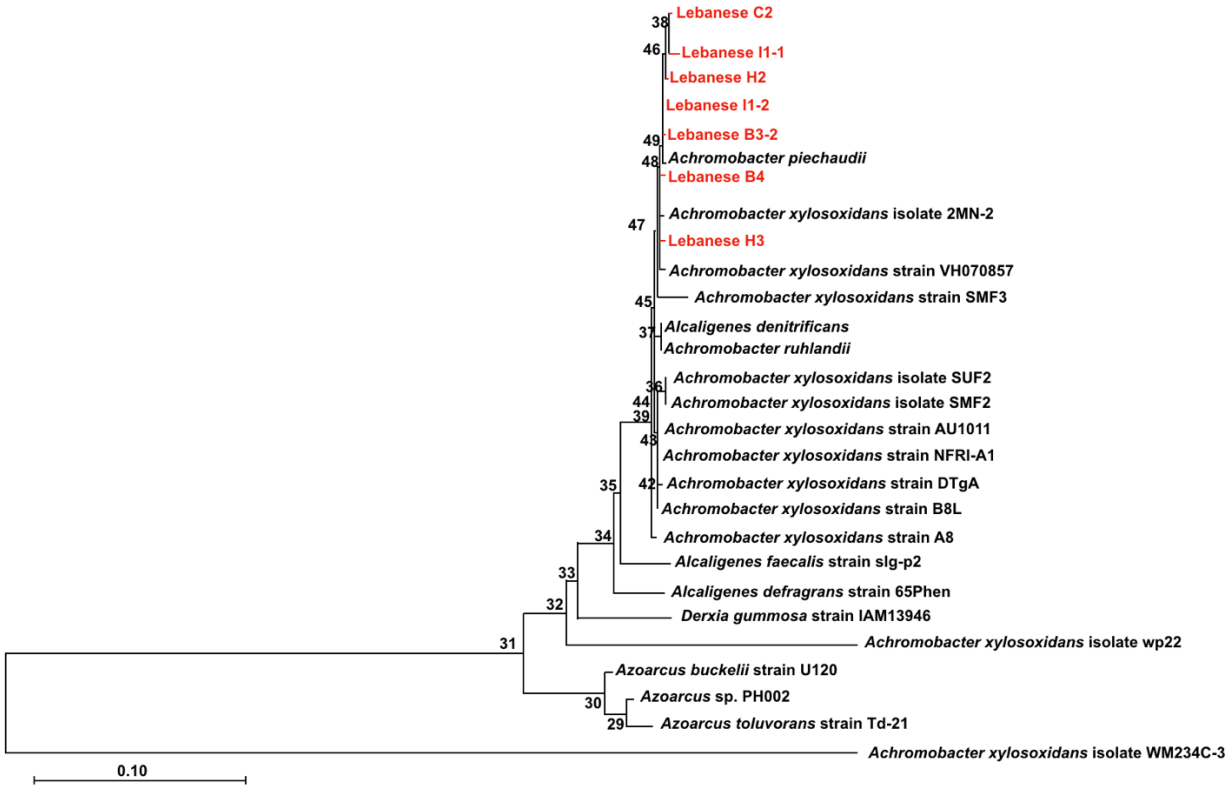

Figure 3.9. Phylogenetic tree showing the position of Lebanese B3-2, Lebanese B4, Lebanese C2, Lebanese H2, Lebanese H3, Lebanese I1-1 and Lebanese I1-2 with *Achromobacter* species based on 16S rRNA sequence. The neighbor-joining tree was rooted by a sequence of *Achromobacter xylosoxidans* isolate WM234C-3 as the outgroup. Bootstrap values (1000 replicates) are indicated. The scale bar represents 10% nucleotide substitutions.

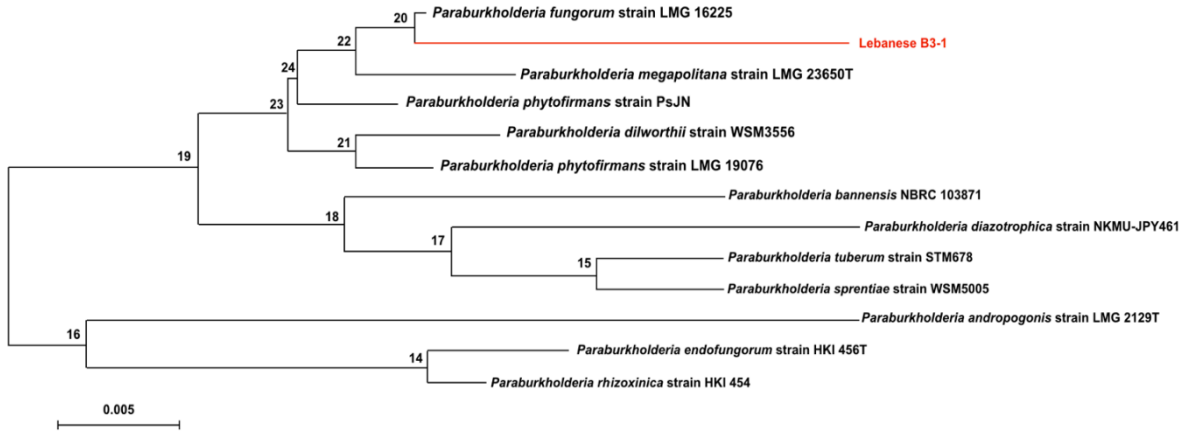

Figure 3.10. Phylogenetic tree showing the relationships of Lebanese B3-1 with *Paraburkholderia* species based on 16S rRNA sequence. Bootstrap values (1000 replicates) are indicated. The scale bar represents 0.5% nucleotide substitutions.

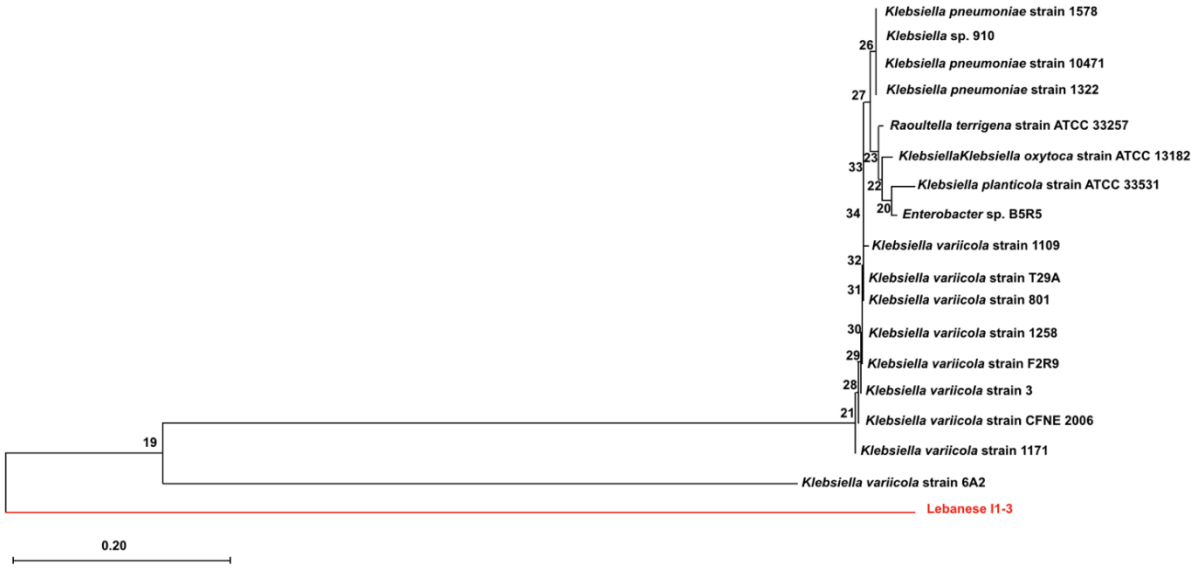

Figure 3.11. Phylogenetic tree showing the position of Lebanese I1-3 with *Klebsiella* species based on 16S rRNA sequence. Bootstrap values (1000 replicates) are indicated. The scale bar represents 20% nucleotide substitutions.

Table 3.1. Taxonomic assignments of the 16 bacterial strains isolated from wheat rhizosphere based on the analysis of their 16S rRNA sequences with the EzBioCloud database (https://www.ezbiocloud.net).

No.	Isolates	Sequence lenght	Completeness (%)	Pairwise Similarity (%)	Accession No.	Identified As
1	Lebanese A10	1,421	100	95.26	JWJH01000079	*Rhizobium nepotum* strain 39/7
			100	95.04	CP002249	*Rhizobium* sp. strain H13-3
			100	95.04	JWIT01000061	*Rhizobium* sp. strain KFB 330
2	Lebanese A11	1,457	100	95.79	MUYX01000273	*Stenotrophomonas* sp. strain AM6
			100	95.65	KJ452162	*Stenotrophomonas indicatrix* strain WS40
			100	95.65	PEJT01000021	*Stenotrophomonas rhizophila* strain LMG 10879
3	Lebanese A12	1,407	100	97.40	CP002249	*Rhizobium* sp. strain H13-3
			100	97.40	JWIT01000061	*Rhizobium* sp. strain KFB 330
			100	97.25	JWJH01000079	*Rhizobium nepotum* strain 39/7
4	Lebanese B1	1,497	100	96.77	MUYX01000273	*Stenotrophomonas* sp. strain AM6
			97.1	96.68	AB021404	*Pseudomonas geniculata* strain ATCC 19374
			100	96.64	KJ452162	*Stenotrophomonas indicatrix* strain WS40
5	Lebanese B2	1,468	100	98.28	CP007597	*Stenotrophomonas rhizophila* strain DSM 14405
			100	98.05	CP016294	*Stenotrophomonas* sp. strain QL-P4
			100	97.99	ALYK02000006	*Stenotrophomonas* sp. strain S028
6	Lebanese B3-1	1,447	97.3	98.13	KF733462	*Paraburkholderia insulsa* strain PNG-April
			100	97.89	BAYC01000104	*Paraburkholderia fungorum* strain NBRC 102489
			97.8	97.78	U96936	*Paraburkholderia phenazinium* strain LMG 2247
7	Lebanese B3-2	1,463	94.83	97.49	EU150134	*Achromobacter marplatensis* strain B2
			100	97.39	HG324053	*Achromobacter deleyi* strain LMG 3458
			100	97.32	HG324052	*Achromobacter kerstersii* strain LMG 3441
8	Lebanese B4	1,476	97.83	98.98	EU150134	*Achromobacter marplatensis* strain B2
			99.51	98.88	AY170848	*Achromobacter spanius* strain LMG 5911
			100	98.75	HG324053	*Achromobacter deleyi* strain LMG 3458
9	Lebanese C1	1,484	100	97.85	CP007597	*Stenotrophomonas rhizophila* strain DSM 14405
			94.41	97.80	LT622838	*Stenotrophomonas bentonitica* strain BII-R7
			100	97.78	ALYK02000006	*Stenotrophomonas* sp. strain S028
10	Lebanese C2	1,448	94.83	97.86	EU150134	*Achromobacter marplatensis* strain B2
			100	97.74	HG324053	*Achromobacter deleyi* strain LMG 3458
			99.5	97.73	AY170848	*Achromobacter spanius* strain LMG 5911
11	Lebanese H1	1,459	100	97.21	CP007597	*Stenotrophomonas rhizophila* strain DSM 14405
			94.4	97.05	LT622838	*Stenotrophomonas bentonitica* strain BII-R7
			100	96.86	ALYK02000006	*Stenotrophomonas* sp. strain S028
12	Lebanese H2	1,491	97.86	98.46	EU150134	*Achromobacter marplatensis* strain B2
			100	97.98	HG324053	*Achromobacter deleyi* strain LMG 3458
			99.5	97.9	AY170848	*Achromobacter spanius* strain LMG 5911
13	Lebanese H3	1,449	94.83	97.93	EU150134	*Achromobacter marplatensis* strain B2
			100	97.81	HG324053	*Achromobacter deleyi* strain LMG 3458
			99.5	97.80	AY170848	*Achromobacter spanius* strain LMG 5911
14	Lebanese I1-1	1,449	97.83	96.52	EU150134	*Achromobacter marplatensis* strain B2
			99.51	96.09	AY170848	*Achromobacter spanius* strain LMG 5911
			100	96.05	HG324053	*Achromobacter deleyi* strain LMG 3458
15	Lebanese I1-2	1,475	94.83	98.83	EU150134	*Achromobacter marplatensis* strain B2
			66.51	98.60	AY170848	*Achromobacter spanius* strain LMG 5911
			100	98.53	HG324053	*Achromobacter deleyi* strain LMG 3458
16	Lebanese I1-3	1,454	70.51	97.27	MH179329	*Klebsiella huaxiensis* strain WCHKl090001
			100	97.00	BCNN01000001	*Lelliottia amnigena* strain NBRC 105700
			93.70	96.95	MK049964	*Enterobacter huaxiensis* strain 090008

Finally, the ability of the 16 bacterial strains to use insoluble sources of Pi and K^+ was tested as described in Chapter 2 (§ 2.10 and Figures 2.9 and 2.10), and assessed using the so-called *Solubilizing Indices* (SI). Representative growth tests on agar plates in presence of an insoluble Pi source or of both Pi and K^+ insoluble sources are displayed by Figures 3.12 and 3.13, respectively. Phosphate solubilizing activity was displayed by all the strains except the *Stenotrophomonas*-related A11 strain. Table 3.2 provides SI values derived from these experiments. Differences in SI occurred between the 15 strains able to use insoluble source of Pi, but these differences remained within a rather narrow range of variations (below about 3 times) when compared with the very large variations in nitrogenase activity, by at least 10^3 times, as assessed by ARA tests (Figure 3.3).

Ability to use the insoluble source of K^+ (in presence of an insoluble source of Pi) was clearly displayed by 2 strains, the *Achromobacter*-related C2 and *Klebsiella*-related I1.3 strains (Figure 3.13 and Table 3.2). It is worth to note that these two strains displayed also the highest ability to use the insoluble source of Pi (largest values of SI in Table 3.2).

A summary of the results obtained in these experiments, regarding the phylogenetic relationships, *BOX-A1R* amplification patterns, nitrogenase activity (ARA tests), SI for the insoluble source of Pi ("SI for Pi") and SI for the insoluble source of K^+ (in presence of the insoluble source of Pi) ("SI for K") is provided in Table 3.3.

Detailed examination of this figure reveals that differences in "SI for K", "SI for P" and/or nitrogenase activity can be observed between the 7 strains that phylogenetic analyses identified as related to the *Achromobacter* genus and that PCR experiments identified as displaying the same *BOX A1R* amplification pattern. This indicates that different genotypes are present amongst these 7 strains although they display the same ***BOX-A1R*** amplification pattern. On the other hand, within the 5 *Stenotrophomonas*-related strains, the 2 ones that displayed similar *BOX-A1R* amplification patterns also displayed similar SI for Pi (SI for K being "0" in both cases), and similar nitrogenase activity. The 2 *Rhizobium*-related strains, which display similar *BOX-A1R* amplification patterns, also display similar nitrogenase activity and SI for Pi (SI for K being 0 in both strains).

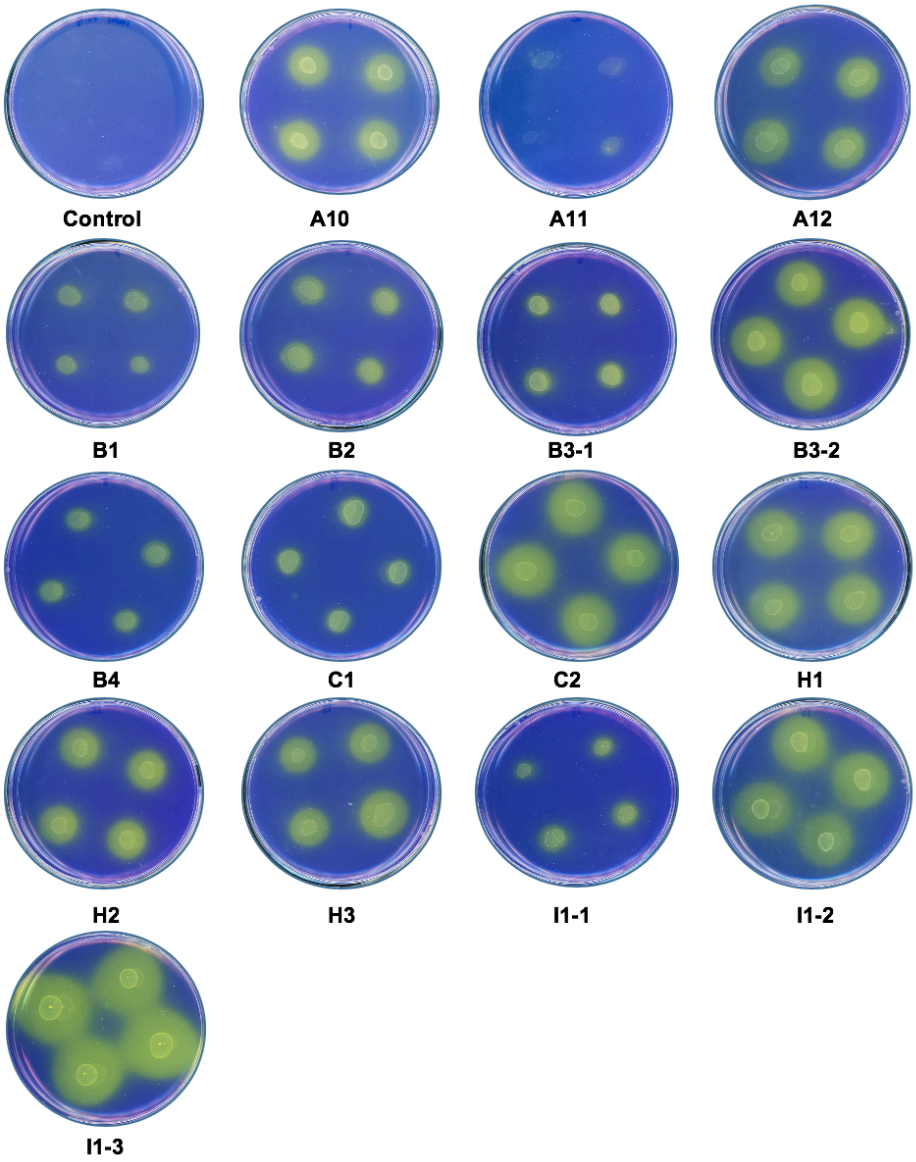

Figure 3.12. Assessment of the capacity of the 16 bacterial strains to use an insoluble source of Pi. Bacterial growth (drop tests) occurred on modified Pikovskaya's agar medium added with tricalcium phosphate as a poorly soluble P source and supplemented with bromocresol purple as a pH indicator (see § 2.10). The plates were incubated for 3 days at 27°C. The initial pH of the medium was 7.0. Bacterial growth results in medium acidification, which shifts the color of the pH indicator from purple to yellow.

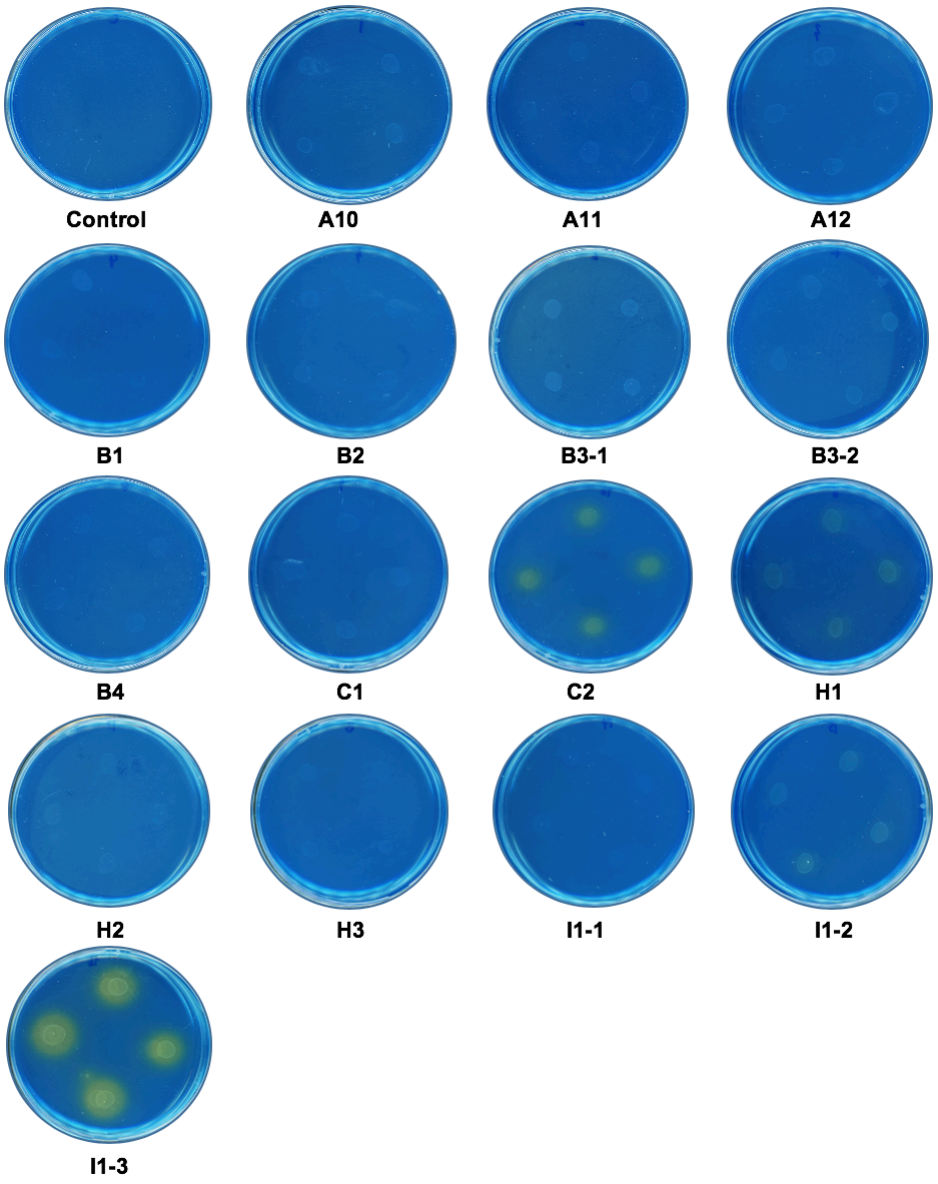

Figure 3.13. Assessment of the capacity of the 16 bacterial strains to use an insoluble source of K^+ in presence of an insoluble source of Pi. Bacterial growth (drop tests) occurred on Alexandrov agar medium added with potash feldspar (potassium aluminosilicate) as a poorly soluble K^+ source, tricalcium phosphate as a poorly soluble P source, and bromothymol blue as a pH indicator (see § 2.10). The plates were incubated for 3 days at 27°C. The initial pH of the medium was 7.2. Bacterial growth results in medium acidification, which shifts the color of the pH indicator from blue to yellow.

Table 3.2. Mean P and K *Solubilizing Indexes* (SI) of the 16 bacterial isolates purified from Lebanon wheat rhizosphere. Purification rounds and protocol: see Chapter 2, Figure 2.7. SI (see Chapter 2, Figures 2.9 & 2.10, and § 2.10). SI is calculated as follows from the photos displayed by Figures 3.12 and 3.13: diameter of the yellow zone induced by the spotted colony reported to the diameter of the spotted colony. "0" indicates that no yellow zone appeared around the colony.

Isolate codes	P solubilization (SI) [a]	K solubilization (SI) [a]
Control	0	0
A10	2.4 ± 0.1	0
A11	0	0
A12	2.3 ± 0.3	0
B1	1.2 ± 0.1	0
B2	1.4 ± 0.1	0
B3-1	1.3 ± 0.2	0
B3-2	2.6 ± 0.4	0
B4	1.3 ± 0.3	0
C1	1.2 ± 0.1	0
C2	3.0 ± 0.3	1.3 ± 0.1
H1	2.8 ± 0.3	0
H2	2.1 ± 0.5	0
H3	2.5 ± 0.5	0
I1-1	1.6 ± 0.4	0
I1-2	2.9 ± 0.5	0
I1-3	3.7 ± 0.5	1.4 ± 0.1

[a] Results: Means of 8 replicates followed by standard error.

Table 3.3. Molecular and physiological characterization of the 16 Lebanese strains isolated from wheat rhizosphere: summary of the data. *BOX-A1R*: data from the amplification pattern of *BOX-A1R* amplicons (see Figure 3.6). Columns with same letters correspond to similar amplification patterns. Nitrogenase activity: see Figure 3.3. P and K *Solubilizing Indexes* (SI for P and SI for K): see Figures 3.12 and 3.13, and Table 3.2

Genus	***Achromobacter***							***Stenotrophomonas***					***Rhizobia***		***Paraburkholderia***	***Klebsiella***
Isolate code	**B3-2**	**B4**	**C2**	**H2**	**H3**	**I1-1**	**I1-2**	**A11**	**B1**	**B2**	**C1**	**H1**	**A10**	**A12**	**B3-1**	**I1-3**
BOX-A1R	**a**	**a**	**a**	**a**	**b**	**b**	**b**	**c**	**d**	**e**	**e**	**d**	**f**	**f**	**g**	**h**
Nitrogenase activity	**2,996.5 ± 43.4**	**2.9 ± 0.3**	**1.2 ± 0.3**	**3,811.8 ± 142.2**	**4.5 ± 0.4**	**3,608.3 ± 98.5**	**3,861.5 ± 105.5**	**0.6 ± 0.1**	**0.5 ± 0.2**	**0.4 ± 0.2**	**1.9 ± 0.4**	**2.2 ± 0.5**	**1.0 ± 0.2**	**1.0 ± 0.2**	**678.9 ± 13.6**	**3,398.7 ± 168.0**
SI for P	**2.6 ± 0.4**	**1.3 ± 0.3**	**3.0 ± 0.3**	**2.1 ± 0.5**	**2.5 ± 0.5**	**1.6 ± 0.4**	**2.9 ± 0.5**	**0**	**1.2 ± 0.1**	**1.4 ± 0.1**	**1.2 ± 0.1**	**2.8 ± 0.3**	**2.4 ± 0.1**	**2.3 ± 0.3**	**1.3 ± 0.2**	**3.7 ± 0.5**
SI for K	**0**	**0**	**1.3 ± 0.1**	**0**	**0**	**0**	**0**	**0**	**0**	**0**	**0**	**0**	**0**	**0**	**0**	**1.4 ± 0.1**

3.3.3. Effects of bacterial strains on plant growth

Five laboratory classical bacterial strains, *B. japonicum* strain ORS285, *B. japonicum* strain ORS285Δ*nif*, *Frankia* sp. R43, *A. lipoferum* 4B and *A. brasilense* Sp245 known to be able to engage beneficial symbiotic interactions with different plant species, and 7 bacterial strains isolated from Lebanon soil, A11 and B1 (*Stenotrophomonas*-related), B3-1 (*Parabulkholderia*-related), B3-2, H2 and I1-2 (*Achromobacter*-related) and I1-3 (*Kebsiella* related) were tested for the effects on wheat (*T. turgidum* spp. durum, cv. Oued Zenati) growth on artificial soil (peat/soil/perlite, 1/1/1, v/v/v) for 30 days in growth chamber as described in Chapter 2 (§ 2.7). Low N solution (LN: 0.7 mM assimilable N; see § 2.3) was used for plant watering. Non-inoculated plants watered with either LN or HN (5.2 mM assimilable N; see § 2.3) solution were grown in parallel and used as control. Roots and shoots were collected, dried and weighted (biomass dry weight: DW).

Several bacterial strains were found to significantly increase root, shoot and/or total biomass (Figure 3.14). The most pronounced effects on total biomass were observed with B3-2, B1, *A. lipoferum* 4B, B3-1, A11 and I1-2. Inoculation with each of these strains also resulted in an increase in shoot to root biomass ratio, indicating that the stimulating effect on plant growth benefited shoot more than root growth. An inverse situation was observed in the case of Frankia inoculation.

Based on the whole set of results, we selected 6 bacterial strains, *B. japonicum* strain ORS285 (abbreviation: Brad), *Frankia* sp. R43 (abbreviation: *Frankia*), *Azospirillium lipoferum* 4B (abbreviation: Azo4B), B1 (*Stenotrophomonas* related), B3-2 (*Achromobacter* related) and I1-3 (*Kebsiella* related) for further analyses of the plant responses. B1 and B3-1 were selected based on their strong effects on plant growth (Figure 3.14). The effect of I1-3 on plant growth was weaker but this strain was selected because it was found to be the most efficient one in using poorly soluble sources of Pi and K^+ (Table 3.3 and Figure 3.13).Figure 3.15; obtained by using the same data as those displayed by Figure 3.14, provides the values of the root and shoot biomass, total biomass and shoot to root biomass ratio of the plants inoculated with each of these 6 strains but expressed in % of the corresponding values displayed by the non-inoculated control plants (watered with LN solution).

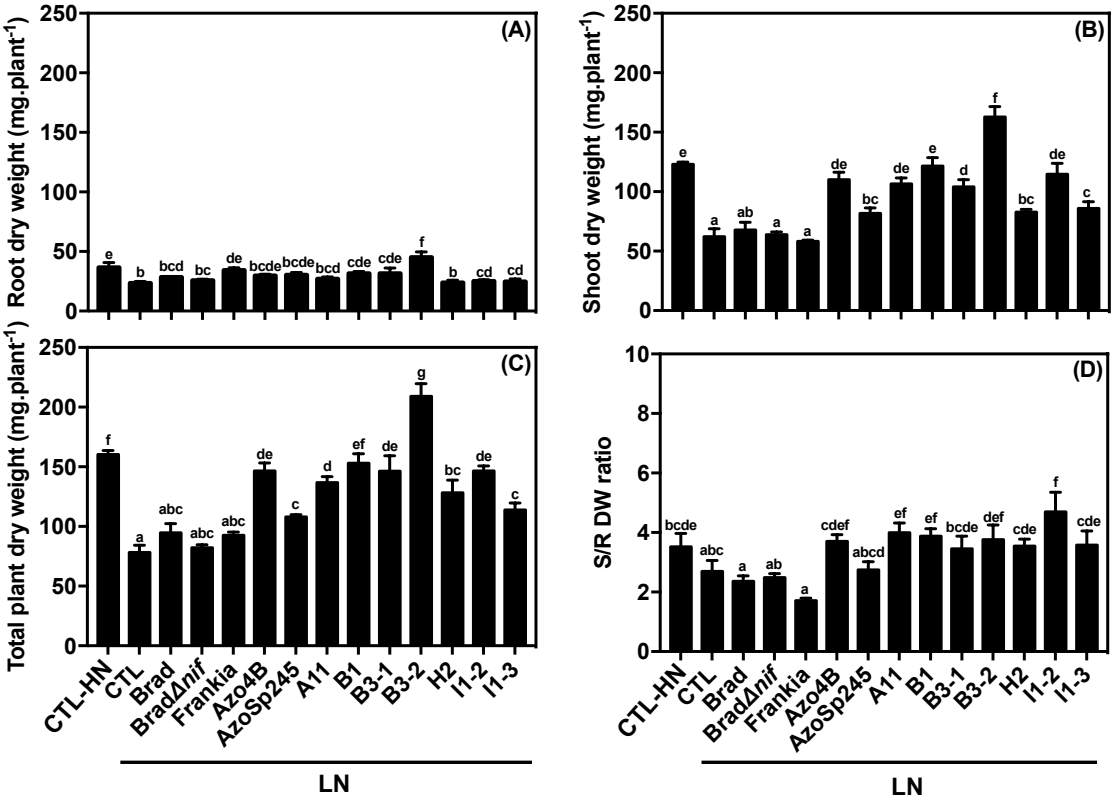

Figure 3.14. Effect of 12 rhizobacterial strains on wheat growth on soil in growth chamber. Plants (*T. turgidum* spp. durum cv. Oued Zenati) were grown on artificial soil (peat moss/sand/perlite, 1/1/1; v/v/v) for 30 days after seedling transplantation. The plants were watered every 3 days with Hoagland solution, containing 5 mM NH_4NO_3 (HN treatment: high N condition) or with Hoagland-modified solution containing 0.5 mM NH_4NO_3 (LN treatment: low N condition). LN-treated plants were inoculated (inoculation of the soil and of the seedlings before transplantation) with one rhizobacterial strain according to the procedure described in § 2.2 and 2.7. Control HN and LN treatments: the soil and the transplanted seedlings were not-inoculated. A set of 12 rhizobacterial strains was tested: *B. japonicum* strain ORS285 (Brad), *B. japonicum* strain ORS285Δ*nif* (BradΔ*nif*), *Frankia* sp. R43 (*Frankia)*, *A. lipoferum* strain 4B (Azo4B), *A. brasilense* Sp245 (LN/AzoSp245), Lebanese A11 isolate (LN/A11), Lebanese B1 isolate (B1), Lebanese B3-1 isolate (B3-1), Lebanese B3-2 isolate (B3-2), Lebanese H1 isolate (H1), Lebanese I1-2 isolate (I1-2) and Lebanese I1-3 isolate (I1-3).

(A) Root biomass (dry weight: DW) of the plants at the end of the 30-day growth period.
(B) Shoot biomass
(C) Total biomass
(D) Shoot:root biomass ratio

Values are means ± SE (n = 5). Different letters above histogram bars indicate statistical significance at $p<0.05$ (ANOVA, performed using Statistix 8, Analytical software, SXW, Tallahassee, FL USA)

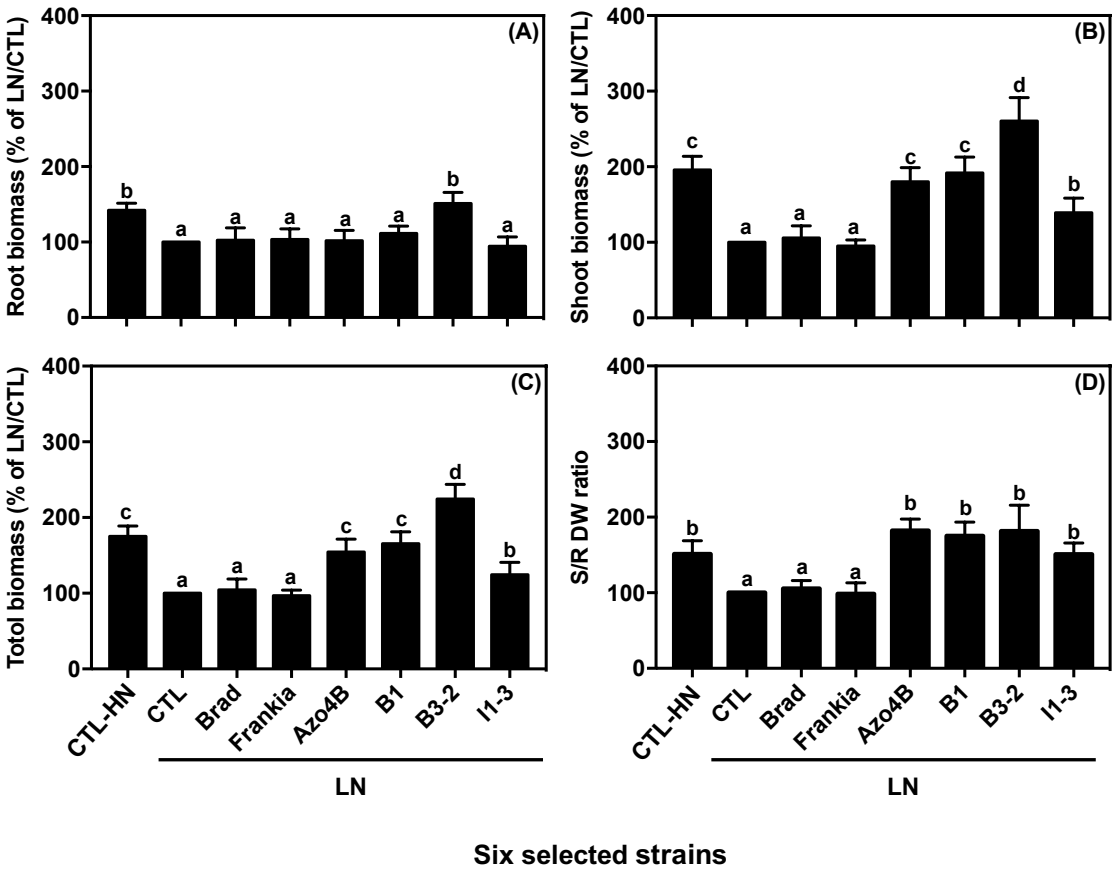

Figure 3.15. Effects on plant growth of the 6 bacterial strains selected from the data displayed by Figure 3.14. Same data as in Figure 3.14 but expressed in % of the non-inoculated control plants (CTL) watered with LN solution. See legend to Figure 3.14.

(A) Root biomass (dry weight: DW) of the plants at the end of the 30-day growth period.
(B) Shoot biomass
(C) Total biomass
(D) Shoot:root biomass ratio

Values are means ± SE (n = 5). Different letters above histogram bars indicate statistical significance at $p<0.05$ (ANOVA).

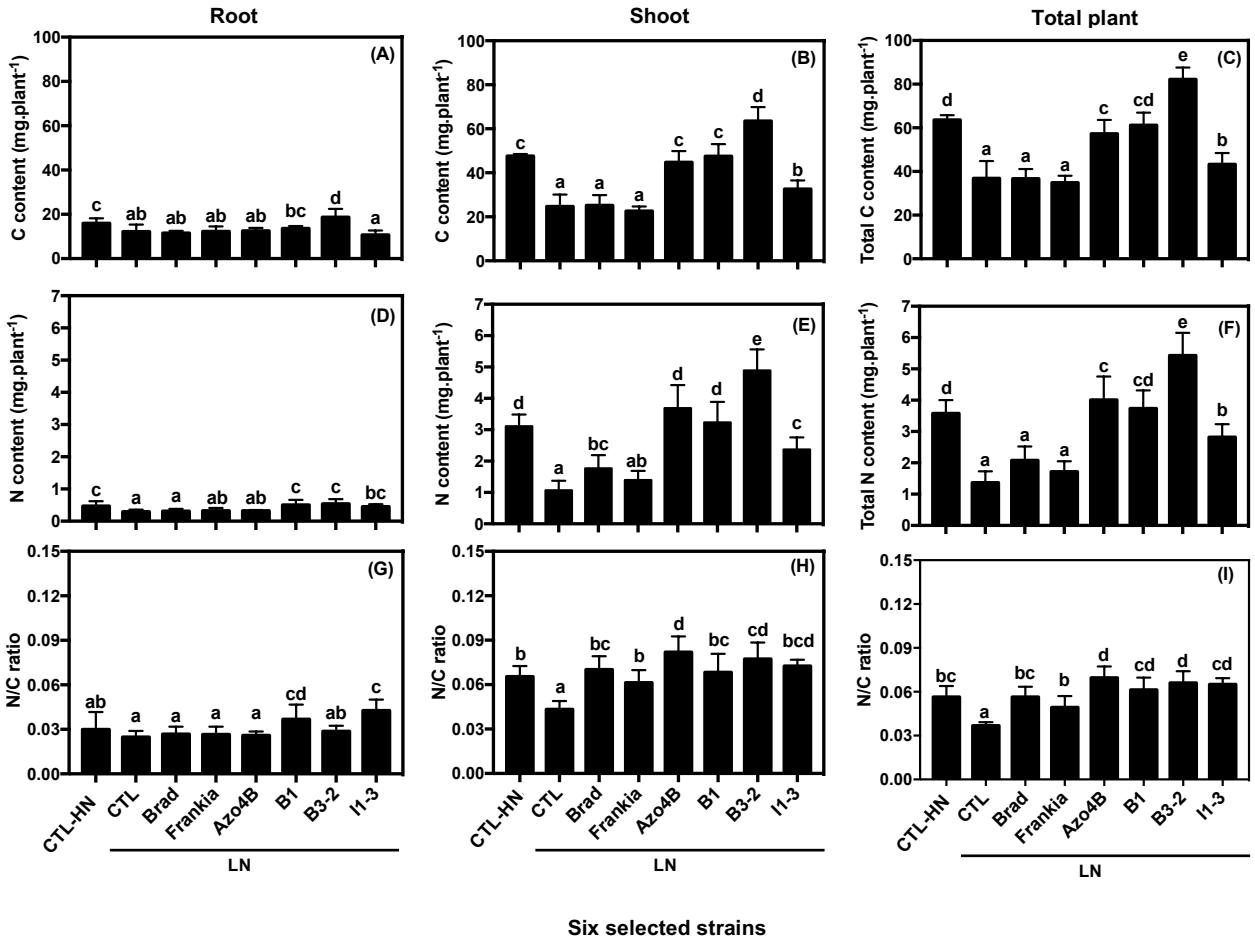

Figure 3.16. Carbon and nitrogen contents in the plants inoculated by the 6 selected bacterial strains. Same plants as in the experiments described by Figure 3.14 (and Figure 3.15). Plant growth conditions (HN and LN treatments) and inoculation: see Legend to Figure 3.14. HN and LN control plants: non-inoculated plants. The 6 selected bacterial strains are *B. japonicum* strain ORS285 (Brad), *Frankia* sp. R43 (Frankia), *A. lipoferum* strain 4B (Azo4B), Lebanese B1 isolate (B1), Lebanese B3-2 isolate (B3-2) and Lebanese I1-3 isolate (I1-3).

(A), (B) and (C): C contents (mg per plant) in roots (A) and shoots (B), and total (roots + shoots) (C).
(D), (E) and (F): N contents (mg per plant) in roots (D) and shoots (E), and total N content (F).
(G), (H) and (I): N/C content ratios in roots (G), shoots (H) in total plants (I).

Values are means ± SE (n = 5). Different letters above histogram bars indicate statistical significance at $p<0.05$ (ANOVA).

The root and shoot contents in C and N of the plants inoculated with the 6 selected strains and of the non-inoculated control plants were assayed by mass spectrometry. The values, determined on a per plant basis, are shown in Figure 3.16. Altogether, these data indicated that the identity of the inoculated bacterial strain affected the amounts of C and N present in shoots, roots and whole (shoots + roots) plants, determined on a per plant basis, and the N/C contents.

The C and N content data displayed by Figure 3.16 were then plotted against the corresponding biomass values and linear fits were adjusted to the experimental points (Figure 3.17). A very strong correlation appeared between the C content and biomass values, in roots as well as in shoots, with a slope close to 0.4 in both cases (Figure 3.17, left panels).

C always accounted for about 40% of the wheat biomass, independently of the organ (roots or shoots), of the treatment (inoculation or not) and of the identity of the inoculated bacterial strain. Similar percentages of C content, close to 40%, have been reported in various plant species and tissues (Personal communication of Pascal Tillard, Stable Isotope Analytical Platform, BPMP, SupAgro Montpellier). In contrast, the correlation between the N content and biomass values was different in roots and in shoots, the linear fits displaying a slope of 0.01 and 0.03, respectively. Thus, per unit of biomass, more nitrogen (by about 3 times) was used (stored into vacuoles or metabolized into organic compounds) for shoot production than for root production by the wheat seedlings. Also, in Figure 3.17, the correlation of the C and N contents with biomass appeared weaker in the case of the N contents than in that of the C contents, especially in roots (R^2 lower than 0.4). This suggested that significant differences in nitrogen use efficiency, assessed by the ratio of biomass to nitrogen content (Masclaux-Daubresse *et al.,* 2010), occurred between plants, maybe depending on identity of the inoculated strain.

Root, shoot and whole plant biomass values were then reported to the corresponding N contents (on a per plant basis), the resulting ratio corresponding to the so-called Nutrient Use Efficiency (NUE) index (Good *et al.,* 2004; Masclaux-Daubresse et al., 2010). The data are displayed in Figure 3.18. They indicate that NUE was reduced in inoculated plants, when compared with the non-inoculated LN control plants. This suggested plant growth was not limited by nitrogen availability in inoculated plants (in other words, that growth was limited by other factors).

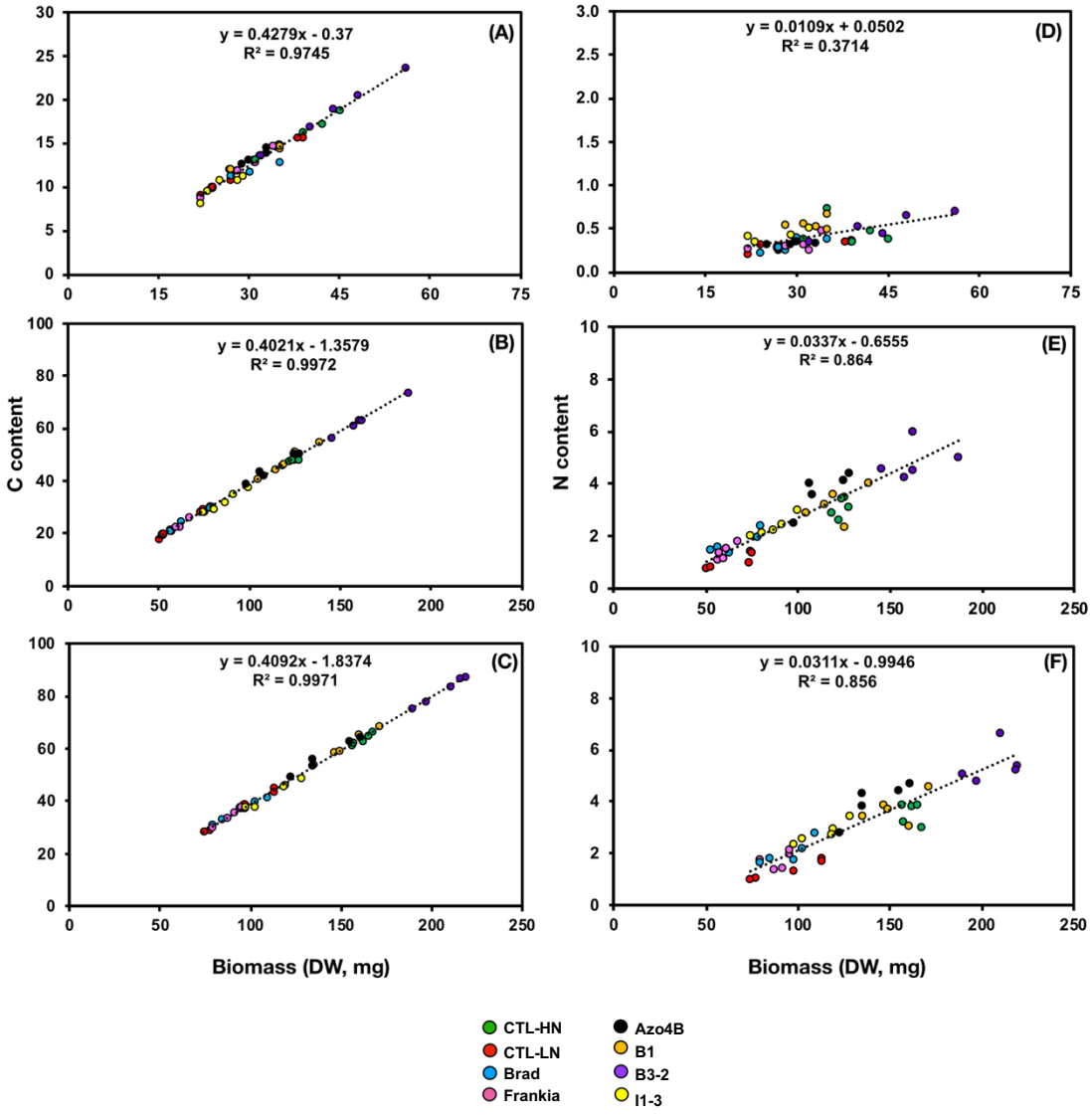

Figure 3.17. Relation between dry weight and total C contents and total N contents. Same plants as in the experiments described by Figure 3.14 (and Figure 3.15). All the data are expressed on a per plant basis. Plant growth conditions (HN and LN treatments) and inoculation: see Legend to Figure 3.14. HN and LN control plants: non-inoculated plants. The 6 selected bacterial strains are *B. japonicum* strain ORS285 (Brad), *Frankia* sp. R43 (Frankia), *A. lipoferum* strain 4B (Azo4B), Lebanese B1 isolate (B1), Lebanese B3-2 isolate (B3-2) and Lebanese I1-3 isolate (I1-3).

(A), (B) and (C): C contents (mg) versus DW (mg) in roots (A), shoots (B) and total plant (C).
(D), (E) and (F): N contents (mg) versus DW (mg) in roots (D), shoots (E) and total plant (F).

Root and shoot contents in P, K, Ca, Mg, Mn, Fe, Cu, Zn and Na were then assayed. The results were expressed on a per-biomass-unit (mg DW) (Figure 3.19). Altogether, the data indicated that both inoculation and the identity of the inoculated bacterial strain can affect the relative abundancy of nutrient elements in plant roots and shoots.

In summary, the results provided evidence that different bacterial strains were able to increase plant biomass production and to alter root and shoot contents in N and other nutrient elements, while reducing NUE. The mechanisms underlying these different effects are probably very diverse and complex, but we assumed that changes in root architecture and root hair development in response to bacterial strain inoculation could contribute to the consequences of the inoculation on plant development. In the following chapter, we present the work we have carried out to phenotype the effects of bacterial strains on root architecture and root hair development.

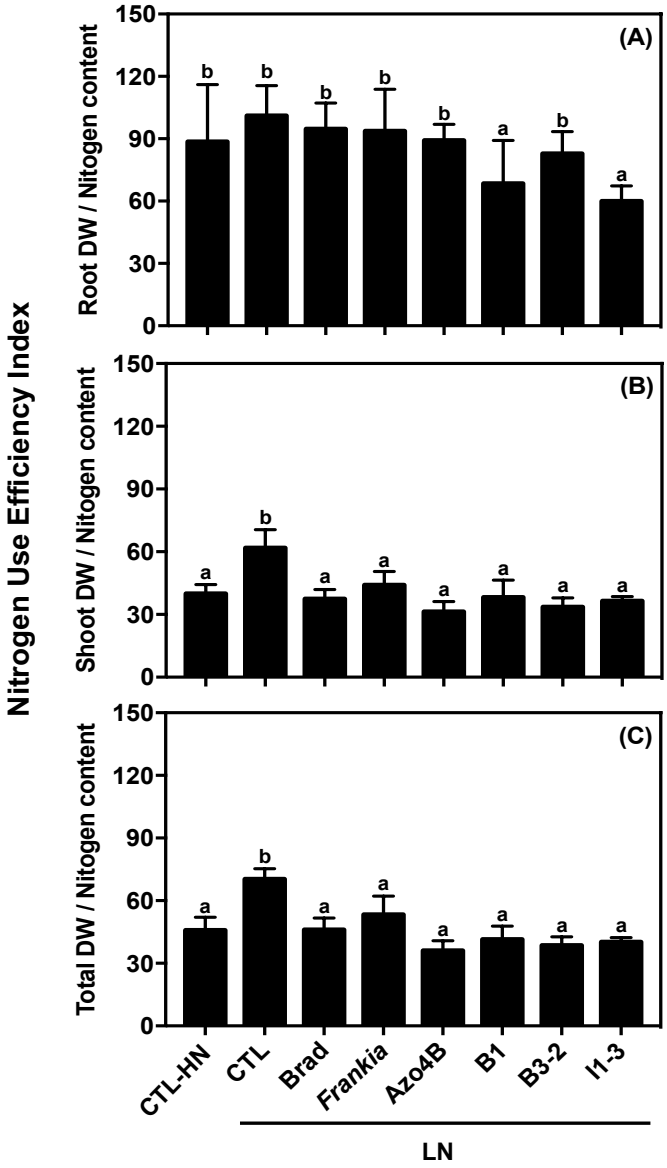

Figure 3.18. Effect of the 6 selected bacterial strains on plant Nitrogen Use Efficiency Index. Nitrogen Use Efficiency (NUE) Index: DW (mg) reported to N content (mg). Same plants as in the experiments described by Figure 3.14 (and Figure 3.15).

(A) Shoots
(B) Roots
(C) Total plant

Plant growth conditions (HN and LN treatments) and inoculation: see Legend to Figure 3.14. HN and LN control plants: non-inoculated plants. The 6 selected bacterial strains are *B. japonicum* strain ORS285 (Brad), *Frankia sp. R43* (Frankia), *A. lipoferum* strain 4B (Azo4B), Lebanese B1 isolate (B1), Lebanese B3-2 isolate (B3-2) and Lebanese I1-3 isolate (I1 3). Values are means ± SE (n = 5).

Values are means ± SE (n = 5). Different letters above histogram bars indicate statistical significance at $p<0.05$ (ANOVA).

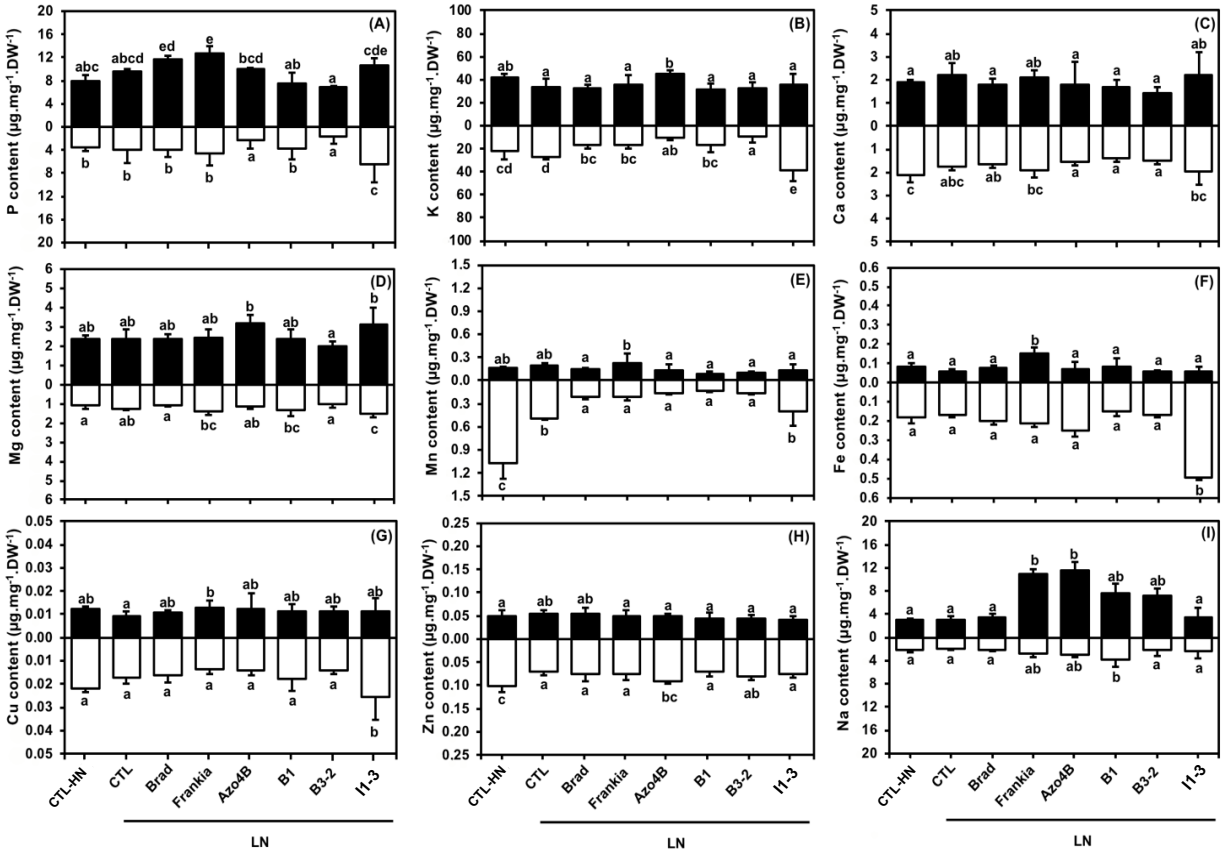

Figure 3.19. Effects of the 6 selected bacterial strains on wheat plant root and shoot nutrient element contents. Same plants as in the experiments described by Figure 3.14 (and Figure 3.15). Plant growth conditions (HN and LN treatments) and inoculation: see Legend to Figure 3.14. HN and LN control plants: non-inoculated plants. The 6 selected bacterial strains are *B. japonicum* strain ORS285 (Brad), *Frankia* sp. R43 (Frankia*)*, *A. lipoferum* strain 4B (Azo4B), Lebanese B1 isolate (B1), Lebanese B3-2 isolate (B3-2) and Lebanese I1-3 isolate (I1-3). P, K, Na, Ca, Mn, Fe, Mn, Zn and Cu (panels A to I, respectively) were assayed in roots and shoots (white and black bars, respectively) from the plants harvested at the end of the 30-day growth period (see legend to Figure 3.14). Means ± SE (n = 5). Different letters above histogram bars indicate statistical significance at $p<0.05$ (ANOVA).

Chapter 4

Development of methodologies for phenotyping root hair traits

4.1. Introduction: objectives and requirement specifications

Root interactions with PGPR strains can result in very diverse beneficial effects, from increased resistance to pathogenic microbes to improved plant mineral nutrition. We are interested in the mechanisms that could underlie this latter effect.

It has been frequently reported that PGPR can both promote root hair production and elongation and affect root system architecture, by inhibiting primary root growth and stimulating production and elongation of secondary roots. Our hypothesis is that these effects on root system and root hair development, by increasing the volume of soil that the plant exploits, can improve nutrient ion acquisition and thereby favor plant development and fitness. We have especially discussed the various roles of root hairs, at the crossroad of plant nutrition and interaction with soil microorganisms, in Chapter 1.

Within the framework of the above hypothesis, it can be reciprocally assumed that the magnitude of the effects of a given PGPR strain on root system architecture development and root hair elongation in a given plant species/cultivar is likely to reflect the capacity of this plant-PGPR couple to develop beneficial interactions. Thus, development of procedures allowing to quantitatively describe root responses to PGPR strains could allow, for instance, to screen collections of bacterial strains and/or of plant cultivars, as a first step in the search for most efficient couples of interacting partners under given environmental conditions, and to identify the underlying mechanisms via GWAS analyses.

Based on this consideration, we have aimed at developing methodologies allowing to describe root and root hair development with quantitative parameters in order to "quantify" the effects of abiotic and biotic conditions, especially reduced nutrient ion availability and presence of PGPR strains, on root traits.

The preliminary experiments we performed in order to assess the capacity of 6 different bacterial strains to promote root hair elongation on durum wheat (Chapter 5, Figure 5.5a and b) were carried out by using very young seedlings grown on agar plates. Such a methodology is often used in the literature, especially with the model plant Arabidopsis. Our objective has been to develop other types of procedures for the following 3 considerations:

- After germination, wheat seedlings develop more rapidly than Arabidopsis seedlings, and Petri dishes with classical sizes appear to be too small to allow wheat seedling development for more than a few days after germination. Thus, one objective of our work has been to develop

procedures allowing to use seedlings older than those grown on agar plates in Petri dishes.

- In seedlings grown on agar plates, parts of the root systems are present within the agar, while others roots grow just at the surface of the agar plate or above the agar plate in the Petri dish (in the air at about 100% relative humidity). In our tests, root hairs grown within the agar are found to display reduced elongation while those grown in the air display the longest size. Such differences can lead to a "subjective" choice of the portion of the root systems that are analyzed, likely to introduce some bias in the quantitative analysis of root hair elongation.
- Root manipulation and transfer onto a glass slide for observation under microscope can result in root hair loss of turgidity and damage. An example of such problems is provided by Figure 4.1. Thus, we aimed at reducing the risk of introducing such artifacts, resulting for instance from larger damage to the longest root hairs, or from the fact that the longest root hairs would have fallen along the root surface and therefore become poorly distinguishable.

Based on these considerations, we developed two different methodologies during my PhD work, as previously indicated in the § 2.5 and 2.6 of the *Material and Methods* Chapter. The first one is strictly dedicated to the observation of root hair zones under microscope. The plants are hydroponically grown for in a home-made device, named "cuvette", that can be directly transferred onto the microscope stage without manipulation of the root system. Photographs are taken about 7-days after plant germination. The second methodology allows to get images of the whole root systems of *ca.* 2-week old seedlings grown at the surface of a dark tissue in a rhizobox-like device. Images of the rhizobox are high resolution scans that allow to analyze root hair length and density all over the root system. These two methodologies are described in details in the next paragraphs.

4.2. The "cuvette" methodology to phenotype root hair traits

4.2.1. The experimental setup

Since transfer of root samples on glass slides for observation under microscope is likely to result in root hair damage, the objective was to use a plant growth device allowing direct observation of root hair zones without any transfer on a glass slide. Several prototypes of home-made devices have been successively tested. They were produced using 3-D printers. Their design allowed to adapt a glass slide and coverslip, with a space of 3 mm between them, forming a "window" through which roots could be seen and photographed.

The general shape of the device is adapted to the microscope stage. The dimensions and design of the prototypes currently in use are provided by Figure 4.2. The side view in Panel C allows to see the position of the glass slide and coverslip in

the device, and the way they can be adjusted and fixed with a dentistry silicone glue to the plastic device. The main root of a germinated seedling is introduced in a 4-mm diameter tunnel that allows the growing root to reach the "window" through which it can be photographed by the microscope system (Figure 4.3). A 2 mm diameter tunnel present in the upper part of the device and a 3-mm diameter tunnel present in the lower part (Figure 4.2) allow air and water movements through the device, and thereby rapid re-equilibrium of the hydrostatic pressure and level of solution within the device when the level of the solution outside the device is varied in order to oxygenate the solution within the device.

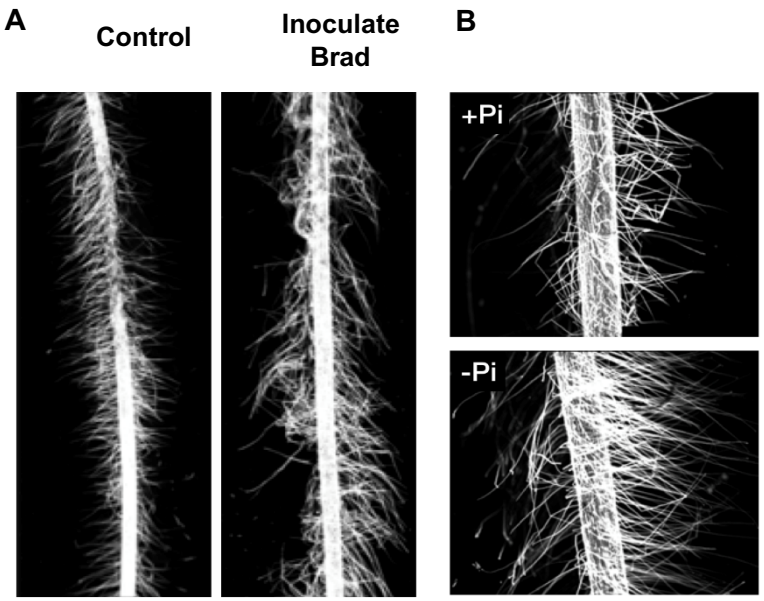

Figure 4.1. Root hair zones after translocation of root samples onto a glass slide for observation under microscope. Wheat seedlings were grown on agar plates (Hoagland medium) for 5 days after germination. Root segments (about 1 cm long) observed were present just above the surface of the agar plate and were excised at 1.5 cm from the root tips. They were transferred onto a glass slide, immerged in water and covered with a glass cover slip for observation under microscope. Panel A: the plants were non-inoculated (left) or inoculated with *B. japonicum* strain ORS285 (right). Panel B: non-inoculated plants were grown on Hoagland-agar medium containing 0.5 mM Pi ($H_2PO_4^-$) or on modified Hoagland medium without Pi (top and bottom photographs, respectively).

Figure 4.3 illustrates the position of the seedling and of the growing roots in the device. Only the coverslip has been adjusted to this prototype, and not the glass slide.

Such a "cuvette", with its seedling, is placed into a container filled with the nutrient solution to be tested as displayed by Figure 4.4, the seedling having been inoculated or not before its transplantation to the cuvette. In the experimental setup illustrated by Figure 4.4, the cuvette is inclined by about 30 degrees with respect to vertical direction. In such position, because of gravitropism, roots preferentially grow along the surface of the lower face of the cuvette, to which the coverslip has been fixed. In this experiment, the corresponding glass slide was not fixed to the opposite face (the upper face) of the cuvette.

A setup comprising 2 pumps and 2 water level sensor allows to pump out the solution from the container into a second container and to pump it back, with an automatic and continuous flow of solution from one compartment to the other. The total volume of solution and the positions of the water level sensors are set to allow the maximal level of the solution to be 2 cm below the seed, and the minimal level at about 3 cm above the bottom of the container. The successive emptying and refilling of the container results in similar displacements of the level of the solution within the cuvette, ensuring that the oxygen partial pressure within the cuvette remains at the same value as that in the bulk solution despite O_2 consumption by the growing roots within the cuvette. A scheme of the electrical circuit that controls the pumps is provided by Figure 4.5.

Figure 4.6 provides a photo of a wheat seedling and its roots in a cuvette device (Panel A), the device on the microscope slide (Panel B), and a root segment with root hairs under the microscope (Panel C). Such photos can be analyzed using the MRI-RHT program, also named MRHT (Montpellier Rio Imaging-Root Hair Tool) that is described here below. This program has also been more shortly named MRHT in the following text).

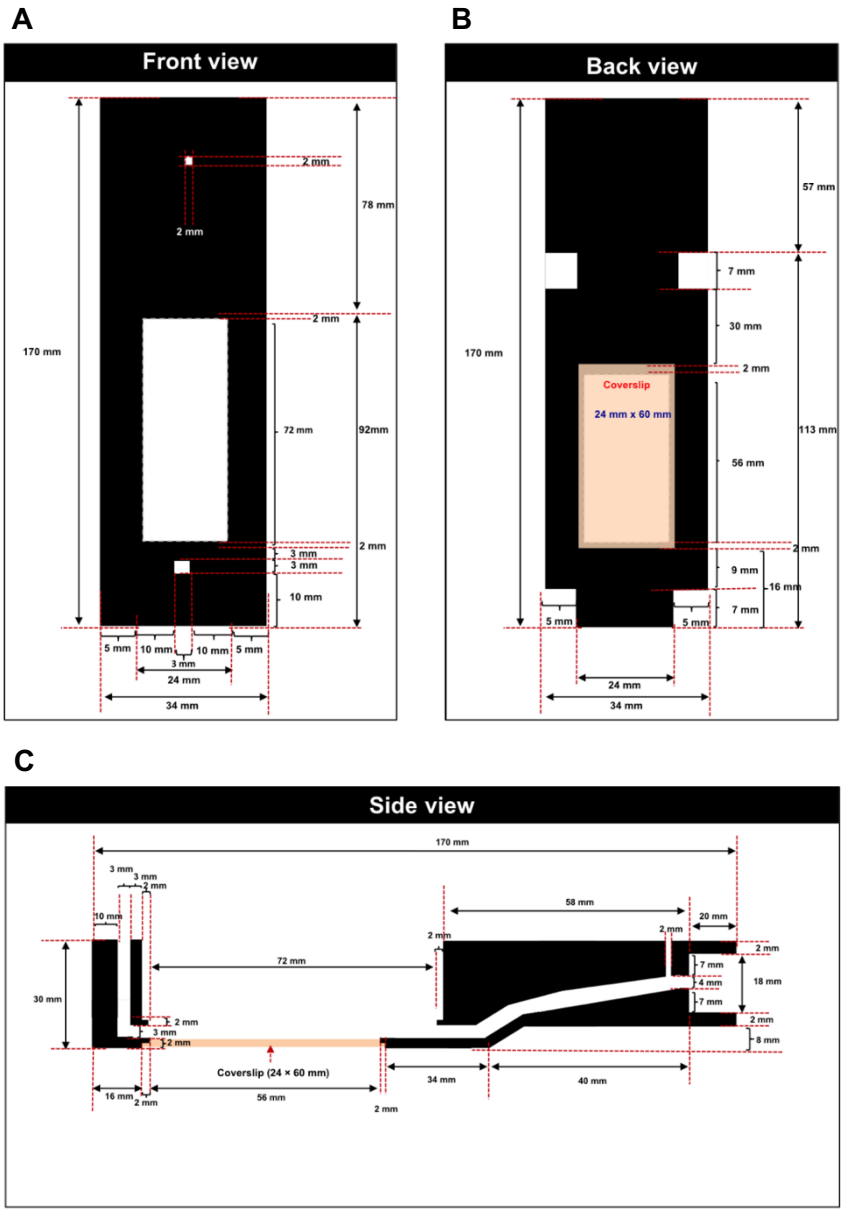

Figure 4.2 Schematic description of the "cuvette" device: 2D drawing into a 3D model. Front view (A), Back view (B) and side view (C).

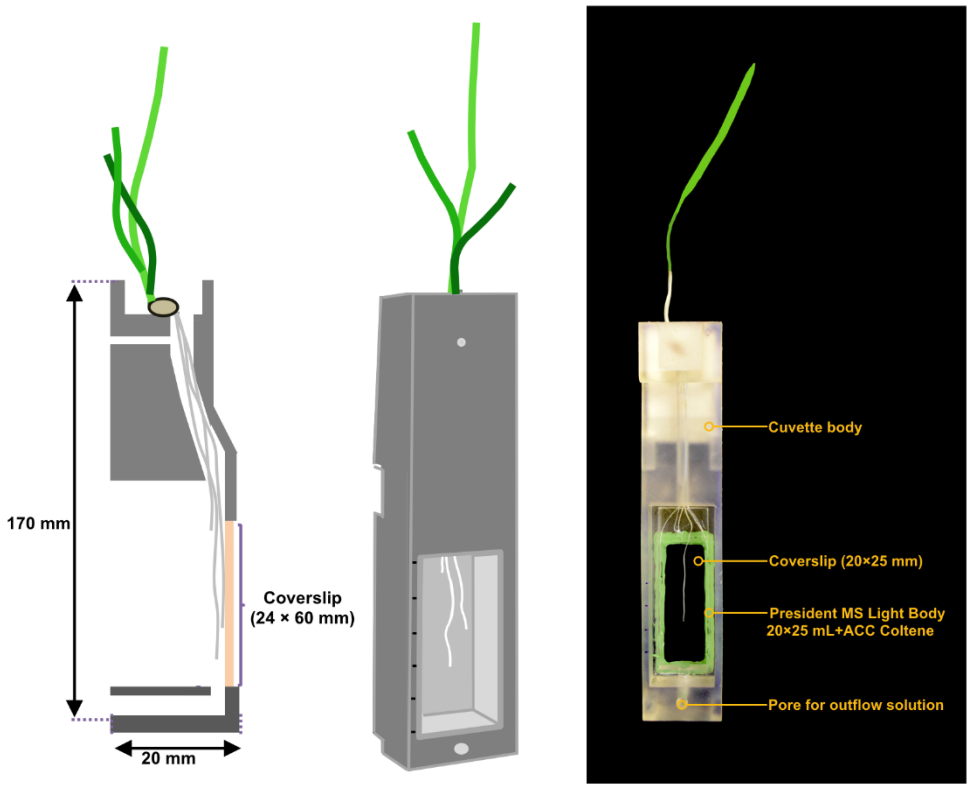

Figure 4.3. Representation of a wheat seedling grown in a cuvette device. The whole shape of the device is adapted, when horizontally placed, to the stage of the microscope (Zeiss Apotome). The growing roots can be observed through the "window" formed by a cover slip, and a glass slide fixed to the cuvette frame (see Figures 4.2 and 4.4).

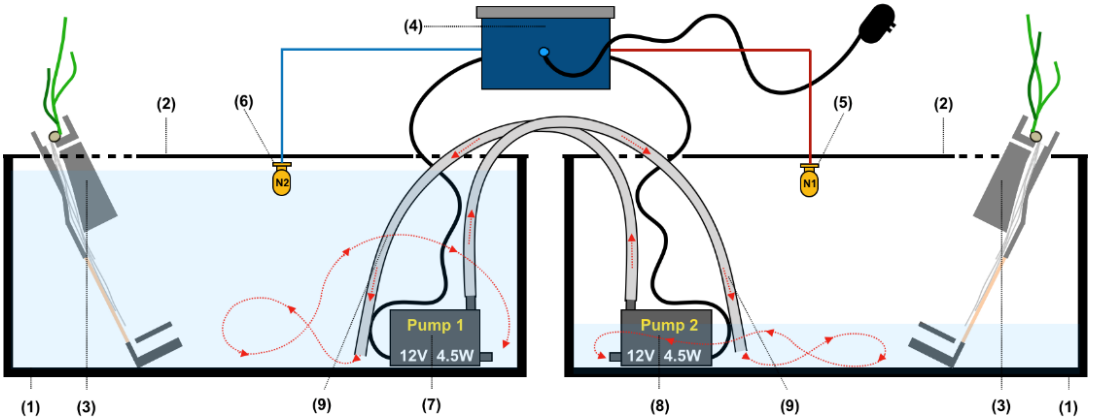

Figure 4.4. Schematic diagram of the pumping system ensuring renewal and oxygenation of the solution within the cuvette devices placed in containers filled with the tested nutrient solution.

(1) Plastic containers (10 L)
(2) Plastic container lids
(3) Cuvette
(4) Controller box (see Figure 4.6)
(5) Sensor 1 (Level sensor normally open (Floodsw2 contact of)
(6) Sensor 2 (Level sensor normally open (Floodsw2 contact of)
(7) and (8) Pumps: Mini Water Pump DC 12V 4.5W 240L/H Flow Rate, Waterproof Brushless (Mini Submersible Water Pump QR30E)
(9) Polyethylene tube (diameter 1.2 mm)

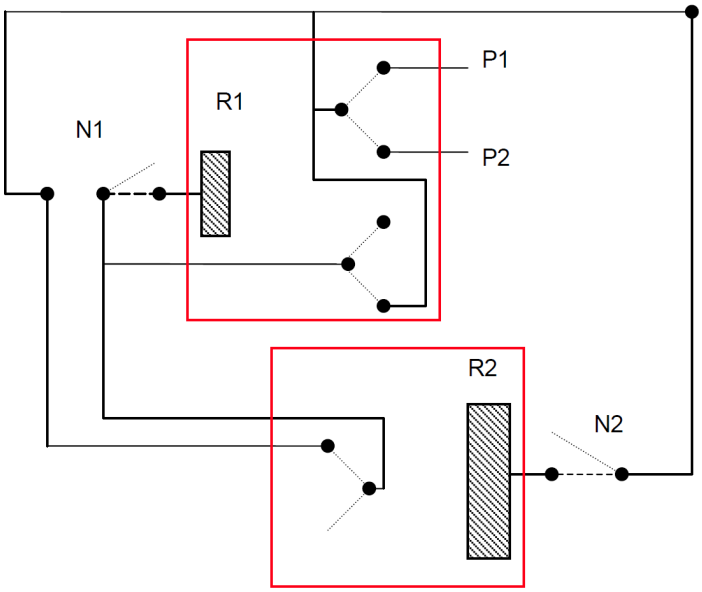

Figure 4.5. Schematic diagram of the electrical circuit in the controller box ensuring alternative solution transfers between the 2 containers and their cuvette devices.

R1 : Double inverter relay (control coil-figured by the hatched rectangle- powered in 12Vcc depending on switch N1, both inverters at up position at rest, at down position if 12Vcc is applied on control coil)
R2 : Single inverter relay (same as R1 but single inverter and coil power depending on switch N2)
N1 : Liquid level sensor in container 1, consisting in a switch normally open (i.e. OFF) while liquid level is down and becoming closed (i.e. ON) when liquid level reached the desired up position.
N2 : Liquid level sensor in container 2 (same operation mode as N1).
P1 : Pump 1 (Mini Water Pump DC 12Vcc 4.5W, powered through first inverter of R1). It empties container 1 if ON
P2 : Pump 2 (Mini Water Pump DC 12Vcc 4.5W, powered through first inverter of R1) . It empties container 2 if ON

Example of operation step sequence;

1) Container 2 being emptied / container 1 being filled: N1ON, N2ON, R1DOWN, R2DOWN, P2ON, P1OFF
2) Container 1 filled, initiation of its emptying: N1OFF, N2ON, R1UP, R2DOWN, P2OFF, P1ON
3) Container 1 being emptied / container 2 being filledN1ON, N2ON, R1UP*, R2DOWN, P1ON, P2OFF
4) Container 2 filled, initiation of its emptying: N1ON, N2OFF, R2UP, R1DOWN, P1OFF, P2ON
5) Container 2 being emptied / container 1 being filled: N1ON, N2ON, R1DOWN, R2DOWN, P2ON, P1OFF (same as step 1, and so on)

With the nominal flow rate of the pumps and the diameter of the tubing, the period of the cycle from step 1 to step 5 is approximately 3 minutes.

*The R2 state depends solely of the one of the N2 level detector/switch : DOWN if N2 is ON and UP if N2 is OFF) . Control of R1 UP/DOWN is as follows : R1 gets UP when N1 gets OFF and it remains locked UP as long as N2 stays ON : thus, when N1 changes for ON, R1 keeps UP. When N2 gets OFF, this unlocks the UP state of R1 that can get DOWN (as N1 is ON) and this makes the commutation from pump1 ON and pump2 OFF to pump1 OFF and pump 2 ON.

Electrical design by Dr. Jean-Baptiste Thibaud, UMR 5247, IBMM, Montpellier

4.2.2. Description of the MRI-RHT program developed for automatic phenotyping of root hair traits

Using the ImageJ software, a program dedicated to the analysis of images such as those obtained with the "cuvette" device (Figure 4.6) has been written for automatic root hair trait phenotyping by Volker Baecker (Bioimage Analyst, Montpellier Ressources Imagerie, CNRS-INSERM), in interaction with us. This program has been named MRHT, for Montpellier RIO Imaging_Root Hair Tool.

From such images, the MRHT program can provide estimations of root hair density, mean root hair length, maximal length, and total surface (number of pixels) of the root hairs. The program and its code are available at:
http://dev.mri.cnrs.fr/projects/imagej-macros/wiki /MRI_Root_Hair_Tools

A schematic description of the way the program works is provided by Figure 4.7. In summary, the photo is cleaned, segmented and binarized (black pixels for root tissues and white pixels for the background) (Figure 4.7, panel A). Then two lines are drawn along the frontiers of the root in the image, one line along the upper side and one line along the lower side of the root in Panel B of Figure 4.7 (lines drawn in blue in the Figure, but in yellow on the screen when the program is running (see later, Figure 4.10D). These lines, which will be used to "describe" root hair traits, are named "analyzing lines" in Figure 4.7. Each line is shifted away from the root surface, pixel by pixel, letting it to remain "parallel" to the root surface (Figure 4.7, Panel C for the upper line). These successive displacements are stopped as soon as the line does not cross any black pixel (*i.e.*, does not cross any root hair). Then, the distance between this position of the line and the root surface provides an estimate of the length of the longest root hair(s) (Figure 4.7, Panel C, and Figure 4.8). Furthermore, at each position of the line between its initial position along the root surface and its final position at the extremity of the longest root hair(s), the line is "analyzed" from left to right with respect to the "color" (white or black) of the pixels it crosses: a transition from a white to a black pixel in the movement from left to right means that the line has entered a new root hair, and "+1" is added to a counter (Figure 4.7, Panel D). The number of root hairs that the line crosses at each position from the root surface is thereby determined. The relationship between the distance x of the line to the root surface and the number of root hairs n that the line has crossed when present at this distance of the root surface allows to determine the number of root hairs that have a given length (Figure 4.7, Panel E, and Figure 4.8) and thereby, for instance the root hair mean length. The number of root hairs that the line crosses when it is close to the root surface (Figure 4.8) provides an estimate of the root hair density at this "side" of the root in the photo. Finally, this procedure allows also to "count" the total number of "black" (root hair) pixels that the two lines have crossed, and thus a parameter that reflects the total surface occupied by root hairs in the photograph.

Figure 4.9 explains how to install and use the MRHT tool within the ImageJ software, and Figure 4.10 describes the program workflow.

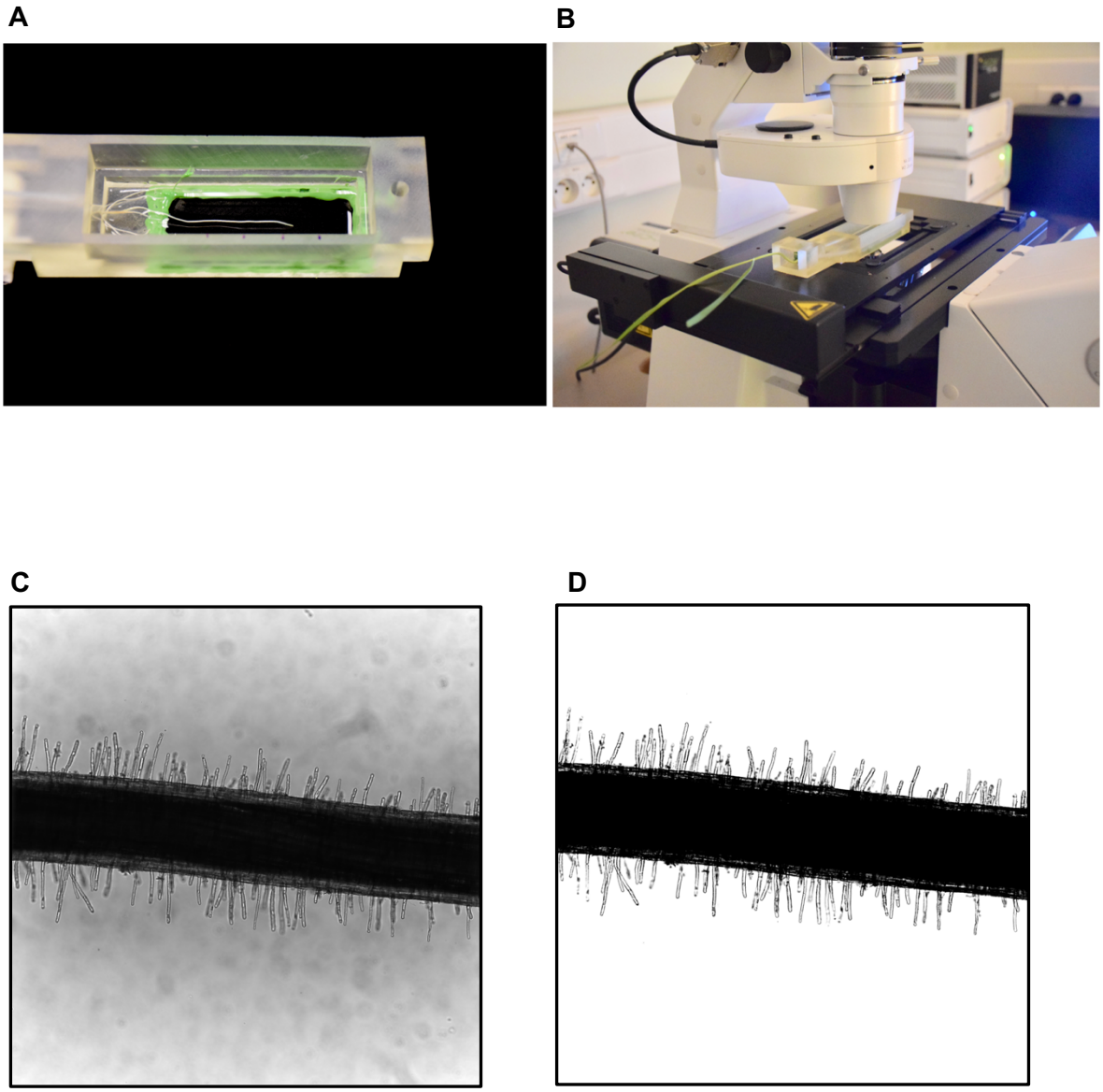

Figure 4.6. Observation of the growing roots at the surface of the cover slip of the cuvette window.

(A) Preparation of the seedling main root immerged in the solution contained in the cuvette.
(B) Cuvette under the Microscope (Zeiss Apotome).
(C) Example of photos obtained with the cuvette device.
(D) Same photo but after background cleaning and binarization using the ImageJ software.

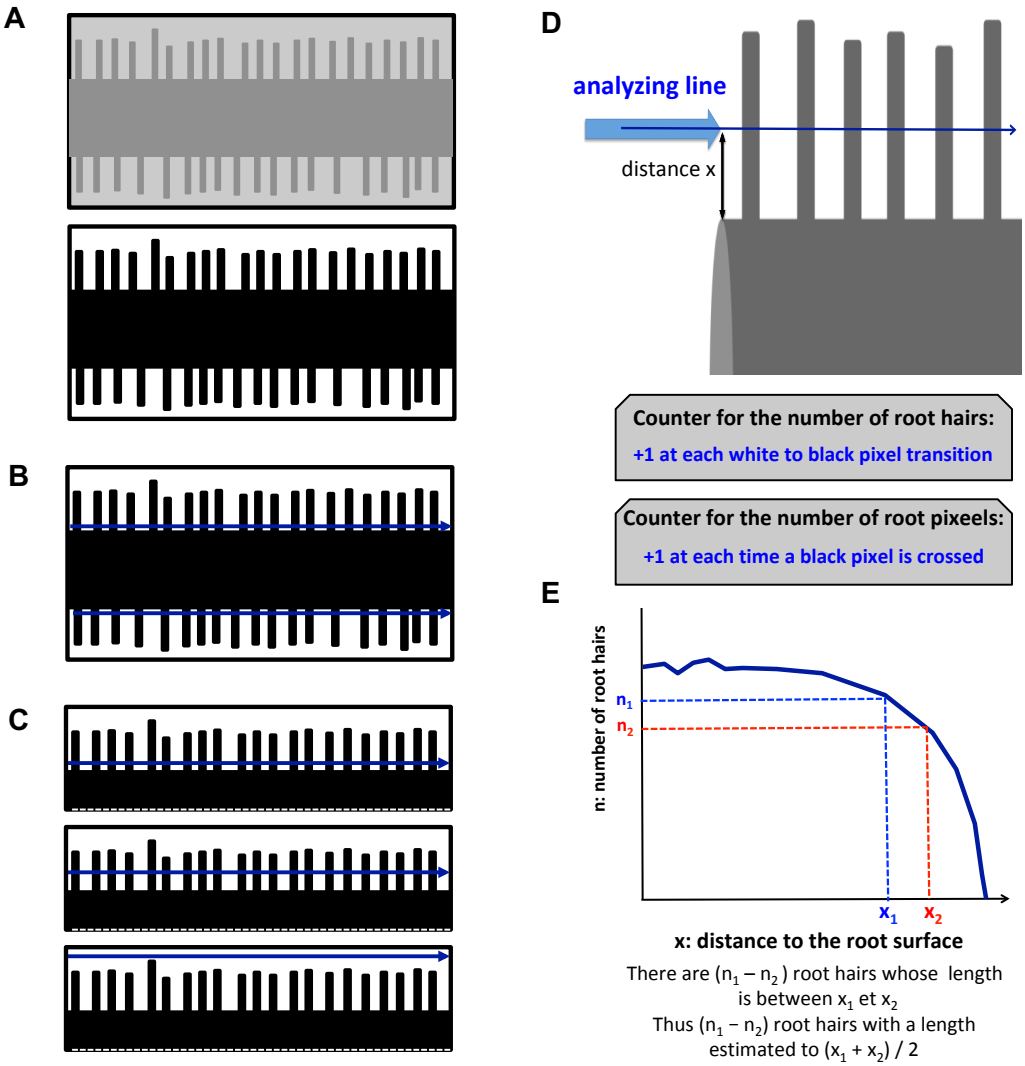

Figure 4.7. Representation of the MRHT program that has been developed for phenotyping root hair length and density. (A) Binarization of the root segment (the pixels are set to white for the background and to black for the root). (B) The root surface is identified and a line ("analyzing line") is drawn along the surface on both side of the root (lines in blue). (C) The program moves each analyzing line away from the root surface, pixel after pixel, until the line does not cross any root hair. The corresponding position provides the maximal length of the root hairs. Note that a single line and only the upper half "view" of the root are displayed in the Panel. (D) At each distance x (in pixels) from the root surface, the "analyzing line" explores the photo from left to right and identifies the presence of a root hair (and adds +1 to the corresponding counter) when it finds a transition from a white to a black pixel. (E) Curve displaying the relationship between the distance x of the analyzing line to the root surface and the number n of root hairs that the line has crossed at this position. This relationship allows to determine the number of root hairs having a given length.

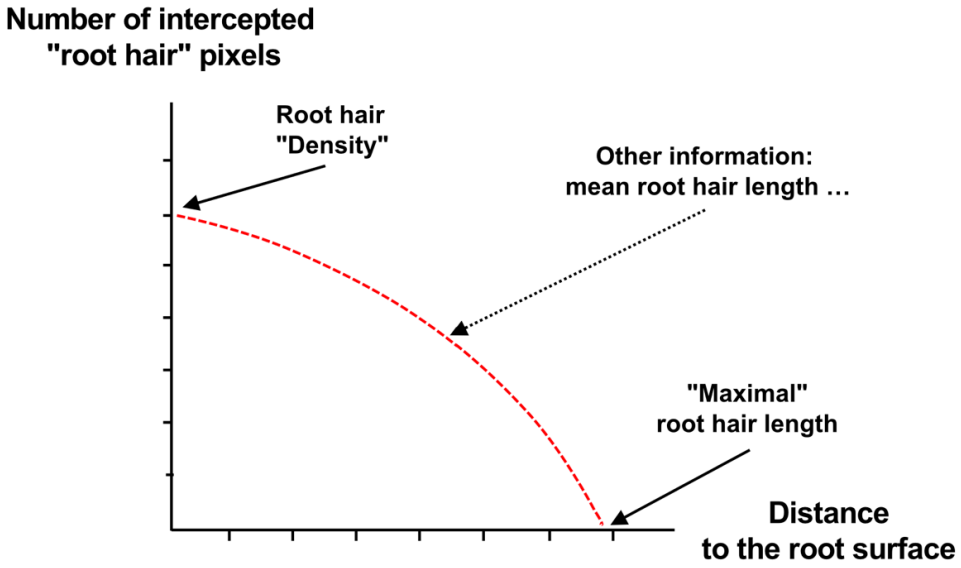

Figure 4.8. Summary of the phenotyping information that the MRHT program provides from the analysis of the curve describing the relationship between the distance to the root surface and the number of root hairs that are longer than this distance.

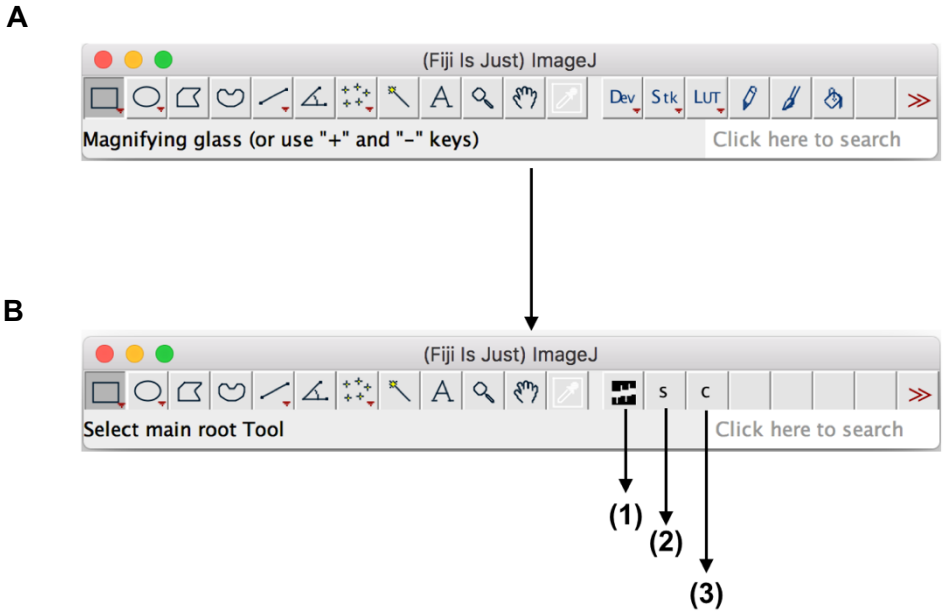

Figure 4.9. Running the MRHT program.

(A) The ImageJ launcher window

(B) The toolset menu of the MRHT program on the ImageJ launcher window.

(1) Open the MRHT (MRI_Root_Hair_Tools) page.

(2) The s button selects the main root and measures its diameter.

(3) The c button starts the analysis of the root hair traits as described by the panels B to E of Figure 4.7. The upper and lower "side" of the root in the photo are independently analyzed. This will provide, for each "side" of the root, the following plot: (i) the number of root hairs as a function of root hair length, (ii) root hair density as a function of the distance to the root surface, and (iii) the number of root hair pixels reported to the number of root hairs as a function of the distance to the root surface (in each case for both the upper and lower sides of the root).

Installation of the MRHT program into the ImageJ macros and workflow of the program: see Figure 4.10.

Program written by Volker Baecker (CNRS-INSERM, Montpellier RIO Imaging)

A

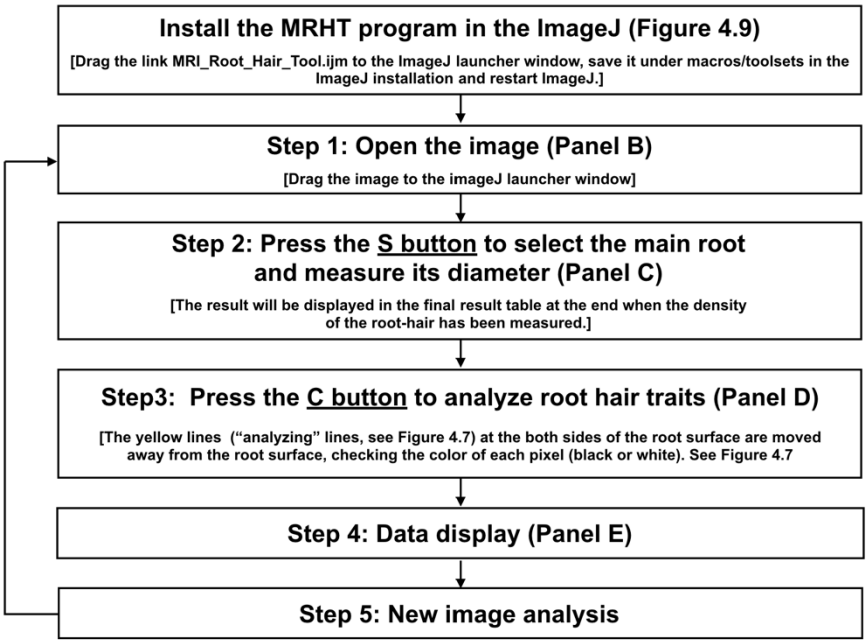

B C D

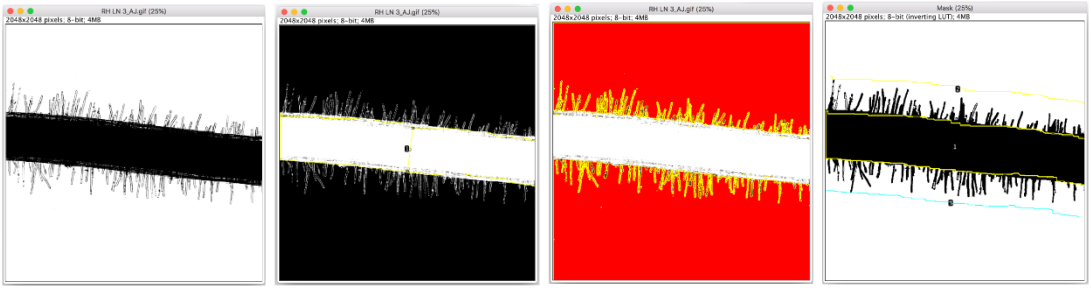

E

root hair measurements

n	image	side	length	width	nr. hairs	max Length	average length	nr. of Pixel	area	density
1	RH LN 3_AJ.gif	top	2138.4698	349.9057	59	271	98.5203	133201.806	133201.806	0.2171
2	RH LN 3_AJ.gif	bottom	2130.8222	349.9057	61	252	94.3533	119690.997	119690.997	0.2079

Figure 4.10. Workflow of the MRHT program. See Figures 4.7, 4.9 and main text.

Program written by Volker Baecker (CNRS-INSERM, Montpellier RIO Imaging)

4.2.3. Test of the MRHT program

In order to test the outputs of the MRHT program when compared with "manual" analysis directly carried out using the ImageJ software, photographs of root zones were taken using the Apotome microscope at about 1 cm from the main root tip from 13 durum wheat seedlings grown in different conditions. The values of the root hair mean length and maximal length provided by MRHT for this set of 23 images are compared on Figures 4.11 and 4.12 to the corresponding values obtained by "manual" analysis. Taken as a whole, these analyses indicate that the MRHT program can be considered as sufficiently operational and trustable for carrying out our analyzes.

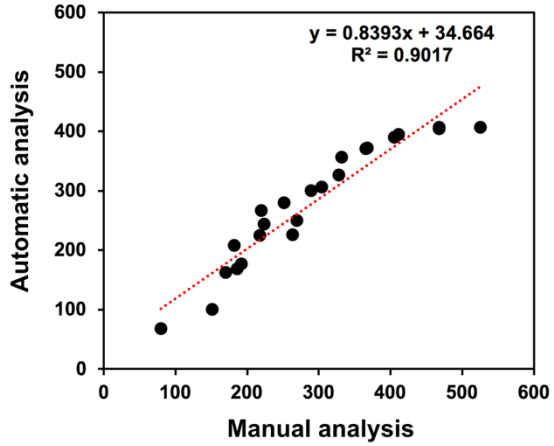

Figure 4.11. Test of the MHRT program. Comparison of the number of root hairs identified by manual analysis or by the MRHT program. A set of 23 photos of root hair regions from wheat seedlings grown in different conditions and for different times have been used for this test.

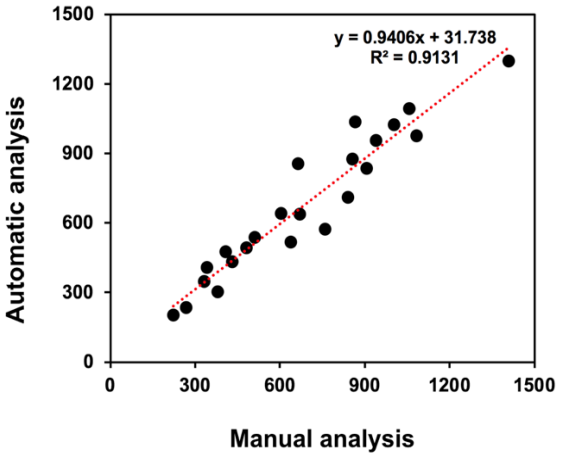

Figure 4.12. Test of the MHRT program. Comparison of the maximal root hair length determined by manual analysis or by the MRHT program. A set of 23 photos of root hair regions from wheat seedlings grown in different conditions and for different times have been used for this test. ImageJ was used for manual analysis of the images.

4.3. The "rhizobox-like" methodology to phenotype root hair traits from whole root systems

4.3.1. The experimental setup

Different kinds of rhizobox-like prototypes have been successively tested. They differed, for instance, in the substrate, artificial soil, filter paper, or tissue, in which - or at the surface of seedling roots can grow. Growth at the surface of a piece of tissue appearing as the best solution, different kinds of tissue were tested (different material and mesh size). Then, we considered that a solid substrate was to be introduced "behind" the tissue, filling the interspace between the two glass plates of the rhizobox, in order to "buffer" and control the level of humidity at the tissue surface. Trials performed using artificial soils (sand, perlite, vermiculite and mixes) revealed that the pressure of the substrate against the tissue and the glass plate displayed strong local heterogeneities, probably especially when the substrate was rendered humid by watering, and that such heterogeneities profoundly affected the final development of the root system architecture, the roots growing through the zones where the pressure is weaker, and the quality of the scan (mist droplets). The solution to this problem has been to introduce a "solid board" of polyurethane foam "behind" the tissue. The polyurethane foam board has the dimensions of an A4 (or A3) sheet of paper, since the rhizoboxes are scanned with a A4/A3 high resolution scanner, and a thickness of 10 mm. In practice, a piece of tissue a little bit larger than two A4 sheets is sewed to form a bag of A4 dimensions, within which the polyurethane board is introduced. The rhizobox is thus rendered symmetric and seedlings can be grown between the tissue and the glass plate on both sides of the rhizobox.

A schematic description of presently used rhizobox prototypes is provided by Figure 4.13. An automatic plant watering system was fitted to the experimental device, as shown in Figure 4.14. Sets of rhizoboxes, sharing the same watering device (and timer), are installed within supports made of polystyrene boards (Figure 4.15).

4.3.2. Description of the ACRT program developed for analyzing root systems from plants grown in rhizobox devices

An example of the images that were obtained using the rhizobox-like method is provided by Figure 4.16. Parts of the image have been enlarged, showing that large portions of the root systems harbor root hairs.

The MRHT program developed for phenotyping root hair traits (density, length…; see above) from photos obtained using the "cuvette" methodology did not appear to be actually adapted to the analysis of images of whole root systems such those provided by the rhizobox methodology. We are currently testing the commercially available WINRHIZO^{TM} software (see chapter 5), but we have also started to work at defining a strategy to characterize from such images root (hair) traits likely to be relevant to soil foraging and nutrient acquisition.

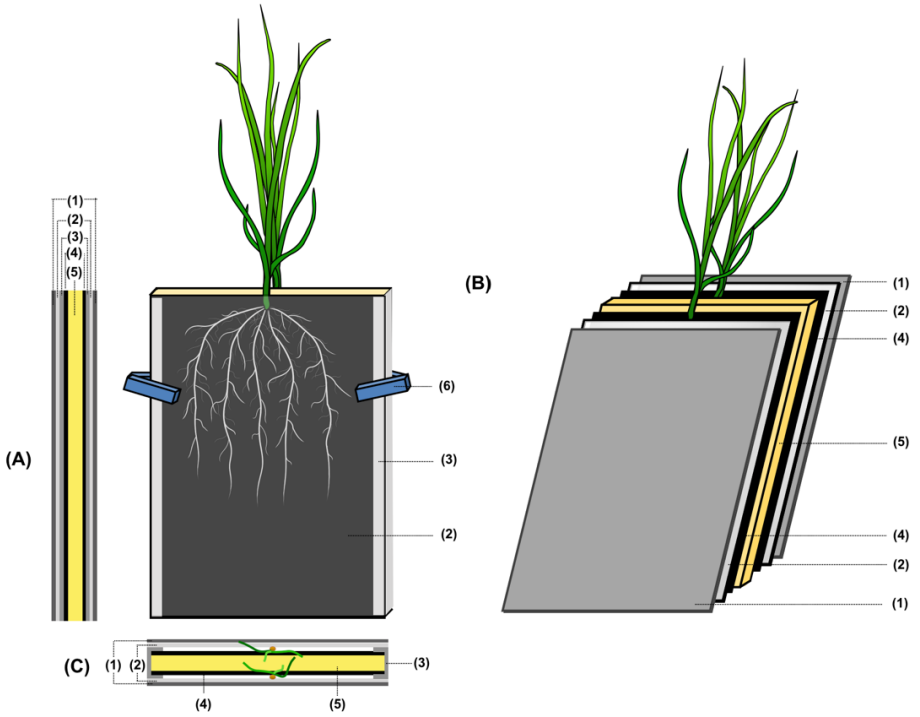

Figure 4.13. Schematic diagram of the presently used glass-wall rhizoboxes. Side view (A), Front view (B) and Top view (C).

(1) Non-transparent foam board with aluminium foil (260×320×4 mm.): external protection against light (i.e., preventing light to reach roots).
(2) Glass plate (260×320×2 mm.)
(3) Aluminum slide bar (200×320×15 mm.)
(4) 100% Black polyester (PES 18/13)
(5) Solid polyurethane foam board (260×320×15 mm.)
(6) Nylon spring clamp 100 mm (Dexter)

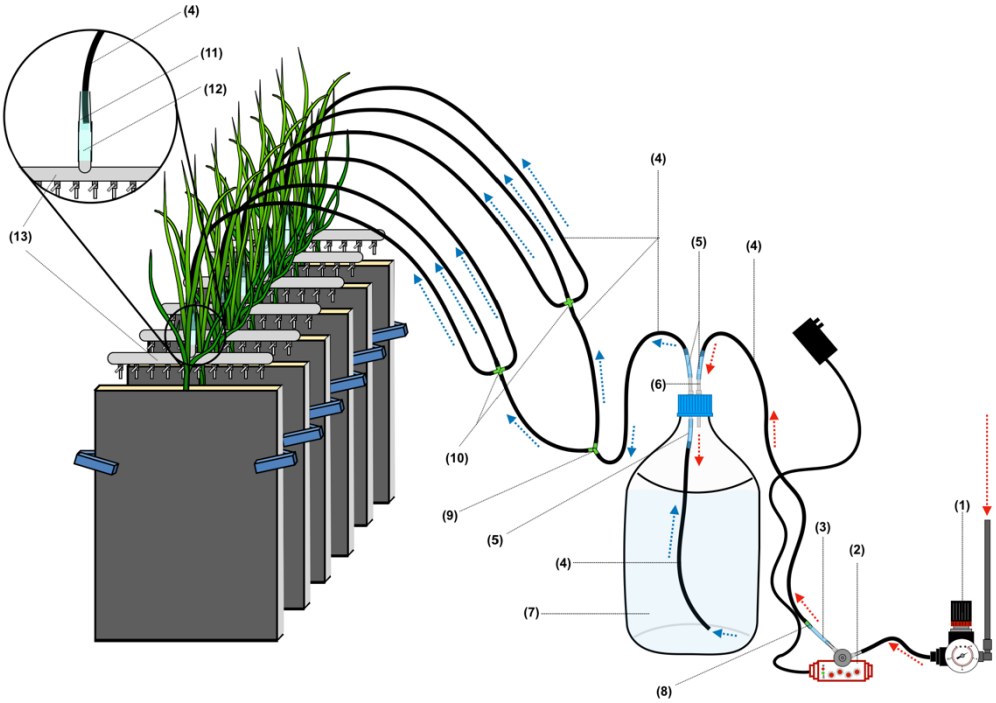

Figure 4.14. Schematic description of the automatic irrigation system for growing wheat seedlings in the rhizoboxes.

(1) Air pressure regulator (Gauge regulator & pressure regulating valve)
(2) Timer allowing to fix the duration of the watering episode and of the inter-episode.
(3) Polyethylene tubing (diameter 0.6 mm)
(4) Polyethylene tubing (diameter 1 mm)
(5) Polyethylene tubing (diameter 1 mm)
(6) Connector tubing (2 ways, 1/8” to 1/8”)
(7) Lab Schott bottle (5 liters) with blue cap
(8) Two- way air valve line connector
(9) Aquarium tank plastic 3 way air valve line connector
(10) Four-way air valve line connector
(11) Polyethylene tubing (diameter 1 mm)
(12) Polyethylene tubing (diameter 1.2 mm)
(13) Stainless steel air flow splitter, 1 (input) + 10 ways (see inset).

Figure 4.15. Assembly of a set of rhizoboxes with a polystyrene tray.

Images such as that displayed by Figure 4.16 clearly show that root hair development resulted in a very strong increase in the absorptive surface of the root system. We have considered that assessing the root surface by counting the number of pixels belonging to the root system in the image, with respect to the distance to the line corresponding to the soil surface, i.e. the "depth in the soil" or to the distance to the initial germinated grain could reflect.

- the contribution of root hair development to the root absorptive surface
- the root system capacity to explore and mine the soil.

Within this framework, as a preliminary step, a program has been written (as an ImageJ macro) to determine the "area" of root tissue in dependency of the "*depth*" in the soil or the distance to the germinated grain. This program, which has been written by Volker Baecker (CNRS-INSERM Montpellier Ressources Imagerie) like the MRHT program, has been named ACRT (Analysis of Complex Root system Tool). The toolset menu within ImageJ and the workflow of this program are described in Figures 4.17 and 4.18.

The program is available at:
https://github.com/MontpellierRessourcesImagerie/imagej_macros_and_scripts/wiki/Analyze_Complex_Roots_Tool

First analyses using the ACRT program of images provided by the rhizobox methodology are reported in Chapter 5.

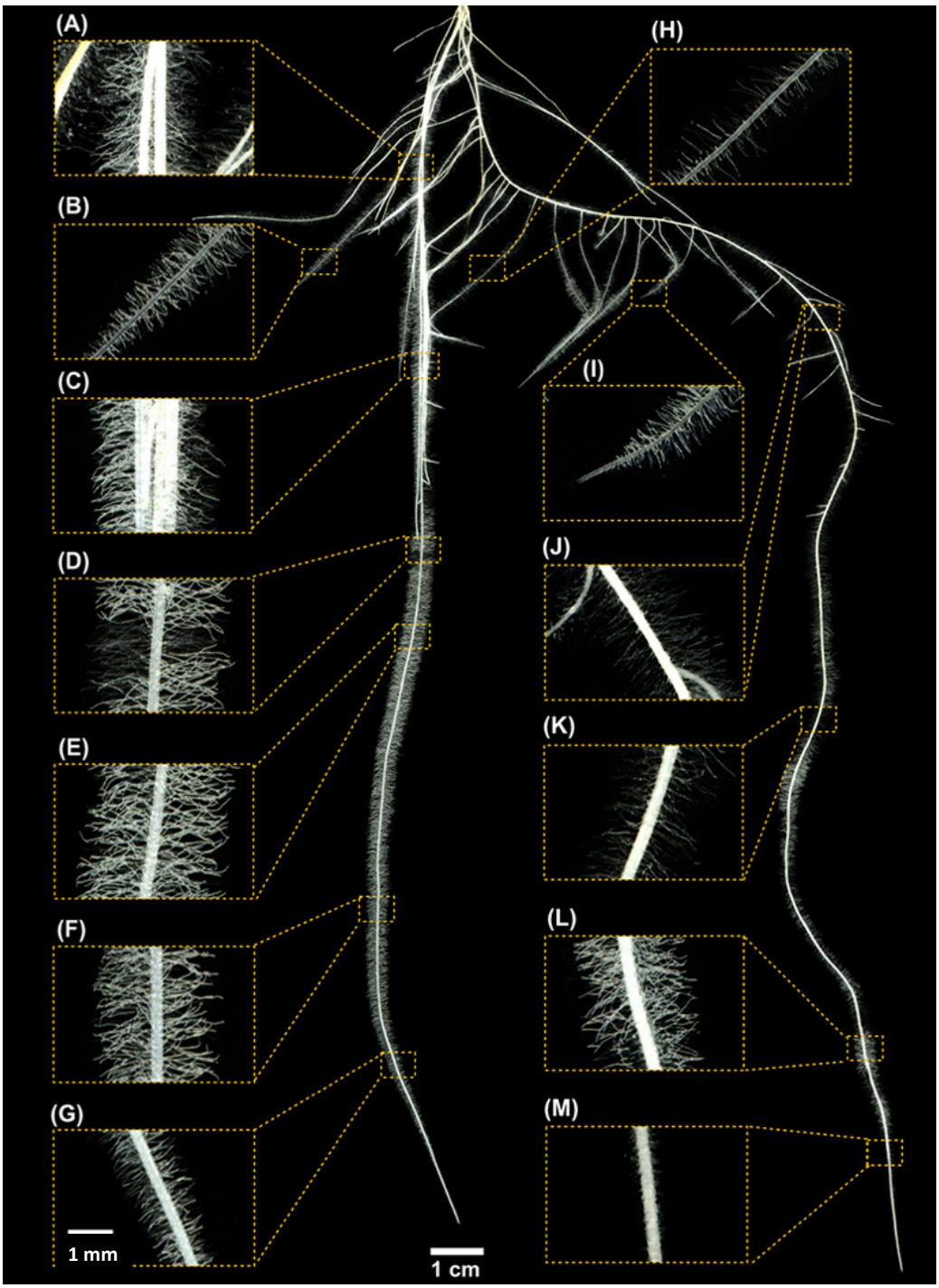

Figure 4.16. Representative example of root system images obtained from the rhizobox methodology. Durum wheat seedling grown for 12 days on LN (low nitrogen) medium.

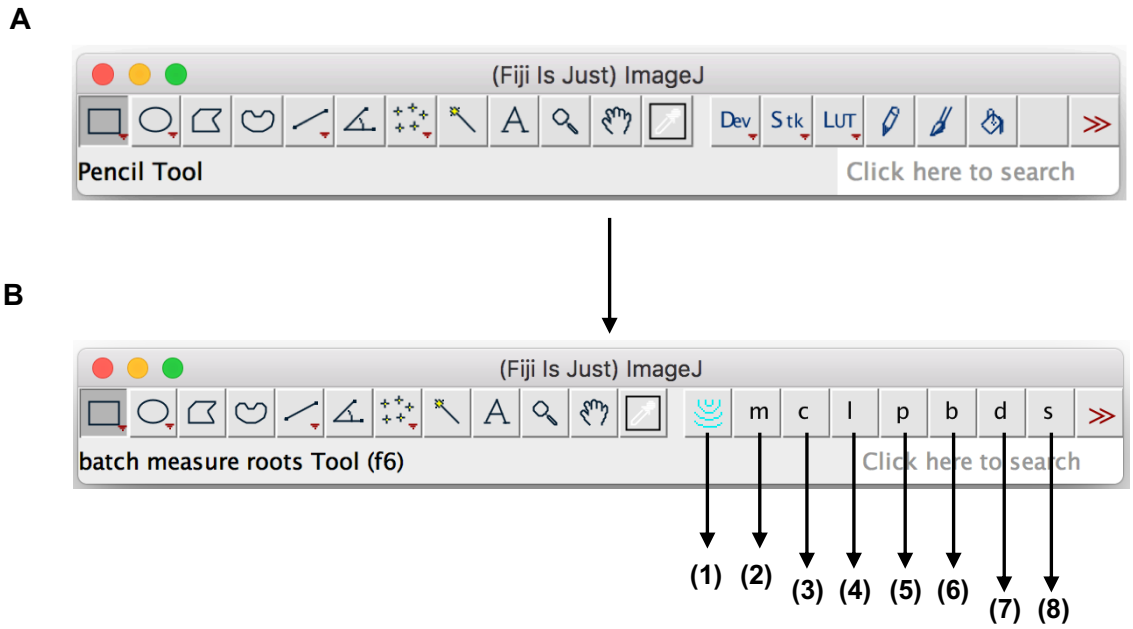

Figure 4.17. The toolset menu of the ACRT program in the ImageJ launcher window and program running.

(1) Open the ACRT (analyze_complex_root_tool) page.
(2) m-button: create the binary mask, and distance transformation of the image.
(3) c-button: activate the circle tool.
(4) l-button: activate the line tool.
(5) p-button: select the features per distance or depth.
(6) b-button: select the features to export depending on the option chosen with the p-button, and start the batch-process.
(7) d-button: delete the data column
(8) s-button: calculate the average, SD and SE

Program written by Volker Baecker (CNRS-INSERM, Montpellier RIO Imaging)

Installation of the ACRT program into the ImageJ macros and workflow of the program: see Figure 4.18.

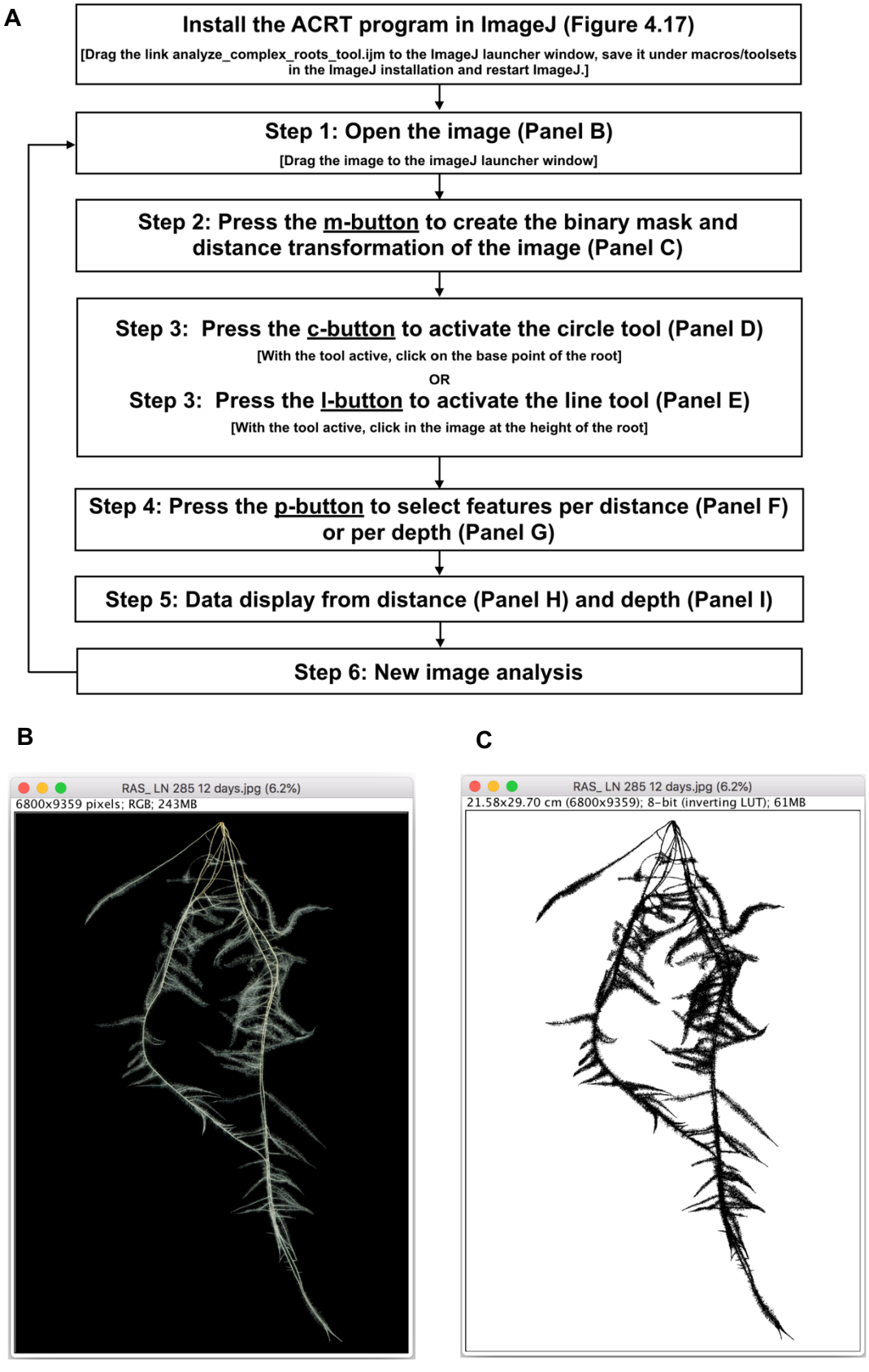

Figure 4.18. Workflow of the ACRT program (continue).

D

E

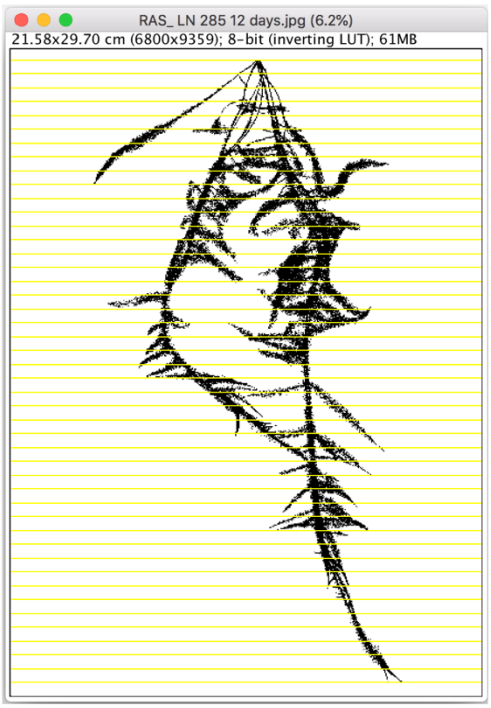

F

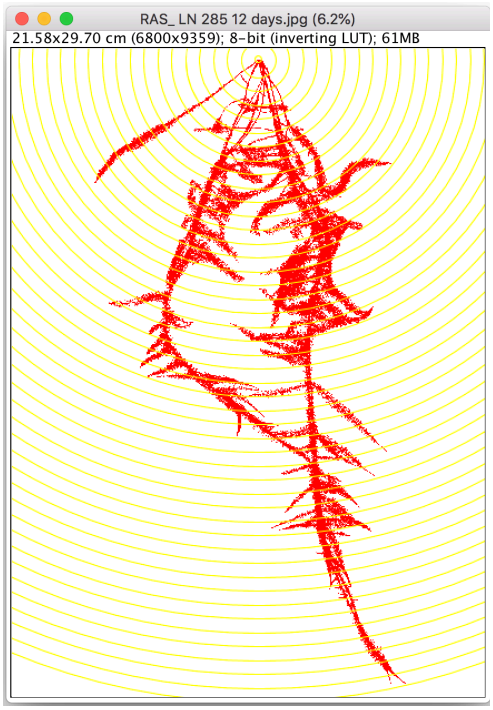

G

Figure 4.18. Workflow of the ACRT program (continue).

H

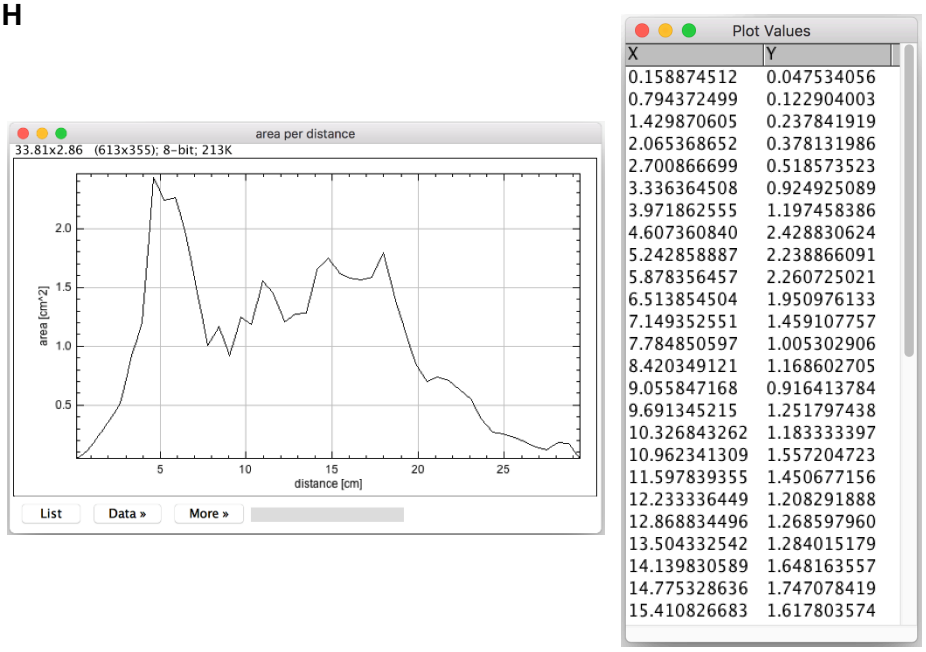

I

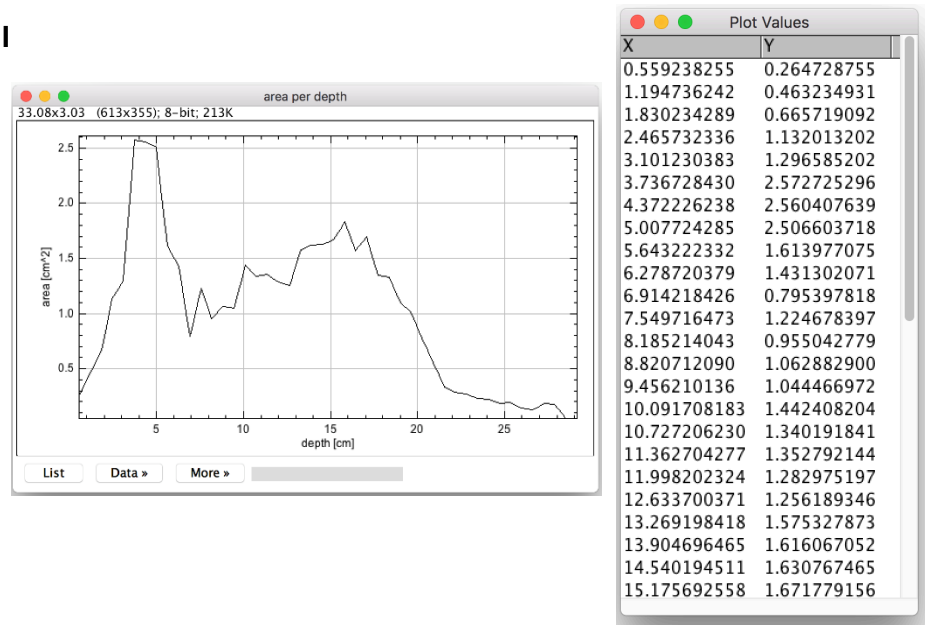

Figure 4.18. Workflow of the ACRT program. See main text.

Program available at:
https://github.com/MontpellierRessourcesImagerie/imagej_macros_and_scripts/wiki/Analyze_Complex_Roots_Tool

Written by Volker Baecker (CNRS-INSERM, Montpellier Ressources Imagerie)

Chapter 5

Root development responses to biotic and abiotic conditions: effects of bacterial strains and reduced Pi availability

While developing procedures for phenotyping root system responses to biotic and abiotic conditions, my PhD work at has been interspersed with various experiments, carried out in different environmental conditions in order to test the effects of nutrient deficiencies or inoculation with bacterial strains using prototype devices that were under development. A large part of these experiments, which resulted in adaptation of protocols or changes in the design of the prototypes, were not carried out in order to provide publishable scientific information. Such experiments will be therefore not reported in the present manuscript.

Here below I present 4 recent experiments carried out by growing inoculated or non-inoculated plants in soil conditions, or on agar plates, or in hydroponics in cuvette devices, or in rhizobox devices. Taken as a whole, the results of these experiments both allow to address methodological questions and provide scientific information.

5.1. Root system responses to inoculation in plants grown on soil for 30 days.

Inoculation with several bacterial strains tested in Chapter 3 was found to lead to an increase in biomass production and to affect the contents in nutrient elements. A working hypothesis was that these effects involved changes in root development. Before being weighted for nutrient element content assays, the root systems of these plants had been carefully washed, in order to remove adhering soil particles, and thereafter photographed. Representative photographs are provided by Figure 5.1. The tested bacterial strains (6 in total) were *Bradyrhizobium japonicum* strain ORS285, *Frankia* sp. R43, *Azospirillum lipoferum* strain 4B, and the Lebanese B1, B3-2 and I1-3 isolates.

Many root hairs had been probably damaged by the isolation and washing procedure of the root systems, or "bent" along the roots and thus no longer visible. It should however be noted that careful examinations allowed detection of root hairs in some loci (see enlargement in Figure 5.1), indicating that roots displayed root hairs in the experimental conditions that we used. However, the visible root hairs were always hardly detectable and were not taken into account in our analysis of the photos.

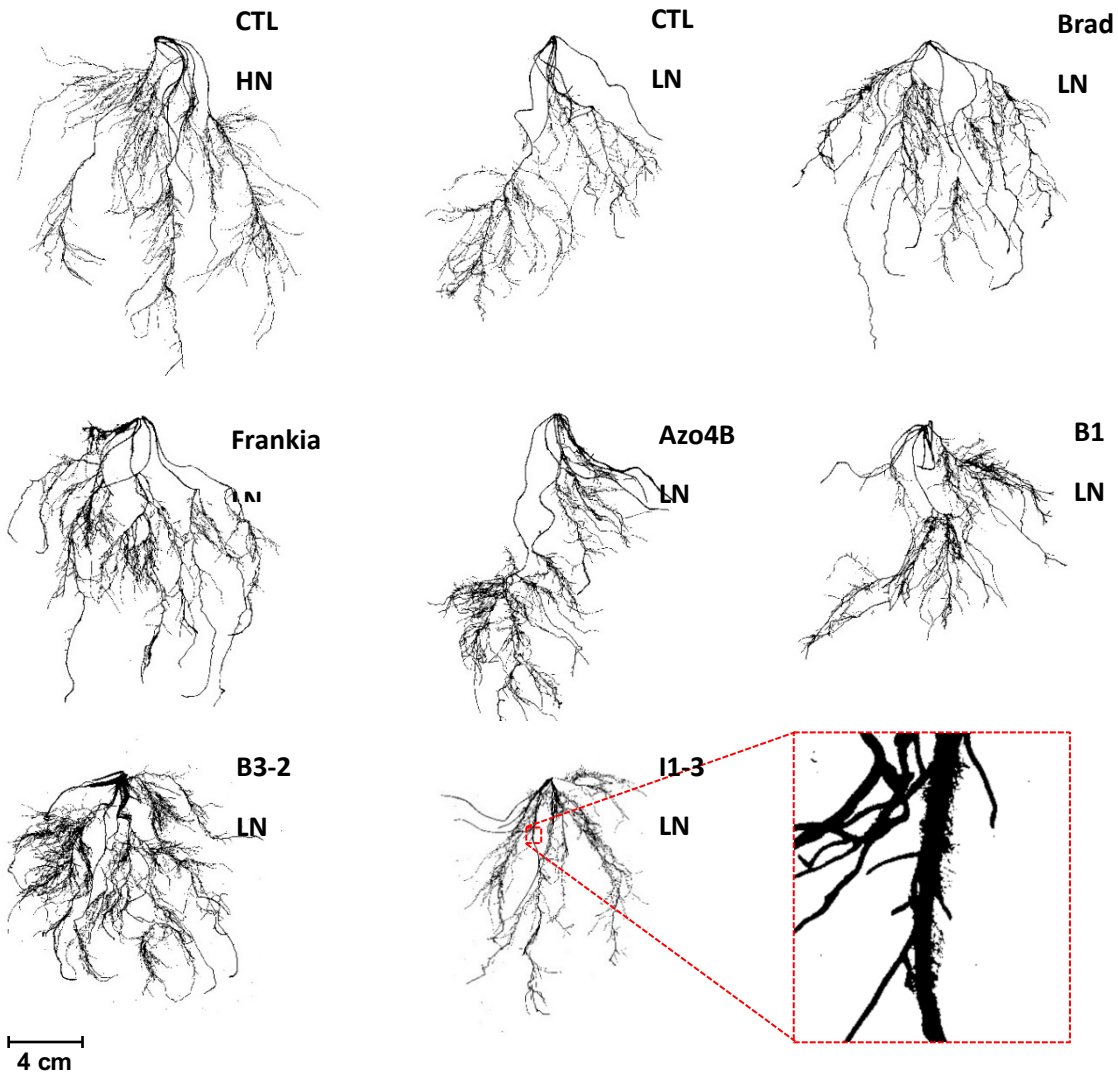

Figure 5.1. Root systems from wheat plants grown on soil in growth chamber for 30 days. Same plants as those phenotypes in Chapter 3 (Figures 3.14 to 3.19). Plants (*Triticum turgidum* spp. durum cv. Oued Zenati) were grown on artificial soil (peat moss/sand/perlite, 1/1/1; v/v/v) for 30 days after seedling transplantation. The plants were watered every 3 days with HN solution (5.2 mM assimilable N: high N condition) or with LN solution (0.7 mM assimilable N; low N condition). LN-treated plants were inoculated (inoculation of the soil and of the seedlings before transplantation) with one rhizobacterial strain according to the procedures described in § 2.2 and 2.7. Control HN and LN treatments: the soil and the transplanted seedlings were not-inoculated. Root systems were excised at the end of the growth period, gently washed from soil particles and photographed. Examples of photographs are provided (scale bar: 4 cm). For image analysis and statistics: see Figure 5.2. Inoculated strains; *B. japonicum* strain ORS285 (Brad), *Frankia* sp. R43 (Frankia), *A. lipoferum* strain 4B (Azo4B), Lebanese B1 isolate (B1), Lebanese B3-2 isolate (B3-2) and Lebanese I1-3 isolate (I1-3). Shoot and root biomass of the plants: see Figure 3.14 and 3.15. N contents, C contents and NUE indices: Figures 3.15 to 3.18. Nutrient element contents: Figure 3.19.

The photos were analyzed using IJ-Rhizo program (Pierret *et al.,* 2013) to get estimates of the total length and total root area of each root system (Figure 5.2). When compared with the control plants, statistically significant increase in the total root length and area estimates was only observed in the case of root inoculation with the Lebanese B3-2 strain. It is worth to note that this strain was previously found to be the only one, from the 6 tested strains, to induce a statistically significant increase in root biomass (see Chapter 3, Figure 3.14 and 3.15).

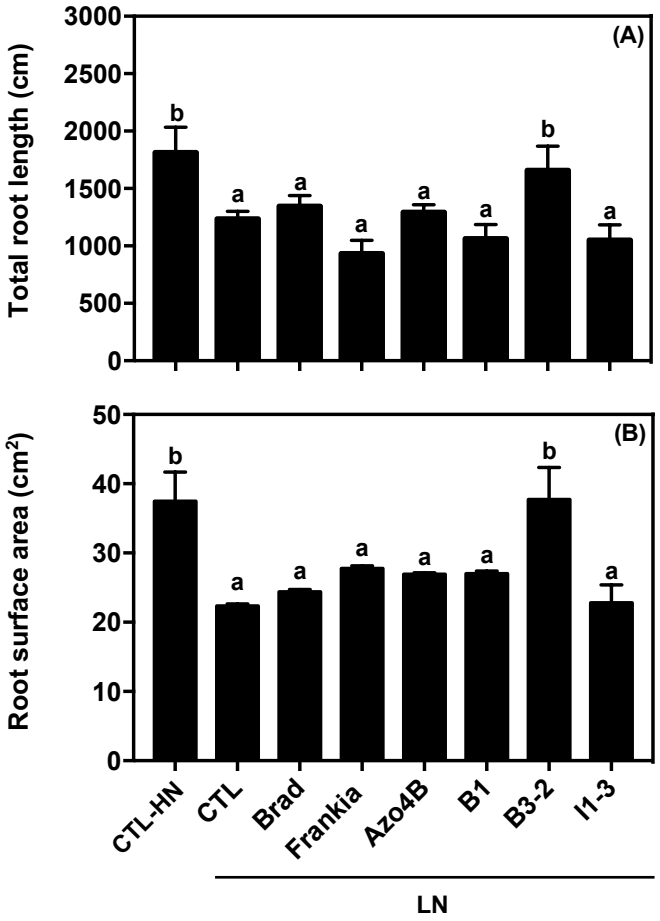

Figure 5.2. Root system development of wheat plants grown in soil for 30 days and inoculated or not inoculated with bacterial strains. Same plants as those characterized in Chapter 3 (Figures 3.14 to 3.19). Examples of root system images: see Figure 5.1. Image analysis was carried out using IJ-Rhizo program (see Figure 2.5).

(A) Total root length
(B) Root surface area

Inoculated strains: *B. japonicum* strain ORS285 (Brad), *Frankia* sp. R43 (Frankia), *A. lipoferum* strain 4B (Azo4B), and Lebanese B1, B3-2 and I1-3 isolates. Values are means ± SE (n = 5). Different letters above histogram bars indicate statistical significance at $p<0.05$ (ANOVA).

The total length and total root area data were then plotted against root biomass (previously determined in the experiment described by Figure 3.14). The resulting curves are displayed by Figure 5.3A and B. A rather good correlation was observed between root area and root biomass (Panel A). The correlation appeared weaker between root length and root biomass. The "root area" data were then divided by the corresponding "root length" data, in order to obtain a parameter reflecting a "mean root diameter". The ratios were poorly variable between the different plants, non-inoculated or inoculated, including inoculation with the Lebanese B3-2 isolate, and no correlation appeared with root biomass. Altogether, these results suggested that inoculation with B3-2, which resulted in increased root biomass and increased root area, poorly affected root radial growth.

5.2. Effect of inoculation with bacterial strains on root hair elongation in young seedlings grown on agar plates

Inoculation of the germinated seedlings and of the agar plates was carried out as described in Chapter 2, § 2.2 to 2.4. Six bacterial strains were tested, *B. japonicum* strain ORS285, *Frankia* sp. R43, *A. lipoferum* strain 4B, and the Lebanese isolates B1, B3-2 and I1-3, thus the same set of strains as the one used in the above experiment. The seedlings grew for 3 days in LN agar conditions. Representative photos of root hairs, taken at about 1.5 cm from the root tip, are provided in Figure 5.4. The results of root hair length analysis are reported in Figure 5.5. The two sides of each root hair zone in the photos were examined separately (Figure 5.5A), yielding very similar data, which was taken as a validation of the measurement procedure (performed using ImageJ).

Each of the 6 bacterial strains induced an increase in root hair length, by *ca*. 25% to 45% when expressed in % of root hair length in non-inoculated control plants. The increase was statistically significant in the case of *B. japonicum* strain ORS285, *Frankia* sp. R43, B3-2 and I1-3 (Increase in root hair length by 35%, 29%, 34% and 43%, respectively).

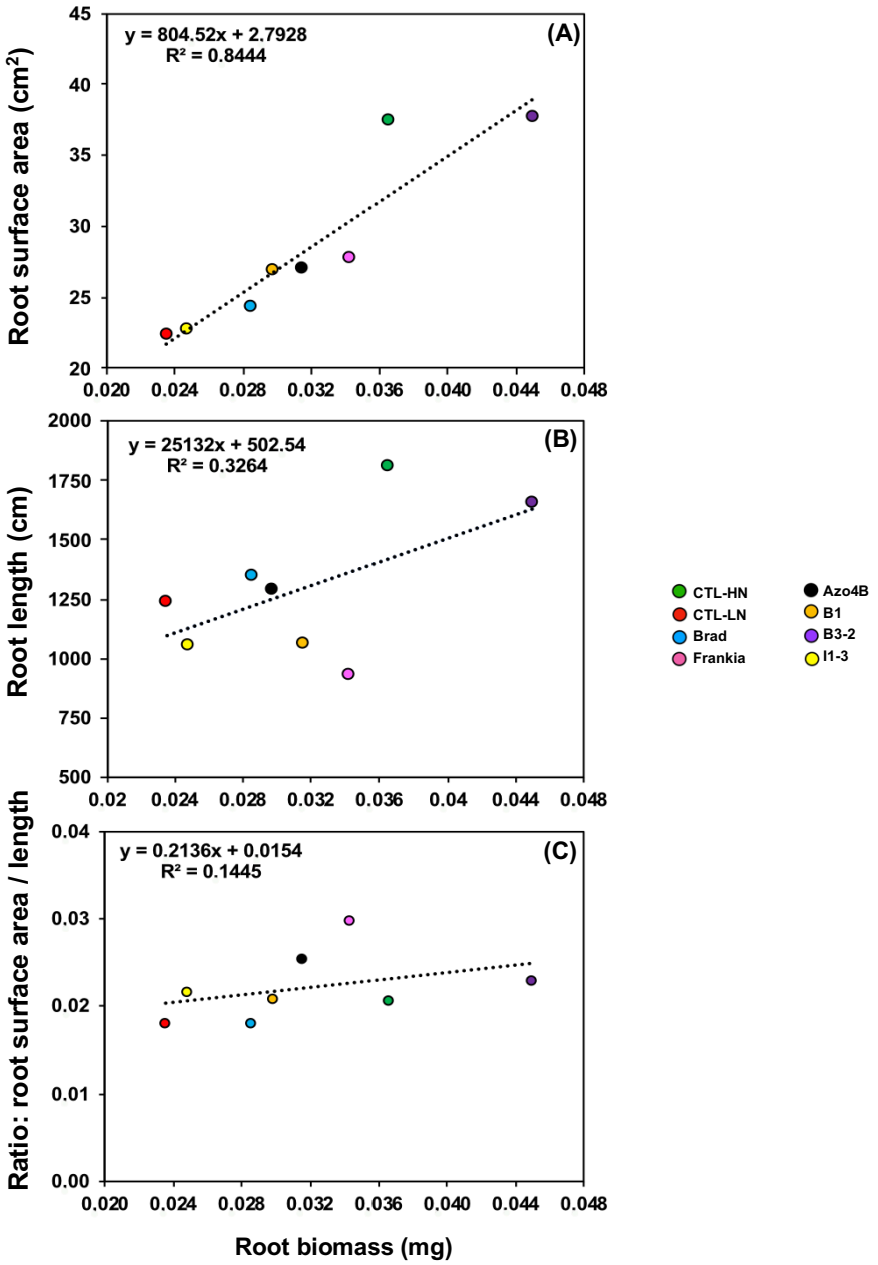

Figure 5.3. Relationships on LN conditions between root biomass, total root surface and root length in non-inoculated plants and in plants inoculated with different bacterial strains. Same plants as in the experiments described by Figure 3.14 (and Figure 3.15). Root system biomass (DW); data from Figure 3.14. Total root surface and root length: data from Figure 5.2. Plant growth conditions (HN and LN treatments) and inoculation: see Legend to Figure 3.14. HN and LN control plants: non-inoculated plants. The 6 inoculated bacterial strains were *B. japonicum* strain ORS285 (Brad), *Frankia* sp. R43 (Frankia), *A. lipoferum* strain 4B (Azo4B), Lebanese B1, B3-2 and I1-3 isolates.

(A) Total root surface plotted against root system biomass
(B) Total root length plotted against root system biomass
(C) Ratio of total root surface to root length expressed against root system biomass

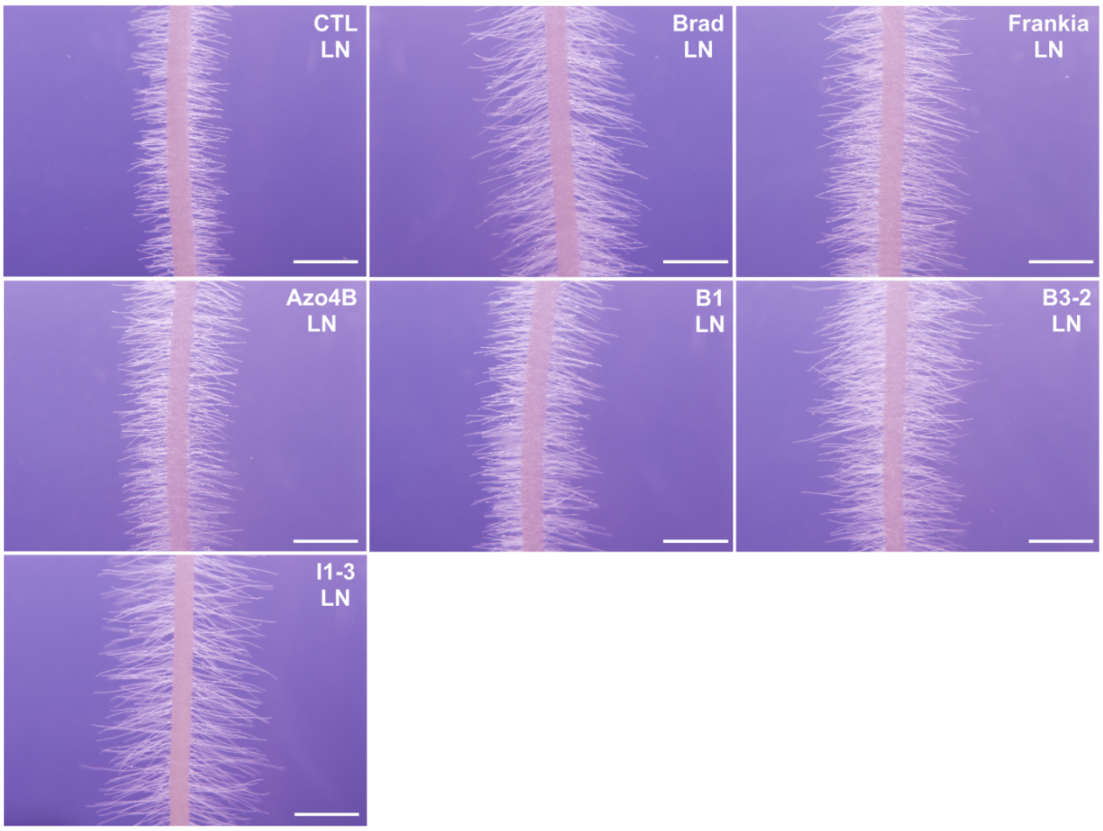

Figure 5.4. Root hair development in wheat plants grown on agar plates and inoculated or not inoculated with bacterial strains. Plants (*T. turgidum* spp. durum cv. Oued Zenati) were grown for 3 days on low nitrogen (LN) agar plates as described in § 2.4. LN medium (0.7 mM assimilable nitrogen): see § 2.3. Root inoculation and agar plate inoculation: see § 2.2 and 2.4. Inoculated strains: *B. japonicum* strain ORS285 (abbreviation: Brad), *Frankia* sp. R43 (Frankia), *A. lipoferum* strain 4B (Azo4B), Lebanese B1 isolate (B1), Lebanese B3-2 isolate (B3-2) and Lebanese I1-3 isolate (I1-3). Values are means ± SE (n = 5). Photos of the roots were taken at 1.5 cm from the root tip using an Olympus binocular (bright field mode). After contrast adjustment, the images were analyzed using ImageJ focusing on root hair length measurements (see Figure 5.4). Scale bar: 2.5 mm.

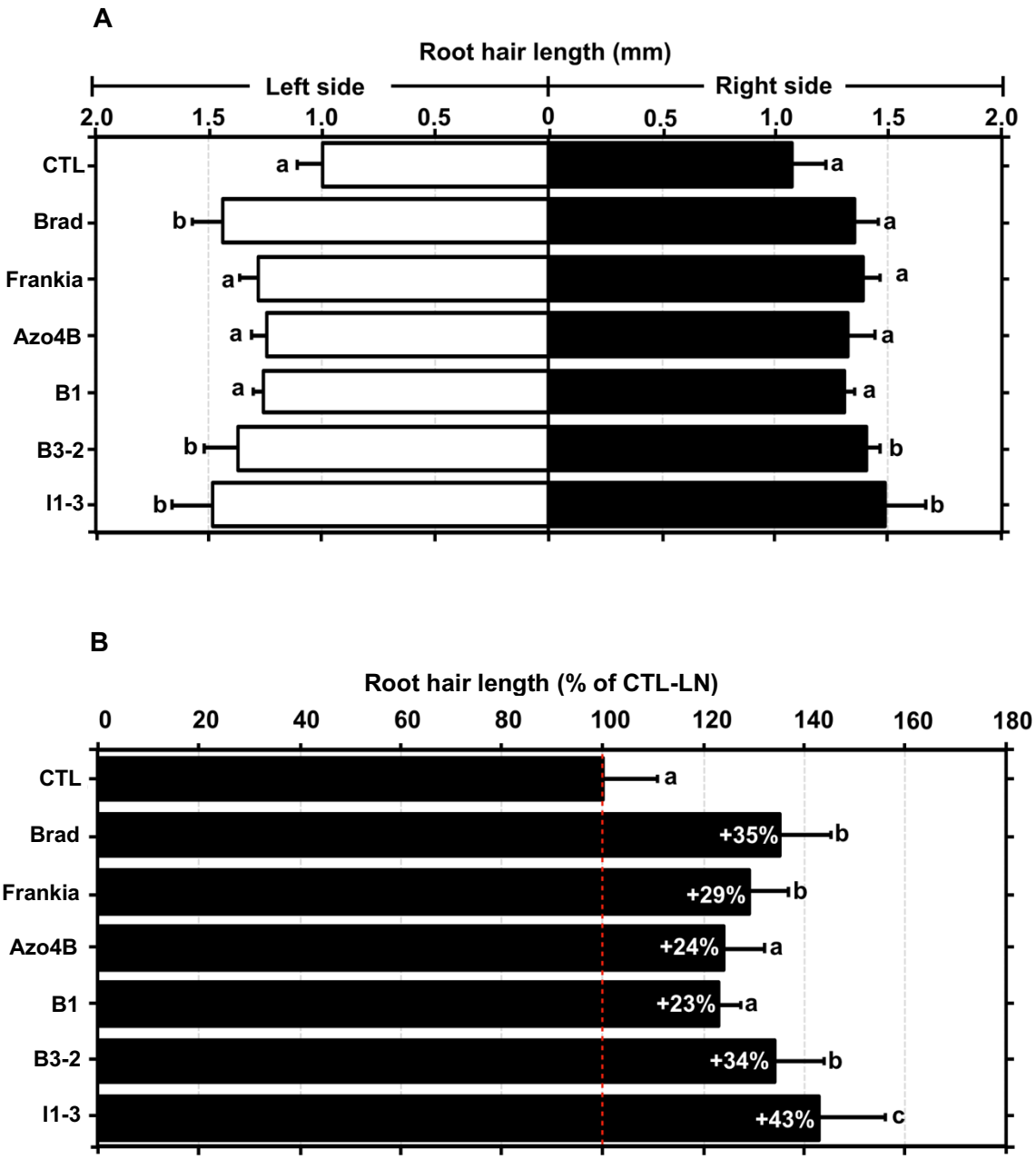

Figure 5.5. Effect of bacterial inoculation on root hair length in plants grown on LN-medium agar plates for 3 days. Experimental conditions and examples of images: see Figure 5.3. Root hair length was assessed using ImageJ, separately on each side (left and right) of the root (Panel A) before values for the two sides were computed (Panel B). Inoculated strains: *B. japonicum* strain ORS285 (abbreviation: Brad), *Frankia* sp. R43 (Frankia), *A. lipoferum* strain 4B (Azo4B), Lebanese B1 isolate (B1), Lebanese B3-2 isolate (B3-2) and Lebanese I1-3 isolate (I1-3).

(A) Values obtained on each side of the root image.
(B) Mean values for the whole root segments (both sides) computed from the data shown in (A) and expressed in % of the control (non-inoculated) plants (CTL).
Means ± SE (n = 8). Different letters above histogram bars indicate statistical significance at $p<0.05$ (ANOVA).

5.3. Effect of *B. japonicum* strain ORS285 on root hair elongation in plants hydroponically grown in "cuvette" devices

Seedlings inoculated with *B. japonicum* strain ORS285 were hydroponically grown in LN solution for 4 days in "cuvette" devices (Chapter 4, § 4.2 and Figures 4.2 to 4.6). Photos were taken of the region located at about 1.5 cm from the root tip. Representative images are provided by Figure 5.6A. Phenotyping root hair development using the MRHT program revealed that inoculation with *B. japonicum* strain ORS285 resulted in statistically significant increases in root hair density (by about 8%), mean root hair length (by *ca.* 26%) and maximal root hair length (by *ca.* 22%) (Figure 5.6B), when compared with non-inoculated control plants. Thus, the increase in mean root hair length (*ca*. 26%) in these experimental conditions was close to the one induced by the same bacterial strain in the experiment carried out on agar plates (35%; Figure 5.5B).

5.4. Effects of *B. japonicum* strain ORS285 and of reduced Pi availability on root development in rhizobox devices

Plants inoculated with *B. japonicum* strain ORS285 or non-inoculated were grown in rhizobox devices for 12 days as described in § 2.6 (Chapter 2). Inoculation was achieved as described in § 2.2. Non-inoculated plants were watered with either LN or LP ("Low Pi availability") solution. Inoculated plants were watered with LN solution.

LN solution (detailed composition provided in § 2.3) contained 0.7 mM assimilable nitrogen (0.1 mM NH_4NO_3 and 0.5 mM KNO_3) and 1 mM Pi (introduced as KH_2PO_4). LP solution contained 5.2 mM assimilable nitrogen (0.1 mM NH_4NO_3 and 5 mM KNO_3, like HN solution: see § 2.3) and 0.1 mM Pi (provided as KH_2PO_4). The other macro-elements and the micro-elements were the same in LN and LP solutions.

Figures 5.7, 5.8 and 5.9 provide images of root systems from (i) non-inoculated plants grown in LN conditions, (ii) inoculated plants grown in LN conditions, and (iii) non-inoculated plants grown in LP conditions, respectively (10 plants in each case).

As previously shown in Figure 4.16, and further illustrated by the presence in each of these figures of a panel displaying an enlargement of a root region, large parts of the root systems were covered with dense and long root hairs in these experimental conditions.

A

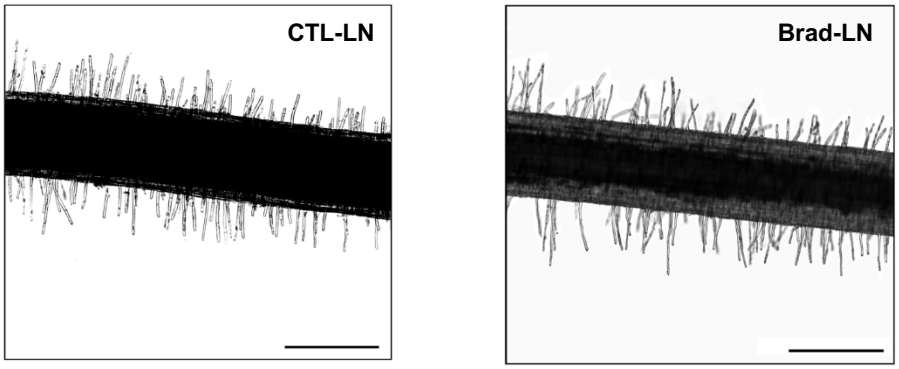

B

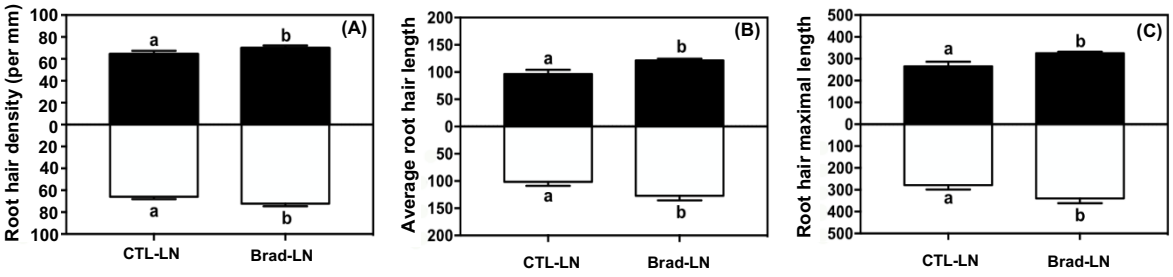

Figure 5.6. Sensitivity of root hair development to inoculation with *B. japonicum* strain ORS285 in wheat plants hydroponically grown in "cuvette" devices for 4 days. The plants (*T. turgidum* spp. durum cv. Oued Zenati), either inoculated with *B. japonicum* strain ORS285 (abbreviation: Brad) or not inoculated (control: CTL), grew in LN solution (containing a low concentration of assimilable nitrogen: 0.1 mM NH_4NO_3 and 0.5 mM KNO_3). Growth conditions, inoculation and "cuvette" device: see Chapter 2, § 2.2 to 2.5, and Chapter 4, § 4.2. Four days after transfer of the plant into the device, an image of the region at about 1.5 cm from the root tip was taken (Microscope Zeiss Apotome, Bright field, Z-stacks mode).

(A) Images from a control plant (left panel) and an inoculated plant (right panel). Scale bar: 500 µm.

(B) Analysis of root hair development using the MRHT program. Assessment of root hair density, maximal root hair length and average root hair length on both side of the root. Black bars correspond to the data obtained for the upper side of the image and white bars to those obtained for the lower side. ImageJ plugin MRHT: see § 4.2.2. Values are means ± SE (n = 3 images). Different letters above histogram bars indicate statistical significance at $p<0.05$ (ANOVA).

Non-inoculated plants grown in low N conditions

Figure 5.7. Images of wheat root systems from non-inoculated plants grown in rhizobox devices in LN conditions for 12 days. Seedling (*T. turgidum* spp. durum cv. Oued Zenati) germination and transfer in rhizoboxes: see Chapter 2, § 2.2, 2.3 and 2.6. Rhizobox devices: see Chapter 4, § 4.3. Scale bar: 3 cm. An enlargement of a root segment, rendering root hairs visible, is displayed.

Inoculated plants grown in low N conditions

Inoculated strain: *B. japonicum* strain ORS285

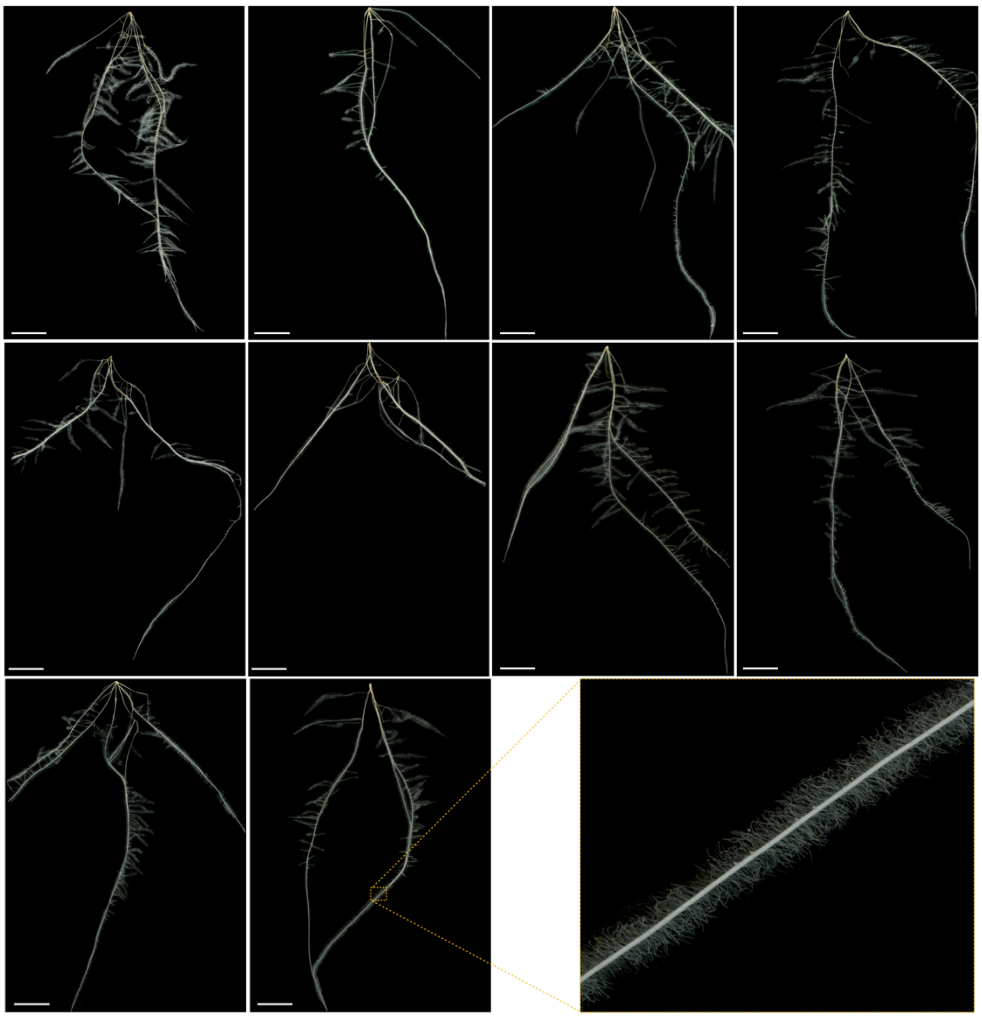

Figure 5.8. Images of wheat root systems from plants inoculated with *B. japonicum* strain ORS285 and grown in rhizobox devices in LN conditions for 12 days. Seedling (*T. turgidum* spp. durum cv. Oued Zenati) germination, inoculation and transfer in rhizoboxes: see Chapter 2, § 2.2, 2.3 and 2.6. Rhizobox devices: see Chapter 4, § 4.3. Scale bar: 3 cm. An enlargement of a root segment, rendering root hairs visible, is displayed.

Non-inoculated plants grown in low P conditions

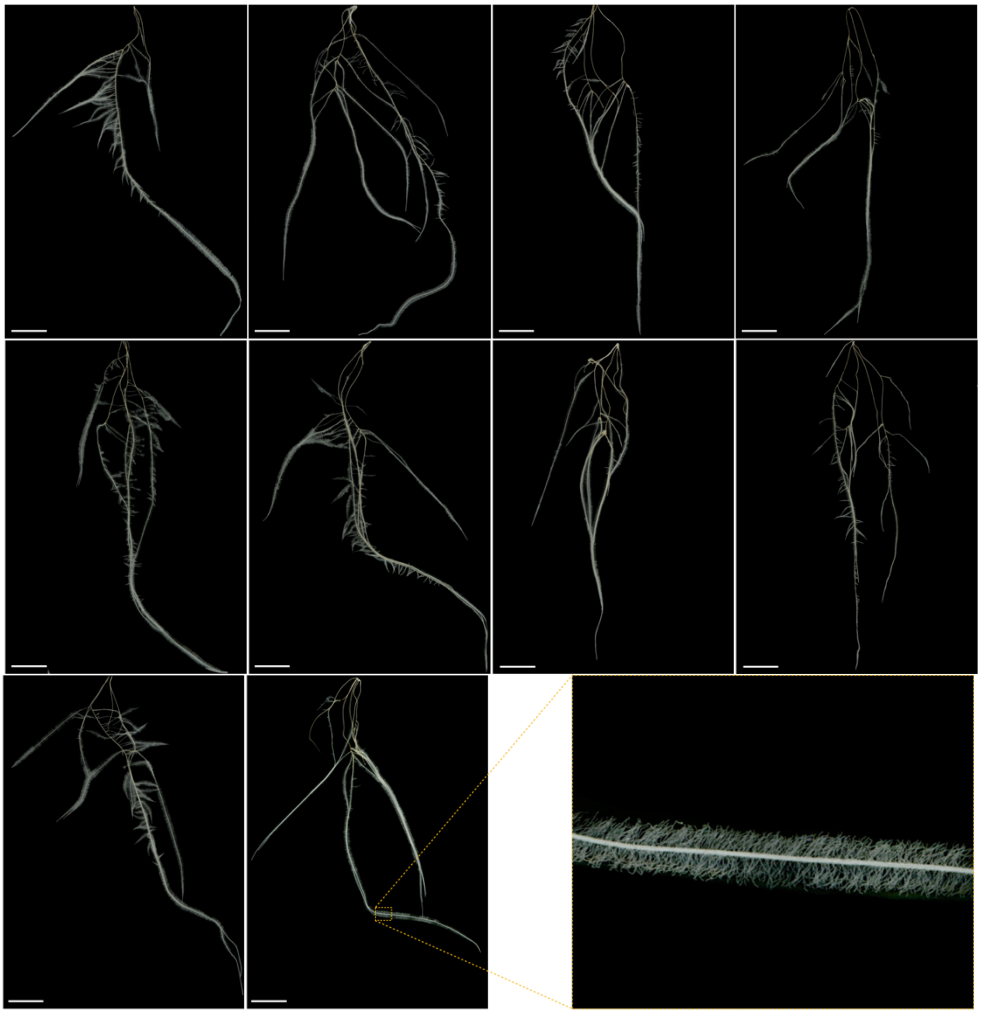

Figure 5.9. Images of wheat root systems from non-inoculated plants grown in rhizobox devices in LP ("low Phosphate") conditions for 12 days. Seedling (*T. turgidum* spp. durum cv. Oued Zenati) germination and transfer in rhizoboxes: see Chapter 2, § 2.2, 2.3 and 2.6. Rhizobox devices: see Chapter 4, § 4.3. Scale bar: 3 cm. An enlargement of a root segment, rendering root hairs visible, is displayed. Low P solution contained 0.1 mM KH_2PO_4 (instead of 1 mM KH_2PO_4 as in LN solution; see main text).

The images were analyzed using the ACRT program (plugin of ImageJ developed by Volker Baecker; see § 4.3.2 and Figures 4.17 and 4.18), and the commercially available WINRHIZO™ software (Regent Instruments Inc, Canada). Both procedures take into account the presence of root hairs, but in a different way.

The ACRT program sorts the pixels of the image into two categories, "background pixels" or "root pixels". With respect to root pixels, the program does not distinguish between the pixels corresponding to root hairs and those corresponding to the roots from which root hairs have developed, but pools all these pixels together, and determines the area that these pixels cover. Then, the program provides the root area as a function of the "distance" to the germinated seed at the surface of the rhizobox foam, or as a function of the "depth" in the rhizobox, *i.e.*, the distance to the horizontal line at the top if the rhizobox where the germinated seed has been deposited. Figure 5.10 provides the plots describing the relationship between the *root surface area* and either the *distance* to the seed (left panel) or the *depth* from the seed level (right panel) in the case of the "non-inoculated roots grown in LN conditions (open symbols) and the "*B. japonicum* strain ORS285-inoculated roots grown in LN conditions" (black symbols). Figure 5.11 allows to compare in a similar way the development of non-inoculated roots grown in either LN (open symbols) or LP (black symbols") conditions.

The WINRHIZO™ software has been developed (as indicated by the Regent Instruments Inc. company website: http://regent.qc.ca/assets/winrhizo_software.html) for "*Analysis of washed root systems*". It provides "*global measurements* such as *average root diameter, total root length, area, volume and number of tips …root morphology measurement as a function of user definable diameter classes…".* Figure 5.12 provides the values of "*Total root length*" (Panel A of this Figure), "*Total root surface*" (Panel B), "*Total root length*" per class of root diameter (Panel C), and "*Total root area*" per class of root diameter (Panel D) obtained from WINRHIZO™ for the images of the root systems displayed by Figures 5.7, 5.8 and 5.9 in order to compare non-inoculated LN-watered roots, *B. japonicum* strain ORS285-inoculated LN-watered roots and non-inoculated LP-watered roots. In this analysis, we have set the "diameter class" parameters so as root hairs are taken as "roots of very thin diameter" (the thinnest diameter: between 0 and 0.20 mm).

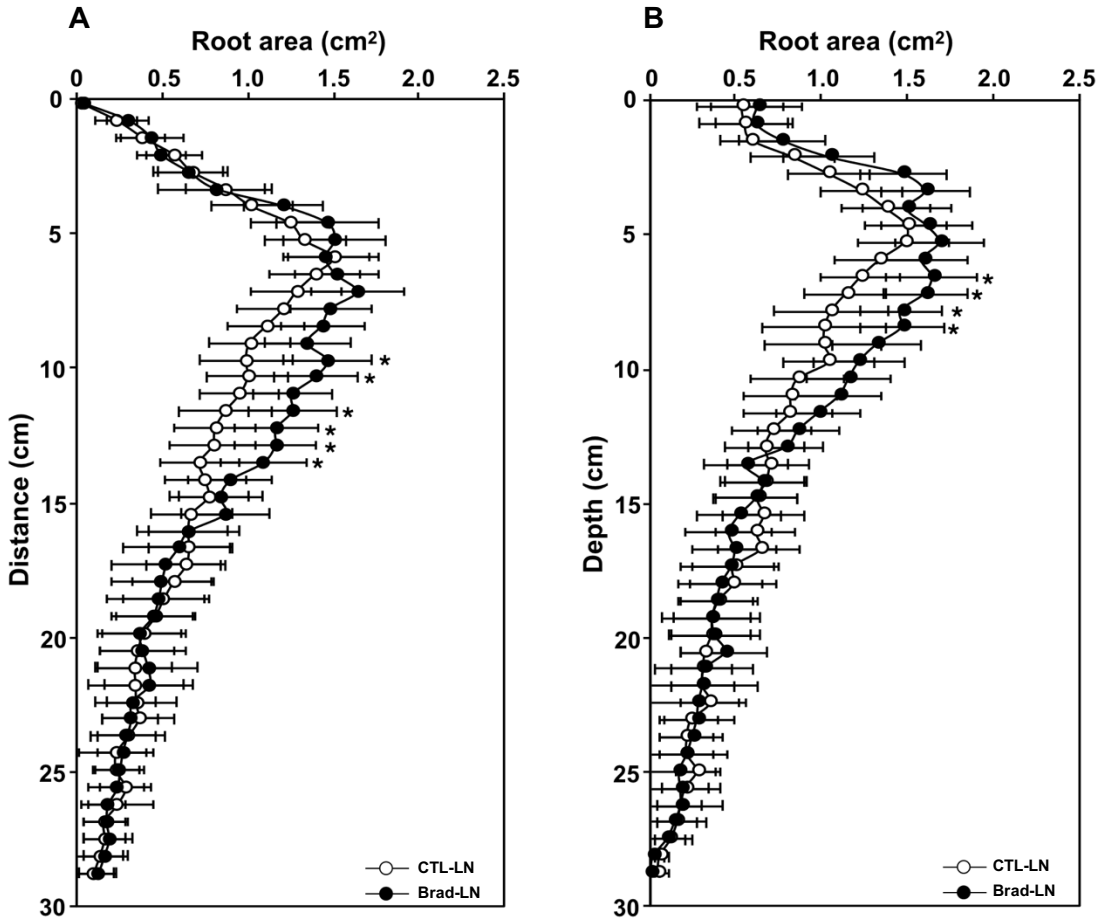

Figure 5.10. Effect of *B. japonicum* strain ORS285 on root system development. Plants were either inoculated with *B. japonicum* strain ORS285 (black symbols) or non-inoculated (open symbols) and grown in rhizobox devices for 12 days in LN solution. Images (scans) of 10 root systems at the end of the 12-d growth period are provided by Figure 5.7 for non-inoculated plants and 5.8 for inoculated plants. Root development was analyzed using the ACRT program, allowing to plot root surface area (derived from the number of root pixels on the 2-D image) as a function of either the distance to the seed (panel A) or the depth "in the soil" (panel B), *i.e.*, the distance to the horizontal line at the top of the rhizobox that would correspond to the "soil surface where germination would have occurred". ACRT program: see Chapter 4, Figure 4.17 and 4.18, and § 4.3.2.

Means ± SE (n = 10 root systems per condition). Corresponding root system images: Figures 5.7 and 5.8. The symbol * indicates a statistically significant difference at $p<0.05$ (Student's t-test).

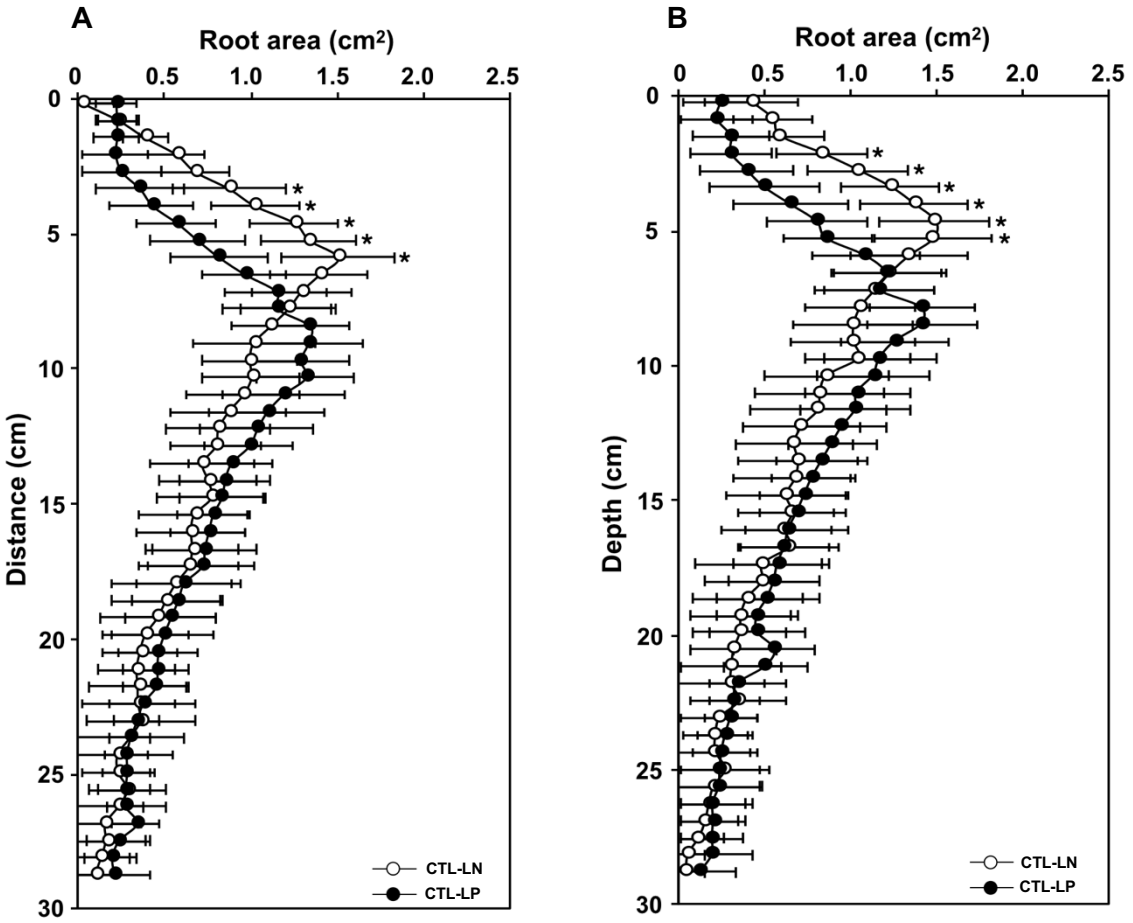

Figure 5.11. Comparison of the effects of low N and low P conditions on root system development. Non-inoculated plants were grown in rhizobox devices for 12 days, being watered either with LN ("low N", open circles) or LP ("low P"; black symbols) solution. Images (scans) of 10 root systems at the end of the 12-d growth period are provided by Figure 5.7 for LN plants and Figure 5.9 for LP plants. Root development was analyzed using the ACRT program, allowing to plot root surface area (derived from the number of root pixels on the 2-D image) as a function of either the distance to the seed (panel A) or the depth "in the soil" (panel B), i.e., the distance to the horizontal line at the top of the rhizobox that would correspond to the "soil surface where germination would have occurred". ACRT program: see Chapter 4, Figure 4.17 and 4.18, and § 4.3.2.

Means ± SE, n = 10 root systems per condition. Corresponding root system images: Figures 5.7 and 5.9. The symbol * indicates a statistically significant difference at $p<0.05$ (Student's t-test).

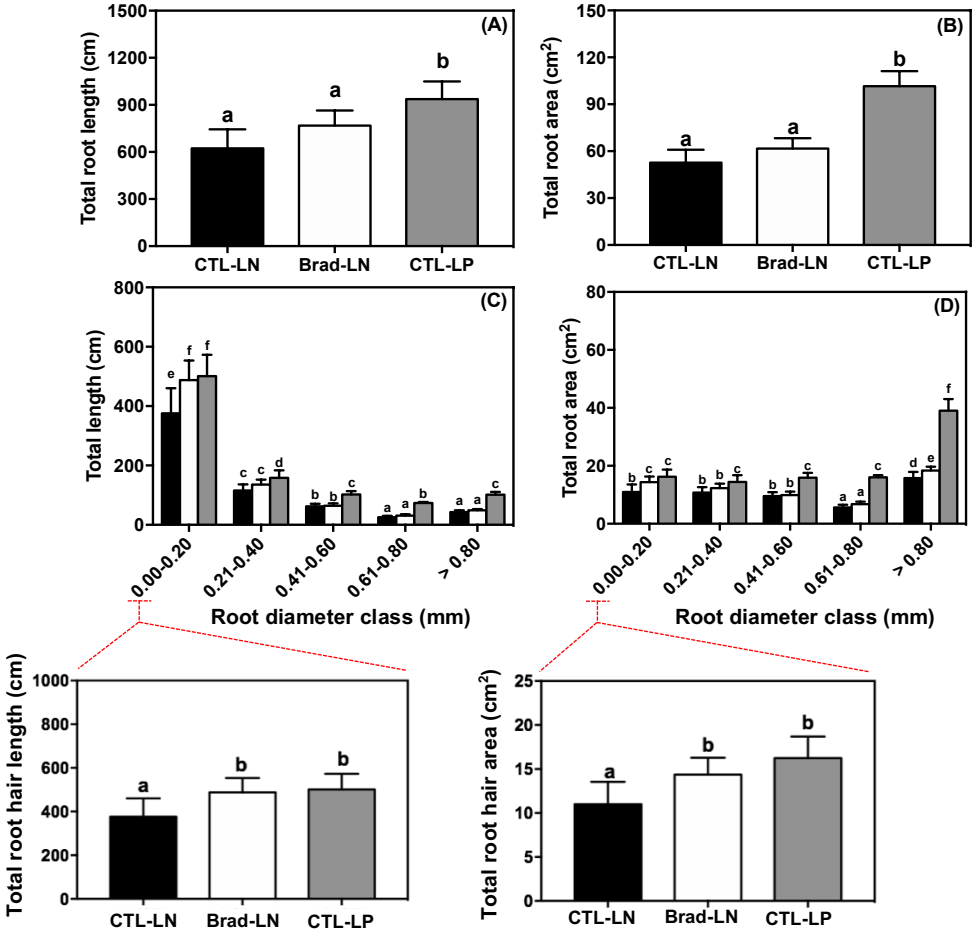

Figure 5.12. Root phenotyping of non-inoculated plants grown in LN and LP conditions, and of *B. japonicum* strain ORS285-inoculated plants grown in LN conditions. Plants were grown as described in the legends to Figures 5.7 (non-inoculated plants grown in LN conditions), 5.8 (plants inoculated with *B. japonicum* and grown in LN conditions) and Figure 5.9 (plants grown in LP conditions). Images of the root systems: see these Figures. Images were analyzed using the WINRHIZO™ software.

(A) and (B) Total length of the whole root system (A) and corresponding root area (B). "Total length" is the sum of the length of every root element detected by WINRHIZO™, including root hairs that were taken as the thinnest root elements by WINRHIZO™ (see main text).

(C) and (D) Root length of each root diameter class (C) and corresponding surface area (D). Five root diameter classes were defined within WINRHIZO™ (arbitrary user definition) to analyze the root systems: thinner than or equal to 0.20 mm, between 0.21 and 0.40 mm, between 0.41 and 0.60 mm, between 0.61 and 0.80 mm, and larger than

0.80 mm. The thinnest diameter class (0 to 0.20 mm) corresponds essentially to root hairs. The total length of all the roots elements identified in each of these 5 classes was determined and plotted in the histogram displayed Panel C. Panel D provides the corresponding surface areas. Panel E and F indicated the total length and total area of root hair which had the diameter thinner than or equal to 0.20 mm.

Taken as a whole, the analyses carried out with ACRT and WINRHIZO™ provide evidence that, when compared with non-inoculated plants grown in LN conditions, root development was altered in the inoculated plants and in the plants grown in LP conditions. For instance, inoculation resulted in an increase in total root hair length (compare first two bars of the histogram in Figure 5.12C) and in an increase in root area detected in the half upper part of the rhizobox devices (Figure 5.10B). Growth in LP conditions resulted in a decrease in root area detected in the 25% upper part of the rhizobox devices, and then in an increase in root area in the 75% lower part of the devices. It also resulted in an increase in total root hair length (compare the first and third bars of the histogram in Figure 5.12C).

These results are further discussed in the following chapter (Chapter 6: "*Discussion and Perspectives*").

Chapter 6

Discussion and Perspectives

The general objective of my PhD work is to contribute to the research efforts aimed at gaining knowledge allowing agriculture to progress towards ecological intensification. In this perspective, reducing the fertilization inputs, and their ecological costs and damages, appears as one of the major challenges. Within this framework, I have focused my research project on root development and physiological functions contributing to plant mineral nutrition, including interactions with beneficial soil microbes, since evidence is available that such interactions can be of crucial importance for nutrient ion acquisition. I have chosen to carry out my work on wheat, since it is a cereal of high agronomical importance, and its interactions with soil bacteria likely to behave as *Plant growth promoting rhizobacteria* (PGPR).

Different kinds of mechanisms can underlie the beneficial effects of PGPR on plant growth, amongst which stimulation of root development and root hair production and elongation. I have isolated bacterial strains likely to interact with wheat roots and then worked at developing methodological procedures allowing to phenotype root responses to abiotic and biotic conditions.

6.1. Characterization of rhizobacterial strains able to interact with wheat

6.1.1. Diversity in the panel of bacterial isolates obtained from Lebanon wheat rhizosphere

The set of 16 bacterial isolates that have been purified from rhizospheric soil of wheat plants grown in a Lebanon field can be sorted, at the genus level (Table 3.1), in 7 *Achromobacter* (B3-2, B4, C2, H2, H3, I1-1, I1-2), 5 *Stenotrophomonas* (A11, B1, B2, C1 and H1), 2 *Rhizobia* (A10 and A12), 1 *Paraburkholderia* (B3-1) and 1 *Klebsiella* (I3-1).

From the PUBMED web site, in October 2019, the terms "PGPR" associated to either "*Achromobacter*", "*Stenotrophomonas*", "*Paraburkholderia*" or "*Klebsiella*" allowed to retrieve 5 references (the first one being published in 2014), 17 references (first one: 2012), 3 references (first one: 2016) references, and 15 references (first one: 2013), respectively. More references were obtained for PGPR and "Rhizobium" (66 publications, the first on published in 1995) or "*Azospirillum*" (51 references; first one: 1999). Thus, this kind of survey of the literature indicates that knowledge on PGPR activities within the genera *Achromobacter*, *Paraburkholderia*, *Stenotophomonas* and *Klebsiella* is less developed than within *Azospirillum* or *Rhizobium*. *Azospirillum brasiliense* appears as a model PGPR species.

Achromobacter (class: Betaproteobacteria) are Gram-negative straight rods, motile by using one to 20 peritrichous flagella. They are strictly aerobic and are found in water and soils (Garrity *et al.,* 2005). *Achromobacter piechaudii* ARV8 has been shown to display PGPR activity in Tomatoes and peppers grown in challenging biotic conditions (drought and/or salt stress) (Mayak *et al.,* 2004). It has also been shown that Inoculation of canola with *Achromobacter* sp. strain U80417 resulted in an increase in biomass production, a stimulation of both NO_3^- and K^+ net influx rates per root surface area unit and a promotion of root hair development (Bertrand *et al.,* 2000). A strain of *Achromobacter xylosoxidans*, endowed with the capability of producing indole acetic acid (IAA), of solubilizing inorganic phosphate and of increasing root length in *Brassica juncea*, has been shown to significantly improved Cu uptake in this species (Ma *et al.,* 2009). *Achromobacter xylosoxidans* strain WM234-C, initially isolated as an endophyte in wheat roots, has been shown to promote biomass production (fresh weight) and to increase chlorophyll a contents in rice (Jha and Kumar, 2009).

Stenotrophomonas (Class: Gammaproteobacteria) is a genus of Gram-negative bacteria, comprising at least ten species (Palleroni and Bradbury, 1993; Ryan *et al.,* 2009). The main reservoirs of *Stenotrophomonas* are soil and plants. *Stenotrophomonas* species range from common soil organisms (*S. nitritireducens*) to opportunistic human pathogens (*S. maltophilia*). *Stenotrophomonas rhizophila* sp. nov. has been characterized as a plant-associated bacterium endowed with antifungal activity against plant-pathogenic fungi (Wolf *et al.,* 2002). Inoculation of *Stenotrophomonas maltophilia* SBP-9 to wheat roots has been shown to result in increased plant growth and plant chlorophyll content (Singh and Jha, 2017). Inoculation with this bacterial strain also led to increased adaptation to nitrogen deficiency in *Arachis hypogea* (Alexander *et al.,* 2019).

Paraburkholderia (class: Betaproteobacteria) are Gram-negative, slightly curved rods that are motile by means of flagella. Members of this genus have been found in in nitrogen-fixing nodules of legumes (e.g., in mimosa, *Lebeckia ambigua* and *Hypocalyptus sophoroides*; *Paraburkholderia diazotrophica*, *Paraburkholderia dilworthii*, *Paraburkholderia strydomiana* sp. nov. and *Paraburkholderia steynii* sp. nov; De Meyer *et al.,* 2013; Beukes *et al.,* 2019). *Paraburkholderia phytofirmans* PsJN has been shown to behave as a PGPR upon interaction with *Arabidopsis*, increasing the plant tolerance to salinity (Ledger *et al.,* 2016) and providing protection against a virulent strain of *Pseudomonas syringae* through the activation of induced resistance (Timmermann *et al.,* 2017).

Klebsiella (Gammaproteobacteria) are gram-negative and usually non-motile bacteria (lacking a flagellum). They typically occur as straight rods with rounded or slightly pointed ends. Members of the genus *Klebsiella* are a part of the human and animal's normal flora in the nose, mouth and intestines. In plants, *Klebsiella* can be found in a variety of hosts. *K. pneumoniae* and *K. oxytoca* are able to fix atmospheric nitrogen into a form that can be used by plants (Cakmakci *et al.,* 1981). Inoculation with *Klebsiella pneumoniae* 342 has been shown to lead to enhanced maize

productivity in field conditions (Riggs *et al.,* 2001). In wheat, it has been shown to relieve nitrogen (N) deficiency symptoms and to increase total N and N concentration in the plant (Iniguez et al., 2004). It is worth to note that this nitrogen fixation phenotype appears as specific to one wheat cultivar (Trenton) as it was not observed with two other cultivars. Furthermore, wheat tolerance to salinity has been shown to be increased by inoculation with *Klebsiella* sp. SBP-8 (Singh *et al.,* 2015). Plant growth promotion and alleviation of Cd_2^+ toxicity has been reported in *Vigna mungo* upon inoculation with *Klebsiella pneumoniae* HR1 strain (Dutta *et al.,* 2018).

6.1.2. Characterization of PGPR ability of Lebanese isolates

The 16 bacterial isolates that we have obtained are all diazotrophic species since they have been selected after 6 successive rounds of growth on "nitrogen-free" medium. Furthermore, growth tests in presence of a poorly soluble phosphate source indicates that these 16 isolates are endowed with Pi solubilization capacity. Two from them, C2 and I1-3, also displayed significant growth in presence of poorly soluble sources of both Pi and K^+ (Figure 3.13 and Table 3.2).

Amongst these 16 isolates, the 7 strains that have been selected (based on the fact that their colonies differed in their visual aspect) and tested for their effects on wheat growth have all led to an increase in biomass production, when compared with non-inoculated control plants (Figure 3.14). Furthermore, for 5 out these 7 strains, a statistically significant increase in biomass production was also observed when compared with the control *Bradyrhizobium japonicum* and *Frankia* strains (Figure 3.14). Finally, when compared with the 2 control bacterial strains that induced the largest increase in plant growth, *Azospirillum lipoferum* 4B and *Azospirillium brasilense* Sp245, 4 Lebanese strains led to a statistically similar increase in biomass and one, B3-2, in a still larger increase plant growth (Figure 3.14). Altogether, these results provide evidence that at least 4 to 5 of the tested Lebanese strains are indeed endowed with "*Plant Growth Promotion*" ability. It is worth to note that assessment of plant Nitrogen Use Efficiency in 3 of these Lebanese strains, B1, B3-2 and I1-3, and the 3 control strains, *Bradyrhizobium japonicum* ORS285, *Frankia* sp. R43 and *Azospirillum lipoferum* 4B, revealed that the promotion of plant growth was accompanied by a decrease in "Nitrogen Use Efficiency", suggesting that the availability of assimilable nitrogen was not the main factor limiting plant growth in these experimental conditions (Figure 3.18). Assays of nutrient element contents (Figure 3.19) revealed that inoculation with different bacterial strains resulted in differences in nutrient element contents, *e.g.*, in P, K or Fe contents, but did not provide any simple hypothesis about the origin of the increase in plant growth. Secretion of stimulating phytohormones might have played a role, together with other processes, in the promotion of plant growth.

6.2. Phenotyping root development and responses to abiotic and biotic conditions

6.2.1. Methodological issues

A process that can be predicted to contribute to plant growth promotion by PGPR strains is stimulation of root growth and root hair development. Frequently reported effects of PGPR strains are inhibition of main root growth, stimulation of secondary root growth and promotion of root hair production and elongation (Vacheron *et al.,* 2013; Poitout *et al.,* 2016).

Quantitative analyses of such effects of PGPR strains on root and root hair development have been mainly carried out in plants grown on agar plates, and most often in Arabidopsis thaliana (Poitout *et al.,* 2016).

I have been working at analyzing the effects of PGPR strains on root and root hair development in wheat plants grown either in agar plates, in hydroponic conditions, in modified rhizoboxes providing "aeroponics" conditions at the surface of a humid polyester tissue and in soil. The experiments carried out using soil-grown plants were not aimed at taking into account root hair development. These cells were very hardly visible and probably often damaged during root system recovery from the soil, since long root hairs are fragile (Figure 4.1). Image analyses of root systems inoculated with different PGPR strains revealed differences, in terms of total root length and total root surface area, according to the inoculated strain but these differences were not statistically significant except in one case, inoculation with the Lebanese B3-2 isolate, which led to a ca. 20% increase in total root surface area (Figure 5.2). One may consider that such analyses are biased since they do not take into account root hair surface area while, altogether, my experiments provide evidence that wheat can produce dense and long root hairs that strongly increase the area of the root-soil interface (Figure 1.1; see also below). Furthermore, images of young seedlings grown on agar plates revealed that inoculation with various bacterial strains resulted in statistically significant promotion of root hair elongation, by more than 30% in the case of the Lebanese B3-2 and I1-3 strains (Figure 5.5).

In this context, I have been working at developing strategies and experimental devices in order to describe with quantitative parameters the effects of PGPR strains on root and root hair development. Two methodologies have been described in Chapter 4, using the so-called "Cuvette" and "Rhizobox" devices.

The "Cuvette" methodology allows to get high-resolution images under microscope (see Figure 5.6A) of root hair regions at a given distance of the root apex, and thereby to describe the phenotype using quantitative parameters such as root hair density, mean and maximal root hair length, in a quasi-automatic way using the MRHT program. I have used this methodology to investigate the effect of *Bradyrhizobium japonicum* on root hair development in wheat seedlings (Figure 5.6). The results indicated that the inoculation resulted in a statistically significant but weak increase in root hair density, and in mean and maximal root hair length. *B. japonicum* strain appears now as poorly active on wheat (e.g., Figure 3.15 regarding growth promotion).

Clearly, it would be interesting to further test the cuvette methodology with other bacterial strains.

The cuvette methodology suffers from 2 major scientific drawbacks. First, the plants are grown in hydroponic conditions, which is not actually relevant at the physiological level (in the case of wheat) and might affect root interactions with bacteria. Secondly, the present device allows to get images of short regions (chosen close to the root apex) of the root system and thus cannot describe the root system as a whole, and root hair development on the whole system. These drawbacks have been taken into account to develop the rhizobox methodology (Chapter 4).

Growing plants in our rhizobox devices clearly allows to get high-quality images of the whole root system, from about 2-week-old seedlings. Growth occurs in the "air" at the surface of a tissue maintained humid by automatic watering of a polyurethane foam adjusted "behind" the tissue. Such conditions are likely to mimic root growth in some soil conditions, when growth occurs along soil particles in soil pores displaying an atmosphere similar to that above the soil (in terms of O_2 availability) but more humid. Examples of images of root systems grown in such conditions (Figures 1.1, 5.7 to 5.9) show that dense and long root hairs can cover large portions of the whole root system. Clearly, estimates of parameters such as "root hair density" or "mean root hair length" cannot be easily obtained from such images. On the other hand, analysis of small root regions like those enlarged in panels of Figure 1.1 indicate that the total root hair surface area can be about 10 times larger than that of the corresponding root segment that would be "free from root hairs" (see Table 6.1).

Table 6.1. Examples of contribution of root hairs to total root surface area in different regions of a root systems developed in a rhizobox. Panels E, F and L: see Figure 14.6. Root hair surface area and total root area have been estimated by using the WINRHIZO™ software, root hairs being identified as root elements of the smallest diameter.

Panels in Figure 4.16	Area		
	Root hair (cm^2)	Total root (cm^2)	Root hair contribution (%)
E	0.239	0.262	91
F	0.201	0.227	88
L	0.141	0.176	80

Our working hypothesis to describe the complex root system images obtained using the rhizobox methodology has been that plotting root surface area against distance to the germinated seed (or depth with respect to the germinated seed) could support first quantitative analyses of the effects of biotic (as well as abiotic) conditions on root system development. A program (plugin of ImageJ) named ACRT has been developed (by Volker Baecker, MRI, Montpellier) in this perspective. I have then carried out two different experiments to compare the effects of low P condition with respect to low N (LN) conditions, and the effect of root inoculation with *Bradyrhizobium japonicum*, versus no inoculation, on root development.

6.2.2. Effect of LP conditions and of inoculation with B. japonicum on root development

The sets of 10 images obtained for each treatment, either LN, or LN and inoculation with *B. japonicum*, or LP, provided by Figures 5.7, 5.8, and 5.9, respectively, have been analyzed using the ACRT program. The results have been plotted in Figure 5.10, for comparison between LN treated plants and inoculated LN-treated plants, and in Figure 5.11 for comparison between LN-treated and LP-treated plants.

For complementary analyses, we have decided to withdraw 2 images, from each set of 10 Figures. This allowed me to take into account that parts of root systems developed just along the rhizobox left and right sides cannot be properly imaged and analyzed using the ACRT program. Thus, the first 2 images of the second row in Figure 5.8 were suppressed. I also suppressed the 2 images of the last row in Figure 5.7, as they looked rather different from the other 8 images, and suppressed the last 2 images of the second row in Figure 5.9 for the same reason. The "restricted" sets of 8 images are provided by Figures 6.1 (LN treated plants), 6.2 (inoculated LN-treated plants) and 6.3 (LP-treated plants). The analyses of these new sets of 8 images using ACRT are provided by Figure 6.4 (comparison of non-inoculated LN-treated and inoculated LN-treated plants) and Figure 6.5 (comparison of non-inoculated LN-treated or LP-treated plants).

The curves provided by Figures 6.4 and 6.5, obtained from the selected sets of 8 images are very similar to those provided by Figures 5.10 and 5.11, obtained from the whole sets of 10 images. This can be taken as an indication that the rhizobox methodology can support robust analyses of root system and root hair development.

Comparison between the non-inoculated and inoculated plants. Figure 5.10 (like Figure 6.4) indicates that inoculation with *B. japonicum* resulted in an increase in total root surface area. This conclusion is also supported by the results from the analyses of root surface area carried out using WINRHIZO™ and displayed in Figure 5.12. Interestingly, the increase in root surface area due to plant inoculation mainly appears at depths, with respect to the position of the germinated seed, between *ca.* 5 cm and 14 cm (Figure 5.10B) (distances from the germinated seed between *ca.* 6 to 15 cm; Figure 5.10A), Above or below this region, root surface area appears as strictly similar in the inoculated and non-inoculated root systems.

In both the inoculated and non-inoculated root systems, the largest root surface areas are found in this range of 5 to 15 cm from the germinated seed Visual observation of the initial images (Figures 5.7 and 5.8) allows to conclude this region in the rhizobox displays colonization by well-developed secondary roots. The data displayed by Figure 5.12 (WINRHIZO™ analyses) suggest that the increase in root surface area in this region due to inoculation mainly results from an increase in root hair surface area, rather than an increase in root growth (length) in this region (compare the white and black bars in Figure 5.12).

Figure 6.1. Images of wheat root systems from non-inoculated plants grown in rhizobox devices in LN conditions for 12 days. Set of 8 images selected from the 10 images displayed by Figure 5.7. See main text and Figure 5.7.

Seedling (*T. turgidum* spp. durum cv. Oued Zenati) germination and transfer in rhizoboxes: see Chapter 2, § 2.2, 2.3 and 2.6. Rhizobox devices: see Chapter 4, § 4.3. Scale bar: 3 cm. An enlargement of a root segment, rendering root hairs visible, is displayed.

Comparison between root systems developed in LN or LP conditions. Figure 5.11 (like Figure 6.5) reveal differences in root system development (colonization of the rhizoboxes) between LN treated and LP treated plants. Analyses with WINRHIZO™ (Figure 5.12) provide evidence that the differences result in an increase in total root surface area, due to both a significant increase in root growth (length) and root hair development (Figure 5.12, compare black and grey bars). It should be noted however that in the 5 to 6 first cm from the germinated seedlings, total root surface area was clearly more important in the LN treated than LP¬-treated plants. Beyond this distance, the inverse situation was observed, and larger root surface area was systematically observed in LP treated plants. This is likely to suggest the root growth within the first 5-6 upper cm of the rhizoboxes occurred with less secondary root production and elongation in LP than LN conditions. Beyond this distance, the inverse situation would occur. Such a difference in rot architecture development was not observed in the comparison between inoculated and non-inoculated plants (above paragraph).

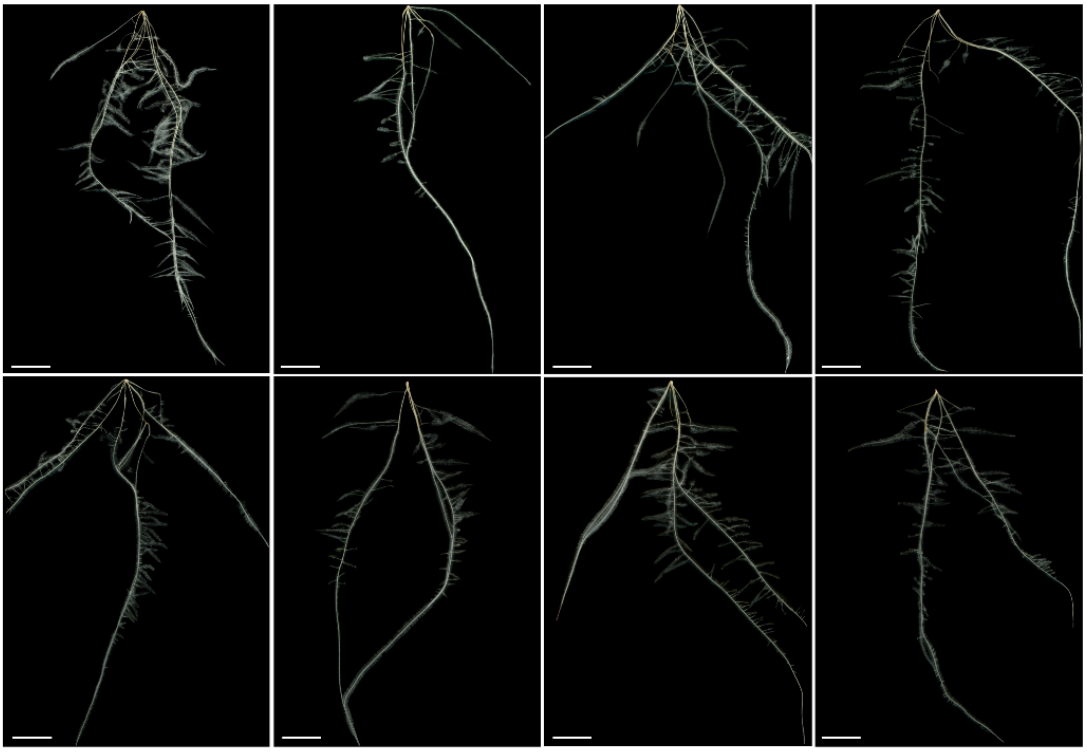

Figure 6.2. Images of wheat root systems from plants inoculated with *Bradyrhizobium japonicum* strain ORS285 and grown in rhizobox devices in LN conditions for 12 days. Set of 8 images selected from the 10 images displayed by Figure 5.8. See main text and Figure 5.8.

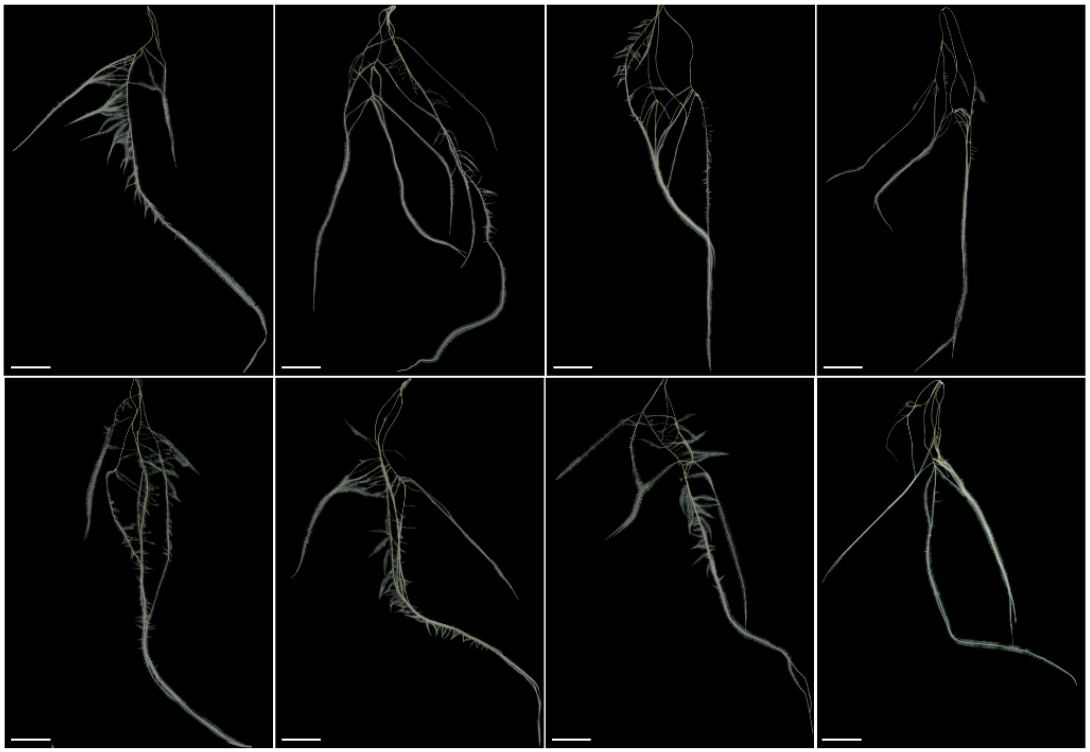

Figure 6.3. Images of wheat root systems from non-inoculated plants grown in rhizobox devices in LP ("low Phosphate") conditions for 12 days. Set of 8 images selected from the 10 images displayed by Figure 5.9. See main text and Figure 5.9.

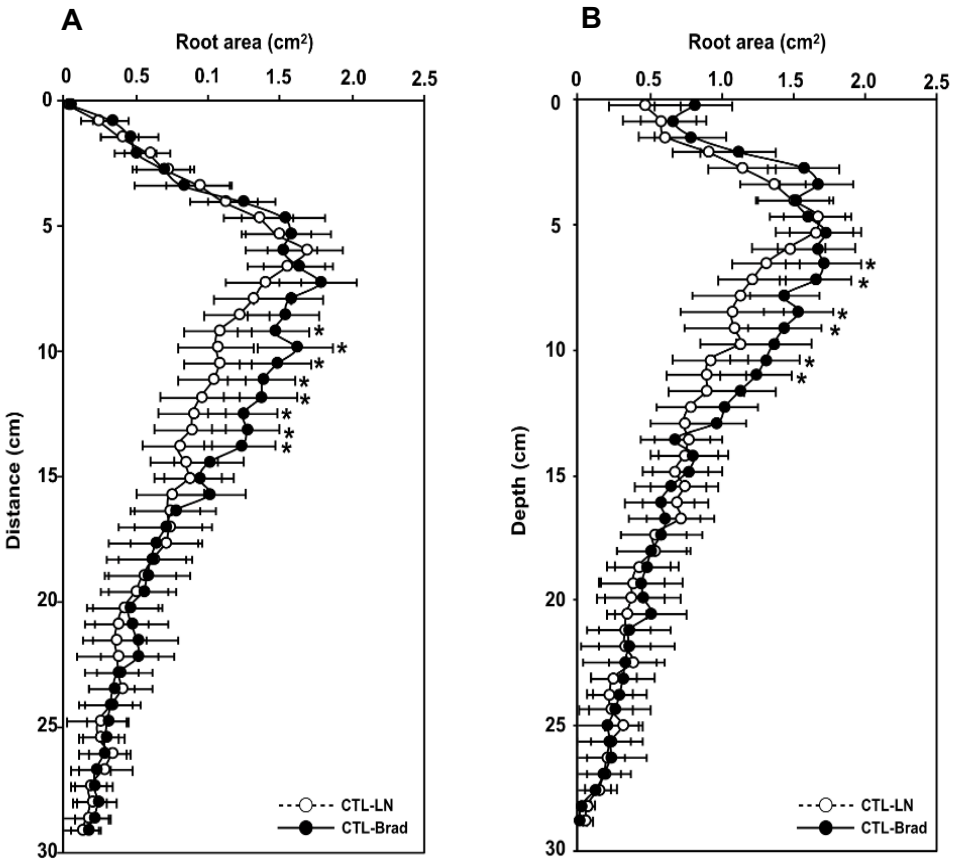

Figure 6.4. Effect of *B. japonicum* on root system development. Analyses from the sets of the 8 selected images provided in Figure 6.2 (non-inoculated LN treated plants) and Figure 6.3 (*B. japonicum* inoculated LN treated plants). See main text and Figures 5.10 for the corresponding analyses with the full sets of 10 images. Means ± SE (n = 8 root systems per condition). The symbol * indicates a statistically significant difference at $p<0.05$ (student's t-test).

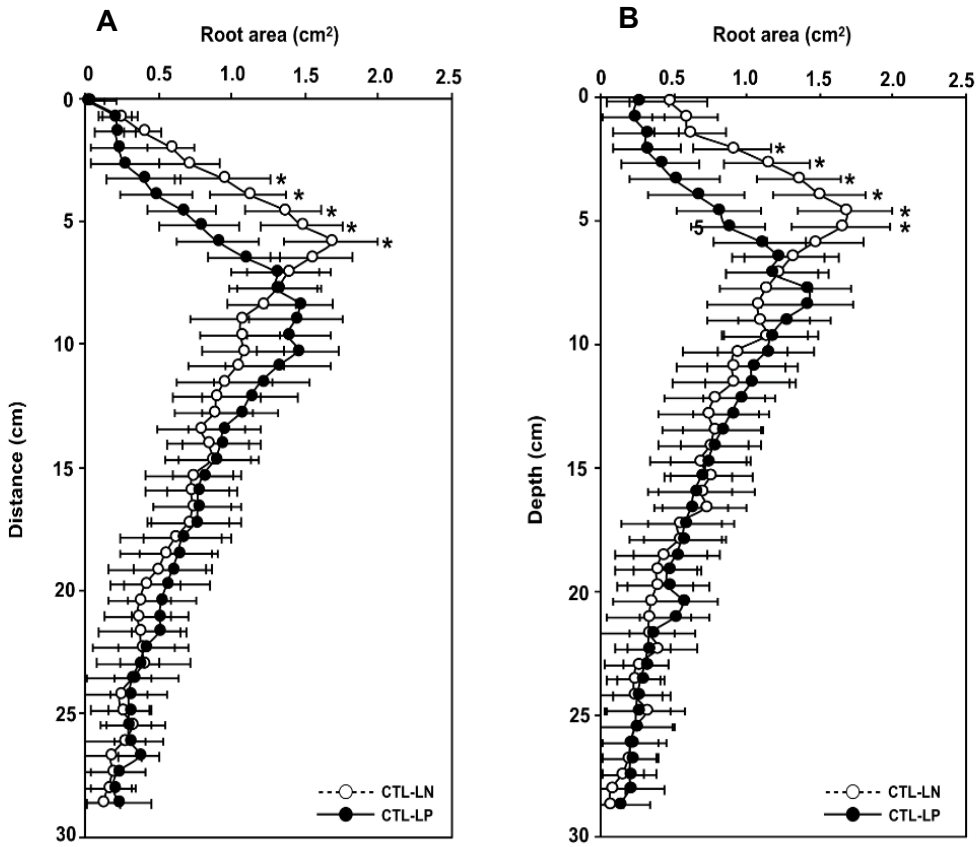

Figure 6.5. Comparison of the effects of low N and low P conditions on root system development. Analyses from the sets of the 8 selected images provided in Figure 6.2 (non-inoculated LN treated plants) and Figure 6.3 (non-inoculated LP treated plants). See main text and Figures 5.11 for the corresponding analyses with the full sets of 10 images. Means ± SE (n = 8 root systems per condition). The symbol * indicates a statistically significant difference at $p<0.05$ (student's t-test).

6.3. Conclusions and perspectives

The results I have obtained indicate that the *Bradyrhizobium japonicum* strain I have tested, ORS285, can interact with the wheat cultivar I have used, Oued Zenati, since it affects root development (Figure 5.10 and 6.4; see above) but is poorly active in terms of plant growth promotion, at least in the experimental conditions we have used (Figure 3.14 and 3.15). It is however important to note that evidence is available that beneficial interactions between roots and soil microbes can display a high level of specificity. For instance, as indicated above, inoculation with *Klebsiella pneumoniae* 342 has been shown to relieve nitrogen deficiency symptoms in one wheat cultivar, out of 3 cultivars that were tested (Iniguez *et al.*, 2004). Thus, it may be worth to assess

the effects of other *B. japonicum* strains on wheat growth and root system development, as well as to test the corresponding responses of other wheat cultivars.

Two methodologies have been developed during this work in order to phenotype root and root hair development. Regarding the current protocols and device prototypes, I believe that the "rhizobox" methodology is the most interesting one, since the growth conditions are more physiologically relevant and images of whole root systems, including root hairs, can be obtained.

Downstream of this work, it would certainly be relevant to Improve the ACRT program developed for automatic analysis of root images obtained using the "rhizobox" device, and to develop strategies allowing to complete/associate the services and information that of these programs provide with those provided by WINRHIZO™. A first step would be to "tune" internal parameters of these programs so that they provide very similar analyses, for instance in terms of total root surface area. Some discrepancies regarding this output have indeed been observed between the two programs that might be due to the initial "cleaning", segmentation and binarization of the images. Probably more importantly, it would be very interesting to optimize the possible complementarities between the two programs. For instance, I believe that a first description of root images could be provided by WINRHIZO™, taking into account only root hairs (identified by this software as the "root system elements" having the thinnest diameter) and then analyzed with ACRT in order to describe root system capacity to explore and forage the "soil" at different depths/distances from the germinated seed, and root hair contribution to this foraging function.

Besides such objectives, I consider that the "rhizobox" methodology could now allow to screen large enough collections of bacteria, including the Lebanese isolates that I have obtained (Chapter 3), in order to identify highly efficient strains, in terms of impact on root system development. The working hypothesis underlying such work is that bacterial strains identified as displaying a strong capacity to stimulate root (including root hair) development are likely to be efficient in improving plant nutrition. In a second step, of course, the effects of such strains on root development and plant growth in real soil conditions would have to be checked. Conversely, GWAS analyses could be developed, testing a collection of wheat accessions, for instance a series of genotypes that would recapitulate wheat domestication, against one bacterial strain (previously found to be able to efficiently interact with at least one member of the tested wheat collection) in order to identify genes and mechanisms involved in the interaction and its impact on root development and plant nutrition. The general objective of all these investigations is to gain knowledge on root PGPR in order to use such bacteria as biofertilizers favoring development of sustainable agricultural practices.

References

Ahmad, I., A. Mian and F. J. M. Maathuis. 2016. Overexpression of the rice AKT1 potassium channel affects potassium nutrition and rice drought tolerance. J. Exp. Bot. 67(9): 2689-2698.

Ahmed, M. A., J. Passioura and A. Carminati. 2018. Hydraulic processes in roots and the rhizosphere pertinent to increasing yield of water-limited grain crops: a critical review. J. Exp. Bot. 69: 3255-3265.

Ahn, S. J., R. Shin and D. P. Schachtman. 2004. Expression of KT/KUP genes in Arabidopsis and the role of root hairs in K^+ uptake. Plant physiol. 134: 1135-1145.

Albalasmeh, A. A. and T. A. Ghezzehei. 2014. Interplay between soil drying and root exudation in rhizosheath development. Plant Soil. 374: 739-751.

Alexander, A., V. K. Singh, A. Mishra and B. Jha. 2019. Plant growth promoting rhizobacterium *Stenotrophomonas maltophilia* BJ01 augments endurance against N_2 starvation by modulating physiology and biochemical activities of *Arachis hypogea*. PLoS ONE 14(9): e0222405.

Babourina, O., B. Hawkins, R. R. Lew I. Newman and S. Shabala. 2001. K^+ transport by Arabidopsis root hairs at low pH. Aust. J. Plant Physiol. 28: 635-641.

Bai, L., X. Ma, G. Zhang, S. Song, Y. Zhou, L. Gao, Y. Miao and C. P. Song. 2014. A receptor-like kinase mediates ammonium homeostasis and is important for the polar growth of root hairs in *Arabidopsis*. Plant Cell. 26: 1497-1511.

Baird, W. V. and J. L. Riopel. 1983. Experimental studies of the attachment of the parasitic angiosperm *Agalinis purpurea* to a host. Protoplasma. 118: 206-218.

Baird, W. V. and J. L. Riopel. 1985. Surface characteristics of root and haustorial hairs of parasitic Scrophulariaceae. Bot. Gaz. 146: 63-69.

Baldani, J. I., V. M. Reis, S. S. Videira, L. H. Boddey and V.L. D. Baldani. 2014. The art of isolating nitrogen-fixing bacteria from non-leguminous plants using N-free semi solid media: a practical guide for microbiologists. Plant Soil. 384: 413-431.

Bashan, Y and L. E. de-Bashan. 2010. How the plant growth-promoting bacterium *Azosprillum* promotes plant growth-a critical assessment. Adv. Agron. 108: 77-136.

Bates, T. R. and J. P. Lynch. 1996. Stimulation of root hair elongation in *Arabidopsis thaiiana* by low phosphorus availability. Plant Cell Environ. 19: 529-538.

Bayley, P. H. J., J. D. Currey and A. H. Fitter. 2002. The role of root system architecture and root hairs in promoting anchorage against uprooting forces in *Allium cepa* and root mutants of *Arabidopsis thaliana*. J. Exp. Bot. 53 (367): 333-340.

Baylis, G.T.S. 1970. Root hairs and phycomycetous mycorrhizas in phosphorus-deficient soil. Plant Soil. 33: 713-716.

Bengough, A. G., K. Loades and B. M. McKenzie. 2016. Root hairs aid soil penetration by anchoring the root surface to pore walls. J. Exp. Bot. 67(4): 1071-1078.

Berg, G. and K. Smalla. Plant species and soil type cooperatively shape the structure and function of microbial communities in the rhizosphere. 2009. FEMS Microbiol Ecol 68: 1-13.

Bernhardt, C., M. Zhao, A. Gonzalez, A. Lloyd and J. Schiefelbein. 2005. The bHLH genes GL3 and EGL3 participate in an intercellular regulatory circuit that controls cell patterning in the Arabidopsis root epidermis. Development. 132: 291-8.

Bertrand, H., C. Plassard, X. Pinochet, B. Touraine, P. Normand, and J. C. Cleyet-Marel. 1999. Stimulation of the ionic transport system in *Brassica napus* by a plant growth-promoting rhizobacterium (*Achromobacter* sp.). Can. J. Microbiol. 46: 229-236.

Beukes, C. W., E. T. Steenkamp, E. van Zyl, J. Avontuur, W. Y. Chan, A. I. Hassen, M. Palmer, L. S. Mthombeni, F. L. Phalane, T. K. Sereme, S. N. Venter. 2019. *Paraburkholderia strydomiana* sp. nov. and *Paraburkholderia steynii* sp. nov.: Rhizobial symbionts of the fynbos legume *Hypocalyptus sophoroides*. Antonie van Leeuwenhoek. 112(9): 1369-1385.

Bhosale, R., J. Giri, B. K. Pandey, R. F. H. Giehl, A. Hartmann, R. Traini, J. Truskina, N. Leftley, M. Hanlon, K. Swarup, A. Rashed, U. Voß, J. Alonso, A. Stepanova, J. Yun, K. Ljung, K. M. Brown, J. P. Lynch, L. Dolan, T. Vernoux, A. Bishopp, D. Wells, N. von Wirén, M. J. Bennett and R. Swarup. 2018. A mechanistic framework for auxin dependent Arabidopsis root hair elongation to low external phosphate. Nat. Commun. 9: 1409, doi: 10.1038/s41467-018-03851-3

Bibikova, T. N, A. Zhigilei and S. Gilroy. 1997. Root hair growth in Arabidopsis thaliana is directed by calcium and an endogenous polarity. Planta 203(4): 495-505.

Bonfante, P. and A. Genre. 2008. Plant and arbuscular mycirrhizal fungi: an evolutionary-developmental perspective. Trands Plant Sci. 13(9): 492-498.

Bouteau, F., A. M. Pennarun, A. Kurkdjian, M. Convert, D. Cornel, M. Monestiez, J. P. Rona and U. Bousquet. 1999. Ion channels of intact young root hairs from *Medicago sativa.* Plant. Physiol. Biochem. 37(12): 889-898.

Brown, A.C., and W. A. Sinclair.1981. Colonization and infection of primary roots of Douglas fir seedlings by the ectomycorrhizal fungus *Laccaria laccata*. Forest Sci. 27: 111-124.

Brown, L. K., T. S. George, J. A. Thompson, G. Wright, L. Lyon, L. Dupuy, S. F. Hubbard and P. J. White. 2012. What are the implications of variation in root hair length on tolerance to phosphorus deficiency in combination with water stress in barley (*Hordeum vulgare*)? Ann. Bot. 110: 319-32.

Brown, L. K., T. S. George, G. Barrett, S. F. Hubbard and P. J. White. 2013. Interactions between root hair length and arbuscular mycorrhizal colonisation in phosphorus deficient barley (*Hordeum vulgare*). Plant Soil. 372: 195-205.

Brown, L. K., T. S. George, K. Neugebauer and P. J. White. 2017. The rhizosheath - a potential trait for future agricultural sustainability occurs in orders throughout the angiosperms. Plant Soil. 418: 115-128.

Bruex, A., R. M. Kainkaryam, Y. Wieckowski, Y. H. Kang, C. Bernhardt, Y. Xia, X. Zheng, J. Y. Wang, M. M. Lee, P. Benfey, P. J. Woolf and J. Schiefelbein 2012. A gene regulatory network for root epidermis cell differentiation in *Arabidopsis.* PLoS Genet 8: e1002446.

Brundrett, M. C. 2002. Coevolution of roots and mycorrhizas of land plants. New Phytol. 154: 275-304.

Brusetti, A. A., M. M. Jadaon, A. M. Abdulsamad and H. M. Dashti. 2009. Heat treatment of bacteria: A simple method pf DNA extraction for molecular techniques. Kuwait Med. J. 41(2): 117-122.

Bulgarelli, D., K. Schlaeppi, S. Spaepen, E. V. L. van Themaat and P. Schulze-Lefert. 2013. Structure and functions of the bacterial microbiota of plants. Annu. Rev. Plant Biol. 64: 807-838.

Burris, J. N. 2016. *Nanocomposite Adhesive of English ivy (Hedera helix): Bioproduction, Nanoparticle Isolation, and Molecular Analysis* (Doctoral dissertation, University of Tennessee, Knoxville). Retrieved from https://www.semantic scholar.org/paper/Nanocomposite-Adhesive-of-English-ivy-(-Hedera-)%3A-Burris/ad75824bc00e66182707bc2d4cebe20ae9ff9269

Burris, J. N., S. C. Lenaghan, M. Zhang and C. N. Stewart. 2012. Nanopartical biofabrication using English ivy (*Hedera helix*). J. Nanobiotechnology. 10: 7p.

Cakmakci, M. L., H. J. Evans and W. S. Seidler. 1981. Characteristics of nitrogen-fixing *Klebsiella oxytoca* isolated from wheat roots. Plant Soil. 61: 53-63.

Camacho-Cristobal, J. J., E. M. Martin-Rejano, M. B. Herrera-Rodriguez, M. T. Navarro-Gochicoa, J. Rexach and A. Gonzalez-Fontes. 2015. Boron deficiency inhibits root cell elongation via an ethylene/auxin/ROS-dependent pathway in *Arabidopsis* seedlings, J. Exp. Bot. 66: 3831-3840.

Cannales, J., O. Contreras-López, J. M. Álvarez and R. A. Gutiérrez. 2017. Nitrate induction of root hair density is mediated by TGA1/ TGA4 and CPC transcription factors in *Arabidopsis thaliana*. Plant J. 92: 305-316.

Carminati, A., J. B. Passioura, M. Zarebanadkoiki, M. A. Ahmed, P. R. Ryan, M. Watt and E. Delhaize. 2017. Root hairs enable high transpiration rates in drying soils. New Phytol. 216: 771-781.

Cerezo, M., P. Tillard, S. Filleur, S. Muños, F. Daniel-Vedele and A. Gojon. 2001. Major alterations of the regulation of root NO_3^- uptake are associated with the mutation of *Nrt2.1* and *Nrt2.2* genes in Arabidopsis. Plant Physiol. 127: 262-271.

Chang, M. X., M. Gu, Y. M. Xia, X. L. Dai, C. R. Dai, J. Zhang, S. C. Wang, H. Y. Qu, N. Yamaji, M. J. Feng M. and G. H. Xu GH. 2019. OsPHT1;3 Mediates Uptake, Translocation, and Remobilization of Phosphate under Extremely Low Phosphate Regimes. Plant Physiol. 179(2): 656-670.

Chaparro, J. M., D. V. Badri, M. G. Bakker, A. Sugiyama, D. K. Manter and J. M. Vivanco. 2013. Root exudation of phytochemicals in *Arabidopsis* follows specific patterns that are developmentally programmed and correlate with soil microbial functions. PLoS One 8: e55731

Chen, G., Q. Hu, L. Luo, T. Yang, S. Zhang, Y. Hu, L. Yu and G. Xu. 2015. Rice potassium transporter OsHAK1 is essential for maintaining potassium-mediated growth and functions in salt tolerance over low and high potassium concentration ranges. Plant Cell Environ. 38: 2747-2765.

Chen, C. Y., K. Wu. And W. Schmidt. 2015. The histone deacetylase HDA19 controls root cell elongation and modulates a subset of phosphate starvation responses in *Arabidopsis*. Sci. Rep. 5: 11p, doi: 10.1038/srep15708

Clarkson, D. T. 1985. Factors affecting mineral nutrient acquisition by plants. Ann. Rev. Plant Physiol. 36: 77-115.

Comas, L. H., S. R. Becker, V. M. V. Cruz, P. F. Byrne and D. A. Dierig. 2013. Root traits contributing to plant productivity under drought. Front. Plant Sci. 4: 442, doi.org/10.3389/fpls.2013.00442.

Contesto, C., G. Desbrosses, C. Lefoulon, G. Béna, F. Borel, M. Galland, L. Gamet, F. Varoquaux, B. Touraine. 2008. Effects of rhizobacterial ACC deaminase activity on *Arabidopsis* indicate that ethylene mediates tocal root responses to plant growth-promoting rhizobacteria. Plant Sci. 175: 178-189.

Cui, S., T. Wakatake, K. Hashimoto, S. B. Saucet, K. Toyooka, S. Yoshida and K. Shirasu. 2016. Haustorial hairs are specialized root hairs that support parasitism in the facultative parasitic plant *Phtheirospermum japonicum*. Plant Physiol. 170: 1492-1503.

Cui, S., T. Suzakic, R. Tominaga-Wadad and S. Yoshida. 2018. Regulation and functional diversification of root hairs. Semin. Cell Dev. Biol. 83: 115-122.

Damiani, I., A. Drain, M. Guichard, S. Balzergue, A. Boscari, J. C. Boyer, V. Brunaud, S. Cottaz, C. Rancurel, M. D. Rocha, C. Fizames, S. Fort, I. L. Gaillard, V. Maillol, E. G. J. Danchin, H. Rouached, E. Samain, Y. H. Su, J. Thouin, B. Touraine, A. Puppo, J. M. Frachisse, N. Pauly and H. Sentenac. 2016. Nod factor effects on root hair-specific transcriptome of *Medicago truncatula*: focus on plasma membrane transport systems and reactive oxygen species networks. Front. Plant Sci. 7: 794, doi.org/10.3389/fpls.2016.00794

Dashti, L., I. Malkhazova, M. Gtari, I. Tamagnini, S. Borin, M. Merabishvili, N. Chanishvili, D. Mora, F. Cappitelli and D. Daffonchio. 2008. Fluorescent-BOX-PCR for resolving bacterial genetic diversity, endemism and biogeography. BMC Microbiology. 8: 13p.

Datta, S., H. Prescott and L. Dolan. 2015. Intensity of a pulse of RSL4 transcription factor synthesis determines *Arabidopsis* root hair cell size. Nat. Plants 1: 15138.

Dauphin, A., H. El-Maarouf, N. Vienney, J. P. Rona and F. Bouteau. 2001. Effect of desiccation on potassium and anion currents from young root hairs: Implication on tip growth. Physiol. Plant. 113: 79-84.

Davies, J., L. G. Briarty and J. O. Rieley. 1973. Observations on the swollen lateral roots of the Cyperace. New Phytol. 72: 167-174.

De Meyer, S. E., M. Cnockaert, J. K. Ardley, B. E. Van Wyk, P. A. Vandamme and J. G. Howieson. 2014. *Burkholderia dilworthii* sp. nov., isolated from Lebeckia ambigua root nodules. Int. J. Syst. Evol. Microbiol. 64: 1090-1095.

De Michele, R., D. Loqué, S. Lalonde and W. B. Frommer. 2012. Ammonium and urea transporter inventory of the *Selaginella* and *Physcomitrella* genomes. Front. Plant Sci. 62(3): 19p, doi.org/10.3389/fpls.2012.00062

Delhaize, E., T. M. Rathjen and C. R. Cavanagh. 2015. The genetics of rhizosheath size in a multiparent mapping population of wheat. J. Exp. Bot. 66 (15): 4527-4536.

Ditengou, F., A., M. Raudaskoski and F. Lapeyrie. 2000. Root hair elongation is inhibited by hypaphorine, the indole alkaloid from the ectomycorrhizal fungus *Pisolithus tinctorius,* and restored by indole-3-acetic acid. Planta. 211: 722-728.

Ditengou, F., A., M. Raudaskoski and F. Lapeyrie. 2003. Hypaphorine, an indole-3-acetic acid antagonist delivered by the ectomycorrhizal fungus *Pisolithus tinctorius*, induces reorganisation of actin and the microtubule cytoskeleton in *Eucalyptusglobulus* ssp *bicostata* root hairs. Planta. 218: 217-225.

Dittmer, H.J. 1937. A quantitative study of the roots and root hair of a winter rye plant (secale cereale). Am. J. Bot. 24: 417-420.

Dolan, L. 2017. Root hair development in grasses and cereals (Poaceae). Curr. Opin Genet Dev. 45: 76-81.

Downey, P., I. Szabò, N. Ivashikina, A; Negro, F. Guzzo, P. Ache, R. Hedrich, M. Terzi and F. L. Schiavo. 2000. *KDC1,* a novel carrot root hair K^+ channel. J. Biol. Chem. 275(50): 39420-39426.

Drouge, B., H. Doré, S. Borland, F. Wisniewski-Dyé, C. Prigent-Combaret. 2012. Which specificity in cooperation between phytostimulating rhizobacteria and plants? Res. Microbiol. 163: 500-510.

Dutta, P., A. Karmaker, S. Majumdar and S. Roy. 2018. *Klebsiella pneumoniae* (HR1) assisted alleviation of Cd(II) toxicity in Vigna mungo: a case study of biosorption of heavy metal by an endophytic bacterium coupled with plant growth promotion. Euro-Mediterranean J. Environ. In. 3: 10p.

Felle, H. H. 1994. The H^+/Cl^- symporter in root-hair cells of *Sinapis alba*. Plant Physiol. 106: 1131-1136.

Felle, H. H. and P. K. Helper. 1997. The cytosolic Ca^{+}_{2} concentration gradient of Sinapis alba root hairs as revealed by Ca^{+}_{2}-selective microelectrode tests and fura-dextran ratio imaging. Plant Physiol. 114: 39-45.

Felle, H. H., É. Kondorosi, Á. Kondorosi and M. Schultze. 1998. The role of ion fluxes in Nod factor signalling in *Medicago sativa*. Plant J. 13(4): 455-463.

Felle, H. H., É. Kondorosi, Á. Kondorosi and M. Schultze. 1999. Nod factors modulate the concentration of cytosolic free calcium differently in growing and non-growing root hairs of *Medicago sativa* L. Planta. 209: 207-212.

Feng, H., M. Yan, X. Fan, B. Li, Q. Shen, A. J. Miller and G. Xu. 2010. Spatial expression and regulation of rice high-affinity nitrate transporters by nitrogen and carbon status. J. Exp. Bot. 62(7): 2319-2332.

Finkel, O. M, G. Castrillo, S. H. Paredes, I. S. González and J. L. Dangl. 2017. Understanding and exploiting plant beneficial microbes. Curr Opin Chem Biol. 38: 155-163.

Franciosini, A., B. Rymen, M. Shibata, D. S. Favero and K. Sugimoto. 2017. Molecular networks orchestrating plant cell growth. Curr. Opin. Plant Biol. 35: 98-104.

Gahoonia, T. S. and N. E. Nielsen. 1998. Direct evidence on participation of root hairs in phosphorus (^{32}P) uptake from soil. Plant and Soil. 198: 147-152.

Gahoonia, T. S. and N. E. Nielsen. 2004. Barley genotypes with long root hairs sustain high grain yields in low-P field. Plant and Soil. 262: 55-62.

Galland, M., L. Gamet, F. Varoquaux, B. Touraine, B. Touraine and G. Desbrosses. 2012. The ethylene pathway contributes to root hair elongation induced by the beneficial bacteria *Phyllobacterium brassicacearum* STM196. Plant Sci. 190: 74-81.

Gans, J., M. Woilinsky and J. Dunbar. 2005. Computational improvements reveal great bacterial diversity and high metal toxicity in soil. Science. 309: 1387-1390.

Garciadeblas, B., J. Barrero-Gil, B. Benito and A. Rodríguez-Navarro. 2007. Potassium transport systems in the moss *Physcomitrella patens*: *pphak1* plants reveal the complexity of potassium uptake. Plant J. 52: 1080-1093.

Garrido-Oter, R., R. T. Nakano, N. Dombrowski, K.W. Ma, T. Team, A. C. Mchardy and P. Schulze-Lefert. 2018. Molecular traits of the rhizobiales root microbiota and their evolutionary relationship with symbiotic rhizobia. Cell Host Microbe. 24: 155-167.

Garrity, G. M., D. J. Brenner, N. R. Krieg, J. T. Staley. (Eds.). 2005. *Bergey's Manual of Systematic Bacteriology, Volume Two: The Proteobacteria, Part C: The Alpha-, Beta-, Delta-, and Epsilonproteobacteria*. New York: Springer.

Gassmann, W. and J. I. Schroeder. 1994. Inward-rectifying K^+ channels in root hairs of wheat: A mechanism for aluminium-sensitive low-affinity K^+ uptake and membrane potential control. Plant Physiol. 105: 1399-1408.

George, T. S., L. K. Brown, L. Ramsay, P. J. White, A. C. Newton, A. G. Bengough, J. Russell and W. T. B. Thomas. 2014. Understanding the genetic control and physiological traits associated with rhizosheath production by barley (*Hordeum vulgare*). New Phytol. 203: 195-205.

Gierth, M., P. Mäser and J.I. Schroeder. 2005. The potassium transporter *AtHAK5* functions in K^+ deprivation-induced high-affinity K^+ uptake and *AKT1* K^+ channel contribution to K^+ uptake kinetics in *Arabidopsis* roots. Plant Physiol. 137: 1105-1114.

Gomes, N. C. M., C. G. Flocco, R. Costa, H. Junca, R. Vilchez, D. H. Pieper, E. Krögerrecklenfort, R. Paranhos, L. C. Mendonça-Hagler and K. Smalla. 2010. Mangrove microniches determine the structural and functional diversity of enriched petroleum hydrocarbon-degrading consortia. FEMS Microbiol. Ecol. 74: 276-290.

Gong. X. and G. McDonald. 2017. QTL mapping of root traits in phosphorus-deficient soils reveals important genomic regions for improving NDVI and grain yield in barley. Theor. Appl. Genet. 130: 1885-902.

Good, A. G., A. K. Shrawat and D. G. Muench. 2004. Can less yield more? Is reducing nutrient input into the environment compatible with maintaining crop production? Trends in plant science. 9: 597-605.

Grierson, C., E. Nielsen, T. Ketelaar and J. Schiefelbein. 2014. Root hairs. *Arabidopsis Book.* 12: e0172. doi: 10.1199/tab.0172

Haichar, F. Z., T. Heulin T, J. Guyonnet and W. Achouak. 2016. Stable isotope probing of carbon flow in plant-holobionte. Curr. Opin. Biotechnol. 41: 9-13.

Haling, R. E., L. K. Brown, A. G. Bengough, I. M. Young, P. D. Hallett, P. J. White, I. and T. S. Georage. 2013. Root hairs improve root penetration, root-soil contact, and phosphorus acquisition in soils of different strength. J. Exp. Bot. 64(12): 3711-3721

Haling, R. E., L. K. Brown, A. G. Bengough, T. A. Valentine, P. J. White, I. M. Young and T. S. George. 2014. Root hair length and rhizosheath mass depend on soil porosity, strength and water content in barley genotypes. Planta 239(3): 643-651

Halperin, S. J. and J. P. Lynch. 2003. Effects of salinity on cytosolic Na^+ and K^+ in root hairs of *Arabidopsis thaliana*: in vivo measurements using the fuorescent dyes SBFI and PBFI. J. Exp. Bot. 54(390): 2035-2043.

Han, Y., M. Xin, K. Huang, Y. Xu, Z. Liu, Z. Hu, Y. Yao, H. Peng, Z. Ni and Q. Sun. 2016. Altered expression of *TaRSL4* gene by genome interplay shapes root hair length in allopolyploid wheat. New Phytologist. 209: 721-732.

Henry, C. H. and J. W. Deacon. 1981. Natural (non-pathogenic) death of the cortex of wheat and barley seminal roots, as evidenced by nuclear staining with acridine orange. Plant and Soil. 60: 255-274.

Hinsinger, P., A. G. Bengough, D. Vetterlein and I. M. Young. 2009. Rhizosphere: biophysics, biogeochemistry and ecological relevance. Plant Soil. 321: 117-152.

Hirsch, R. E., B. D. Lewis, E. P. Spalding and M. R. Sussman. 1998. A role for the AKT1 potassium channel in plant nutrition. Science. 281(5365): 918-921.

Hogg, B. V., J. Kacprzyk, E. M. Molony, C. O'Reilly, T. F. Gallagher, P. Gallois and P. F. McCabe. 2011. An in vivo root hair assay for determining rates of apoptotic-like programmed cell death in plants. Plant Methods. 7:45, 9p.

Holden, J. 1975. Use of nuclear staining to assess rates of cell death in cortices of cereal roots. Soil Biol. Biochem. 7, 333-334.

Holz, M., M. Zarebanadkouki, Y. Kuzyakov, J. Pausch and A. Carminati. 2018. Root hairs increase rhizosphere extension and carbon input to soil. An. Bot. 121: 61-69.

Horn, R., L. U. Wingen, J. W. Snape and L. Dolan. 2016. Mapping of quantitative trait loci for root hair length in wheat identifies loci that co-locate with loci for yield component. J. Exp. Bot. 67: 4535-4543.

Huang, N. C., K. H. Liu, H. J. Lo and Y. F. Tsay. 1999. Cloning and functional characterization of an *Arabidopsis* nitrate transporter gene That encodes a constitutive component of low-affinity uptake. Plant cell. 11: 1381-1392.

Huang, L., X. Shi, W. Wang, K. H. Ryu and J. Schiefelbein. 2017. Diversification of root hair development genes in vascular plants. Plant Physiol. 174: 1697-1712.

Huang, Y., Y. Wang, L. Tan, L. Sun, J. Petrosino, M. Z. Cui, F. Hao and M. Zhang. 2016. Nanospherical arabinogalactan proteins are a key component of the high-strength adhesive secreted by English ivy. PNAS. 113 (23): E3193-E3202.

Ibáñez, F., L. Wall and A. Fabra. 2017. Starting points in plant-bacteria nitrogen-fixing symbioses: intercellular invasion of the roots. J. Exp. Bot. 68: 1905-1918.

Inguez, A. L., Y. Dong and E. W. Triplett. 2004. Nitrogen fixation in wheat provided by *Klebsiella pneumonia* 342. Mol. Plant Microbe In. 14(10) 1078-1085.

Ivashikina, N., D. Becker, P. Ache, O. Meyerhoff, H. H. Felle and R. Hedrich. 2001. K^+ channel profile and electrical properties of *Arabidopsis* root hairs. FEBS lett. 508: 463-469.

Jackson, M.L. 1973. Soil Chemical Analysis. Printice Hall of India (Pvt.) Limited, New Delhi, India.

Jain, D. K. and D. G. Patriquin. 1984. Root hair deformation, bacterial attachment, and plant growth in wheat-*Azospirillum* associations. Appl. Environ. Microbiol. 48(6): 1208-1213.

Jakobson, I., B. Chen, L. Munkvold, T. Lundsgaard and Y. G. Zhu. Contrasting phosphate acquisition of mycorrhizal fungi with that of root hairs using the root hairless barley mutant. Plant Cell Environ. 28(7): 928-938.

James, R. A., C. Weligama, K. Verbyla, P. R. Ryan, G. J. Rebetzka, A. Rattey, A. E. Richardson and E. Delhaize. 2016. Rhizosheaths on wheat grown in acid soils: phosphorus acquisition efficiency and genetic control. J. Exp. Bot. 67(12): 3709-3718.

Janes, G., D. von Wangenheim, S. Cowling, I. Kerr, L. Band, A. P. Frenc and A. Bishopp. 2018. Cellular Patterning of Arabidopsis Roots Under Low Phosphate Conditions. Front. Plant Sci. 9: 735. doi: 10.3389/fpls.2018.00735

Jha, P. and A. Kumar. 2009. Characterization of novel plant growth promoting endophytic bacterium *Achromobacter xylosoxidans* from wheat plant. Microbe Ecol. 58(1): 179-188.

Jones, D. L., J. K. Shaff and L. V. Kochian. 1995. Role of calcium and other ion in directing root hair tip growth in *Limnobium stonoloniferum*. Planta 197: 672-680.

Jones, A. R., E. M. Kramer, K. Knox, R. Swarup, M. J. Bennett, C.M. Lazarus, H. M. Leyser and C.S. Grierson. 2009. Auxin transport through non-hair cells sustains root-hair development. Nat. Cell Biol. 11: 78-84.

Kanno, Y., Y. Kamiya and M. Seo. 2013. Nitrate does not compete with abscisic acid as a substrate of AtNPF4.6/NRT1.2/AIT1 in *Arabidopsis*. Plant Signal Behav. 8: 12, e26624.

Klinsawang, S., T. Sumranwanich, A. Wannaro and P. Saengwilai. 2018. Effect of root hair length on potassium acquisition in rice (*Oryza sativa* L.). Appl. Ecol. Env. Res. 16(2): 1609-1620.

Krapp, A., L. C. David, C. Chardin, T. Girin, A. Marmagne, A. S. Leprince, S. Chaillou, S. Ferrario-Méry, C. Meyer, F. Daniel-Vedele. 2014. Nitrate transport and signalling in *Arabidopsis*. J. Exp. Bot. 65 789–798.

Krouk, G., B. Lacombe, A. Bielach, F. Perrine-Walker, K. Malinska, E. Mounier, K. Hoyerova, P. Tillard, S. Leon, K. Ljung. E. Zazimalova. E. Benkova, P. Nacry and A. Gojon. 2010. Nitrate-regulated auxin transport by *NRT1.1* defines a mechanism for nutrient sensing in plants. Dev. Cell. 18(6): 927-937.

Kwak, S. H., R. Shen and J. Schiefelbein. 2005. Positional signaling mediated by a receptor-like kinase in *Arabidopsis*. Sciences. 307: 1111-1113.

Kyselková M., J. Kopecký, M. Frapolli, G. Défago, M. Ságova-Marecková, G. L. Grundmann and Y. Moënne-Loccoz. 2009. Comparison of rhizobacterial community composition in soil suppressive or conducive to tobacco black root rot disease. ISME J. 3: 1127-1138.

Lagarde, D., M. Basset, M. Lepetit, G. Conejero, F. Gaymard, S. Astruc and C. Grignon. 1996. Plant J. 9(2): 195-203.

Lamont, B. B.1974. The biology of dauciform roots in the sedge Cyathochaete avenacea. New Phytol. 73: 985-996.

Lauter, F. R., O. Ninnemann, M. Bucher, J. W. Riesmeier and W. B. Frommeer. 1996. Preferential expression of an ammonium transporter and of two putative nitrate transporters in root hairs of tomato. Proc. Natl. Acad. Sci. USA. 93: 8139-8144.

Ledger, T., S. Rojas, T. Timmermann, I. Pinedo, M. J. Poupin, T. Garrido, P. Richter, J. Tamayo and R. Donoso. 2016. Volatile-Mediated Effects Predominate in *Paraburkholderia phytofirmans* Growth Promotion and Salt Stress Tolerance of *Arabidopsis thaliana*. Front Microbiol. 17: 18p, doi:10.3389/fmicb.2016. 01838

Lee, R. D. W. and H. T. Cho. 2013. Auxin, the organizer of the hormonal/ environmental signals for root hair growth. Front. Plant Sci. 448(4): 7p, doi.org/10.3389/fpls.2013.00448

Leitner, D., S. Klepsch, M. Ptashnyk, A. Marchant. G. J. D. Kirk, A. Schnepf and T. Roose. 2010. A dynamic model of nutrient uptake by root hairs. New Phytol. 185: 792-802.

Lejay, L., P. Tillard, M. Lepetit, F. D. Olive, S. Filleur, F. Daniel-Vedele and A. Gojon. 1999. Molecular and functional regulation of two NO_3^- uptake systems by N^- and C^- status of *Arabidopsis* plants. Plant J. 18(5): 509-519.

Léran, S., S. Muños, C. Brachet, P. Tillard, A. Gojon and B. Lacombe. 2013. The *Arabidopsis* NRT1.1 is a bidirectional transporter involved in root-to-shoot nitrate translocation. Mol. Plant. 6: 1984-1987.

Léran, S., K. Varala, J. C. Boyer, M. Chiurazzi, N. Crawford, F. Daniel-Vedele, L. David, R. Dickstein, E. Fernandez, B. Forde, W. Gassmann, D. Geiger, A. Gojon, J. M. Gong, B. A. Halkier, J. M. Harris, R. Hedrich, A. M. Limami, D. Rentsch, M. Seo, Y. F. Tsay, M. Zhang, G. Coruzzi and B. Lacombe. 2014. A unified nomenclature of NITRATE TRANSPORTER 1/PEPTIDE TRANSPORTER family members in plants. Trends Plant Sci. 19(1): 5-9.

Lew, R. R. 1998. Immediate and steady state extracellular ionic fluxes of growing Arabidopsis thaliana root hairs under hyperosmotic and hypoosmotic conditions. Physiol. Plant. 104: 397-404.

Li, T., G. Lin, X. Zhang, Y. Chen, S. Zhang and B. Chen. 2014. Relative importance of an arbuscular mycorrhizal fungus (*Rhizophagus intraradices*) and root hairs in plant drought tolerance. Mycorrhiza. 24: 595-602.

Li, W., Y. Wang, M. Okamoto, N.M. Crawford, M.Y. Siddiqi, A.D. Glass. 2007. Dissection of the *AtNRT2.1:AtNRT2.2* inducible high-affinity nitrate transporter gene cluster. Plant Physiol. 143: 425-433.

Li, S. J. Yu, M. Zhu, F. Zhao and S. Luan. 2012. Cadmium impairs ion homeostasis by altering K^+ and Ca^{2+} channel activities in rice root hair cells. Plant Cell Environ. 35: 1998-2013.

Lin, C. M., S. Koh, G. Stacey, S. M. Yu, T. Y. Lin and Y. F. Tsay. 2000. Cloning and functional characterization of a constitutively expressed nitrate transporter gene, *OsNRT1*, from rice. Plant Physiol. 122(2): 379-388.

Lin, Q., Y. Ohashi, M. Kato, T, Tsuge, H. Gu, L.J. Qu and T. Aoyama. 2015. GLABRA2 directly suppresses Basic Helix-Loop-Helix transcription factor genes with diverse functions in root hair development. Plant Cell. 27: 2894-2906.

Liu, K. H., C. Y. Huang and Y. F. Tsay. 1999. CHL1 is a dual-affinity nitrate transporter of Arabidopsis involved in multiple phases of nitrate uptake. Plant Cell. 11: 865-874.

Liu, M., T. Rathjen, K. Weligama, K. Forrest, M. Hayden and E. Delhaize. 2017. Analysis of aneuploid lines of bread wheat to map chromosomal locations of genes controlling root hair length. J. Exp. Bot.199: 1333-1341.

López-Bucio, J., J. C. Campos-Cuevas, E. Hernández-Calderón, C. Velásquez-Becerra, R. Farías-Rodríguez, L. I. Macías-Rodríguez, and E. Valencia-Cantero. 2007. *Bacillus megaterium* rhizobacteria promote growth and alter root-system architecture through an auxin- and ethylene-independent signaling mechanism in *Arabidopsis thaliana*. Mol. Plant Microbe. 20(2): 207-207.

Lu, M., T. Rathjen, K. Weligama, K. Forrest, M, Hayden and E. Delhaize. 2017. Analysis of aneuploid lines of bread wheat to map chromosomal locations of genes controlling root hair length. An. Bot. 119: 1333-1341.

Ludewig, U., B. Neuhäuser and M. Dynowski. 2007. Molecular mechanisms of ammonium transport and accumulation in plants. FEBS Letters 581: 2301-2308.

Lugtenberg, B. and F. Kamilova. 2009. Plant-growth-promoting rhizobacteria. Annu. Rev. Microbiol. 63: 541-556.

Luo, B., J. Chen, L. Zhu, S. Liu, B. Li, H. Lu, G. Ye, G. Xu and X. Fan. 2018. Overexpression of a high-affinity nitrate transporter *OsNRT2.1* increases yield and manganese accumulation in rice under alternating wet and dry condition. Front Plant Sci. 9: 12p, doi: 10.3389/fpls.2018.01192.

Lynch, J.P. 2007. Roots of the second green revolution. Aust. J. Bot. 55: 493-512.

Ma, Z., T. C. Walk, A. Marcus and J. P. Lynch. 2001. Morphological synergism in root hair length, density, initiation and geometry for phosphorus acquisition in *Arabidopsis thaliana*: A modeling approach. Plant Soil. 236: 221-235.

Maherali, H. 2014. Is there an association between root architecture and mycorrhizal growth response? New Phytol. 204: 192-200.

Marschner, H. 1995. Mineral Nutrition of Higher Plants, Ed 2. Academic Press, London.

Marzec, M., M. Melzer and I. Szarejko. 2015. Root hair development in the grasses: what we already know and what we still need to know. Plant Physiol. 168: 407-414.

Masclaux-Daubresse, C., F. Daniel-Vedle, J. Dechorgnat, F. Chardon, L. Gaufichon and A. Suzuki. 2010. Nitrogen uptake, assimilation and remobilization in plant: challenges for sustainable and productive agriculture. Ann. Bot. 105:1141-1157.

Massicotte, H. B., R. L. Peterson and L. H. Melville. 1989. Hartig net structure of ectomycorrhizae synthesized between *Laccaria biocolor* (Tricholomataceae) and two hosts: *Betula alleghaniunis* (Betulaceae) and *Pinus resinosa* (Pinaceae). Am. J. Bot. 76: 1654-1667.

Masucci, J. D. and J. W. Schiefelbein. 1996. Hormones act downstream of TTG and GL2 to promote root hair out growth during epidermis development in the *Arabidopsis* root. Plant Cell 8: 1505-1517.

Mayak, S., T. Tsipora and G. R. Bernard. 2004. Plant growth-promoting bacteria that confer resistance to water stress in tomatoes and peppers. Plant Sci. 166: 525-530.

McCully. M. E. 1999. Roots in soil: Unearthing the complexities of roots and their rhizospheres. 50: 695-718.

McElgunn, J. D. and C.M. Harrison. 1969. Formation, elongation and longevity of barley root hairs. Agron. J. 61. 79-81.

Meharg, A. A. and M. R. Blatt. 1995. NO^-_3 transport across the plasma membrane of *Arabidopsis thaliana* root hairs: kinetic control by pH and membrane voltage. J. Membrane Biol. 145: 49-66.

Melzer, B., T. Steinbrecher, R; Seidel, O. Kraft, R. Schwaiger and T. Speck. 2010. The attachment strategy of English ivy: a complex mechanism acting on several hierarchical levels. J. R. Soc. Interface. 7: 1383-1389.

Menand, B., K, Yi, S. Jouannic, L. Hoffmann, E. Ryan, P. Linstead, D.G. Schaefer and L. Dolan. 2007. An ancient mechanism controls the development of cells with a rooting function in land plants. Science 316: 1477-1480.

Miedema, H., V. Demidchik, A. A. Véry J. H. F. Bothwell, C. Brownlee and J. M. Davies. 2008. Two voltage-dependent calcium channels co-exist in the apical plasma membrane of *Arabidopsis thaliana* root hairs. New Phytol. 179: 378-385.

Mirza, M. S., W. Ahmad, F. Latif, J. Haurat, R. Bally, P. Normand and K. A. Malik. 2001. Isolation, partial characterization, and the effect of plant growth promoting bacteria (PGPB) on micro propagated sugarcane in vitro. Plant Soil. 237: 47–54.

Moreno-Espíndola, I, P., F. Rivera-Becerril, M. Ferrara-Guerrero and F. León-González. 2007. Role of root-hairs and hyphae in adhesion of sand particles. Soil. Biol. Biochem. 39: 2520-2526.

Murry, M. A., M. S. Fontaine and J. G. Torrey. 1984. Growth kinetics and nitrogenase induction in *Frankia* sp. HFPArI3 grown in batch culture. Plant and Soil. 78: 61-78.

Nazoa, P., J. Videmar, T.J. Tranbarger, K. Mouline, I. Damiani, P. Tillard, A. D. M. Glass and B. Touraine. 2003. Regulation of the nitrate transporter gene *AtNRT2.1* in *Arabidopsis thaliana*, responses to nitrate, amino acids, and developmental stage. Plant Mol. Biol. 52: 689-703.

Nieves-Cordones, N., F. Alemán, V. Martínez and F. Rubio. 2010. The *Arabidopsis thaliana* HAK5 K^+ transporter is required for plant growth and K^+ acquisition from Low K^+ solutions under saline conditions. Mol. Plant. 3(2): 326-333.

Okamoto, M., A. Kumar, W. Li, Y. Wang, M.Y. Siddiqi, N.M. Crawford and A.D. Glass. 2006 High-affinity nitrate transport in roots of Arabidopsis depends on expression of the NAR2-like gene *AtNRT3.1*. Plant Physiol. 140: 1036-1046.

Olroyd, G. E. D. 2013. Speak, friend, and enter: signalling systems that promote beneficial symbiotic associations in plants. Nat. Rev. Microbiol. 11: 252-263.

Orfanoudakis, M., C.T. Wheeler and J. E. Hooker. 2010. Both the arbuscular mycorrhizal fungus *Gigaspora rosea* and *Frankia* increase root system branching and reduce root hair frequency in *Alnus glutinosa*. Mycorrhiza. 20: 117-126.

Orozco-Mosqueda, M. del C., M. del C. Rocha-Granados and B. R. Glick. 2018. Microbiome engineering to improve biocontrol and plant growth-promoting mechanisms. Microbiol Res. 208: 25-31.

Orsel M., A. Krapp A. and F. Daniel-Vedele. 2002. Analysis of the NRT2 nitrate transporter family in *Arabidopsis*. Structure and gene expression. Plant Physiol. 129: 886-896.

Othman, A. A., W; M. Amer, M. Fayez and N. A. Hegazi. 2004. Rhizosheath of sinai desert plants is a potential repository for associative diazotrophs. Microbiol. Res. 159(3): 285-293.

Palleroni, N. and J. F. Bradbury. 1993. *Stenotrophomonas*, a new bacterial genus for *Xanthomonas maltophilia* (Hugh 1980) Swings et al. 1983. Int. J. Syst. Bacteriol. 43: 606-609.

Pang, J., M. H. Ryan, K. H. M. Siddique and R. J. Simpson. 2017. Unwrapping the rhizosheath. Plant Soil. 418: 129-139.

Pascual, C., P. A. Lawson, J. A. E. Farrow, M. N. Gimenez and M. D. Collins. 1995. Phylogenetic analysis of the genus *Corynebacteriurn* based on 16s rRNA gene sequences. International journal of systematic bacteriology. 45 (4): 724-728.

Pečenková, T., M. Janda, J. Ortmannová, V. Hajná, Z. Stehlíková and V. Žárský. 2017. Early Arabidopsis root hair growth stimulation by pathogenic strains of *Pseudomonas syringae*. An. Bot. 120: 437-446.

Pellizzaro, A., T. Clochard, E. Planchet, A. M. Limami, M. C. Morère-Le Paven. 2015. Identification and molecular characterization of Medicago truncatula NRT2 and NAR2 families. Physiol Plant. 152(2): 256-269.

Peterson, R.L. and M.L. Farquhar. 1996. Root hairs: specialized tubular cells extending root surfaces. Botanical Review. 62: 1-40.

Pierret, A., S. Gonkhamdee, C. Jourdan and J.L. Maeght. 2013. IJ_Rhizo: an open-source software to measure scanned images of root samples. Plant Soil. 373: 531-539.

Pikovskaya, R.I. 1984. Mobilization of phosphorus in soil in connection with the vital activity of some microbial species. Microbiologiya. 17: 362-370.

Pires, N.D., K. Yi, H. Breuninger, B. Catarino, B. Menand and L. Dolan. 2013. Recruitment and remodeling of an ancient gene regulatory network during land plant evolution. Proc Natl Acad Sci USA. 110: 9571-9576.

Poitout, A., A. Martinière, B, Kucharczyk, N. Queruel, J. Silva-Andia, S. Mashkoor, L. Gamet, F. Varoquaux, N. Paris, H. Sentenac, B. Touraine and G. Desbrosses. 2017. Local signalling pathways regulate the *Arabidopsis* root developmental response to *Mesorhizobium loti* inoculation. J. Exp. Bot. 68(5). 1199-1211.

Poly, F., L. J. Monrozir and R. Bally. 2001. Improvement in RFLP procedure to study the community of nitrogen fixers in soil through the diversity of *nifH* gene. Res Microbiol. 152: 95-103.

Poupin, M., M. Greve, V, Carmona and I. Pinedo. 2016. A complex molecular interplay of auxin and ethylene signaling pathways ss involved in *Arabidopsis* growth promotion by *Burkholderia phytofirmans* PsJN. Front. Plant Sci. 492(7): 16p, doi.org/10.3389/fpls.2016.00492

Rajawat, M.V.S., S. Singh, S. P. Tyagi, and A.K. Saxena. 2016. A Modified Plate Assay for Rapid Screening of Potassium-Solubilizing Bacteria. Pedosphere. 26: 768-773.

Reintanz, B., A. Szyroki, N. Ivashikina, P. Ache, M. Godde, D. Becker, K. Palme, and R. Hedrich. 2002. AtKC1, a silent Arabidopsis potassium channel alpha - subunit modulates root hair K+ influx. Proc. Natl. Acad. Sci. USA 99: 4079-4084.

Remans T., P. Nacry, M. Pervent, T. Girin, P. Tillard, M. Lepetit and A. Gojon. 2006. A central role for the nitrate transporter NRT2.1 in the integrated morphological and physiological responses of the root system to nitrogen limitation in *Arabidopsis*. Plant Physiol. 140: 909-921.

Ribaudo, C. M., E. M. Krumpholz, F. D. Cassán, R. Bottini, M. L. Cantore and J. A. Curá. 2006. *Azospirillum* sp. promotes root hair development in tomato plants through a mechanism that involves ethylene J. Plant Growth Regul. 24: 175-185.

Rigas, S., F. A. Ditengou, K. Ljung, G. Daras, O. Tietz, K. Palme and P. Hatzopoulos. 2013. Root gravitropism and root hair development constitute coupled developmental responses regulated by auxin homeostasis in the *Arabidopsis* root apex. New Phytol. 197: 1130-1141.

Riggs, P.J., M. K. Chelius, A.L. Iniguez, S. M. Kaeppler and E. W. Triplett. 2001. Enhanced maize productivity by inoculation with diazotrophic bacteria. Aust. J. Plant Physiol. 28(9): 829–836.

Robertson-Albertyn, S., R. A. Terrazas, K. Balbirnie, M. Blank1, A. Janiak, I. Szarejko, B. Chmielewska, J. Karcz, J. Morris, P. E. Hedley, T. S. George and D. Bulgarelli. 2017. Root hair mutations displace the barley rhizosphere microbiota. Front. Plant Sci. 1094(8): 15p, doi.org/10.3389/fpls.2017.01094

Roesch, L. F. W., R. R. Fulthorpe, A. Riva, G. Casella, A. K. Hadwin, A. D. Kent, S. H. Daroub, F. A. Camargo, W. G. Farmerie and E. W. Triplett. 2007. Pyrosequencing enumerates and contrasts soil microbial diversity. ISME J. 1: 283-290.

Ryan, R. P., S. Monchy, M. Cardinale, S. Taghavi, L. Crossman, M. B. Avison, G. Berg, D. van der Lelie and J. M. Dow. 2009. The versatility and adaptation of bacteria from the genus *Stenotrophomonas*. Nat. Re. Microbiol. 7 (7): 514-525.

Salazar-Henao, J.E. and W. Schmidt. 2016. An inventory of nutrient-responsive genes in *Arabidopsis root* hairs. Front. Plant Sci. 237(7): 11p, doi: 10.3389/fpls.2016.00237

Sasse, J., E. Martioia and T. Northen. 2018. Feed your friends: Do plant exudates shape the root microbiome? Trends Plant Sci. 23(1): 25-41.

Schall, J. A. and R. S. Quatrono. 1992. Abscisic acid elicits the water-stress response in root hairs of *Arabidopsis thaliana*. Plant Physiol. 100: 216-218.

Schmidt, W. and A. Schikora. 2001. Different pathways are involved in phosphate and iron stress-induced alterations of root epidermal cell development. Plant Physiol. 125: 2078-2084.

Segal, E., T. kushnir, Y. Mualem and U. Shani. 2008. Water uptake and hydraulics of the root hair rhizosphere. Vadose Zone J. 7(3): 1027-1034.

Sentenac, H. and C. Grignon. 1987. Effect of H^+ excretion on the surface pH of corn root cells evaluated by using weak acid influx as a pH probe. Plant Physiol. 84: 1367-1372.

Setiawati, T.C. and L. Mutmainnah. 2016. Solubilization of potassium containing mineral by microorganisms from sugarcane rhizosphere. Agriculture and Agricultural Science Procedia. 9: 108-117.

Shane, M. W., G. R. Cawthray, M. D. Cramer, J. Kuo and H. Lambers. 2006. Specialized 'dauciform' roots of Cyperaceae are structurally distinct, but functionally analogous with 'cluster' roots. Plant Cell Environ. 29: 1989-1999.

Shane, M. W., M. E. McCully, M. J. Canny, J. S. Pate and H. Lambers. 2011 Development and persistence of sandsheaths of *Lyginia barbata* (Restionaceae): relation to root structural development and longevity. Ann. Bot. 108(7): 1307-1322.

Shibata, M., C. Breuer, A. Kawamura, N. M. Clark, B. Rymen, L. Braidwood, K. Morohashi, W. Busch, P. N. Benfey, R. Sozzani and K. Sugimoto. 2018. GTL1 and DF1 regulate root hair growth through transcriptional repression of *ROOT HAIR DEFECTIVE 6-LIKE* 4 in *Arabidopsis*. Development. 145: dev159707. doi:10.1242/dev.159707

Shin, H., H.S. Shin, G. R. Dewbre, and M. J. Harrison. 2004. Phosphate transport in Arabidopsis: Pht1;1 and Pht1;4 play a major role in phosphate acquisition from both low- and high-phosphate environments. Plant J. 39(4): 629-642.

Singh, R. P. and P. N. Jha. 2017. The PGPR *Stenotrophomonas maltophilia* SBP-9 augments resistance against biotic and abiotic stress in wheat plants. Front. Microbiol. 8: 15p, doi.org/10.3389/fmicb.2017.01945

Singh, R. P. and P. N. Jha. and P. N. Jha. 2015. The plant-growth-promoting bacterium *Klebsiella* sp. SBP-8 confers induced systemic tolerance in wheat (*Triticum aestivum*) under salt stress. J. Plant Physiol. 184: 57-67.

Smith, S.E. and D.J. Read. 2008. Mycorrhizal symbiosis. New York, NY, USA: Academic Press.

Stetter, M., K. Schmid and U. Ludewing. 2015. Uncovering genes and ploidy involved in the high diversity in root hair density, length and response to local scarce phosphate in *Arabidopsis thaliana*. PLoS One. 10(3): e0120604. doi:10.1371 /journal. pone.0120604

Sun, X.G. and M. Tang. 2013. Effect of arbuscular mycorrhizal fungi inoculation on root traits and root volatile organic compound emissions of *Sorghum bicolor*. South Afr. J. Bot. 88: 373-379.

Takahashi. H. 2019. Sulfate transport systems in plants: functional diversity and molecular mechanisms underlying regulatory coordination. J. Exp. Bot. 70(16): 4075-4087.

Takahashi. H., P. Buchner, N. Yoshimoto, M. J. Hawkesford and S. H. Shiu. 2012. Evolutionary relationships and functional diversity of plant sulfate transporters. Front. Plant Sci. 119(2): 9p, doi.org/10.3389/fpls.2011.00119

Tan, K., C. Wen, H. Feng, X. Chao and H. Su. 2016. Nuclear dynamics and programmed cell death in *Arabidopsis* root hairs. Plant Sci. 253: 77-85.

Tanaka, N., M. Kato, R. Tomioka, R. Kurata, Y. Fukao, T. Aoyama and M. Maeshima. J. Exp. Bot. 65(6): 1497-1512.

Thibaud, J. B., J. C. Davidian, H. Sentenac, A. Soler and C. Grignon. 1988. H^+ cotransports in corn roots as related to the surface pH shift induced by active H^+ excretion. Plant Physiol. 88: 1469-1473.

Thomson, J., L. H. Melville and R. L. Peterson. 1989. Interaction between the ectomycorrhizal fungus *Pisolithus tinctorius* and root hairs of *Picea mariana* (Pinaceae). Amer. J. Bot. 76: 632-636.

Timmermann, T., A. Grace, D. Raúl, S. Aldo, H. Loreto and G. Bernardo. 2017. *Paraburkholderia phytofirmans* PsJN Protects *Arabidopsis thaliana* Against a Virulent Strain of *Pseudomonas syringae* Through the Activation of Induced Resistance. Mol. Plant Mocrobe In. 30(3): 215-230.

Tsujimoto, R., H. Yamazaki, S. Maeda and T. Omata. 2007. Distinct roles of nitrate and nitrite in regulation of expression of the nitrate transport genes in the moss *Physcomitrella patens*. Plant Cell Physiol. 48(3): 484-497.

Vacheron, J., G. Desbrosses, M.L. Bouffaud, B. Touraine, Y. MoënneLoccoz, D. Muller, L. Legendre, F. Wisniewski-Dyé and C. Prigent-Combaret. 2013. Plant growth-promoting rhizobacteria and root system functioning. Front. Plant Sci. 4 (356): 19p.

Vacheron, J., G. Desbrosses, S. Renoud, R. Padilla, V. Walker, D. Muller and C. Prigent-Combaret. 2018. Differential contribution pf plant-beneficial functions from *Psudomonas kilonensis* F113 to root system architecture alterations in *Arabidopsis thaliana* and *Zea mays*. Mol Plant Microbe In. 31(2): 212-223.

Vartanian, N. 1981. Some aspects of structural and functional modifications induced by drought in root systems. Plant Soil. 63: 83-92.

Vartanian, N., L. Marcotte and J. Giraudat. 1994. Drought rhizogenesis in *Arabidopsis thaliana*. Plant Physiol. 104: 761-767.

Venturi, V. and C. Keel. 2016. Signaling in the rhizosphere. Trends Plant Sci. 21: 187-198.

Verbon., E. and L. M. Liberman. 2018. Beneficial microbes affect endogenous mechanisms controlling root development. Trends Plant Sci. 21(3): 218-229.

Véry, A. A. and J. M. Davies. 2000. Hyperpolarization-activated calcium channels at the tip of *Arabidopsis* root hairs. Proc. Natl. Acad. Sci. USA, 97: 9801-9806.

Véry A. A., M. Nieves-Cordones, M. Daly, I. Khan, C izames and H. Sentenac. 2014. Molecular biology of K^+ transport across the plant cell membrane: what do we learn from comparison between plant species? J. Plant Physiol. 171: 748-769.

Véry A. A. and H. Sentenac H. 2002. Cation channels in the Arabidopsis plasma membrane. Trends Plant Sci. 7(4): 168-175.

Véry A. A. and H. Sentenac H. 2003. Molecular mechanisms and regulation of K^+ transport in higher plants. Annu. Rev. Plant Biol. 54: 575-603.

Vincent, J.M. 1970. A manual for the practical study of root-nodule bacteria. IBP Handbook No. 15, Blackwell Scientific Publishers, Oxford, 164p.

Volkens, G; 1887. Die Flora der aegyptisch-arabischen Wuste: auf Grundlage anatomisch-physiologischer Forschungen. Gebrüder Borntraeger, Berlin.

Walkley, A. and I. A. Black. 1934. An examination of Degtjareff method for determining soil organic matter and a proposed modification of the chromic acid titration method. Soil Sci. 37: 29-37.

Wang, L., M. Deng, J. Xu, X. Zhu and C. Mao. 2018. Molecular mechanisms of phosphate transport and signaling in higher plants. Semin Cell Dev Biol. 4: 114-122.

Wang, L., M. Y. Guo, J. B. Thibaud, A. A. Véry and H. Sentenac. 2019. A repertoire of cationic and anionic conductances at the plasma membrane of *Medicago truncatula* root hairs. Plant J. 98(3): 418.433.

Wen, T.J. and P.S. Schnable. 1994. Analyses of mutants of 3 genes that influence root hair development in *Zea mays* (Gramineae) suggest that root hairs are dispensable. Am. J. Bot. 81: 833-842.

Wirth, J., F. Chopin, V. Santoni, G. Viennois, P. Tillard, A. Krapp, L. Lejay, F. Daniel-Vedele and A. Gojon. 2007. Regulation of root nitrate uptake at the *NRT2.1* protein level in *Arabidopsis thaliana*. J. Biol. Chem. 282: 23541-23552.

Wolf, A., F. Antje, H. Martin and G. Berg. 2002. *Stenotrophomonas rhizophila* sp. nov., a novel plant-associated bacterium with antifungal properties. Int. J. Syst. Evol. Microbiol. 52: 1937-1944.

Wu, Q; S., C. Y. Liu, D. J. Zhang, Y. N. Zou, X. H. He and Q. H. Wu. 2015. Mycorrhiza alters the profile of root hairs in trifoliate orange. Mycorrhiza. 26(3): 11p, doi: 10.1007/s00572-015-0666-z

Wullstein, L. H., M. L. Bruening and W. B. Bollen. 1979. Nitrogen fixation associated with sand grain root sheaths (rhizosheaths) of certain xeric grasses. Physiologia Plantarum. 46: 1-4.

Wullstein, L. H. and S. A. Pratt. 1981. Scanning electron microscopy of rhizosheaths of *Oryzopsis hymenoides.* Am. J. Bot. 68: 408-419.

Yang, X. and W. Deng. 2017. Morphological and structural characterization of the attachment system in aerial root of *Syngonium podophyllum*. Planta. 245: 507-521.

Yang, T., S. Zhang, Y. Hu, F. Wu, Q. Hu, G. Chen, J. Cai, T. Wu, N. Moran, L. Yu and G. Xu. 2014. The role of a potassium transporter oshak5 in potassium acquisition and transport from roots to shoots in rice at low potassium supply levels. Plant Physiol. 166: 945-959.

Yeoh, Y. K., P. G. Dennis, C. Paungfoo-Lonhienn, L. Weber, R. Brackin, M. A. Ragan, S. Schmidt and P. Hugenholt. 2017. Evolutionary conservation of a core root microbiome across plant phyla along a tropical soil chronosequence. Nat. Commun. 8: 215. doi: 10.1038/s41467-017-00262-8

Yi, K., B. Menand, E. Bell, and L. Dolan. 2010. A basic helix-loop-helix transcription factor controls cell growth and size in root hairs. Nature Genet. 42: 264-267.

Yong, Z., Z. Kotur and A.D.M. Glass. 2010. Characterization of an intact two-component high-affinity nitrate transporter from *Arabidopsis* roots. Plant J. 63: 739-748.

York, L. M., A. Carminati, S.J. Moone, K. Ritz and M.J. Bennett. 2016. The holistic rhizosphere: integrating zones, processes, and semantics in the soil influenced by roots. J. Exp. Bot. 67: 3629-3643.

Yuan, J., J. M. Chaparro, D. K; Manter, R. Zhang, J. M. Vivanco and Q. Shen. 2015. Roots from distinct plant developmental stages are capable of rapidly selecting their own microbiome without the influence of environmental and soil edaphic factors. Soil Biol Biochem. 89: 206-209.

Yuan, L., D. Loqué, S. Kojima, S. Rauch, K. Ishiyama, E. Inoue, H. Takahashi, and N. von Wirén. 2007. The Organization of High-Affinity ammonium uptake in *Arabidopsis* roots depends on the spatial arrangement and biochemical properties of AMT1-type transporter. Plant cell. 19: 2636-2652.

Zamioudis, C., P. Mastranesti, P. Dhonukshe, I. Blilou, and C. M. J. Pieterse. 2013. Unraveling root developmental programs initiated by beneficial *Pseudomonas* spp. bacteria. Plant Physiol. 162: 304-318.

Zhang, S. L. Huang, A. Yan, Y. Liu, B. Liu, C. Yu, A. Zhang, J. Schiefelbein and Y. Gan. 2016. Multiple phytohormones promote root hair elongation by regulating a similar set of genes in the root epidermis in *Arabidopsis*. J. Exp. Bot. 67(22): 6363-6372.

Zhao, C., Huang, J. P; Gyaneshwar and D. Zhao. 2018. *Rhizobium* sp. IRBG74 Alters *Arabidopsis* root development by affecting auxin signaling. Front. Microbiol. 2556(8): 12p, doi.org/10.3389/fmicb.2017.02556

Zhu, J., S. M. Kaeppler and J. P. Lynch. 2005. Mapping of QTL controlling root hair length in maize (*Zea mays* L.) under phosphorus deficiency. Plant Soil. 270: 299-310.

Zipfel, C. and G. E. D. Oldroyd. 2017. Plant signalling in symbiosis and immunity. Nature. 543: 328-336.

Zygalakis, K. C., G. J. D. Kirk, D. L. Jones, M. Wissuwa and T. Roose. 2011. A dual porosity model of nutrient uptake by root hairs. New Phytol. 192: 67

Réponses développementales des racines aux carences nutritives et aux conditions biotiques chez le blé: identification de bactéries bénéfiques à partir de sol rhizosphérique de blé et nouvelles procédures de phénotypage du développement des racines et des poils absorbants

Résumé

La réduction de la fertilisation chimique et de ses coûts écologiques est l'un des défis majeurs de l'agriculture. Au niveau fondamental, il est donc important d'acquérir des connaissances sur le développement racinaire et les fonctions physiologiques qui contribuent à la nutrition minérale des plantes, y compris les interactions avec les microbes bénéfiques du sol qui améliorent directement ou indirectement l'acquisition d'ions nutritifs. À la surface des racines, les poils absorbants sont au carrefour de la nutrition minérale de la plante et de ses interactions avec les microbes bénéfiques du sol. Nous montrons que des membres d'une collection de 16 souches bactériennes que nous avons isolées à partir de la rhizosphère de plantes de blé, comprenant des espèces appartenant aux genres *Achromobacter*, *Stenotrophomonas*, *Rhizobium*, *Paraburkholderia* et *Klebsiella*, diffèrent par leur capacité à solubiliser des sources peu solubles de phosphate et de potassium, leurs effets sur l'acquisition des ions nutritifs, l'efficacité d'utilisation de l'azote, la croissance racinaire et le développement des poils absorbants, et finalement leur capacité à promouvoir la croissance du blé. De nouvelles méthodologies de phénotypage ont été développées, impliquant des dispositifs de croissance originaux et des programmes d'analyse d'images *in silico*, afin de décrire avec des paramètres quantitatifs le développement des racines et des poils absorbants en réponse aux conditions abiotiques et biotiques. Une première série d'expériences montre des réponses distinctes, en termes de croissance des racines et de développement des poils absorbants, à la faible disponibilité de phosphate ou d'azote et à l'inoculation d'une souche de *Bradyrhizobium japonicum* chez des plants de blé âgés de 2 semaines (*Triticum turgidum* L. spp. durum cv. Oued Zenati).

Mots clés: Blé, racine, poil absorbant, nutrition minérale, PGPR (Plant Growth Promoting Rhizobacteria)

Root developmental responses to nutrient shortage and biotic conditions in wheat: identification of beneficial bacteria from wheat rhizosphere and new procedures for phenotyping root and root hair development

Abstract

Reducing chemical fertilization and its ecological costs is one of the major challenges in agriculture. Knowledge has thus to be gained about root development and physiological functions contributing to plant mineral nutrition. This includes interactions with beneficial soil microbes directly or indirectly improving nutrient ion acquisition. At the root surface, root hairs are at the crossroad of plant nutrition and interactions with beneficial soil microbes. Members from a collection of 16 bacterial strains that we have isolated from wheat rhizospheric soils, comprising species belonging to the genera *Achromobacter*, *Stenotrophomonas*, *Rhizobium*, *Paraburkholderia* and *Klebsiella*, are shown to differ with respect to their ability to solubilize poorly soluble sources of phosphate and potassium, their effects on nutrient ion acquisition and nitrate use efficiency, their impact on root development and root hair elongation, and finally their capacity to promote wheat growth. New phenotyping methodologies have been developed, involving original growth devices and *in silico* image analysis programs, in order to describe with quantitative parameters root and root hair development in response to abiotic and biotic conditions. A first set of experiment shows distinctive responses, in terms of root growth and root hair development, to low availability of phosphate or nitrogen and to inoculation with a *Bradyrhizobium japonicum* strain in 2-week-old wheat seedlings (*Triticum turgidum* L. spp. durum cv. Oued Zenati).

Key words: Wheat, root, root hair, mineral nutrition, PGPR (Plant Growth Promoting Rhizobacteria)